NUMERICAL AND EXPERIMENTAL INVESTIGATION OF PERFORMANCE FOR VERY-LOW-HEAD MICRO AND PICO KAPLAN HYDRO-TURBINES WITH RIM-DRIVEN GENERATORS

by

Ahmad I. Abbas

A Dissertation Submitted in

Partial Fulfillment of the

Requirements for the Degree of

Doctor of Philosophy

in Engineering

at

The University of Wisconsin-Milwaukee

May 2020

ABSTRACT

NUMERICAL AND EXPERIMENTAL INVESTIGATION OF PERFORMANCE FOR VERY-LOW-HEAD MICRO AND PICO KAPLAN HYDRO-TURBINES WITH RIM-DRIVEN GENERATORS

by

Ahmad I. Abbas

The University of Wisconsin-Milwaukee, 2020
Under the Supervision of Professor Ryoichi S. Amano

Renewable energy plays a significant role in new power generation worldwide, and hydropower is contributing to 86% of renewable electricity production within all other renewable energy resources. Simultaneously, hydropower shares 83% of U.S. renewable energy capacity and accounts for 77% of actual renewable electricity generation. However, most of the installed hydropower consists of large plants. Much potential hydro generation remains untapped, particularly at lower power and head levels. There is a substantial opportunity worldwide and across the U.S. in specific to add new hydropower generating capabilities at low-head sites such as non-powered dams, canals, and conduits with a water height of less than 30 meters, especially, where the potential of solar and wind is not available. As stated by the U.S. Department of Energy, there is an estimated potential hydropower capacity of 12,000 MW of the existed 80,000 unpowered dams with at least 3 feet of water head available.

In this research, investigation of power-efficient micro and pico Kaplan hydro turbines at very-low-head with rim-driven generators to be studied and evaluated, specifically, at heads of less than 3 meters (10 ft). Optimization of performance and design for a 3D-printed conventional -with shaft- 7.6 cm (3-inch) Kaplan turbine to be carried out based on an experimental setup in

the Hydro Turbines Laboratory of the University of Wisconsin-Milwaukee in addition to the utilization of Computational Fluid Dynamics (CFD). Then a shaftless rim-driven generator-based turbine (RDT) to be introduced and optimized. Such a new hydro turbine perception will increase the efficiency (of power generation) of hydro turbines in general, and the efficiency of low-head turbines in specific.

The design optimization includes; the number of the blades for the turbine's rotor (runner) and stator, the blade wrap-angle of the rotor, intake and draft tubes angles, lengths and shapes, and the guide vanes. The performance in terms of the power output and the efficiency is evaluated for the conventional turbine by utilizing CFD and by testing a 3D-printed model of the turbine in a custom-built experimental setup at different water heads (from 2.0 m to 2.6 m) and different rotational speeds (0 – 4000 rpm). The CFD setup is based on 3D transient turbulent featuring the Large Eddy Simulation (LES) model, and STAR-CCM+ is the CFD software. In addition, the high-performance computing (HPC) cluster of the University of Wisconsin-Milwaukee is used for solving the complex CFD simulations.

To evaluate the advantage of the RDT over the conventional turbines, the rim-driven shaftless turbine is introduced in this research at the same boundary conditions. The RDT is not expected only to increase the efficiency of hydro turbines. It will also contribute saving the environment by allowing debris or fish to pass through the central area of the turbine, especially in the case of run-a-river hydro turbines applications. Furthermore, some applications of the RDT are presented in this study. The utilization of RDT in wastewater treatment plants (WWTPs) is one example where WWTPs usually have low or very-low head between the discharge point of the plant and the water body where the treated water is supposed to be disposed. At the same time, a significant continuous water flow rate is available all over the year

for feasible hydro turbine installations. Such utilization will improve the energy efficiency of WWTPs.

TABLE OF CONTENTS

LIST OF FIGURES

LIST OF TABLES

3D	Three dimensional
BCDS	Bounded central differential scheme
C	Coefficient of mass flow rate ratio
CAD	Computer-aided design
CAE	Computer-aided engineering
CFD	Computational fluid dynamics
c_m	Meridional component of absolute velocity (m/s)
D	Diameter, m
DC	Direct current
E	Rate of energy loss, J/s or W
EIA	Energy information administration
F	Friction force, N
g	Gravitational acceleration, m/s^2
GOE	Gottingen airfoil
H	Head, m
HOMER	Hybrid optimization model for multiple energy resources
HPC	High-performance computing
I	Radius of the shaft, m
LES	Large-eddy simulation
MDO	Multidisciplinary design optimization
MGD	Million gallons per day
N	Rotational speed, rpm
N-S	Navier-Stokes
NREL	National Renewable Energy Laboratory
p	Pressure
P	Power, kW
PVC	Polyvinyl Chloride
Q	Flow rate, m^3/s
R&D	Research and development
REN21	Renewable energy policy network for the 21st century
RDP	Rim-driven propeller
RDT	Rim-drive turbine
SAS	Scale-adaptive-simulation
SGS	Sub-grid scale
SST	Shear stress transport

t	Time, s
u	Circumferential velocity (m/s)
URANS	Unsteady Reynolds average Navier-Stokes
V	Velocity
VOF	Volume of fluid
W	Power output, W
WALE	Wall-adapting local-eddy
WWTPs	Wastewater treatment plants
y^+	Non-dimensional wall distance
z	Elevation or head
ZLES	Zonal large-eddy-simulation

GREEK SYMBOLS

β_1	Blade angle at the leading edge (^{o})
β_2	Blade angle at the trailing edge (^{o})
$\Delta\varphi$	Blade wrap angle (^{o})
η	Efficiency
ρ	Density, kg/m^3
μ	Dynamic viscosity, Pa.s
Π	Power coefficient

SUBSCRIPTS AND SUPERSCRIPTS

b	Corrected mass flow rate due to the air in the system effect
c	Calculated mass flow rate (CFD)
e	Experimental mass flow rate
f	Corrected mass flow rate due to friction
m	Model
p	Prototype
r	Mass flow rate ratio

ACKNOWLEDGMENTS

First of all, I would like to express my appreciation and thanks to my advisor Professor Ryoichi Amano. I would like to thank him for his tremendous continuous support and for encouraging my research and allowing me to grow as an independent researcher. His supervision has been priceless.

I would like to thank Professors, John Reisel, Istvan Lauko, Wilkistar Otieno, Deyang Qu, and Yongjin Sung for serving on my dissertation committee and for giving me guiding comments during the preliminary exam and the final dissertation. Their input to my research is valuable and contributes to a better version of my work.

My acknowledgment extends to my research mates and colleagues, and I wish them all the best in their future endeavors. Special thanks to my best friend and my colleague Mohammad Qandil for his great assistance in testing and running the experimental setup. Additionally, I would like to thank an alumna of UW-Milwaukee Caleb Rozema for his help in designing the CAD work of the RDT.

Finally, thanks to my family and friends for their continuous support, encouragement, and inspiration.

With all the love I have in my heart and mind, I dedicate my work

To

My parents, my wife Farah, and my son Amir

Chapter 1: Introduction

1.1 Renewable Energy

Energy consumption has increased dramatically over the last decades due to the increase in the population. Fossil fuels (coal, natural gas, and oil) are the primary energy sources in most of the world due to their availability and high calorific value. However, there are limiting factors on the fossil fuels leading the world to seek for new energy resources that are abundant and can be a reliable substitute for fossil fuels. Some of these limiting factors are: fossil fuels are non-renewable, their consumption rate is much higher than their production rate thus expecting to deplete, and such resources are not clean energy sources since their extraction and energy production lead to a high carbon footprint [1]. Due to these reasons, the necessity to rely on and develop new technologies to harvest energy from renewable and clean resources like wind, hydro, and solar becomes a driving factor in the industry to fulfill the demand for electricity.

Currently, renewable energy plays a significant role in new power generation worldwide. Hydropower, wind, biomass, and photovoltaic are the leading renewable energy streams with 99% of total renewable sources. These streams add up to hundreds of gigawatts in global energy generation. Further, these mitigate tons of greenhouse gas emissions [2][3].

Renewable power generation can help countries meet their sustainable development goals through the provision of access to clean, secure, reliable, and affordable energy. Renewable energy has gone mainstream, accounting for the majority of capacity additions in power generation today. Tens of gigawatts of wind, hydropower, and solar photovoltaic capacity are installed worldwide every year in a renewable energy market that is worth more than a hundred billion USD annually.

Based on REN21's[1] 2019 report, renewables contributed 20% to our energy consumption and 26.5% to our electricity generation in 2018 [2][4]. Some indicators for global renewable energy for years (2013-2018) are shown in Table 1-1, and Figure 1-1 shows the estimated renewable energy share of global electricity production at the end of 2018.

Table 1-1: Renewable energy indicators in the world

Selected renewable energy global indicators	2013	2014	2015	2016	2017	2018
Investment in new renewable capacity (annual) (10^9 US$)	232	273	286	274	326	289
Renewables power capacity (GW_e)	1,578	1,701	1,856	2,017	2,197	2,378
Hydropower capacity (GW_e)	1,018	1,036	1,071	1,095	1,112	1,132
Wind power capacity (GW_e)	319	370	433	487	540	591
Solar PV capacity (grid-connected) (GW_e)	138	177	228	303	405	505
Bio-power capacity (GW_e)	88	101	106	114	121	130
Geothermal power capacity (GW_e)	12.1	12.9	13.0	12.1	12.8	13.3
Concentrated solar thermal power (GW_e)	3.4	4.3	4.7	4.8	4.9	5.5
Solar hot water capacity (GW_{th})	373	409	435	456	472	480
Countries with policy targets for renewable energy use	144	164	173	176	179	169

[Renewables global status report 2015, 2016, 2017, 2018 and 2019][4]–[8]

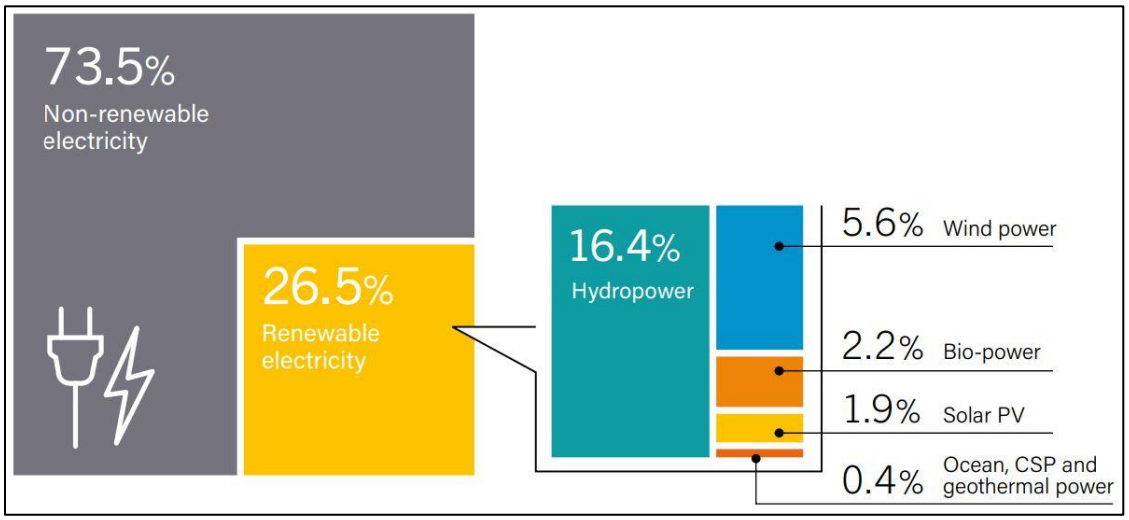

Figure 1-1: Estimated renewable energy share of global electricity production, end-2018[4]

[1] REN21: Renewable Energy Policy Network for the 21st Century; a global renewable energy policy network that provides international leadership for the rapid transition to renewable energy.

1.2 Hydropower

The principle of hydropower is the extraction of kinetic and potential energy from a flow to convert it into mechanical energy and then to electrical power by utilizing the head. The hydro turbine is not a very new concept, however increasing demand for renewable energy leads to expanding and further investigation of the technology.

1.2.1 Hydropower Worldwide

Currently, hydropower energy supplies 16.4% of the global electricity [9]. By comparing with other renewables, hydropower is the most significant contributor as shown in Figure 1-2 with a power capacity of 1,132 GW as of 2018 [4]. Even though the growth rate of hydropower is not as high as wind and solar sources, however, hydropower is sharing almost 40% of the total renewable energy sources in the world, see Figure 1-3.

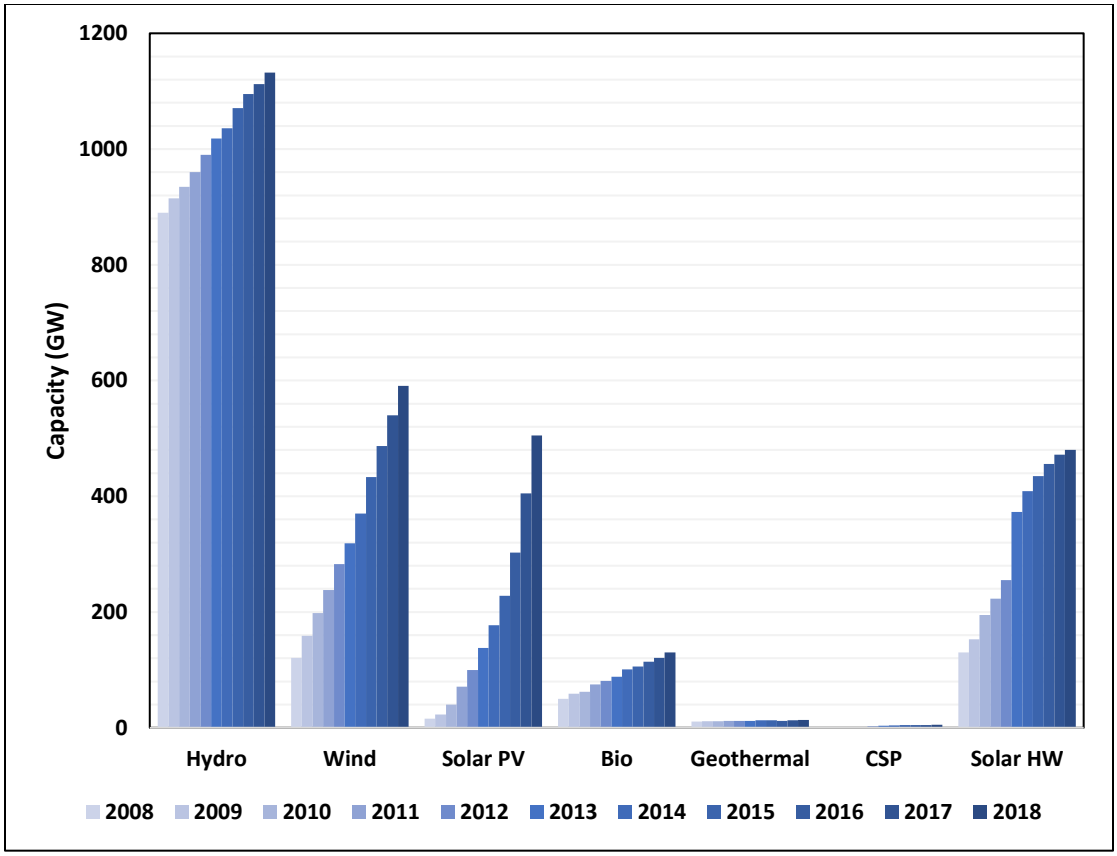

Figure 1-2: Renewable energy capacity and growth rate in the last decade

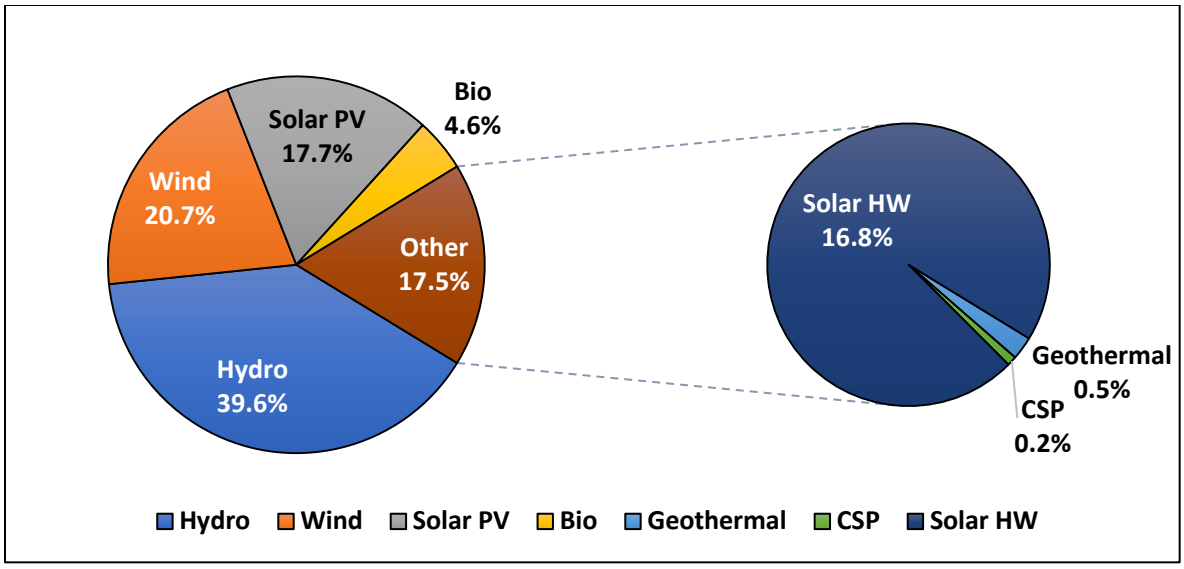

Figure 1-3: Share of renewable energy in the world

1.2.2 Hydropower in the US

In the USA, several renewable energy sources are used to generate power, such as hydro, wind, and biofuels. Figure 1 shows the share percentage of each type of these sources in the production energy in 2017 based on the U.S. Energy Information Administration (EIA) report [10]. It can be inferred from Figure 1-4 that hydroelectric power represents the highest contribution in generating electricity compared to other renewable energy sources with a percentage of 25% of the total renewable energy production. According to U.S. EIA [11], around 50% of the produced electricity from a renewable energy source in Wisconsin are being generated by hydroelectric power. Hydroelectric power is referred to as the electric power generation converted from the potential and kinetic energy stored in a water source (like dams, rivers) by using hydro turbines.

The principle of hydropower is the extraction of kinetic and potential energy from water flow to convert it into mechanical energy and then to electrical power by utilizing the available head. Hydro turbines are far from a new concept, however increasing demand for renewable energy is currently leading to expanding the technology. A particular need is at lower power levels, lower heads in particular, which so far have not been used because of a lack of industrial designs.

Currently, hydropower supplies 16.6% of the global electricity production [9] and 86% of the renewable energy sector [12]. The global installed hydropower capacity is 1171 GW, and the generated power from all different sources is around 3983 TWh/year. In the United States, with about 2400 dams utilized for hydropower, it represents 9.25% of overall generating capacity, accounts for 83% of U.S. renewable energy capacity, and 77% of actual renewable electricity generation [13]. However, most of the installed hydropower consists of large plants. Much potential hydro generation remains untapped, particularly at lower power and head levels [14]. This paper focuses on a study in finding a power-efficient solution to this situation, precisely, at heads, less than 3 m (10 ft), where more energy is available on the aggregate but with a lack of viable solutions both technically (efficiency-wise) and economically. Specifically, the authors envision leveraging 3D-printing techniques to produce units that are both low cost and optimized for specific sites. Such a design methodology, however, requires a thorough design optimization, which this paper addresses.

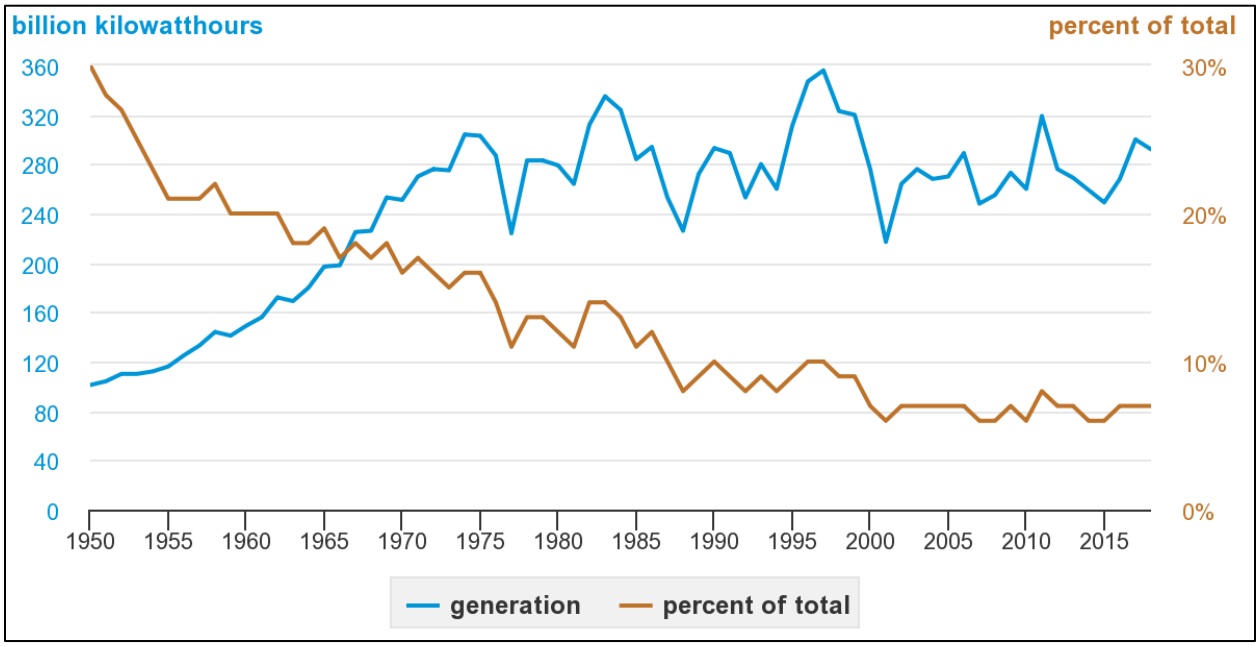

Figure 1-4: Hydroelectricity generation and share of total U.S. electricity generation, 1950-2018

Hydropower is a major energy source as it accounts for 16.6% of the entire electricity generation all over the world [1]. It is considered as a leading renewable energy resource supplying 71% of the global renewable-energy electricity generation [2,3]. In 2017, hydropower contributed to 7.5% of the total United States electricity generation accounting for 44% of electricity generated by renewable energy [4,5]. The United States is ranked fourth in the annual hydroelectric power production after China, Canada, and Brazil, as indicated in Figure 1-5 [6].

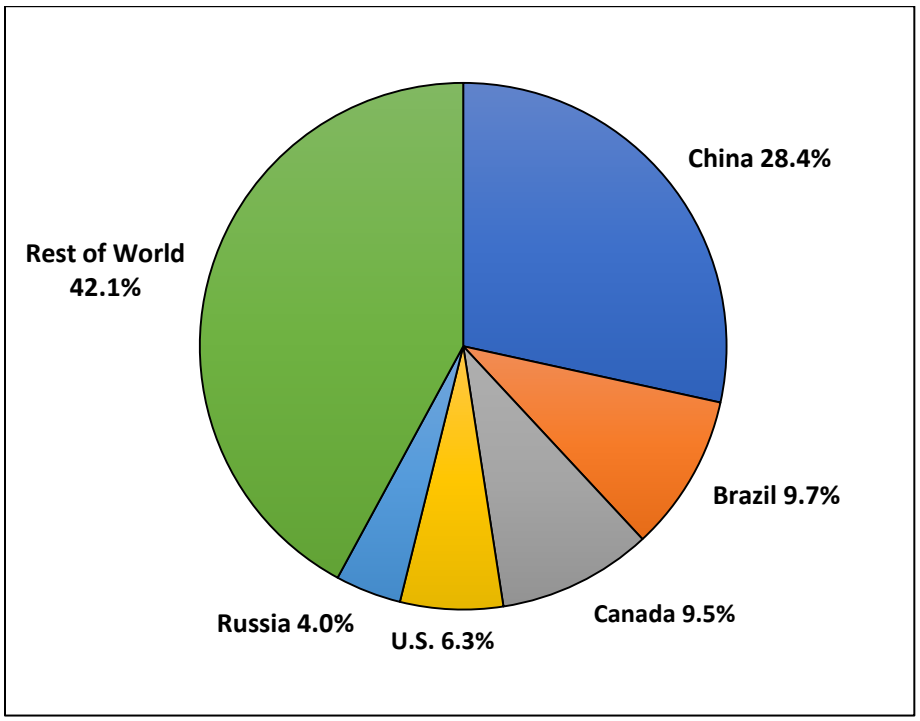

Figure 1-5: Percentage of annual hydropower production per country

There are 2198 active hydropower plants in the United States with a total capacity of 79.64 GW in which half of this capacity is located in Washington, California, and Oregon [15]. The majority of the installed hydropower plants in terms of capacities are located in the Northwest, whereas the northeast has the highest number of facilities. The largest hydroelectric plant in the U.S. is located at the Grand Coulee Dam, WA, with a capacity of 6,809 MW (Table 1-2 shows the top largest hydroelectric power stations in the US). While, the first commercial hydroelectric plant

(12.5 kW) was built in 1882 on the Fox River in Appleton, Wisconsin [16]. Then, commercial power companies began to install many small hydroelectric plants in mountainous regions near metropolitan areas. Construction of the Hoover Dam, see Figure 1-6 (a), started in 1931, and when completed in 1936, it was the largest hydroelectric project in the world with 2 GW [17]. Hoover Dam was then surpassed in 1941 by the Grand Coulee Dam (6.8 GW), see Figure 1-6 (b), on the Columbia River [18]. The more massive power output is due to the higher volume of water available.

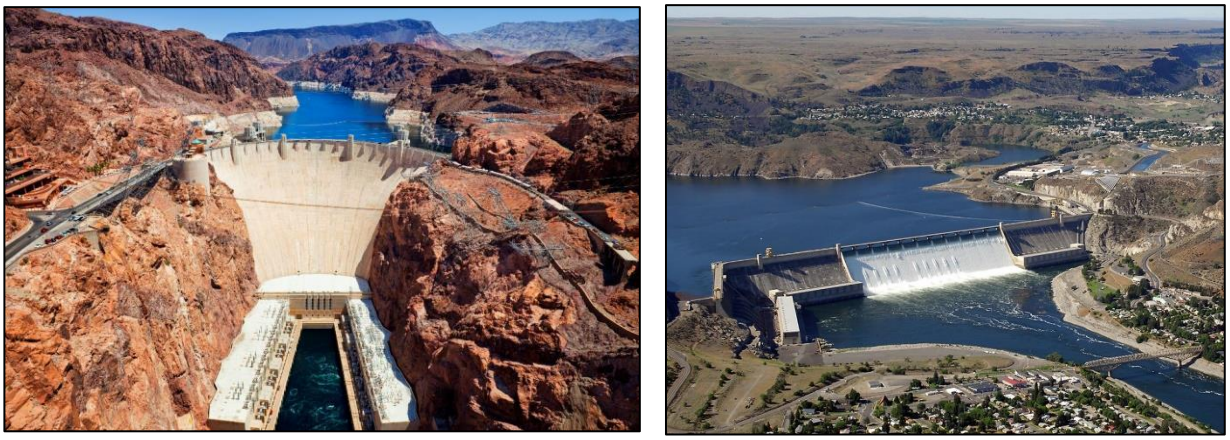

(a) (b)

Figure 1-6: Aerial photo of (a) the Hoover Dam (b) the Grand Coulee Dam

Table 1-2: List of largest hydroelectric power stations in the US

	Name	Location	Year of Completion	Total Capacity (MW)
1	Grand Coulee	Washington	1942/1980	6,809
2	Bath County PSP	Virginia	1985	3,003
3	Chief Joseph Dam	Washington	1958/73/79	2,620
4	Robert Moses Niagara Power Plant	New York	1961	2,515
5	John Day Dam	Oregon/ Washington	1949	2,160
6	Hoover Dam	Nevada/Arizona	1936/1961	2,080
7	The Dalles Dam	Oregon/ Washington	1957	2,038
8	Ludington PSP[2]	Michigan	1973	1,872
9	Raccoon Mountain PSP	Tennessee	1978	1,652
10	Glen Canyon Dam	Arizona	1966	1,320

[2] Pumped-storage plant

1.2.3 Advantages and Disadvantages of Hydropower

The advantages of hydropower can be summarized as follows [19]–[22]:

1) It is a renewable source of energy—and saves scarce fuel reserves.
2) It is a clean power source because there is no air pollution or radioactive waste problems associated with it.
3) Since water power produces no carbon dioxide, it does not contribute to global warming.
4) Hydropower stations have an inherent ability for instantaneous starting, stopping, load variations, etc. and help in improving the reliability of power systems. As a result, hydro stations are the best choice for meeting the peak demand.
5) Hydroelectric projects have a long useful life extending over 50 years. Some hydro projects completed at the end of the 19th century are still in operation (e.g. the plant installed in 1897 in Darjeeling, India).
6) The average cost of generation, operation and maintenance over the lifetime is lower than any other sources of energy.
7) Hydropower has a higher efficiency (over 90%) compared to thermal energy (up to 45%) and gas (up to 60%).
8) The cost of generation is free from inflationary effects after the initial installation.
9) Storage based hydro schemes often provide attendant benefits of irrigation, flood control, drinking water supply, navigation, recreation, tourism, pisciculture, etc.
10) The location in remote regions leads to the development of backward areas inland (education, medical services, road communication, telecommunication, etc.). This advantage is very important in developing and underdeveloped countries.

Despite these advantages, there are a few limitations or disadvantages of hydropower, especially of large hydropower plants:

1) The availability of hydropower is restricted to hilly or foothill areas due to the availability of water and head. This requires extra investment for installing long transmission lines and inevitably leads to transmission losses.
2) Large dams are considered to cause a heavy concentrated load on the earth leading to seismic effects.
3) Rehabilitation and restoration of people and activities in submerged areas is always a matter of concern.
4) In underdeveloped countries, the construction period of hydropower plants is longer than that of other plants. This is especially due to the fact that in hilly areas it is difficult to transport heavy equipment and machinery required to build the plant.
5) During the rainy season, heavy rains in the catchment areas could become a risk to the safety of the dam. At the same time, the release of large amounts of water is also not possible since it creates floods in the downstream side.
6) Some hydropower plants, especially in developing and underdeveloped countries, face serious problems due to an uncontrolled development in the catchment areas. This happens due to improved living conditions and employment opportunities in the area surrounding the power plant and the dam. The construction of housing and other commercial activities in the catchment area, over time, start causing disturbances to the flow of water into the reservoir, which changes the availability of water for power generation.
7) At some locations silt in the water due to soil erosion causes damage to the turbine blades requiring frequent maintenance during the rainy season.

1.2.4 Hydropower Technologies

Basically, there are several ways of hydropower technologies to generate electricity, starting with Impoundment (Modular hydropower, see Figure 1-7) where dams are utilized. The impoundment stores water in a reservoir and then when the water is released, it flows through and spins a turbine, turning a generator that produces electricity [19].

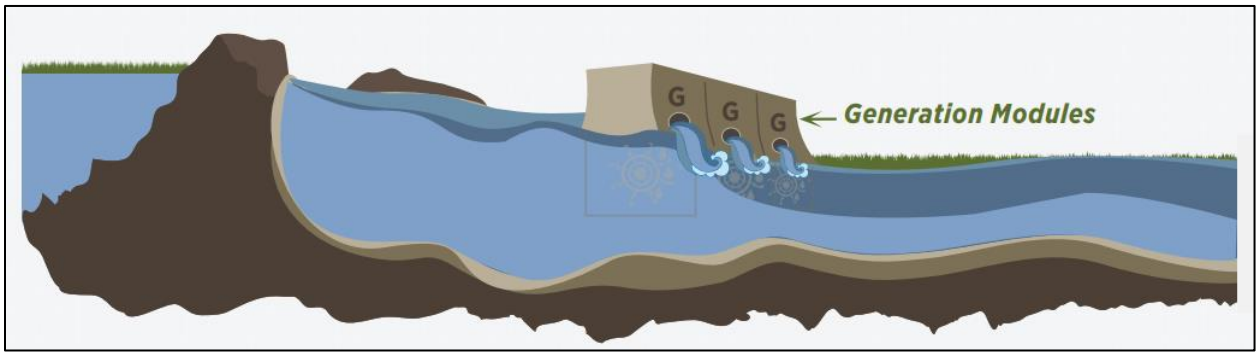

Figure 1-7: Modular hydropower (Impoundment)[23]

A Diversion (run-of-river) is another technology where a portion of a river is channeled through a canal or pipe into a turbine and generator system (see Figure 1-8). The advantage of the previously mentioned technology is that it uses the natural flow of the river and it does not require a large dam. The third technology is called Pumped-storage Hydropower (PSH) or Pumped-storage Plants (PSP) as shown in Figure 1-9, it is considered as a huge battery where the battery is charged by pumping the water back up into a reservoir during periods of low energy use (off-peak hours), and then when more power is needed during the day (on-peak hours), the water is released to produce electricity [24].

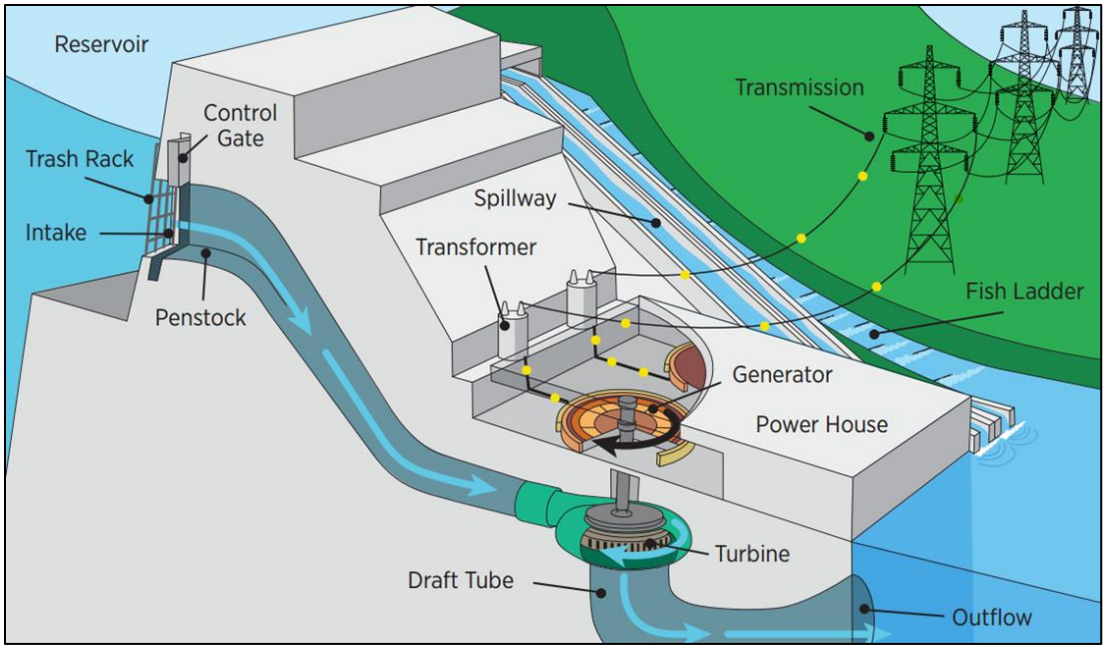

Figure 1-8: Diversion hydropower (run-of-river)[25]

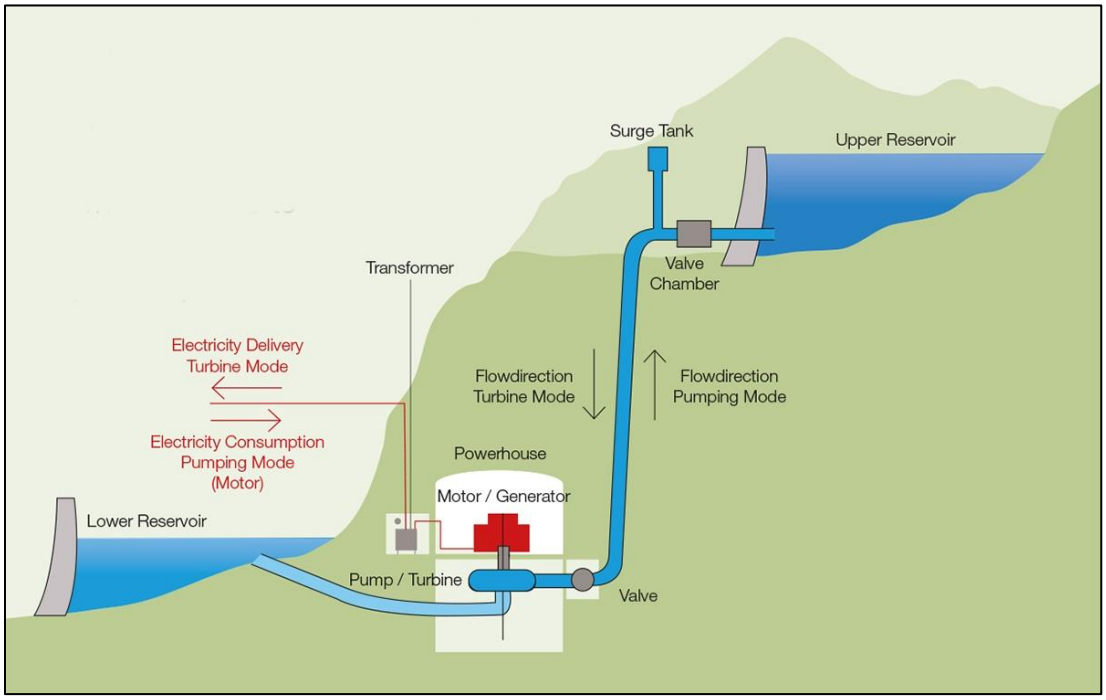

Figure 1-9: The principle of pumped-storage hydropower (PSH) or pumped-storage plants (PSP)[26]

1.3 Hydraulic Turbines

The hydraulic (water) turbine or hydro turbine is a rotary machine that converts kinetic energy and potential energy of water into mechanical work, and thus, this mechanical work can be

utilized to generate electricity through an electric generator. The turbine can be considered as the heart of any hydropower plant. Hydraulic turbines have a row of blades fitted to the rotating shaft or a rotating plate called the hub. Flowing water, while passing through the hydraulic turbine, strikes the blades of the turbine and makes the shaft rotate due to its impact or change of velocity and pressure. While flowing through the hydraulic turbine, the velocity and pressure of water diminish resulting in the development of torque and rotation of the turbine shaft. There are different forms or designs of hydraulic turbines in use depending on the operational requirements. The selection of the turbine is very critical for the success of a hydro-power plant. The optimum output of a specific combination of water flow and head can only be achieved by an adequate type of hydraulic turbine.

1.3.1 Hydro turbines Classifications

There are two main types of hydro turbines: impulse and reaction. The type of hydropower turbine selected for a project is based on the height of water (head) and the flow or volume of water; impulse turbine generally uses the velocity of the water to move the runner and discharges to atmospheric pressure. The water stream hits each bucket on the runner. There is no suction on the downside of the turbine, and the water flows out the bottom of the turbine housing after hitting the runner. An impulse turbine is generally suitable for high head, low flow applications, while the reaction turbine develops power from the combined action of pressure and moving water. The runner is placed directly in the water stream flowing over the blades rather than striking each individually. Reaction turbines are generally used for sites with lower head and higher flows than compared with the impulse turbines [27].

Hydro turbines are classified into three main categories depending on their application: Kaplan, Francis, and Pelton. Kaplan turbines are applicable for low heads and high flow rates

scenarios, whereas Francis turbines for medium heads and flow rates applications and Pelton turbines are used in low flow rates and high heads cases. Francis turbines are the most common type and used in hydropower plants since they possess a wide range of flow rates and head combinations. From 1996 to 2011, 9455 MW identified turbine capacity was installed. 74% of the total installed capacity was Francis turbines, Kaplan with 23%, and 83 MW for Pelton turbines [14]. Figure 1-10 [28] shows the classification of hydro-turbines based on the head (y-axis) and flow (x-axis).

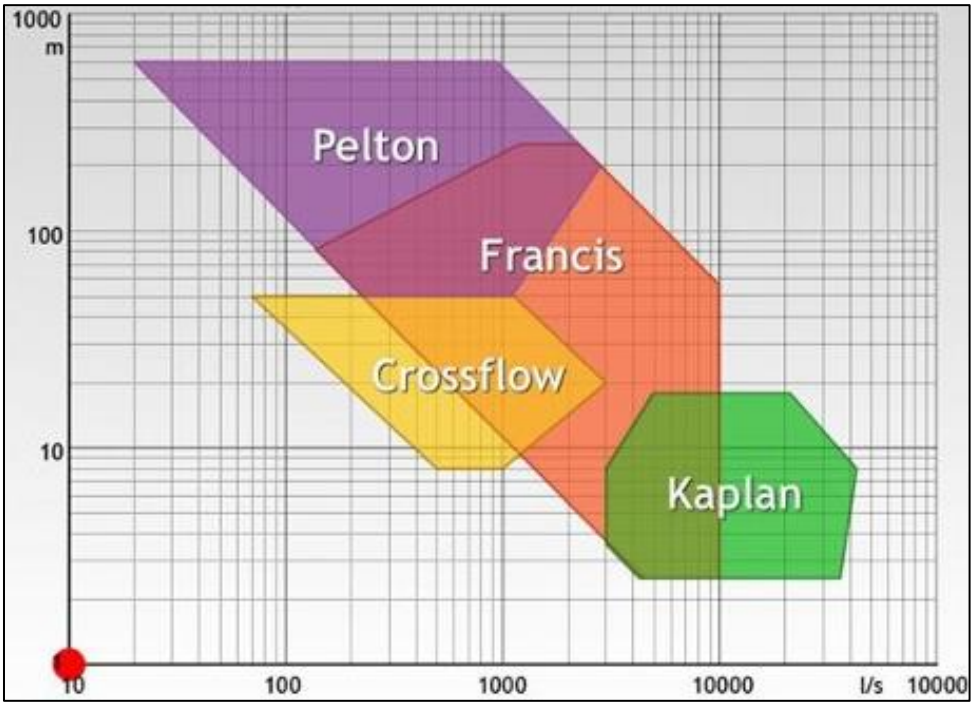

Figure 1-10: Classification of hydro turbines

Based upon the path of water flow, hydraulic turbines can be categorized into three types [16]:

a) Axial flow turbines

In this category of hydraulic turbines, the water flow path is mainly parallel to the axis of rotation. Kaplan and Propeller turbines are the most popular types of axial turbines.

b) Radial flow turbines

This type of hydraulic turbines has water flowing mainly in a plane that is perpendicular to the axis of rotation of the blades. Such a type of turbine is the Pelton turbine.

c) Mixed flow turbines

In practice, for most of the hydraulic turbines, the direction of flow is neither purely axial nor purely radial. It has a significant component of both axial and radial flows. Such types of hydraulic turbines are called mixed flow turbines. The Francis turbine is the most popular type of mixed flow turbine in which water enters in radial direction and exits in axial direction.

1.3.2 Kaplan Hydro turbines

The Kaplan turbine is a propeller-type water turbine and Professor Viktor Kaplan developed it in Austria in 1912. The rotor looks like an ordinary propeller of a ship with adjustable rotor blades (see Figure 1-11). Its major special features are low heights of water till about 25 m, even if it could work with a higher water height and adjustable rotor blades for changes in volume from about 1 m^3/s up to 500 m^3/s [19]. The Kaplan turbine was an evolution of the Francis turbine. Its invention allowed efficient power production in low-head applications which was not possible with Francis turbines. The head ranges from 10–70 meters and the output ranges from 5 to 200 MW. Runner diameters are between 2 and 11 meters. Turbines rotate at a constant rate, which varies from facility to facility. That rate ranges from as low as 55 rpm to 450 rpm [29]. Kaplan turbines are widely used throughout the world for electrical power production. They cover the lowest head hydro sites and are especially suited for high flow conditions.

Current areas of research include computational fluid dynamics (CFD) driven efficiency improvements and new designs that raise survival rates of fish passing through. Because the propeller blades are rotated on high-pressure hydraulic oil bearings, a critical element of Kaplan

design is to maintain a positive seal to prevent the emission of oil into the waterway. Discharge of oil into rivers is not desirable because of the waste of resources and resulting ecological damage.

Figure 1-11: Photograph of a Kaplan turbine runner[30]

1.3.3 Low-Head Hydro turbines

Head is the change in water levels between the hydro intake and the hydro discharge point. It is a vertical height measured in meters. Figure 1-12 shows how the head would be measured on a typical 'low head' and a typical 'high head' site. The more head you have the higher the water pressure across the hydro turbine and the more power it will generate. Higher heads are not only better because they generate more power, but also because the higher water pressure means you can force a higher flow rate through a smaller turbine, and because turbine cost is closely related to physical size, higher-head turbines often cost less than their low-head cousins even though they might generate the same power [31].

Though there is no definite line of demarcation for low, medium, and high heads but the head below 30 meters is considered low head, the head above 30 meters and below 300 meters is considered as medium head and above 300 meters is considered as a high head. A typical low head installation on a river consists essentially of a dam across the stream to back up the river and create

a fall, the water flowing through the turbines and remerging the river below the dam. A dam or barrage constructed across the river creates the necessary head. The power plant is located near the dam and therefore, no surge tank is required. Either one half of the barrage has regulating gates for the discharge of surplus water while the plant is in front of the second half or the plant is constructed by the side of the river [32].

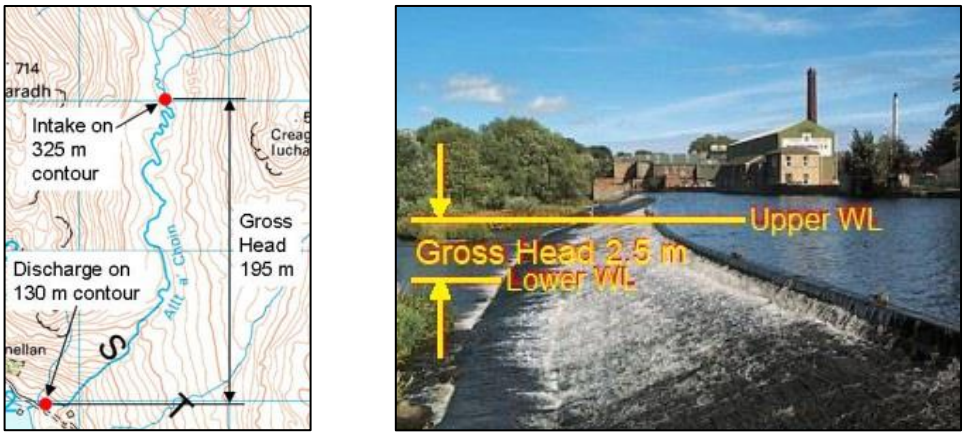

(a) (b)

Figure 1-12: (a) Diagram of measuring head at high head hydropower site (b) Diagram of measuring head at low head hydropower site

In low head power plants, Francis, propeller or Kaplan turbines are employed. Since for given output, a large quantity of water is required, the head is low, therefore pipes of large diameter and short length are required in low head plants. The structure of such plants is extensive and expensive. Generators employed in such plants are of low speed and large diameter.

Low-head hydropower generation with very low discharge using water wheels or other devices which do not require reservoirs or dams across rivers have the advantage that they cause slight or no impact on the environment. They are termed as free-flow turbines and, using small scale power generators, do not require costly high-voltage transmission lines. They are an uninterrupted source of energy. This characteristic is of significance as a renewable energy source and cannot be replaced by other renewables like wind or solar energy.

1.3.4 Micro & Pico Hydro turbines

Besides the previous classifications, hydroelectric power plants can be classified based on the installed capacity of power generation, as large, medium, small, mini, micro, and pico hydropower plants (see Table 1-3). Generally, mini, micro, and pico hydro come under the subcategory of small hydro plants.

Table 1-3: Classification of hydropower based on the power generation capacity

Hydro Power	Capacity	Description
Large-hydro	> 100 MW	Usually feeding a large electricity grid
Medium-hydro	15 – 100 MW	Usually feeding a grid
Small-hydro	1 – 15 MW	Usually feeding into a grid
Mini-hydro	100 kW – 1 MW	Stand-alone scheme
Micro-hydro	5 kW – 100 kW	Provide power for small community or rural industry in remote area
Pico-hydro	< 5 kW	Require only small capacity

Apart from the above classification, there is also a class of very large hydropower plants coming up with capacity ranging from more than 5,000 MW up to 10,000 MW due to the large-scale investment and better technology available. However, as far as small hydro is concerned the upper and lower limit varies from country to country while defining the small hydro. There is a general tendency all over the world to define small hydro by power output. Different countries are following different norms keeping the upper limit ranging from 5 to 50 MW [33].

Hydroelectric plants in the United States are predominantly private (69%); however, 75% of the capacity is owned by federal and nonfederal public owners, primarily from large power plants. The percentage of low and small hydropower plants in terms of numbers is 86%. This indicates future expansion for hydroelectric power in the United States will be from distributed generation [34].

Micro-hydro is a type of hydroelectric power that typically produces from 5 kW to 100 kW of electricity using the natural flow of water. Installations below 5 kW are called pico-hydro [35]. These installations can provide power to an isolated home or small community, or are sometimes connected to electric power networks, particularly where net metering is offered. There are many of these installations around the world, particularly in developing nations, as they can provide an economical source of energy without the purchase of fuel [36]. Micro-hydro systems complement solar PV power systems because in many areas, water flow, and thus available hydropower, is highest in the winter when solar energy is at a minimum. Inexpensive micro-turbines on the Kaplan turbine model are manufactured for individual power production designed for 3 m of head which can work with as little as 0.3 m of head at a highly reduced performance provided sufficient water flow [37].

The advantages of micro-hydro are the following [38]:

1) Efficient energy source. A small amount of flow (0.5 L/min) with a head of 1 m generates electricity with micro-hydro. Power can be delivered up to 1.5 km.
2) Reliable. Hydro produces a continuous supply of electrical energy in comparison with other small-scale renewable technologies. Also, backup, whether diesel or batteries (which causes operation and maintenance and cost problems), is not needed.
3) No reservoir required. The water passing through the generator is directed back into the stream with relatively little impact on the surrounding ecology.
4) It is a cost-effective energy solution for remote locations.
5) Power for developing countries. Besides providing power, developing countries can manufacture and implement the technology.

The disadvantages or problems are as follows:

1) Suitable site characteristics are required, including distance from the power source to the load and stream size (flow rate, output, and head).
2) Energy expansion may not be possible.
3) There is low power in the summer months. In many locations, the stream size will fluctuate seasonally.
4) Environmental impact is minimal; however, environmental effects must be considered before construction begins.

1.3.5 Generators of Hydro turbines

The turbine in a hydropower plant is connected directly to a generator to produce electricity, as shown in Figure 1-13. Generators for large hydropower turbines are normally synchronized to a grid at 50 Hz or 60 Hz, and this controls the speed at which both the turbine and generator must rotate. The turbine speed will vary with the turbine type. For a Pelton turbine -for example- the typical rotational speed is 400-1000 rpm. Francis turbines typically rotate between 100 rpm and 1500 rpm. Propeller turbines, meanwhile, run at speeds between 60 rpm and 300 rpm. In each case, the generator must be tailored to suit the turbine speed [39].

A synchronous generator cannot operate at any speed but instead must turn at one of a number of fixed speeds. The flexibility of generator rotational speed is achieved by varying the number of poles. The smaller the number of poles, the higher the rotational speed needed to achieve a given synchronization frequency. For 50 Hz operation, a two-pole generator must rotate at 3000 rpm, while a 60 Hz machine must operate at 3600 rpm. For eight-pole generators, the necessary speeds would be 750 rpm and 900 rpm. Therefore, generators for slow-speed turbines require a large number of poles [29].

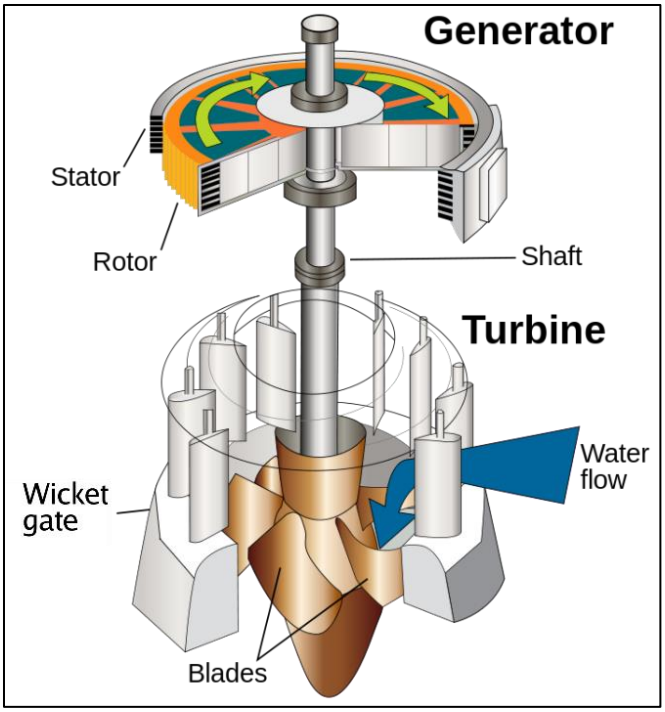

Figure 1-13: Propeller turbine connected to an electric generator through a shaft[40]

For micro-hydro turbines, both synchronous and induction generators can be used. Synchronous generators have always used to produce electricity if no grid supply is available. However, since these machines do not last long in continuous operation, especially when belt driven by a water turbine with rotational speeds higher than its normal operating speeds. Also, synchronous generators are hard to maintain and expensive, so the use of induction motors is another scheme for micro-hydro turbine setups. In general, induction generators (IGs) are more common in the industry, these generators are also called IMAGs (Induction Motors as Generators). In the past, a constant load needs to be maintained all the time as there was no control system available at that time. Recently, with the availability of a low-cost induction generator controller (IGC), a variety of loads can be connected and discounted to the setup [41].

1.4 Rim-driven Propellers (RDP)

A recent design of shaft-less rim-driven propeller (RDP) for ships and submarines, as shown in Figure 1-14, showed some advantages over the traditional designs with the shaft by reducing the vibration and noise, providing a more compact design with less weight, and more flexibility in installations [42]. Also, RDPs configuration can be more cost-effective than the traditional design since fewer components are required. Such technology has reduced the spatial requirements for installation as well as the maintenance needed to operate the system. Moreover, the hubless RDP demonstrated higher efficiencies than the hub one [43][44].

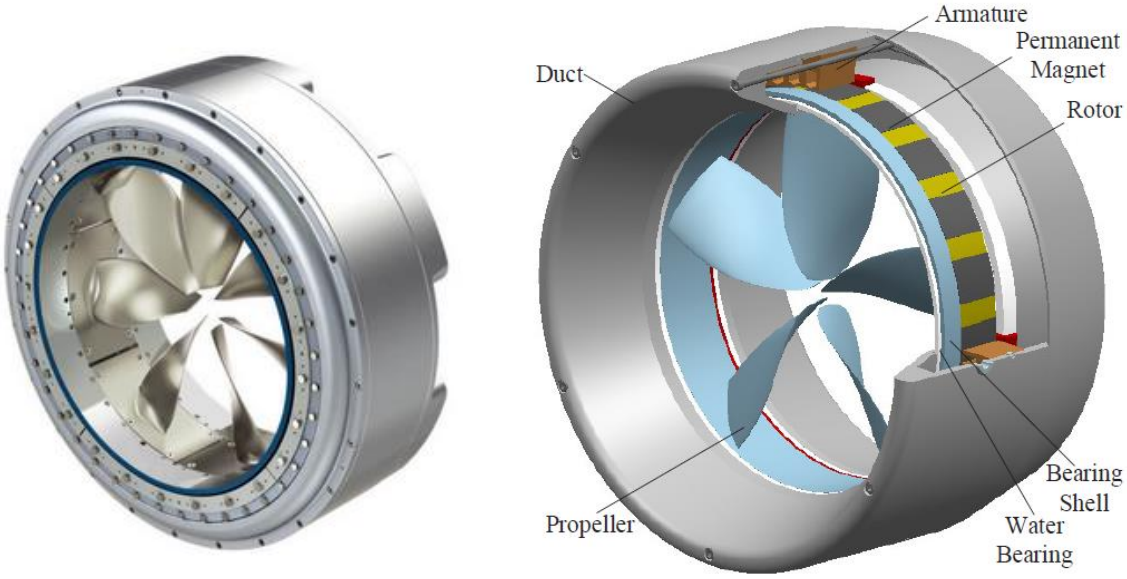

(a) (b)

Figure 1-14: Rim-driven -shaftless- propeller (RDP) for ships and submarines (a) CAD model (b) Structure of the RDP

1.5 Problem Statement

Renewable energy plays a significant role in new power generation worldwide and hydropower is contributing to 86% of renewable electricity production within all other renewable energy resources [12]. Simultaneously, hydropower shares 83% of U.S. renewable energy capacity and accounts for 77% of actual renewable electricity generation. However, most of the installed hydropower consists of large plants. Much potential hydro generation remains untapped, particularly at lower power and head levels [14]. There is a substantial opportunity worldwide and across the U.S. in specific (see Figure 1-15) to add new hydropower generating capabilities at low-head sites such as non-powered dams, canals, and conduits with a water height of less than 30 meters, especially, where the potential of solar and wind is not available (see Figure 1-16) [45]. As stated in the U.S. Department of Energy's report [46], there is an estimated potential hydropower capacity of 12,000 MW of the existed 80,000 unpowered dams with at least 3 feet of water head available.

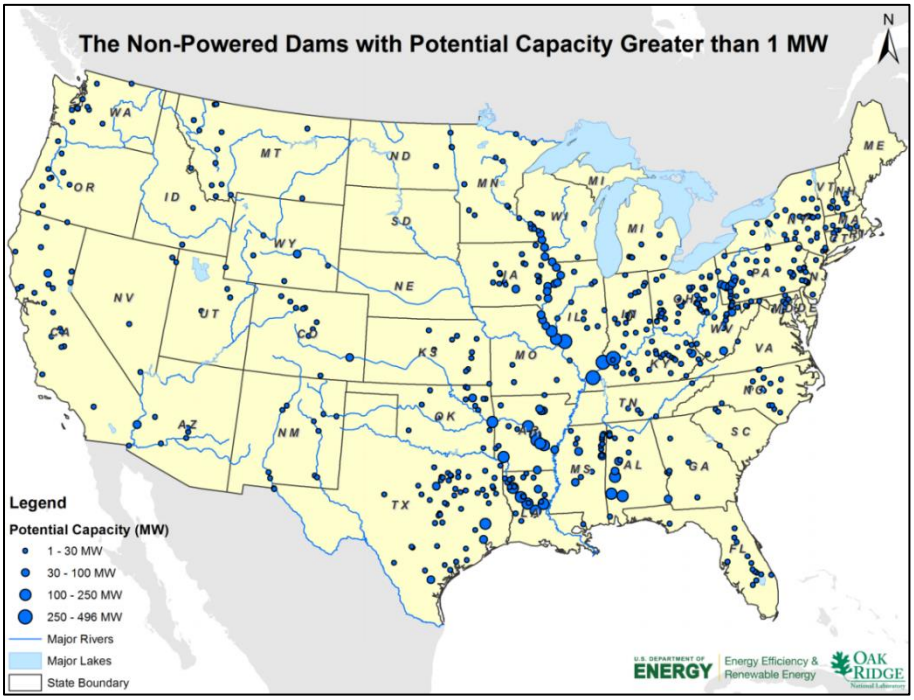

Figure 1-15: The Non-Powered Dams with Potential Capacity greater than 1 MW[47]

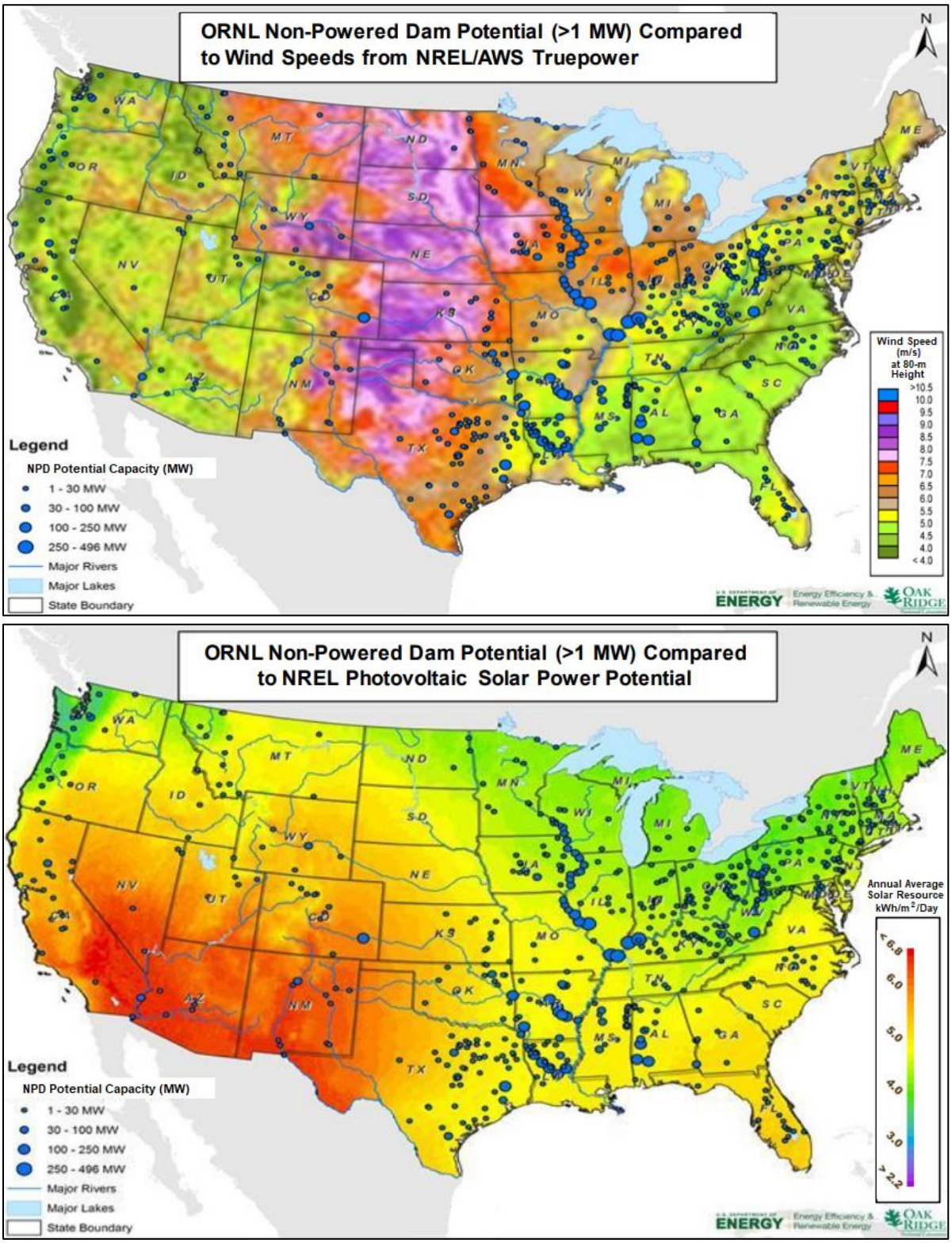

Figure 1-16: Comparison of top NPD sites with potential capacities greater than 1 MW with maps of wind and solar photovoltaic resource potential[47]

In this research, investigation of power-efficient micro and pico Kaplan hydro turbines at very-low-head with rim-driven generators to be studied and evaluated, specifically, at heads of less than 3 meters (10 ft). Optimization of performance and design for a 3D printed conventional -with shaft- 7.6 cm (3-inch) Kaplan turbine to be carried out based on an experimental setup in the Hydro Turbines Laboratory of the University of Wisconsin-Milwaukee in addition to the utilization of Computational Fluid Dynamics (CFD). Then a shaftless (hubless) rim-driven generator-based turbine to be introduced and optimized. Such a new hydro turbine perception will increase the efficiency (of power generation) of hydro turbines in general, and the efficiency of low-head turbines in specific.

The study will follow these main points:

- Design optimization for 7.6 cm (3-inch) and 90 cm (35-inch) conventional Kaplan hydro turbines at specific boundary conditions of 2.6 m (8.5 ft) maximum water head.
- The design optimization includes; the number of the blades for the turbine's rotor (runner) and stator, the blade wrap-angle of the rotor, intake and draft tubes angles, lengths and shapes, and the guide vanes.
- Evaluate the performance (power output and efficiency) of the conventional turbine by utilizing CFD and by testing a 3D printed model of the turbine in a custom-built experimental setup.
- Evaluate the turbine at different water heads (from 2.0 m to 2.6 m) and different rotational speeds (0 – 4000 rpm).
- The CFD setup is based on 3D transient turbulent featuring Large Eddy Simulation (LES) model, and STAR-CCM+ is the CFD software. In addition, the high-performance computing (HPC) cluster of the University of Wisconsin-Milwaukee is used for solving the complex CFD simulations.
- Introduce the rim-driven shaftless (Hubless) turbine (RDT) at the same boundary conditions to evaluate the advantage of the RDT over the conventional turbines.
- Introduce some applications of the rim-driven turbines (RDT), i.e. wastewater treatment plants (WWTPs), where very-low head and high flow of water are available.

Chapter 2: Literature Review

In this chapter, a comprehensive review of previous studies on different aspects of hydropower, i.e. operation, components, economic, parameters, conditions, and optimization methods and hydro turbines optimization studies including small, micro, and pico sizes is presented.

2.1 Hydropower Systems

Barros [48] examined the functionality of a reservoir system with several design parameters such as water flow, energy production, and time interval of the flow by using linear and non-linear optimization techniques. Finardi et al. [49] presented a mathematical model for hydropower plant scheduling. In the model, the electro-mechanical losses in the turbine and the generator were studied and optimized by the lagrangian relaxation method. The results show that the non-linear method is most proper for the actual operation time. Babel et al. [50] investigated the flow duration curve and range of variability method for advancing the efficiency of the power generation. The outcomes show that by using flow duration curve, the power generation can be improved by eight percent as compared with the rule curve-based operation. Power generation can also be enhanced while preserving the environmental flow needs for downstream ecosystems. Labadie [51] concluded the operation of the reservoir system to reduce the cost and improve the efficiency of the plant by using several optimization methods and identified that the genetic algorithm is more convergent as compared to others' optimization methods. Kishor et al. [52] developed the hydropower plant model as a linear or non-linear model and widely classified the research based on hydro plant model development and its controller design. A summary of earlier research work conducted on hydropower systems is presented in Table 2-1.

Table 2-1: Summary of research work on hydropower systems

Author	Components	Parameters	Optimization Technique	Remarks
Barros [48]	Storage hydropower system	Inflow, energy production	Nonlinear, linear and successive linear programming,	Nonlinear programming is found most suitable for real-time operation
Finardi et al. [49]	Hydro unit commitment and loading problem	Head, efficiency, discharge, global loss, mechanical and electrical losses	Lagrangian relaxation, Inexact Augmented Lagrangian	New mathematical model developed including mechanical and electrical losses in the turbine-generator
Babel et al. [50]	Hydropower system	Flow, installed capacity, storage capacity	Flow Duration Curve (FDC) method, and the Range of Variability Approach (RVA)	Reservoir operation considering environmental condition of the river to increase power generation.
Labadie [51]	Multi-reservoir operation review	Efficiency, survivability, sustainability, inflow	Heuristic programming, genetic algorithm, stochastic optimization	Study for improving efficiency and Reducing cost
Kishor et al. [52]	Hydropower plant models	Review paper	Linear and nonlinear models	Broadly categorized the research based on hydro plant model development and its controller design.
Goor et al. [53]	Multi-purpose reservoir Operation	Head, discharge, power	Stochastic dual dynamic programming	More accurate method for optimizing the net production rate and also can be considered when hydraulic head effect is negligible
Ngo et al. [54]	Operation of reservoir	Reservoir level, water level,	MIKE 11 simulation model	Reduces Downstream flood peaks and maintains a high reservoir level for increasing the hydropower production in the flood as well as in the dry season.
Pérez-Díaz et al. [55]	Hydropower plant	Head, scheduling, discharge	Dynamic programming	Obtained scheduling by head and discharge variation to produce maximum power
Connolly et al. [56]	Pumped storage	Time duration to start/stop the turbine	Optimal (24 Historical, 24 Prognostic, and 24 Optimal)	Maximum energy storage to sale in the market for maximizing the profit.
Mahmoud et al. [57]	Cascaded reservoir based hydropower plants	Nonlinear flow rates, and nonlinear dynamical hydraulic heads and gate opening	Dynamic programming, SIMULINK	New dynamical model developed for a cascaded hydropower plant. The head loss due to friction is found key factor in the plant's efficiency.
Chang et al. [58]	Hydropower system	Load, volume of reservoir, flow	Differential dynamic programming	Algorithm developed for better operation of the high head small-tail reservoir plant system.
Soares et al. [59]	Operation of reservoirs	Water head, discount rate, inflow seasonality and system design	Stochastic programming	Operation of reservoir with single as well as cascade system for optimal use of water with high level of head
Naresh et al. [60]	Hydropower system	Discharge, head, reservoir level	Artificial neural network (ANN)	Optimization of interconnected hydropower system.
Shawwash et al. [61]	Hydropower system	Rivers, tributaries, Reservoirs, powerhouses and additional hydraulic facilities such as intake structures, spillway gates and weirs.	Linear programming	Determined the optimal hourly generation and trading schedules in a competitive power market
Birger et al. [62]	Hydropower system	Price forecasting, price node on time interval	Stochastic dual dynamic optimization, Stochastic dual optimization	Discussed about the operation as well as price model for hydropower system

Table 2-1: Summary of research work on hydropower systems (Cont'd)

Author	Components	Parameters	Optimization Technique	Remarks
Cheng et al. [63]	Hydropower reservoir operation	Head, discharge, reservoir level and operating hours	Hybrid genetic algorithm and chaos	Improved convergence speed and solution accuracy in the dynamic programming
Xu et al. [64]	Multi-reservoir system	Storage volume, outflow limit, head, load	Dynamic feasible region genetic algorithm (GA)	Modified GA Improved the refinement of the solution in a more efficient and robust way
Bastos et al. [65]	Hydropower plant	Efficiency, flow, pressure, power	On-offline approach	Used an on-offline optimization procedure for hydro generation in modern power plants
Grygier et al. [66]	Hydropower system	Reservoir inflow, time interval to inflow	Successive linear programming, an optimal control algorithm, and a combination of linear programming and dynamic programming	Successive linear programming, an optimal control algorithm, and a combination of linear programming and dynamic programming (lp-dp) employed to optimize the operation of Multi-reservoir hydro systems for deterministic inflow forecasting
Marino et al. [67]	Reservoir operation	Flow, time of flow, storage level	Dynamic programming (DP)	Increased the size of the DP which requires more core storage. It has been found that the addition of more reservoirs will not affect the DP
Sharif et al. [68]	Multi reservoir system	Storage in reservoir, water level, release of water from reservoir	Genetic Algorithm	A generic genetic Algorithm model developed for the optimization of reservoir systems that can be easily used to any reservoir system.
Jalali et al. [69]	Reservoir system	Water level. Time required to flow	Ant colony method	Ant colony system global-best algorithm provided better and more comparable results with known global optimum results
Ahmed et al. [70]	Multipurpose reservoir	Flow of water	Genetic algorithm, stochastic dynamic programming	GA-derived policies were found promising and competitive. These can be effectively used for reservoir operation.
Jalali et al. [71]	Multi reservoir	Number of reservoirs, number of releases interval, storage	Multi-colony ant algorithm	Multi-colony algorithm is proposed to generate a non-homogeneous and more or less random mesh in entire search space to minimize the possibility of losing global optimum domain
Howard [72]	Hydroelectric system	Head, discharge, planning of operation	Decision support systems	The purpose of hydroelectric system optimization is found to maximize the value of water resources by providing rapid and informative recommendations based on current data and dynamic forecasts of hydrology, energy prices and loads at individual hydro plants within the overall system.
Duckstein et al. [73]	River basin system	Head, discharge, demand, water quality, water level	Multi-objective Optimization	Decision making is found a dynamic process: complex, redundant with feedback and sideways, full of search, detours, information gathering and information ignoring, fueled by fluctuating uncertainty, fuzziness and conflict; it is an organic unity of both pre-decision and post-decision stages of the overlapping regions of partial decisions
Stedinger et al. [74]	Reservoir system	Inflow forecasting, time of inflow, hydrologic state variable	Stochastic dynamic programming	Stochastic dynamic programming derived stationary policies by using the previous period's inflow as a hydrologic state variable. It was found that both stationary and non-stationary SDP models can identify better reservoir operating policies if better hydrologic state variables are employed

Table 2-1: Summary of research work on hydropower systems (Cont'd)

Author	Components	Parameters	Optimization Technique	Remarks
Archibald et al. [75]	Multi-reservoir system	Head, discharge, time of flow, reservoir classes, number of reservoirs	Stochastic dynamic programming	A new method of determining an operating policy for multi-reservoir developed with problems of variable head which reduces the original problem to a series of independent, low dimensional sub problem.
Oliveira et al. [76]	Multi-reservoir system	Probability of spillage, the evaporation losses impacts on water flows and storage volumes	Genetic search algorithm	The genetic algorithms used real-valued vectors containing information needed to define both system release and individual reservoir storage volume targets as functions of total storage in each of multiple within-year period
Mishra et al. [77]	Hydropower plant	Head, discharge, area, length, velocity, friction factor, diameter, thickness	MATLAB/Simulink program	Turbine penstock model has been analyzed to study the effect of water hammer. Also, an attempt has been made to analyze the effect of length, diameter and thickness of the penstock on water hammer.
Jacoby et al. [78]	River basin system	Stream flow, time interval, river basin class	Dynamic programming	Investigated the use of analytical optimization models to 'screen' the set of possible plans and to select a small number worthy of simulation analysis
Ahmadi et al. [79]	Hydro and thermal units	Thermal unit parameters: Fuel cost, valve cost, capacity limits, ramp down limit (RDL), ramp up limit (RUL), fuel limitations, time-varying startup cost, minimum up time and down time. Hydro unit parameters: volume and multi-performance linear curves, power discharge curves, discharge limits, initial and final volume, water balance and operating services.	Multi-objective optimization, Mixed integer programming	Investigated energy generation maximization and reduced thermal emissions. A linearized valve loading effect model developed to facilitate the computation.

2.2 Small Hydropower Systems

Duckstein et al. [80] discussed multi-criterion decision-making techniques to reduce the effect of social and environmental impact of hydropower operation and development. Environmental, ecological, and social consequences of operation and design of small power plants can use multi-criterion decision-making models to reduce the effects of these problems. The results of these studies stated that the plant owner increased the minimum stream flow to protect the ecological values. Garrido et al. [81] developed a new simulation tool for run of river small hydropower plants

by changing its configuration parameters and achieved a good correlation between the developed model and the real data model. Anagnostopoulos [82] highlighted the optimal design of run of river small hydropower plants having the different types of turbines and showed the optimal design of schemes for the best cost benefits of the plant. Aslan et al. [83] discussed the case study where three turbines were installed to utilize the higher flow rates as the best configuration by using dynamic and sensitive analysis programming. Williamson et al. [84] developed a model to select the most suitable turbine configuration for a low-head hydropower plant by using quantitative and qualitative analyses. The individual weighted scores were compared with the perceived relative importance of each of the criteria to select a turbine based on the total weighted score. A summary of earlier research work conducted on small hydropower systems is presented in Table 2-2.

Table 2-2: Summary of research work on small hydropower systems

Author	Components	Parameters	Optimization Technique	Remarks
Duckstein et al. [80]	SHP plant case study	Discharge, economics, environmental	MCDM by Monte Carlo simulation	Environmental, ecological, and social consequences of design and operation of power plants can use MCDM models to reduce conflicts.
Garrido et al. [81]	Run of river hydro plant	Reservoir level, water flows, turbine efficiencies, specific number of turbines and spillway gates	Object-oriented modeling	Found good agreement between the developed tool and the real data. This model can be used to simulate different plants with run-of-river scheme by changing its configuration and parameters.
Anagnostopoulos [82]	Run of river hydro plant	Head, diameter and length of penstock	Stochastic evolutionary algorithm	Used two schemes having different types of turbines for the optimal design and cost benefits
Aslan et al. [83]	Sensitivity analysis for the design of small hydropower plant case study	Turbine type and size decided for SHP plant	Dynamic programming and sensitive analysis	Found best configuration of turbines to utilize the higher flow rates
Williamson et al. [84]	Low head hydro plant	Turbine type, head, discharge, shaft speed	Quantitative and qualitative analyses	Analyzed method to select most appropriate turbine architecture for a low-head pico hydro scheme using quantitative and qualitative analyses.
Singal et al. [85]	Low head run-of-river small hydropower	Head and capacity	Regression method	cost of projects determined based on developed correlations and validated with the cost of recently developed projects
Haddad et al. [86]	Run of river power plants	Turbine types, number of turbines, penstock diameter, as well as scheduling the operation of an RoR power plant	Honey bee mating optimization, Lagrange multipliers	Compared with those of an analytical approach using Lagrange multipliers highlighting the advantages in design, effective operation, ease of application and capability of the proposed HBMO algorithm for solving such complex problems

Table 2-2: Summary of research work on small hydropower systems (Cont'd)

Author	Components	Parameters	Optimization Technique	Remarks
Najmi et al. [87]	Run of River Plant	Discharge design, penstock or tunnel diameter, turbine capacity, number of units and type of turbine	Lagrange optimization	Carried out optimization based on cost effectiveness
Basso et al. [88]	Run of River Plant	Stream flow variability, energy price, costs	Dynamic programming	Energy production and the economic profitability of small run of river power plant based on the underlying stream flow regime
Borges [89]	Small hydropower	uncertainties of rivers inflow and generation units' operation	Stochastic Dynamic Programming	Worked for generation availability and reliability studies of SHP plants to model the energy availability associated with the river inflow variation together with the generation unit availability
Karami et al. [90]	Hydro thermal security constrained generation scheduling	Thermal and hydro unit parameters	Mixed integer programming approach	Aimed to provide reliable information to the ISOs for daily scheduling based on linearized formulations.
Ghadikolaei et al. [91]	Hydro and wind units	Risk constrained scheduling models considering uncertainty and intermittency.	Roulette wheel mechanism is employed for random market price scenario generation. Autoregressive integrated moving average (ARIMA) model employed to characterize the stochastic wind farm generation. Mixed integer stochastic framework for scheduling.	Developed a practical methodology of risk measurement and management model for hybrid wind/hydro generation scheduling that allows generating companies (GENCO) to manage the risk of wind generation and market price uncertainties
Ahmadi et al. [92]	Hydropower generation units	Hydro unit constraints, scenario generation and reduction.	Stochastic self-scheduling and mixed integer programming employed	Refers to the linear nature of the formulations and real size power systems. Results showed a rationale solution time.

2.3 Micro and Pico Hydro turbines

Yadav [93], with his noble and native concept tried to increase the efficiency of the turbine with the modification in the blade and with some auxiliary attachments, which will lead to less wastage of the head and result in better efficiency. Williams [94] utilized a centrifugal pump integrated with an induction motor as a combination of turbine and generator for micro hydropower plants. The unit was found to be a cost effective and a suitable alternative to cross flow turbines for power output up to 5 kW in industrialized and developing countries. Huang et al.

[95] analyzed experimentally a novel three-bladed vertical axis 3 kW micro-hydro turbine. The turbine system used a three-phase permanent magnet symmetric generator that converts mechanical energy into electrical energy. The experimental results showed that the speed ranges of the water flow are narrower than those of wind, and the status transformation from cut-into stable power generation was short. The study also showed that the efficiency of the turbine was constrained by stream flow speed and crossover section area.

The performance, operation and economic analysis of low head turbines for micro hydel power applications were reviewed by Elbatran et al. [96]. They analyzed the effectiveness features of various types of turbines as well as the significant factors that affect their operation and performance. The authors also provided a guideline for selecting the most suitable turbine for use in different low head and micro-hydropower plants. Židonis et al. [97] highlighted the recent developments in the design of Pelton and Turgo impulse turbines and opportunities for future development. The study proved that a significant increase had been made in the computational fluid dynamics for the development of Pelton and Turgo turbines. The study also proved that the simulation results of Pelton turbine simulations were found to match the experimental results, and detailed analysis is required for achieving the same in a Turgo turbine.

An experimental investigation of design parameters for pico hydro Turgo turbine using response surface methodology was done by Gaiser et al. [98]. The design parameters such as nozzle diameter, jet inlet angle, number of blades, and blade speed were used in a three-level central composite response surface experiment. A low-cost Turgo turbine was tested and a second-order regression model was developed to predict its efficiency. The effects of blade orientation angle and jet impact location on efficiency were also investigated. Khan et al. [99] analyzed a micro-hydro turbine to recover flow conditions for optimum power generation. Turbine geometry

modeling was done using computational fluid dynamics (CFD). CFD analysis of the turbine geometry with different configurations of debris protectors was carried out to evaluate the optimal recovery of flow properties for maximum electricity generation. A summary of earlier research work conducted on micro and pico hydro turbines is presented in Table 2-3.

Table 2-3: Summary of research work on micro and pico hydro turbines

No.	Author	Turbine	Net Head (m)	Discharge (l/s)	Output (kW)	Efficiency (%)
1	Bozorgi et al. [100]	Axial Pump as Turbine	4	200	6	61
2	Date et al. [101]	Reaction Turbine	1.45	30	0.28	65–70
3	Motwania et al. [102]	Single Stage Centrifugal Pump Turbine	15	25	3	60
4	Alexander et al. [103]	Propeller Turbine	4–9	–	20	68
5	Derakhshan and Nourbakhsh [104]	Pump as Turbine	25	150	30	–
6	Sinagra et al. [105]	Cross Flow Turbine	–	820	–	89
7	Ikeda [106]	Nano Hydraulic Turbine	1.2	1–3	0.1–0.2	20
8	Yassi and Hashemloo [107]	Axial (Kaplan) Turbine	24	117	–	85
9	Mishra et al. [108]	Cross Flow Turbine	8.5–10	10–70	–	55
10	Andrade et al. [109]	Cross Flow Turbine	35	135	–	70
11	Pereira and Borges [110]	Cross Flow Turbine	5.5	100	3.5	85
12	Khan and Badshah [111]	Cross Flow Turbine	6	175	6.2	60
13	Girma and Dribssa [112]	Cross Flow Turbine	3	420	2.5	83
14	Acharya et al. [113]	Cross Flow Turbine	10	100	7.3	77
15	Bryan and Kendra [114]	Pelton and Turgo Turbine	13–28	–	<5	80
16	Date et al. [115]	Simple Recation Turbine	1–4	1–8	0.150	50
17	Williamson et al. [116]	Turgo Turbine	1–3.5	10	0.250	87–91
18	Giosio et al. [117]	Pump as Turbine	5.98	133	6.2	79

2.4 Hydro Turbines Optimization Techniques

Bijukchhe [118] conducted a comparison between experimental and CFD results of 8-inch diameter, horizontal Kaplan turbines. The study described the numerical simulation of the prototype turbine at full and partial load and compares the results with experimental values for a range of 6-15 meters (20-50 feet) of the head, flow rates of 200-340 l/s (7-12 CFS) and six different runner rotational speeds in the range of 1333-3350 rpm. Steady-state analysis with backward Euler Scheme and Shear Stress Transport (SST) as a turbulence model was used. The simulations match experimental results best for the optimum point but overpredict for the overload conditions.

Yen et al. [119] presented a study of a 30 cm (12-inch) diameter Kaplan hydro turbine geometry with performance optimization through CFD method based on Large Eddy Simulation (LES) of transient turbulence modeling. The study included a selection of horizontal versus vertical setup, tailwater head test, draft tube length test, draft tube angle test, intake tube geometry test, and blade geometry combination test. All of these geometric parameters were used in the computation, and the results compared based on power output, mass flow rate, and efficiency.

ElGammal et al. [120] focused on the turbine's intake tube design based on numerical investigations to maximize energy extraction. Optimizing the efficiency of a system with less material cost was the primary goal of the study. The results showed the merit of higher slopes per side length in enhancing output power, with an average of 2.7% of the output power by full expansion from minimum to the maximum angle. A bell-mouth profile was also investigated and provided an additional 2.2% increase in turbine efficiency.

A previous study by Abeykoon and Hantsch [121] discussed the design of a Kaplan turbine rotor. The aim was to improve the efficiency of the turbine by optimizing the rotor design. A simplified theoretical study was compared with a computational fluid dynamics (CFD) evaluation to analyze further the points of enhancement, such as number of blades and blades' inlet and outlet angles, where the latter showed the significant development on the turbine's power output. Ujwala et al. [122] presented a study for a low head, lightweight Kaplan turbine, this research aimed to boost the hydraulic efficiency by reducing weight, alternating blade rotating angles (-15^{o} to $+20^{o}$) and number of blades (four to eight blades) using CFD, theoretical calculations were also presented. The optimum operation achieved at zero angle and five blades. Janjua et al. [123] utilized CFD and CAD analysis to optimize the blade profile geometry of a low-head Kaplan turbine. Five blade profiles at different blade angles were developed by implementing the

coordinates point system of CAD software on the blade's geometry. The optimized blade geometry improved the power output by 4.4%.

Another investigation of the design and the velocity distribution of a Kaplan runner blade was conducted by Permana and Rudianto [124] by using CFD for predicting the flow and CAE to verify the design. An airfoil profile from Gottingen (GOE) series was selected for the runner's blade. The point of focus of this study was to define the major characteristics of the turbine with a given head and flow rate. Jost et al. [125] presented a comparison between numerical solutions and experiments for a Kaplan turbine with six blades in order to enhance the CFD efficiency prediction by using advanced turbulence models i.e. shear-stress-transport (SST), scale-adaptive-simulation (SAS) SST, and zonal large-eddy-simulation (ZLES). Both steady-state and transient simulations were performed and compared. However, ZLES with a bounded central differential scheme (BCDS) was the only model suitable at all operating points with less than 1% error in the efficiency.

Nan et al. [126] designed a small hydro-turbine with a constant blockage ratio of the blade using a new blade thickness design with a longer and arc chamfered front hub. The experimental and CFD results showed an enhancement in the efficiency of the turbine by up to 2.9% of the original efficiency depends on the system flow rate, as well as a reduction in the separation area and the vortex after the front blade. Ranjan et al. [127] optimized an efficient design of a cross-flow hydro turbine based on an existing turbine and by using ANSYS FLUENT as CFD tool. The investigation tested different angles for the inlet blade, nozzle entry arc angle, and rotational speed. The optimum design with 20% efficiency improvement compared with the existing turbine, was found with 65^{o} nozzle entry arc angle, 10^{o} inlet blade angle and at 600 rpm rotational speed.

A new method for design a swirler for axial micro-hydro turbines was used by Hoghooghi et al. [128] to replace the existing airfoil-shaped inlet guide vanes. Using a CFD analysis and experimental tests, 12 fixed blades swirler lead to reduce the project cost by 60-70%. According to Yildiz and Vrugt [129], the balance between the capital and operating costs with the energy required from the system leads to the best design for a hydro turbine system. The study found that using two different turbines in size or type in a parallel configuration, enhanced the efficiency and the energy production of the system.

2.5 Conclusion

From the past studies, it can be found that very few studies are available for optimum operation of micro and pico hydropower plants. In earlier studies, the main focus was on the operation of large and small hydropower with a reservoir system as well as a cascade system. These systems mainly discussed the operation of the reservoir as well as the interconnected systems and developed the mathematical model for the optimum operation of a reservoir for power generation. These mathematical models generally considered parameters such as reservoir level, time of release water and flow of the stream. As the literature for micro and pico hydropower plants is limited, further study is required for optimum operation of such plants. Various aspects of plant modeling and optimization discussed in the literature presented which can be helpful in future works on the operation of micro and pico hydropower plants.

With the limited research progress made in the turbines in the published literature, used for micro and pico hydropower applications. The salient feature that can be drawn from this work is that efforts have been made by researchers to enhance the efficiency of the turbine used for micro and pico hydro resources. However, there is a research gap from the viewpoint of the design of turbines that large powered turbines are currently being used for low power generation in

hydropower plants. This research gap presents a great challenge to the researchers as turbines that are designed to cater to these specific needs only would be cost effective and reliable for the implementation in hydropower plants. It is deduced that the need for designing a reliable and cost effective turbines for the installation of a micro and pico hydropower plant is essential due to the scarcity of energy. Thus, more research is needed in the fabrication and development of turbines for micro and pico hydro systems.

Chapter 3: Hydro Turbine System Design Optimization

3.1 Research Outline

This chapter focus is optimizing the design of micro and pico Kaplan turbines at a very-low head for their maximum performance by locating the highest possible power generation efficiency. Numerical and experimental approaches were performed to identify the performance of the turbine as well as compare and validate the results. The numerical approach is performed first, using CFD, to optimize the design of the turbine at a range of rotational speeds (0 - 4000 rpm) and a water head ranging from 2 to 2.6 meters. The experimental setup was built based on CFD optimization and tested to validate the results. CFD simulations were executed using STAR CCM+ [27], a commercial software developed by Siemens. Large Eddy Simulation (LES), Volume of Fluid (VOF), and Wall-Adapting Local-Eddy Vis models were used to solve the unsteady multiphase turbulent flow.

3.2 Optimization of the Turbine's Blades

3.2.1 Introduction

In this study, an optimization process is adopted to maximize the power output of a horizontal Kaplan micro-turbines rotor at a very-low head through utilizing computer-aided engineering (CAE) and computational fluid dynamics (CFD) along with a experimental lab setup for validation. An investigation on the number of the blades, the performance at different rotational speeds, and the blade's wrap angle are also considered. An in-house code was developed and utilized for the optimization process. The code function is to create the baseline CAD design for the turbine at given boundary conditions, and then update and optimize the design according to the feedback of the CFD results of the preliminary and the updated designs, where the optimization

compiler is controlled by pre-defined design parameters with considering the fundamentals of turbomachines.

3.2.2 Methodology

The process of design optimization for hydro turbines is complicated due to the rotor and the stator geometries' complexity. Having several variables in the design optimization process entails an engineering optimization technique called multidisciplinary design optimization (MDO). The MDO method is followed in this research to achieve the optimized design of the turbine.

3.2.2.1 *Multidisciplinary Design Optimization*

Several fields of engineering such as aerospace and automotive extensively considered MDO in their applications, where this technique has paved the way for designers to integrate all connected disciplines simultaneously with time and cost is saved. Aerospace engineering applications (i.e., aircraft and spacecraft) were the leading implementer of MDO. [124], [130]–[133] MDO helps in avoiding complications accompanying with sequential design or partial optimization, providing more effective and vigorous convergence than by simple iteration, and supporting the management of the design procedure [134].

Herein, multiple variables involved in the design optimization process of the turbine's rotor, main hub and blades dimensions, meridional contour, number of blades, number of spans, blade's leading edge and trailing edge angles, and blade wrap angle are some examples of the design variables. In this study, the optimization process will be limited to two variables; number of blades and blade wrap angle. Figure 3-1 shows the optimization algorithm followed for the Kaplan turbine rotor's design.

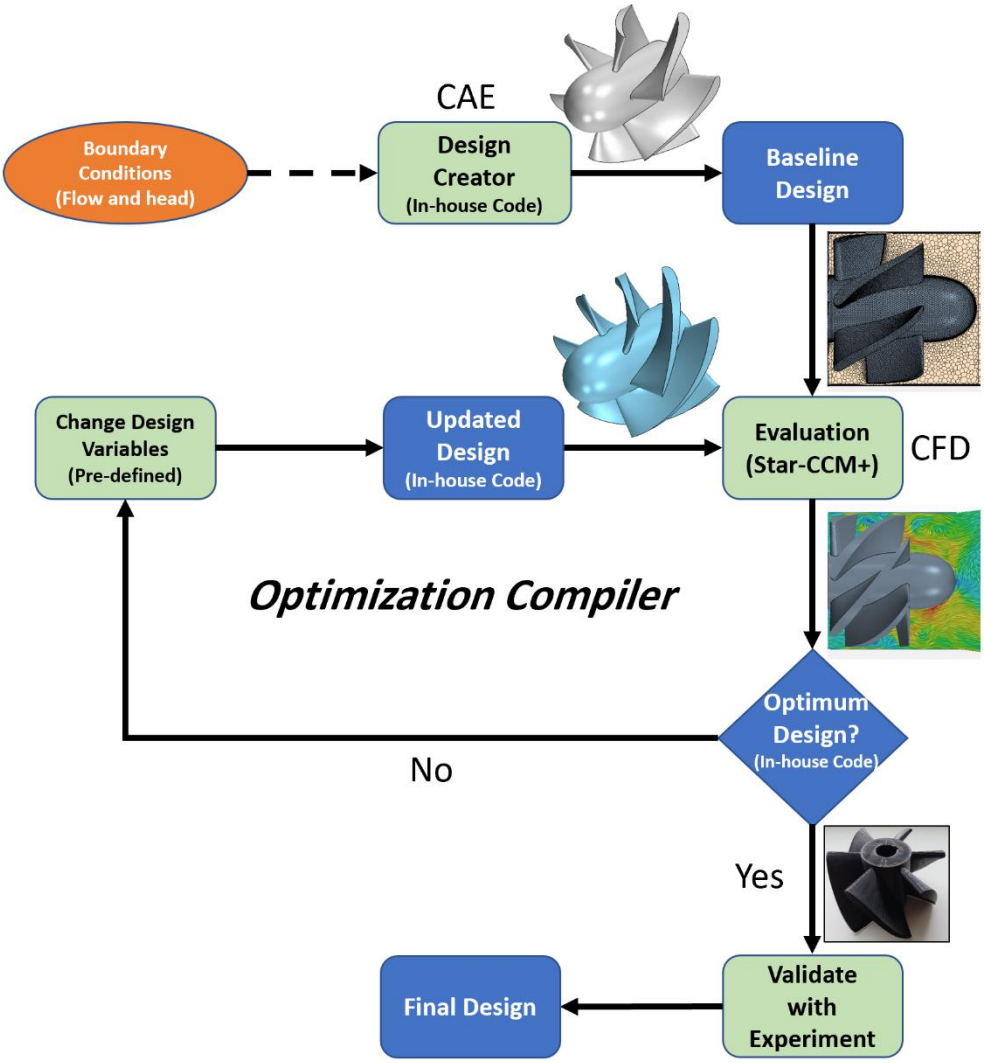

Figure 3-1: Optimization algorithm for the Kaplan rotor's design

3.2.2.2 *Rotor Design with In-house Code*

For given boundary conditions of the system of 2.6 m (8.5 ft) water head and 28 L/s (1.0 CFS) flow rate, a preliminary (baseline) rotor design is created using the in-house code, some parameters of the design are shown in

Table ***3-1***. Figure 3-2 shows the velocity triangles of the inlet and the outlet at the mid-span of the blade. Fixed blades Kaplan turbine is considered for the study to avoid the complexity

in manufacturability, mainly where 3D printed parts are used in this project. The CAD of the baseline design is shown in Figure 3-3.

Table 3-1: Design parameters for the preliminary rotor design

Parameter	Value
Available head (meter)	2.6
Design flow rate (L/s)	28
Minimum flow rate ratio (%)	50
Maximum flow rate ratio (%)	150
Pipe head loss (%)	15
Theoretical power output (W)	230
Rotational speed range (RPM)	500 - 3000
Rotor diameter (cm)	7.6
Number of blades	6
Number of spans	6
Blade angle at leading edge, β_1 (hub to shroud)	30.9^o - 14.3^o
Blade angle at trailing edge, β_2 (hub to shroud)	58.5^o - 16.2^o
Wrap angle, $\Delta\varphi$ (hub to shroud)	80^o - 60^o

The preliminary design is generated to fit the available boundary conditions of the turbine; however, this design might not be the optimum one as some of the design variables depends on the designer's knowledge. Also, some variables have a range of applicable values for the given conditions, which contribute to the development, improvement, and hence optimization of the turbine design.

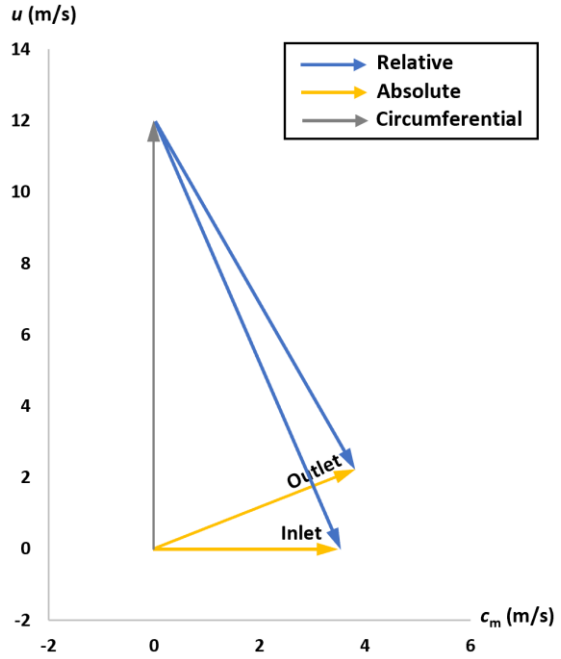

Figure 3-2: Velocity triangles at the mid-span for the inlet and the outlet

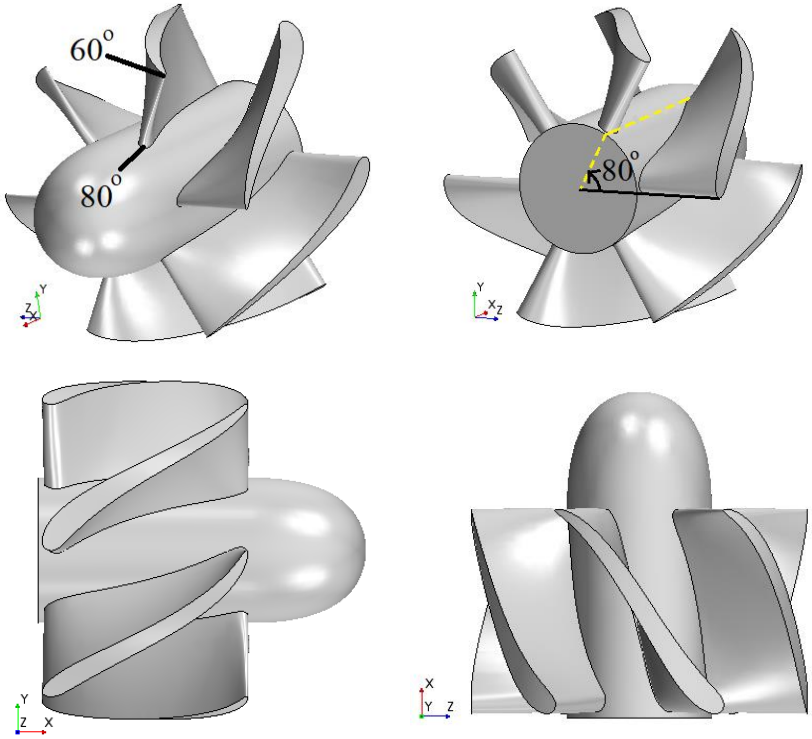

Figure 3-3: CAD for the proposed preliminary rotor design

The first variable selected for the optimization process was the number of the blades. The baseline design is a 6-blade rotor, as shown in Figure 3-3. Three, four, five, and seven blades are

also considered. Evaluation for a matrix of thirty simulations is conducted to locate the maximum power output (in watts) for the five different number of blades rotors at the rotational speed range of 500 – 3,000 RPM for each.

The blade wrap angle ($\Delta\varphi$) is the second variable to exam for further optimization, where the wrap angle is defined as the angle between the leading and trailing edges tangent lines. Also, this angle is recognized by two angles at the trailing edge; starting angle at the hub side and ending angle at the shroud side. In Figure 3-3, for example, the blade wrap angle is 80^o at the hub side of the blade and 60^o at the shroud side of the blade. Thus, the blade wrap angle will be 80^o to 60^o with a linear relation to describe another four angles between the starting and ending angles. The total number of sub-angles for a wrap angle is equal to the number of spans of the blade. Figure 3-4 shows the design details of the baseline rotor; six spans are presented as shown at the suction side of the blade.

Another matrix of 121 simulations is established to evaluate the power output of the rotor at 121 different wrap angles, from 60^o to 110^o, with 5^o increment for both sides (the hub and the shroud).

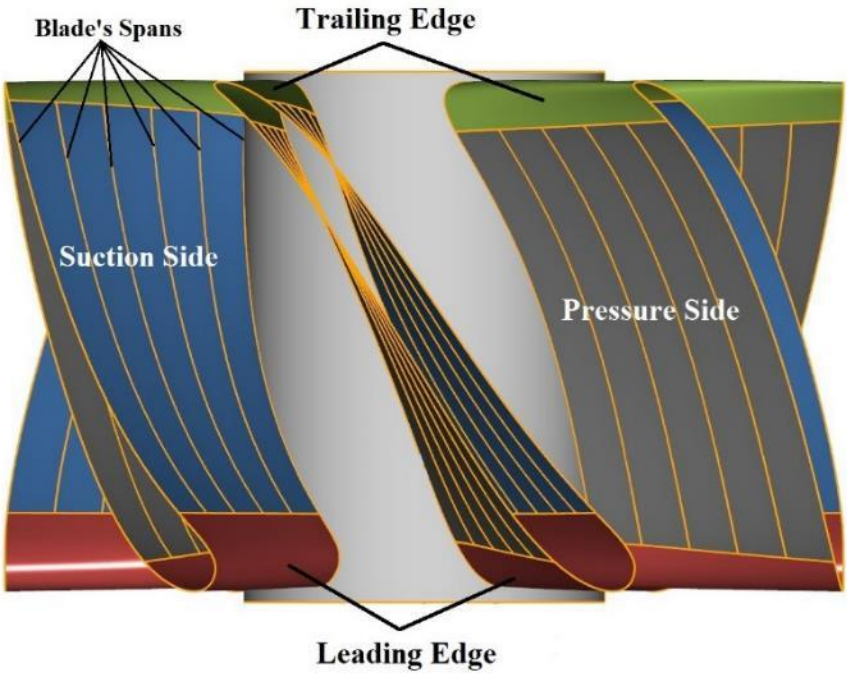

Figure 3-4: Significant design parts of the baseline rotor. Green: Trailing edge. Red: Leading-edge. Blue: Suction side. Dark grey: Pressure side. Light Grey: The hub. Parallel orange lines: Blade's spans

3.2.2.3 *Evaluation of the Rotor Performance by CFD*

Computational Fluid Dynamics is a powerful numerical tool that is used to analyze fluid flow, heat transfer, and mass transfer systems. It is utilized for phase change, multi-phase, and chemical reaction cases to predict the pattern of flow, heat transfer, or mass transfer as well as solving complicated equations numerically. CFD can be employed to a wide range of applications such as turbomachinery, aircraft and vehicle aerodynamics, and metrology, as well as heating, ventilation and air-conditioning of buildings.

CFD has multi advantages over other analytical techniques and experimental approaches. It can be an effective cost and time-saving approach to conduct a new design, investigate some research work, or even for validation purposes. It can study a system that is complicated to perform experimentally and provide different scenarios without building a test rig. There are different commercial software that is capable of executing CFD simulations for various applications.

However, they undergo a similar approach of solving the governing equations and processing the results to a user-friendly interface.

Recently, computational fluid dynamics (CFD) is more common in the R&D units in the industry where satisfying and accurate results for complex problems can be achieved at a lower cost in a timely manner. For such a study with a high number of 3D transient turbulent problems, using CFD with a high-performance computing (HPC) cluster is a necessity. The HPC of the University of Wisconsin-Milwaukee is used with STAR-CCM+ software as the CFD tool.

Hence the numerical problem for turbomachine with a transient-turbulent flow and high swirl, Large Eddy Simulation (LES) model is recommended to solve and model the large and small-scale eddies generated by Navier-Stokes (N-S) equations and by the subgrid-scale (SGS) wall-adapting local-eddy (WALE), respectively [135]. Unsteady Reynolds Average Navier-Stokes (URANS) approach can also be an option. However, LES is more accurate for such a problem despite the fact of being a computationally expensive model [136]–[140].

Table 3-2 presents the physical parameters, conditions, and enabled models for the simulation. As an implicit unsteady simulation model, a time step of 1×10^{-5} seconds (with 20 iterations per the time step) was selected along with the whole solution duration with second-order solution accuracy for temporal discretization. Additionally, the transient rigid body motion was used at the region of the rotor only (see Figure 3-18) to model the periodic interactions of the rotating blades of the rotor with the flow. Although it is time-consuming but more accurate than steady-state approximations.

Table 3-2: Physical parameters, conditions, and enabled models for the simulation

Parameter	Value
Total Head (m)	2.6
Mass flow at the inlet (kg/s)	28
Outlet pressure (kPa)	101.325
Rotor rotational speed (RPM)	500 – 3,000

Timestep (s)	10^{-5}
Number of iterations (per time step)	20
Enabled Models	
Gravity, Rotational motion	
Gradients, Three dimensional	
Turbulent, Segregated Flow	
Implicit Unsteady, Transient	
Large Eddy Simulation (LES), WALE Subgrid Scale	
Multiphase Interaction, Volume of Fluid (VOF)	

Figure 3-5 shows a screenshot of the CFD simulation setup, which mimics the hydro turbine experimental setup at the University of Wisconsin-Milwaukee. A horizontal hydro turbine configuration is presented for this study. The figure indicates the location of the turbine in the system, as well as the inlet and the outlet of the flow.

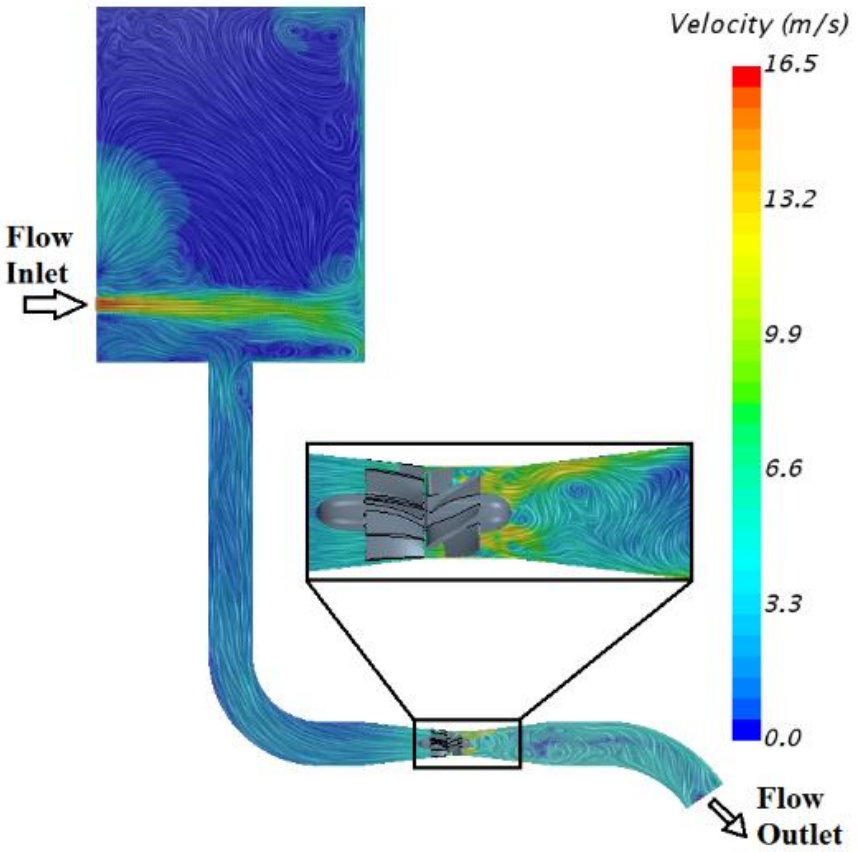

Figure 3-5: The simulation setup for the rotor performance evaluation

3.2.2.4 *Experimental Setup*

Experimentation helps in verifying the numerical computations and can be used as a tool to validate the results obtained from the CFD simulations. It demonstrates the accuracy of the CFD results and can be used to proceed with the simulations with confidence. Additionally, it determines the credibility of the programming and computational results as well as examines the models through comparison with the experimental results.

The experimental setup was developed in the Hydro Turbine lab at the University of Wisconsin-Milwaukee hosting a relatively low-head Kaplan turbine. The system was designed to accommodate a horizontal turbine configuration with an elevated tank, a discharge reservoir, and a circulating pump, as shown in Figure 3-6. The setup is installed on a T-slot table that houses the lower tank providing supports to the hydro turbine system and adjustable configuration. The maximum head that can be achieved through this setup is 2.6m (8.5 ft) and a maximum flow rate of 28 L/s (1.00 CFS). The upper tank has a capacity of 0.60 m^3, Figure 3-7 (a), and the lower reservoir has a capacity of 0.45 m^3. The 10 HP pump circulates the water between the two tanks and is equipped with a Variable Speed Drive (VSD) to control the pump flow rate during testing. The water flowing into the turbine is also controlled through a ball valve installed vertically on the 0.15 m (6 inches) down-pipe as shown in Figure 3-8 (b).

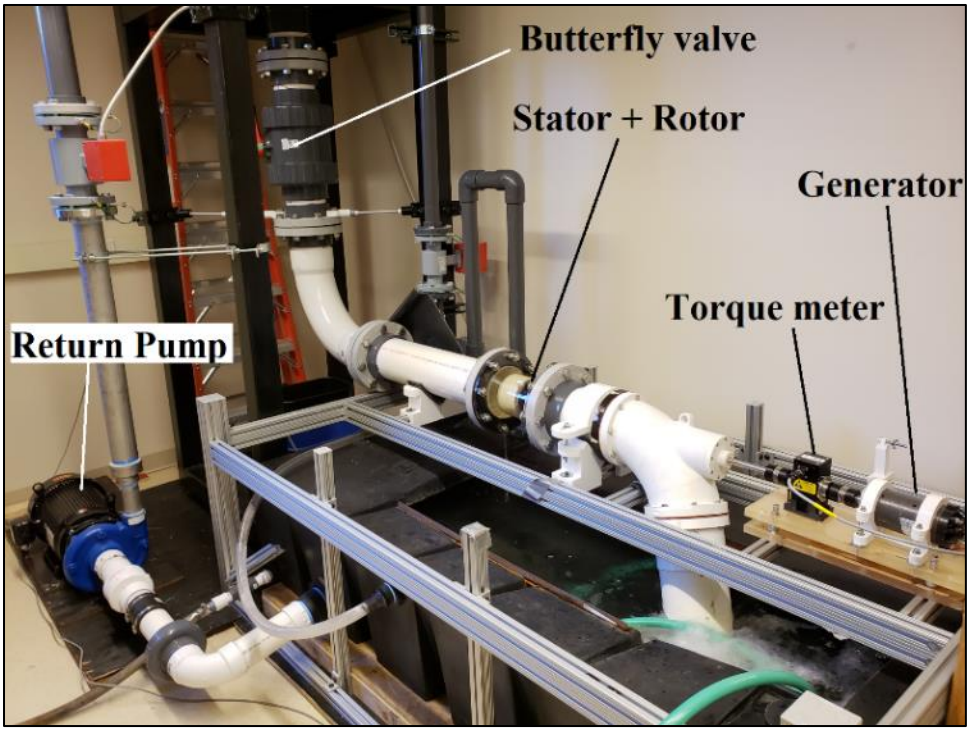

Figure 3-6: Experimental setup of the 7.6 cm turbine's rotor at the UW-Milwaukee's hydro turbines lab

Besides the aforementioned components, the structure has also two flow meters (one before the tank and one in the overflow pipe) and a turbine. The turbine had a transparent housing for observation (see Figure 3-8). The rotor is connected to a 0.016 m (5/8-inch) diameter stainless steel shaft for measurement of speed and torque. As shown in Figure 3-9, the shaft was connected to a torque-meter and a DC generator. Electric power is dissipated in a resistive load bank.

(a) (b)

Figure 3-7: (a) Upper tank (b) Ball valve installed on the down pipe

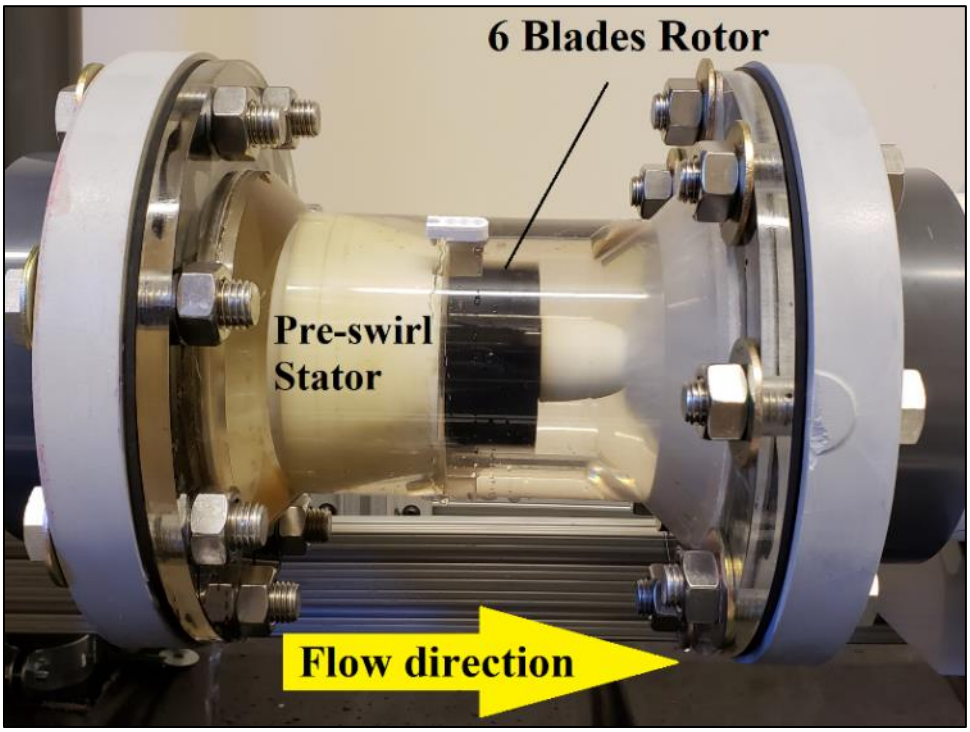

Figure 3-8: Turbine housing includes a 3D printed pre-swirl stator and the 6-blade rotor under operation

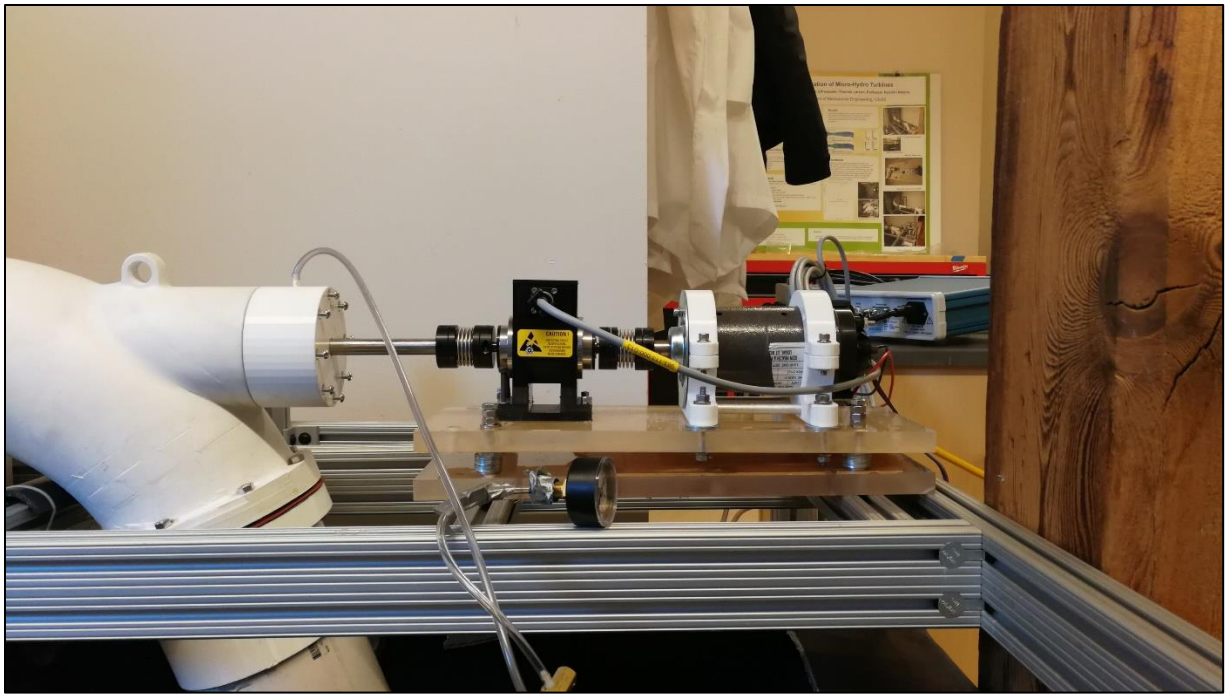

Figure 3-9: Shaft, torque-meter, and motor assembly

The turbine housing is made of clear Acrylic, shown in Figure 3-8, that was cast on the university campus and consisted of three sections:

1- Intake nozzle to convert the pipe diameter from 0.15 m (6”) to 0.076 m (3”)

2- Straight 0.076 m (3”) section hosting the turbine rotor

3- Outlet diffuser changing the diameter back to 0.15 m (6”)

The hydro turbine parts, including the stator and the rotor (runner) were designed and optimized through previous research conducted at the Hydro Turbine lab. These parts along the exit elbow and supports were 3-D printed using Eastman Amphora 3-D Polymer AM3300 commercialized by ColorFabb as nGen [141]. Figure 3-10 shows the 3-D printed 7.6 cm (3-inch) diameter turbine rotor. The parts were designed using a Computer-Aided Design (CAD) modeling software to match with the system configuration and requirements. Ultimaker 2+ [142] was utilized to 3D print the turbine parts and supports used in the experimental setup.

Figure 3-10: The 3D printed 7.6 cm (3-inch) 6-blade rotor for the experimental testing

3.2.2.5 *Instrumentation*

3.2.2.5.1 Ultimaker 2+

Ultimaker 2+ is a 3-D printer with a printing platform of 223 x 223 x 205 mm that has the capability to print complex 3-D parts at various layer resolutions. The printer has high flexibility and provides a wide range of filament materials in addition to printing nozzle sizes. The printing layer resolution can be as fine as 0.6 mm and the maximum printing speed can reach up to 24 mm^3/s [142]. Figure 3-11 shows the 3-D printer that was utilized to print the parts used in building the experimental setup.

Figure 3-11: Ultimaker 2+ 3-D printer

3.2.2.5.2 Flow Meters

Flow rates in the experimental setup were monitored via two electromagnetic flow meters. A 3-inch (0.076 m) flow meter was installed on the pump discharge pipe that fills the upper tank and a 2-inch (0.051 m) was installed on the overflow line of the upper tank. The difference between the two flow rates gives the flow rate going through the turbine while maintaining a constant head. The M-2000 M-series Mag Meter manufactured by Badger Meter was used in the experimentation. The meter has two DC-powered electromagnetic coils and a set of electrodes that create a magnetic field and senses when a conductive fluid like water passes through the meter. The voltage difference between the electrodes is directly proportional to the average velocity of the fluid and then converted to a flow rate. The meter has an accuracy of ±0.25% [143]. Figure 3-12 presents the installed flow meters on the system.

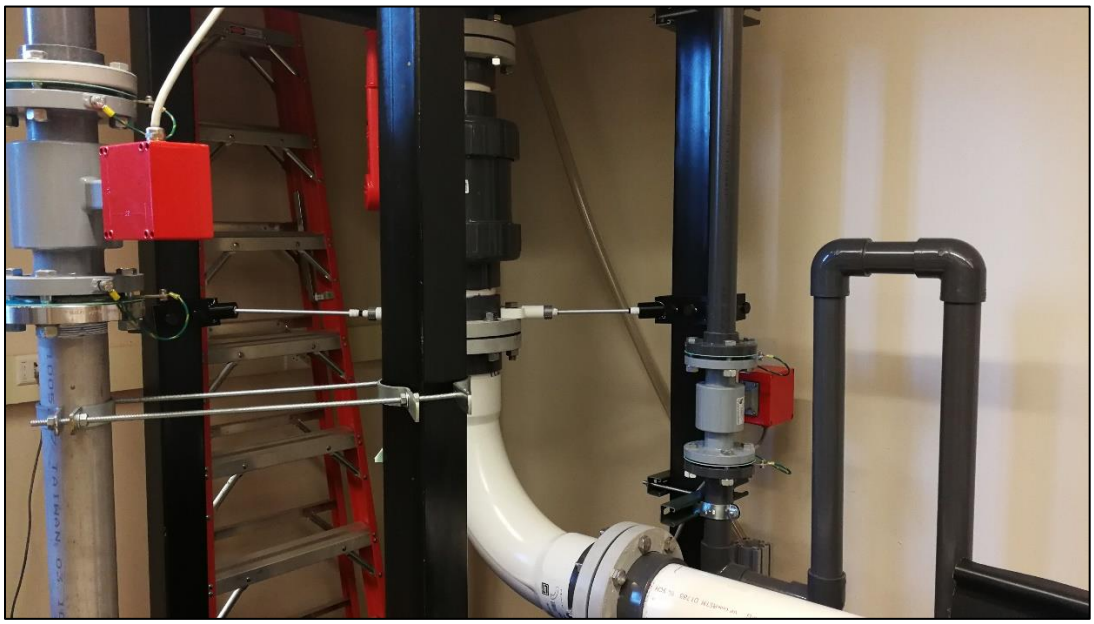

Figure 3-12: Flow meters installed on the filling and overflow lines

3.2.2.5.3 Torque Meter and Torque Display

Torque is measured through an inline torque transducer that is connected to the shaft using a non-slip coupling. The Magtrol TM300 series was utilized to obtain the torque and rotational speed measurements. The non-contact differential transformer has an integrated conditioning electronic module providing a 0 to ±10 VDC torque output as well as a speed output with an accuracy of less than 0.1% [46]. The torque meter was connected to a torque display device that provided the torque, power, and rotational speed measurements. The Magtrol 3411 Torque Display was employed and connected to the torque meter to gather the pertinent data. The device uses a high-speed processor to display the measurements as well as powering the transducer with an accuracy of 0.01% for speed and 0.02% for torque readings [144]. The torque transducer and display are shown in Figure 3-13.

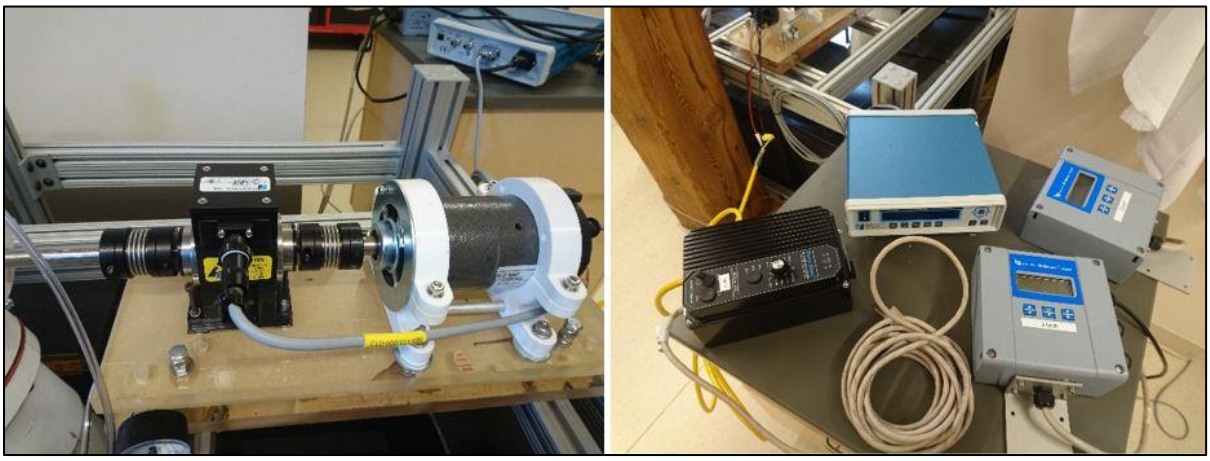

Figure 3-13: Toque transducer and display device

3.2.2.5.4 DC Motor and Motor Controller

The other side of the torque transducer, as shown in Figure 3-13, was connected to a 2.25 HP (1678 W) DC motor that can be re-wired to be used as a generator. The permanent magnet with brushes motor can reach up to 5135 rpm at 130 VDC at no load [145]. Figure 3-14 shows the motor that was used in the lab.

Figure 3-14: DC motor and VSD

3.2.2.5.5 Variable Speed Driven Pump

The water was lifted from the lower (sink) tank to the upper tank via a 10 HP (7460 W) close-coupled centrifugal pump. The 4250 ATM pump can provide a flow rate of up to 7.93 m^3/s (500 GPM) and a maximum head of 30 m (98.4 ft) [146]. The pump is equipped with a VSD to provide a closed control flow rate during the experimental testing. The ABB ACS310-03U-34A1-2 VSD is capable of controlling motors ranging from 7.5 HP to 10 HP with a digital output accuracy of 0.2% [147]. It also has the capability to change the speed manually as well as programmable control to provide an energy-efficient operation. The pump and the VSD installed in the experimental setup are indicated in Figure 3-15.

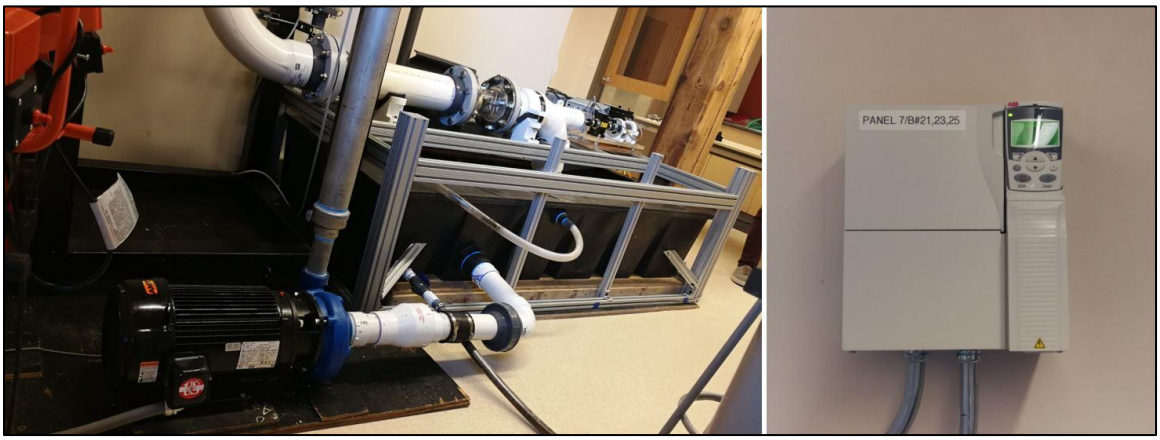

Figure 3-15: Pump-motor set and VSD

3.2.3 Results

The MDO process in this study consist of three main steps; generation and optimization of CADs using an in-house code, CAD designs evaluation using CFD through STAR-CCM+, and finally validating the CFD evaluations with the experimental testing results.

3.2.3.1 *Grid Size Selection*

The mesh size plays a significant role in the CFD simulation results. For example, the discretization error in LES is dependent on the grid size. Also, finer resolutions in the space and time will help in achieving better accuracy to the real case data. However, larger grid size can be computationally expensive. Therefore, compromising between the minimized error and the total computational time was the main criterion in the grid size selection. Five runs were taken into consideration 10, 15, 20, 25, and 30 million cells in which the power output and the computational time are used as the basis of comparison.

Mesh independent study involves analyzing the solution of the simulations based on changing the discretization criteria of the computational domain only. The size of the cell is changed, and the solution time, as well as the accuracy, are monitored. Another way to analyze the mesh sizing is the y^+ and the CFL numbers.

y^+ is a dimensionless wall distance for a wall-bounded flow and also known as the Law of the Wall. It was introduced by Theodore von Karman in 1930 and is defined in Eq. 3-1. It is a function of the shear velocity near the wall, the distance to the nearest wall, and the kinematic viscosity of the fluid. y^+ is used in turbulence models to indicate the effect of the influence of the Reynolds stress tensor [148]. The wall function approach is used to apply boundary conditions to a distance away from the wall, so the turbulence model equations are not solved close to the wall [149].

$$y^+ = \frac{u_\tau y}{\nu} \qquad \text{Eq. 3-1}$$

The Courant-Friedrichs-Lewy (CFL) is a conditional stability requirement that is dependent on the time step and the mesh spacing. It was introduced and discussed at length by Courant et al. in 1928 [150]. CFL condition states that the distance traveled by any information during the time step must be less than the distance between the mesh elements. The information is transferred from a cell and propagates to the immediate neighboring cells. The Courant number, or mean of Convective Courant number, is a dimensionless number that is a function of the time step and the mesh size. It is defined in Eq. 3-2.

$$C = \frac{u\Delta t}{\Delta L} \qquad \text{Eq. 3-2}$$

Based on the results shown in Figure 3-16, the error in the power output between these simulations exceeds 5% for the cases of 10 and 15 million cells, which is a reason for avoiding these two cases regardless of their affordable computational time. While the error in the rest of the cases is less than 2%, however, the 25 and 30 million cells need 1.25 and 1.50 times more, respectively, compared to the 20 million cells case. Since the 20 million cells simulation has a moderate number of cells with an acceptable error percentage of less than 2%, the 20 million cells case is used for this study. This case will provide an optimum solution for working on this study without jeopardizing the simulation resolution or increasing the simulations time making them unfeasible.

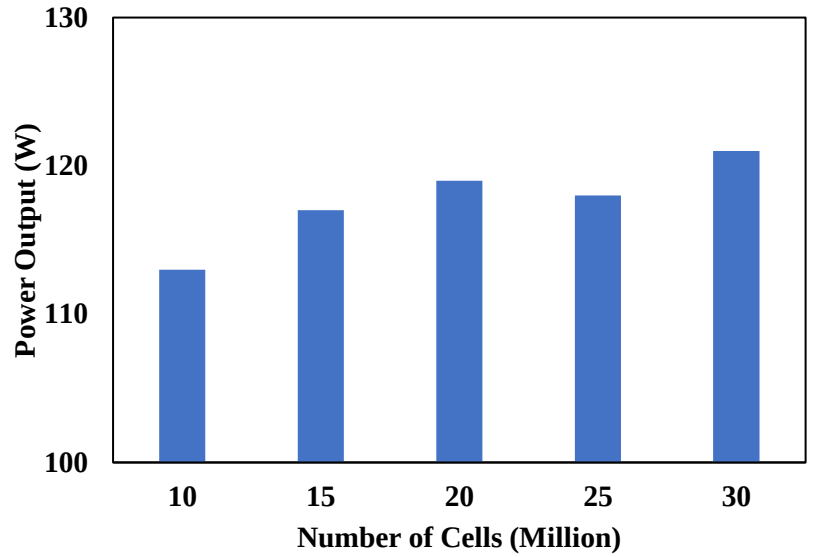

Comp. Time	1.0x	1.5x	2.0x	2.5x	3.0x

Figure 3-16: Power output and computational time at different grid size

Moreover, and for the confirming the validity of the results with the selected mesh size, an assessment for the time-averaged y^+ on the turbine blades was checked to be found in the viscous sublayer zone ($y^+ < 1$) as shown in Figure 3-17, where 15 prism layers were used with 1.3 growth rate. Finally, and though using unconditionally-stable implicit time marching, the time-averaged convective Courant number was below 0.6 (see Figure 3-18) to validate the accuracy for the LES computation.

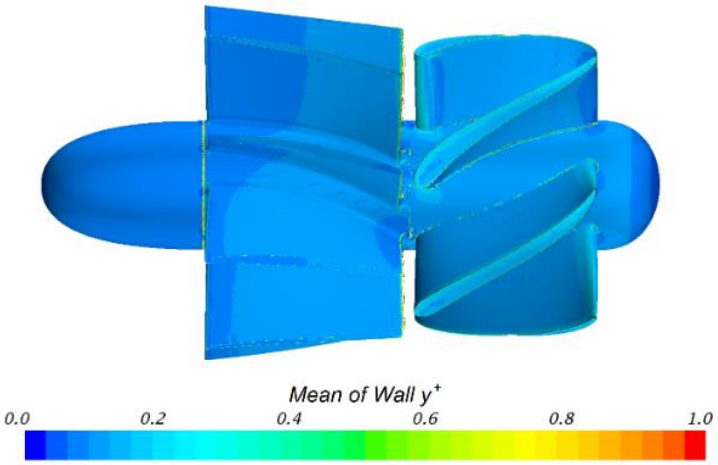

Figure 3-17: Mean of wall y+ values at the rotor and the stator

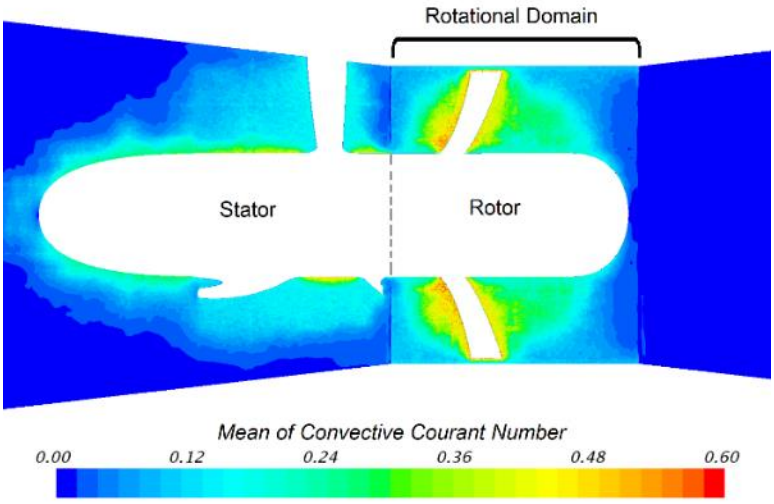

Figure 3-18: Mean of convective Courant number nearby the rotor and the stator

3.2.3.2 *CFD Simulation Results*

The performance of different rotor designs was analyzed using CFD at various rotational speeds starting from 500 RPM up to 3,000 RPM with a 500 RPM step. Figure 3-19 shows the power output of these rotors at the aforementioned rotational speeds range. As can be inferred from the figure, the six blades rotor has the highest power output reaching up to 121 W at 1,500 RPM followed by the seven blades rotor, five blades rotor, four blades rotor, and the three blades rotor. The losses in the seven blades rotor were higher than in the six blades one which justifies the power drop in the former case.

The optimum rotational speed of the turbine is not only limited to 1,500 RPM, as the trendlines in Figure 3-19 show that the turbine is capable of keeping the highest power output within the range of 1,450 – 1,700 RPM. Error bars are representing a fixed error percentage of 5% for all data points.

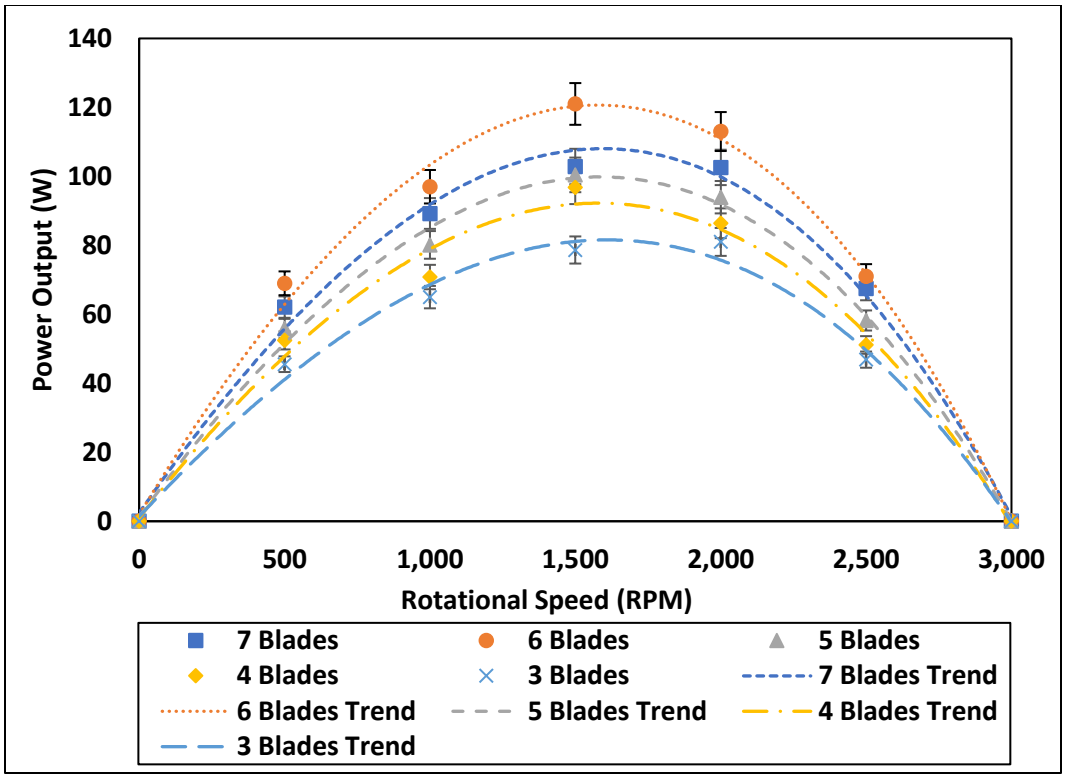

Figure 3-19: Performance curve of the baseline rotor design at a different number of blades and different rotational speeds

Based on the previous first iteration of optimization, the 6-blade rotor is considered for the wrap angle simulation matrix. Figure 3-20 presents the geometry of the baseline design with 80^{o}-60^{o} wrap angle versus the optimized design with the 100^{o}-100^{o} angle; the latter showed nearly 23% improvement in the power output (137 W) of the turbine over the baseline design (111 W). One reason for this increment can be the longer blade in the optimized design which increases the blade passage area as a result.

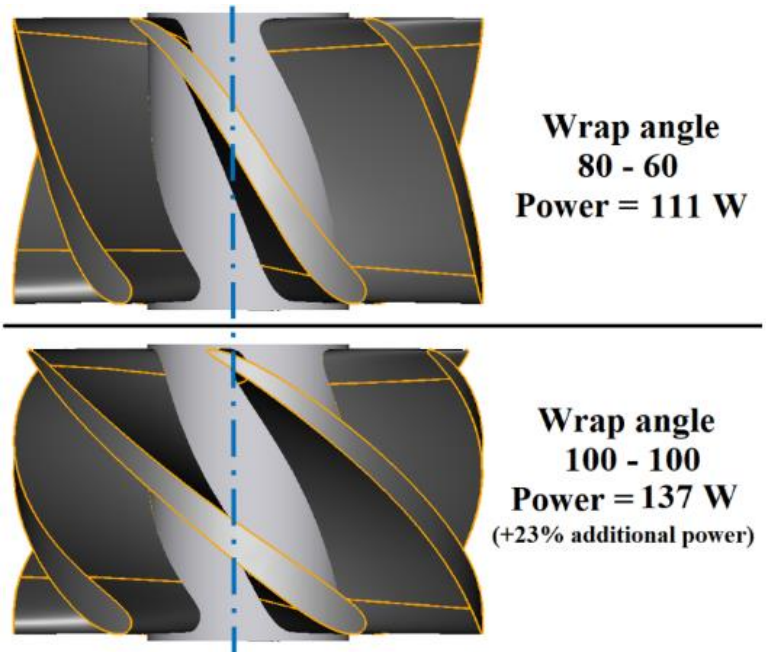

Figure 3-20: Effect of the blade wrap angle (hub to shroud) on the turbine power output

The complete solution of the matrix is shown in Figure 3-21. The figure illustrates the effect of the blade wrap angle on the turbine power output, 0% represents the baseline design where no improvements exist. Regardless of the five wrap angles would decrease the power output below the baseline for the cases 60º-60º/65, 65º-60º, 70º-60º, and 75º-60º (hub-shroud), most of the angles caused improving in the turbine performance. The four wrap angles 100º-100º, 100-105º, 105º-100º, and 105º-105º marked the highest positive effect of 23% on the turbine power output with up to 25% additional power, compared to the lowest power output at the wrap angle of 60º-60º (-2%).

For all angles larger than 105º-105º, it was anticipated that the improvement would be greatest as the blade supposed to have a larger passage area, though, the largest the angles the highest the losses occurred nearby the trailing edge which affected the performance negatively. Eventually, for optimum power output for the turbine, the range of the blade's wrap angle should be within 100º-105º at both the hub and the shroud sides.

Angle at the hub (°)	Angle at the shroud (°)										
	60	65	70	75	80	85	90	95	100	105	110
60	-2%	-1%	2%	3%	4%	6%	8%	10%	12%	13%	15%
65	-1%	2%	3%	4%	6%	8%	9%	11%	13%	14%	15%
70	-1%	3%	5%	6%	8%	9%	9%	12%	13%	15%	16%
75	-1%	4%	6%	7%	9%	10%	11%	13%	14%	16%	17%
80	0%	5%	8%	9%	11%	12%	13%	15%	15%	17%	18%
85	1%	5%	9%	11%	12%	13%	14%	16%	17%	18%	19%
90	2%	6%	10%	12%	13%	14%	15%	17%	19%	20%	20%
95	3%	7%	10%	13%	14%	16%	17%	20%	22%	21%	21%
100	4%	8%	11%	13%	15%	17%	19%	21%	23%	23%	21%
105	4%	8%	12%	13%	16%	18%	20%	22%	23%	23%	22%
110	5%	9%	13%	15%	17%	19%	21%	21%	21%	22%	22%

Figure 3-21: Effect of the blade wrap angle on the power output of the turbine

3.2.3.3 *Validation with Experiments Results*

The performance of the turbine simulated in STAR-CCM+ is compared and validated with the experimental run as indicated in Figure 16. Both runs, CFD and experimental, have the same trend in which the power output increases with increasing the rotational speed up to 1,600 RPM for the experimental data and up to 1,700 RPM for the CFD results, then the power starts to decrease afterward. Regardless of the difference in the peak power output of each result, it can be concluded that this turbine optimum operational rotational speed is in the range of 1,400 – 1,600 RPM.

Although the power outputs are not similar regarding values, however, it can be deduced that the simulations are validated with the experimental work. Due to some limitations in the CFD simulations, the friction losses and the mass of the shaft were not taken into account. The friction losses in the PVC pipes and elbows decreased the power generated by the turbine. Also, the shaft used in the experimental setup is made of stainless steel that has a diameter of 5/8 inches and 90 cm length causing a starting torque that reduced the power output of the turbine. Additionally, the

mechanical losses in the bearings and couplings of the shaft contributed to the difference between the results of the experimental setup and the CFD work. Considering all previous statements, the power output values calculated by CFD were higher than those recorded by the experimental testing, with an average of 47%.

The uncertainty of the experimental data was estimated with a 95% confidence level [151], and it was represented in error bars, as shown in Figure 3-22. Both systematic and random errors were included in the uncertainty analysis. On the other hand, a fixed error percentage of 5% was assumed for the CFD results. Positive error bars were added to the experimental results, while negative bars considered for the CFD results to minimize the average difference percentage of 47% to 35% only.

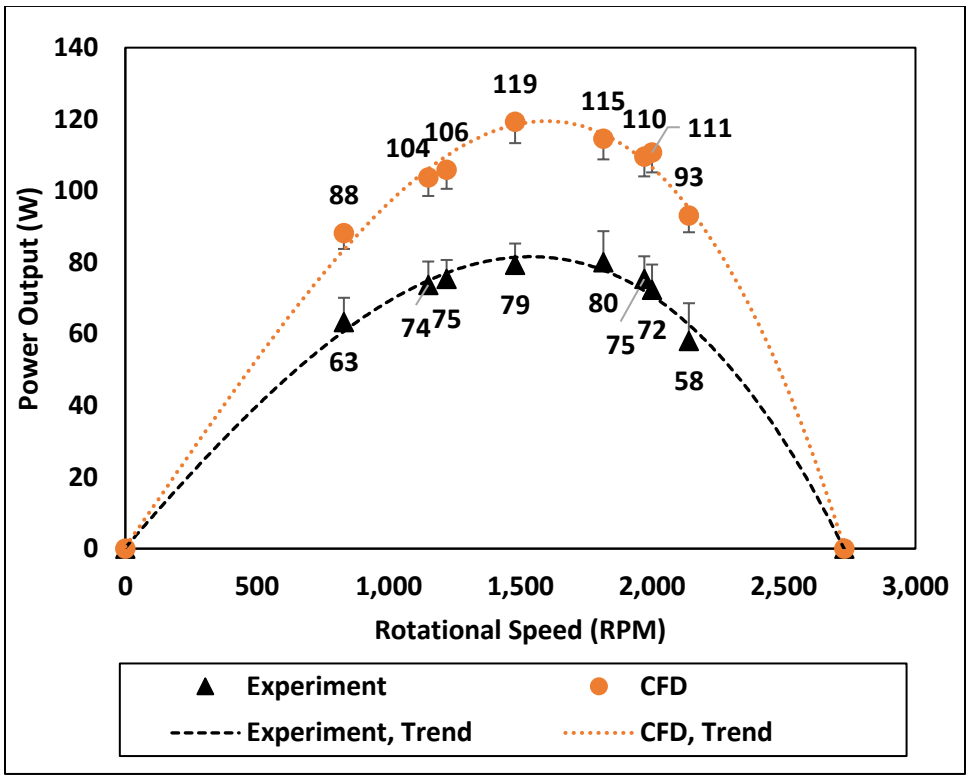

Figure 3-22: Characteristics curve of the optimized rotor, CFD and experiment results

3.3 Optimization of Intake and Draft Tubes

This study presents an optimization for the design of each the intake (nozzle) and the draft tube (diffuser) for a 7.6 cm (3-inch) diameter horizontal-oriented and 90 cm (35-inch) diameter vertical-oriented Kaplan micro-hydro turbine systems at the very low head (less than 3 meters). It is necessary to utilize Computation Fluid Dynamics (CFD) analysis to test a variety of design parameters for the intake and the draft tubes to obtain a consistent overall design with maximum possible efficiency based on Large Eddy Simulation (LES) of transient turbulence modeling. Six angles (18, 24, 30, 36, 42, and 48 degrees) for the intake tube and five angles (12, 18, 24, 30, and 36 degrees) for the draft tube with four tube-lengths for both tubes were investigated for both systems. After that, the shape of the channel of a bellmouth i.e. simple radius and elliptical profiles was considered in this study. All the cases have been tested and compared based on the power output and the efficiency of the turbine

3.3.1 Introduction

These days, tip leakage, friction, and exit kinetic energy from the draft tube are considered the most of the efficiency losses in turbines [152]. The previous statement indicates that Kaplan turbines have been designed to the highest efficiencies; nevertheless, the improvement on the components of the turbine (i.e. the intake and the draft tubes) of the turbine is still an option.

The draft tube is an essential part of the hydro turbine system. It plays a role in controlling the pressure and velocity head differential. As a result, the power across the system. As shown in Figure 3-23, the velocity decreases, while the pressure increases as the fluid passed the draft tube. The concept could be confirmed for an incompressible flow by implementing the law of conservation of energy over the draft tube’s control volume. By continuity definition, it can be seen at a constant volumetric flow rate through the control volume with the draft tube area

increased, that a lower velocity will be obtained. Equation 3-3 and 3-4 show Bernoulli equation [153], which is describing the relation between the pressure, the velocity, and the head.

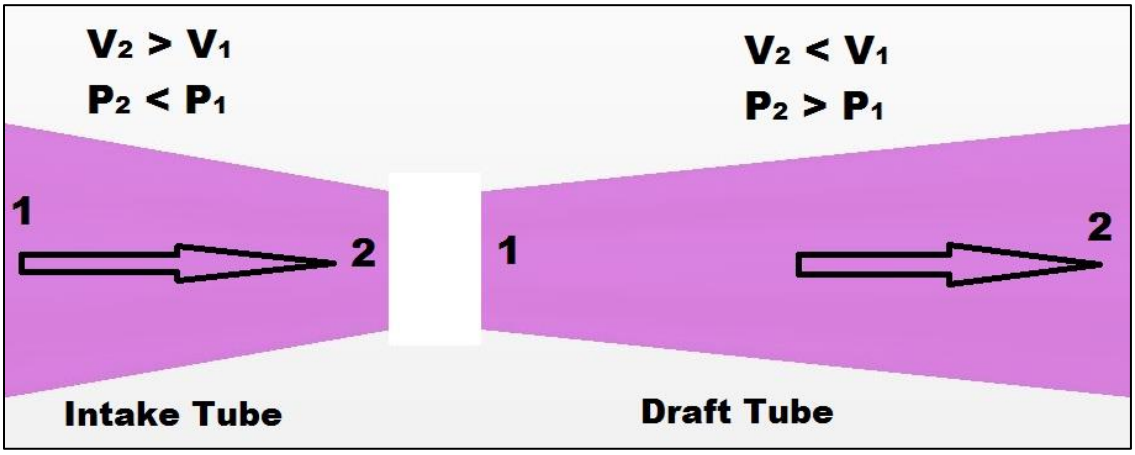

Figure 3-23: Velocity and pressure relation in the intake and the draft tubes

$$\frac{p_1}{\rho} + \frac{V_1^2}{2} + gz_1 = \frac{p_2}{\rho} + \frac{V_2^2}{2} + gz_2 \qquad \text{Eq. 3-3}$$

$$\frac{p_1}{\rho} + \frac{V_1^2}{2} = \frac{p_2}{\rho} + \frac{V_2^2}{2} \qquad \text{Eq. 3-4}$$

The draft tube should be full of water all the time to ensure the optimum operation of the hydro-turbine system, as the pressure and the velocity will be affected if there are any fluid losses in the system as well as the total efficiency. In the ideal case, the outlet pressure should be close to the ambient pressure, and hence only the end of the draft tube might be immersed in the outlet stream. There is a relation between the total head of the system and the output mechanical power obtained from the water. Correspondingly, the geometry design of the draft tube depends on attaining the high performance and the innovation at the same time, if its duty is to be optimized.

Yen et al. present a study of a 30 cm (12-inch) diameter Kaplan hydro turbine geometry with performance optimization through CFD method based on Large Eddy Simulation (LES) of transient turbulence modeling. The study includes a selection of horizontal versus vertical setup, tailwater head, draft tube length, draft tube angle, intake tube configuration, and blade shape

combination tests. All of these geometric parameters were tested and compared based on power output, mass flow rate and efficiency [154].

ElGammal et al. focus intensely on the turbine's intake tube design based on numerical investigations to maximize energy extraction with a set of initial design parameters in the mean of intake tube length and intake tube angle. Optimizing the efficiency of a system with less material cost was the primary goal of the study. Outcomes had proven the merit of higher slope per side length in enhancing output power with an average of 2.7% by full expansion from minimum to the maximum angle. After that, the bellmouth profile was also adopted to find out that there was a significant improvement in the system performance with an additional 2.2% increase in turbine efficiency [120].

The purpose of this study is to optimize design of both the intake and the draft tubes (nozzle and diffuser) for two different diameter sizes Kaplan micro-hydro turbine (7.6 cm and 90 cm) with two different orientations (horizontal for the 7.6 cm system and vertical for the 90 cm system), by finding the optimum angle, length and shape for both tubes, to minimize the losses and achieve the maximum available energy, and as a result, obtaining the maximum power output as well as the efficiency of the hydro turbine system.

3.3.2 Methodology

The optimization of the design in this study conducted for two systems; 7.6 cm (3-inch) diameter horizontal-oriented system and 90 cm (35-inch) diameter vertical-oriented system, as shown in Figure 3-24 and Figure 3-25. Both systems were designed based on a gross head of 3 meters.

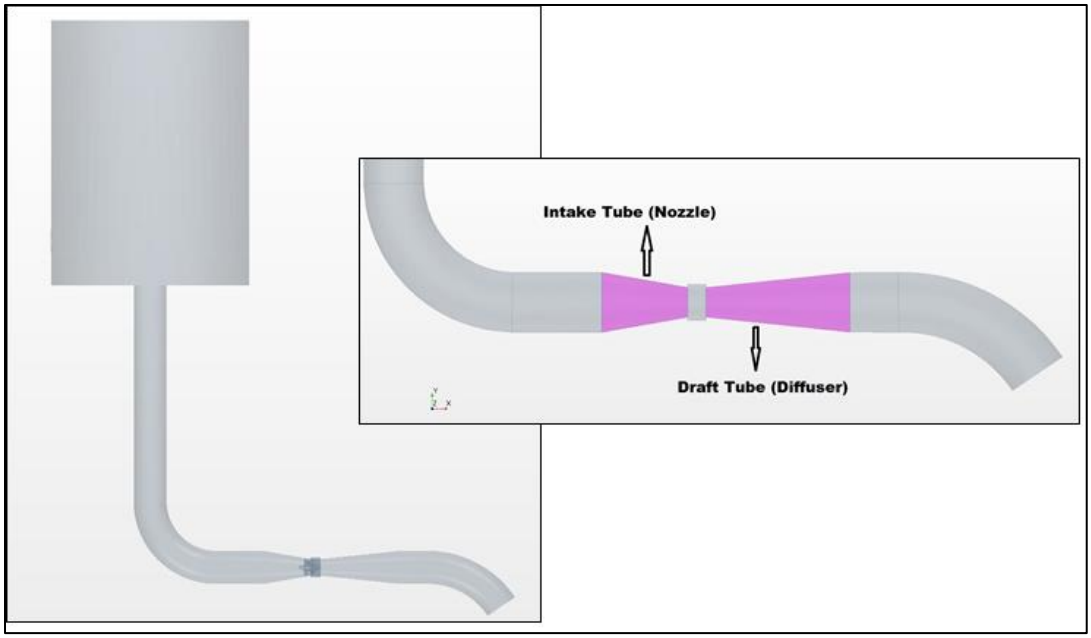

Figure 3-24: The draft and intake tubes in the 7.6 cm (3-inch) horizontal-oriented hydro turbine

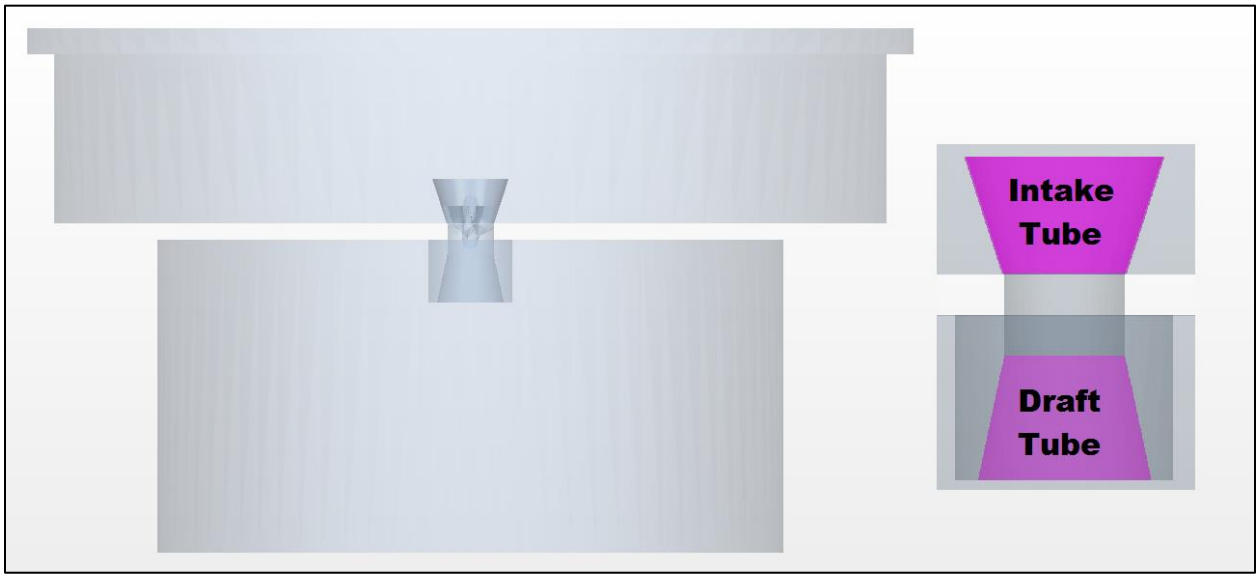

Figure 3-25: The draft and intake tubes in the 90 cm (35-inch) vertical-oriented hydro turbine

3.3.2.1 *Angles*

Six angles in the range of (18 - 48) degrees were tested for the intake tube as shown in Table 3-3, and the definition of the angle for the intake tube in the horizontal 7.6 cm system is shown in Figure 3-26, 30 degrees intake tube angle shown as an example. While five angles in the

range of (12 - 36) degrees were tested for the draft tube as shown in Table 3-4, and the definition of the angle for the draft tube in the horizontal 7.6 cm system is shown in Figure 3-27, 12 degrees draft tube angle shown as an example. The same ranges of angles for both tubes were considered for both the vertical and the horizontally-laid systems.

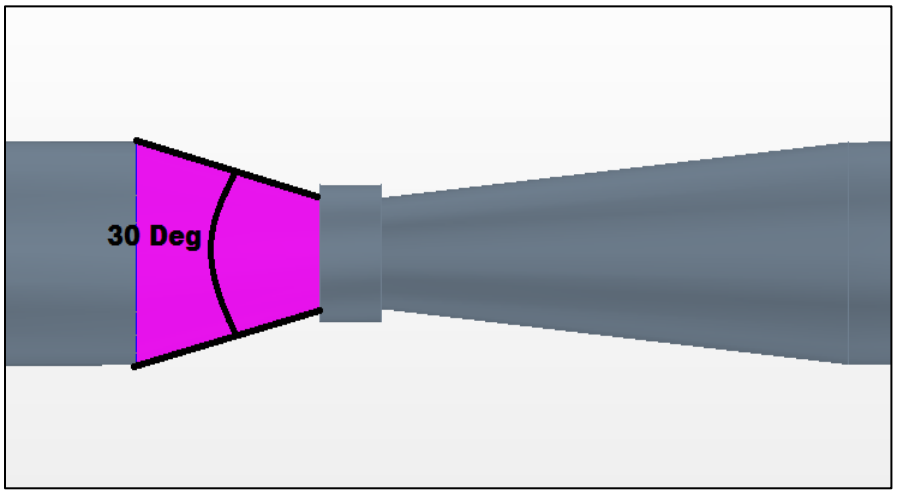

Figure 3-26: Definition of the angle for the intake tube in the horizontal 7.6 cm system, 30 degrees shown in this figure

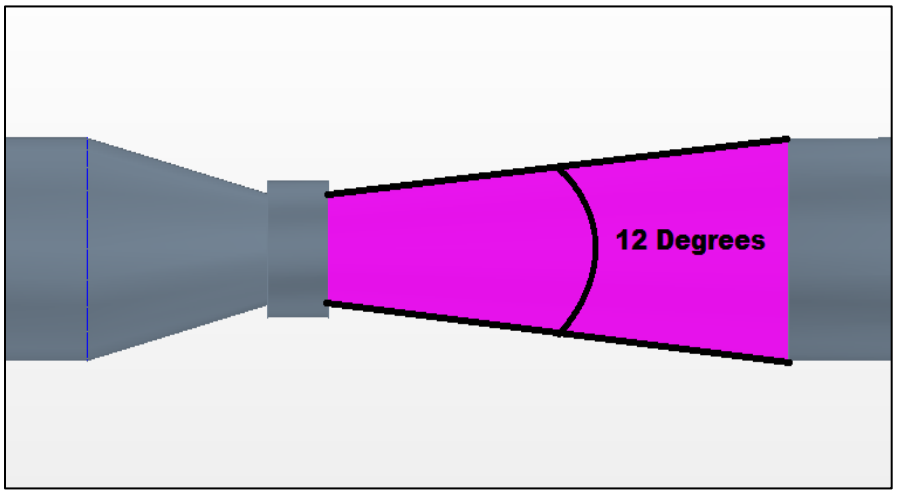

Figure 3-27: Definition of the angle for the draft tube in the horizontal 7.6 cm system, 12 degrees shown in this figure

Table 3-3: Range of angles for the intake tube

No.	Intake Tube Angle
1	18
2	24
3	30
4	36
5	42
6	48

Table 3-4: Range of angles for the draft tube

No.	Draft Tube Angle
1	12
2	18
3	24
4	30
5	36

3.3.2.2 *Length*

Another significant design parameter of the intake and the draft tubes is the length of the tube (as shown in Figure 3-28**)**. Four lengths were investigated (0.4 m, 0.9 m, 1.4 m, and 1.9 m) for both tubes. This parameter was only studied for the vertical 90 cm system, as the horizontal 7.6 cm system has length limitations as the intake and the draft tube are connected to 15.2 cm diameter pipe, and hence the length of the tube is controlled by changing the tube angle.

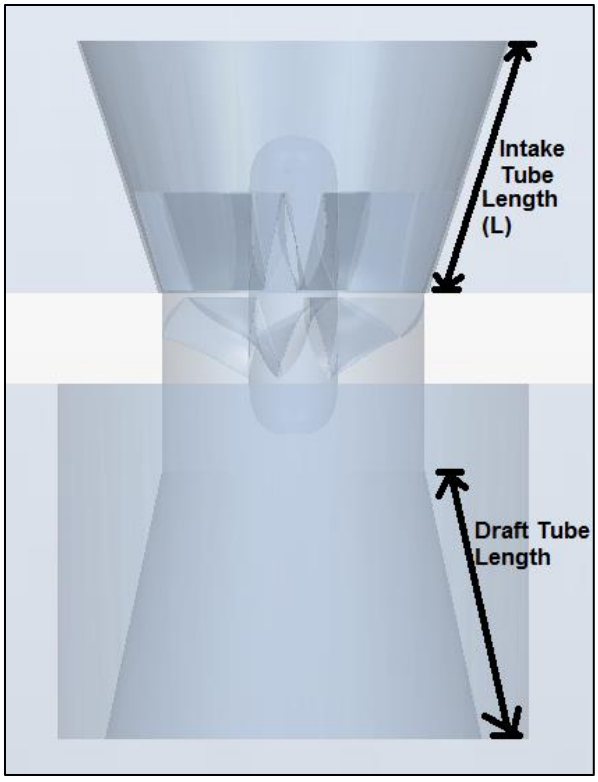

Figure 3-28: Definition of the tube length in the vertical 90 cm system

3.3.2.3 *Shapes*

Besides the angles and the lengths of the tubes, two bell-mouth shapes for the tubes were introduced in this paper; Simple Radius (SR) and elliptical profile, as shown in Figure 3-29. A case of a simple radius was tested with a range of radii of curvature (0 - 16 inches). Figure 3-30 shows the comparison between the straight, simple radius bellmouth (10-inch radius of curvature as an example) and elliptical profile for the intake and the draft tubes. As shown in Table 3-5, eight radii were selected for the simple radius profile, while three (L x W) arbitrary configurations for the elliptical one, as shown in Table 3-6.

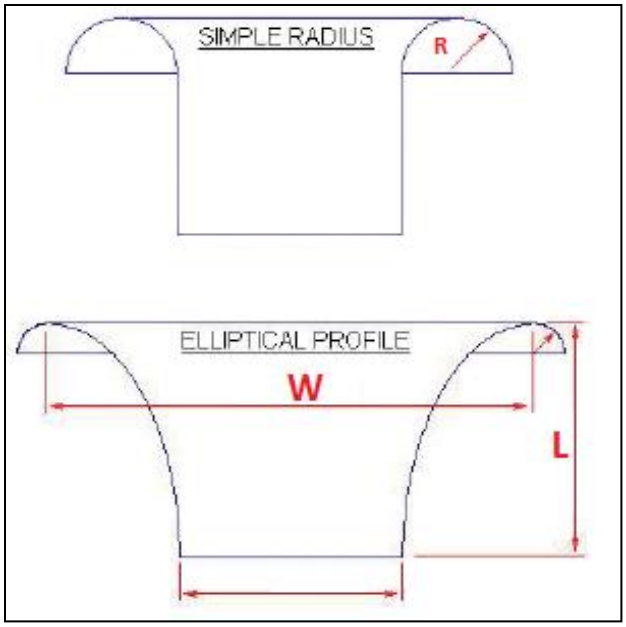

Figure 3-29: Proposed bellmouth profiles

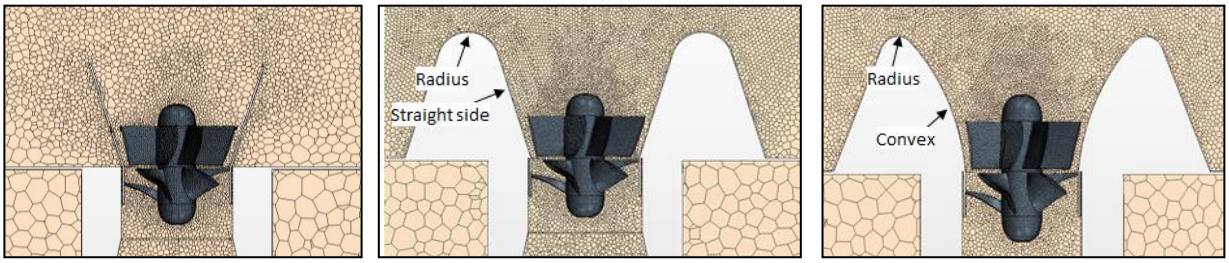

(a) Straight (b) Bellmouth (c) Elliptical

Figure 3-30: Comparison between the straight, simple radius bellmouth (10-inch radius of curvature) and elliptical profiles for the intake tube

Table 3-5: Range of radii for the SR profile

No.	Radius of Curvature (in)
1	2
2	4
3	6
4	8
5	10
6	12
7	14
8	16

Table 3-6: Three configurations of the elliptical profile

No.	Length (L)-in	Width (W)-in
1	35	70
2	50	88
3	50	60

3.3.2.4 *Simulation Approach*

In simulations of the flow in hydro turbine systems, large-scale and small-scale eddies are generated due to turbulence in the flow as a result of high swirl in the rotational part. Turbulence is transient in nature, and eddies evolved have spatial and temporal variations. Navier-Stokes (N-S) equations become more complicated with the addition of turbulence terms of random character, and based on that, N-S equations became Reynolds's Averaged Navier-Stokes (RANS) equation which is the sum of the statistically averaged component and fluctuation component.

While for this study, the CFD approach employs Large Eddy Simulation (LES) as a transient turbulence model, which is considered to be more accurate compared to Unsteady Reynolds Average Navier-Stokes (URANS) approach regarding unsteady simulation.

Large Eddy Simulation (LES) is a natively transient technique that solved large scales of the turbulence and modeled the small-scale motions, where the large scales to be solved by N-S equations while the small scales to be shaped by one of a subgrid-scale model (SGS). LES usually uses either a Smagorinsky or wall-adapting local-eddy (WALE) as an SGS to compute the turbulent viscosity. The WALE SGS employs an algebraic formulation to model the subgrid-scale stresses, while Smagorinsky SGS uses the mixing length hypothesis. The latest model is straightforward and not computationally expensive, but there is a limitation due to the damping effects near the wall; hence a damping function is needed for the accurate simulation of wall-bounded calculations. Therefore, WALE is the simplest with better performance and more accurate scaling near the wall without damping effects [136].

As a result, LES could be the best model for predicting the turbulent flow behavior, but the shortcoming of this technique is that it is computationally expensive. As an implicit unsteady simulation model, the time step was 0.001 second along the whole solution time with 1st order solution accuracy for temporal discretization; since this approach leads the simulation to stability in a reasonable computational time with comparison to the 2nd order solution accuracy.

Physical parameters and simulations' conditions for both systems are described in Table 3-7 below:

Table 3-7: Physical parameters and conditions for the simulations

Parameter	7.6 cm Horizontal System	90 cm Vertical System
Total Head	8.5 (feet) / 2.59 (m)	
Mass flow at tank inlet	28.5 (kg/s)	4600 (kg/s)
Rotor rotational speed	4000 (rpm)	300 (rpm)
Timestep	10^{-3} (s)	
Number of inner iterations/step	5 (per time step)	

3.3.2.5 *Mesh Independent Study*

The mesh independent study applies three different polyhedral mesh setups of 0.8, 1.5, and 4.4 million cells simulation, respectively, and details of these systems are shown in Table 3-8. While the difference between mesh setups for a mesh scene of the runner of the turbine -as an example- is shown in Figure 3-31 (a) as a coarse mesh with 0.8 million cells, and in Figure 3-31 (b) as a fine mesh with 1.5 million cells, while as a very fine mesh with 4.4 million cells as shown in Figure 3-31 (c). The performance comparison is judged by mass flow rate and power output from the turbine.

Table 3-8: Three mesh setups for the 7.6 cm (3-inch) system

Number of Cells	0.8 Million	1.5 Million	4.4 Million
Computational Time	1.0x	1.9x	5.5x
Simulation Detail	Coarse	Fine	Very Fine

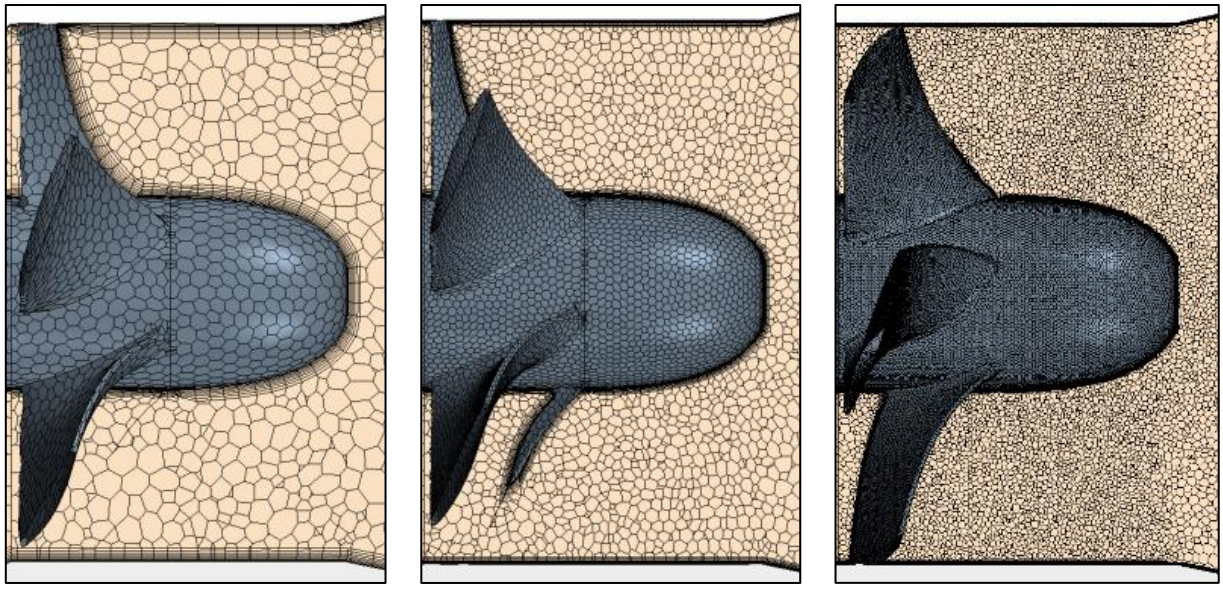

(a) (b) (c)

Figure 3-31: Mesh scene for the runner as (a) coarse mesh 0.8 M, (b) fine mesh 1.5 M and (c) very fine mesh 4.4 M

Based on the results of both the power output and the flow rate, as shown in Figure 3-32 and Figure 3-33, the difference between 0.8 million and 1.5 million setups is about 6.4% and 6.0% in power output and flow rate, respectively. While the difference between 1.5 million and 4.4 million settings for the same perspective is 10.8% and 2.3%, respectively, It could be noticed here that both 0.8 million and 4.4 million setups present higher values for both the power output and the flow rate. However, due to lousy simulation resolution of the 0.8 million setup and high computational time required for the 4.4 million setup; the 1.5 million cells setup was considered for both 7.6 cm (3-inch) and 90 cm (35-inch) systems simulations due to a better balance between simulation resolutions and computational time. Based on the mesh independent study of the 7.6 cm horizontal system, the 90-cm vertical system was scaled, hence no mesh independence shown here for the latest mentioned system. Besides, eight prism layers were used in order to keep the range of the first layer (Wall y^+) value between zero to five, as shown in Figure 3-34; since this is considered as an indicator for the accuracy of the results.

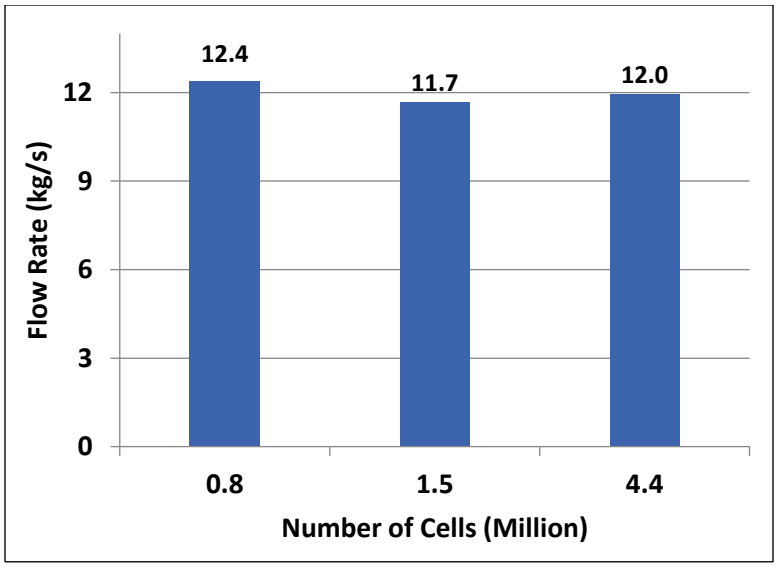

Figure 3-32: Mesh comparison in term of power output

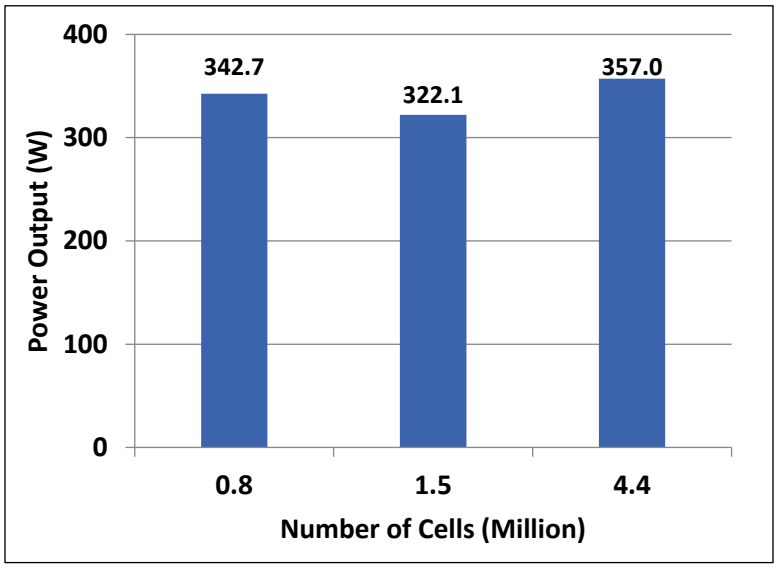

Figure 3-33: Mesh comparison in term of flow rate

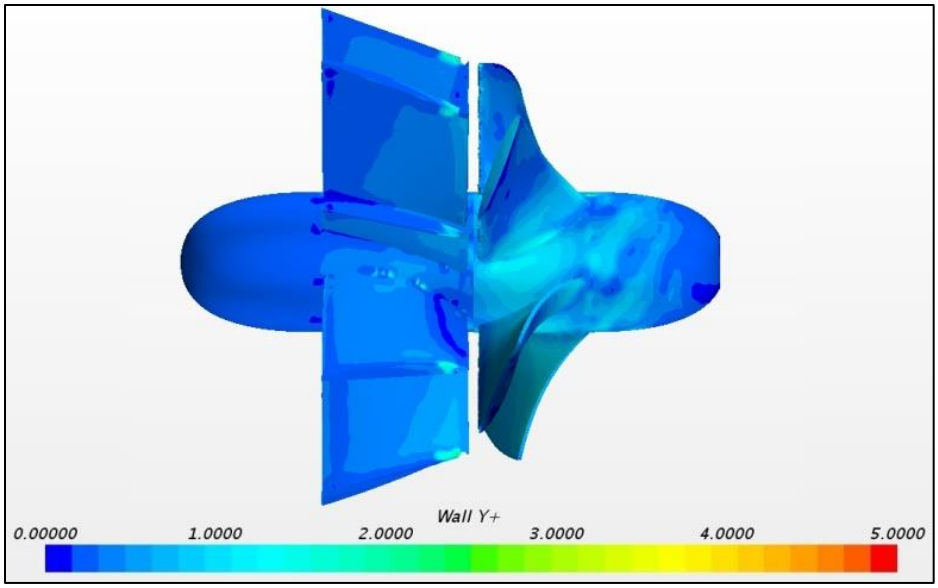

Figure 3-34: Wall y+ values for the runner and the stator

3.3.3 Results

After running different simulations for both 7.6 cm (3-inch) horizontal and 90 cm (35-inch) vertical systems, groups of results were gained for investigating the angles, lengths, and shapes of the intake and draft tubes as indicated below:

3.3.3.1 *Angles*

Four curves were obtained for the performance of the two systems, as can be seen in Figure 3-35, Figure 3-36, Figure 3-38, and Figure 3-39. For the 7.6 cm horizontal system, it was found that the maximum power and efficiency can be obtained around 24 degrees for the intake tube and based on 12 degrees angle of the draft tube angle, to end up with a maximum mechanical power output of about 397 W, and maximum efficiency of 52% for that system. It can be noticed from the Figure 3-35 and Figure 3-36 that changing the draft tube angle have a higher impact on the performance of the system more than the changing the intake tube angle, despite that the angles range of the intake tube (18 - 48 degrees) is wider than the range of the draft tube (12 - 36 degrees). And such a result can be justified by observing the profile of the velocity vector for two angles of

the draft tube as shown in Figure 3-37. With the larger of the two, it is seen that the flowing water leaves the boundary and cause flow separation, which brings down the efficiency, resulting in lower power output.

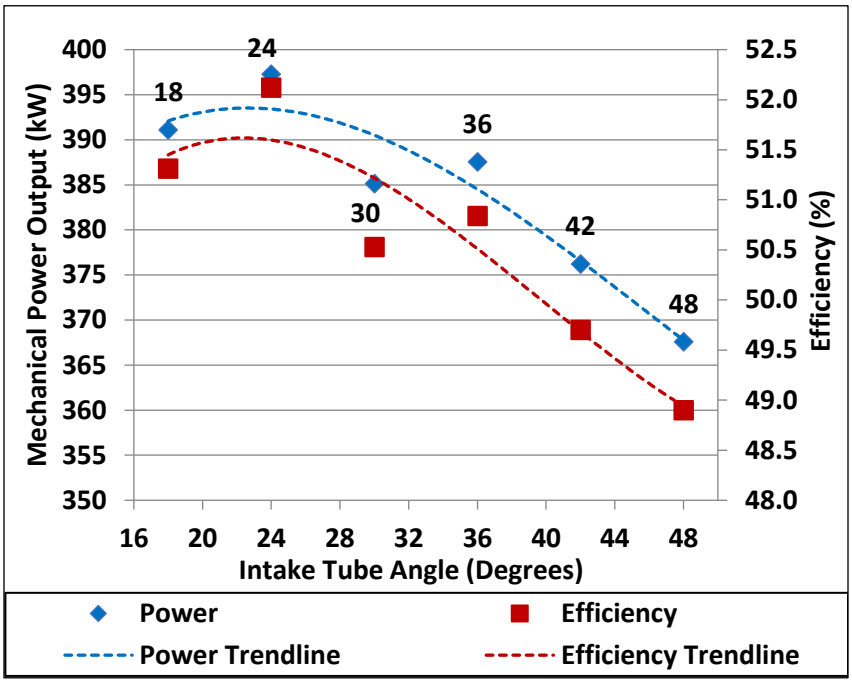

Figure 3-35: Impact of the intake tube angle on the performance of the 7.6 cm horizontal system

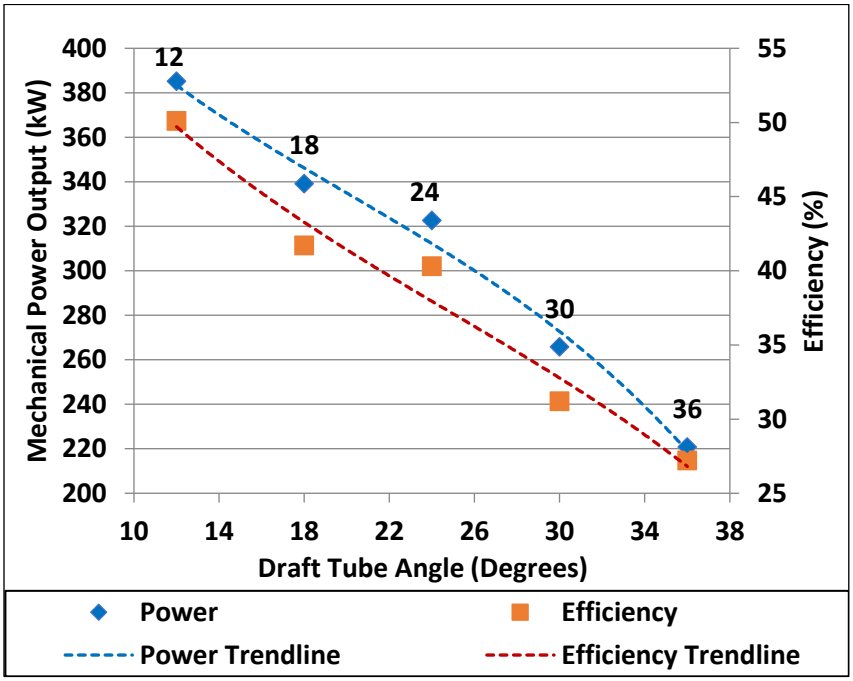

Figure 3-36: Impact of the draft tube angle on the performance of the 7.6 cm horizontal system

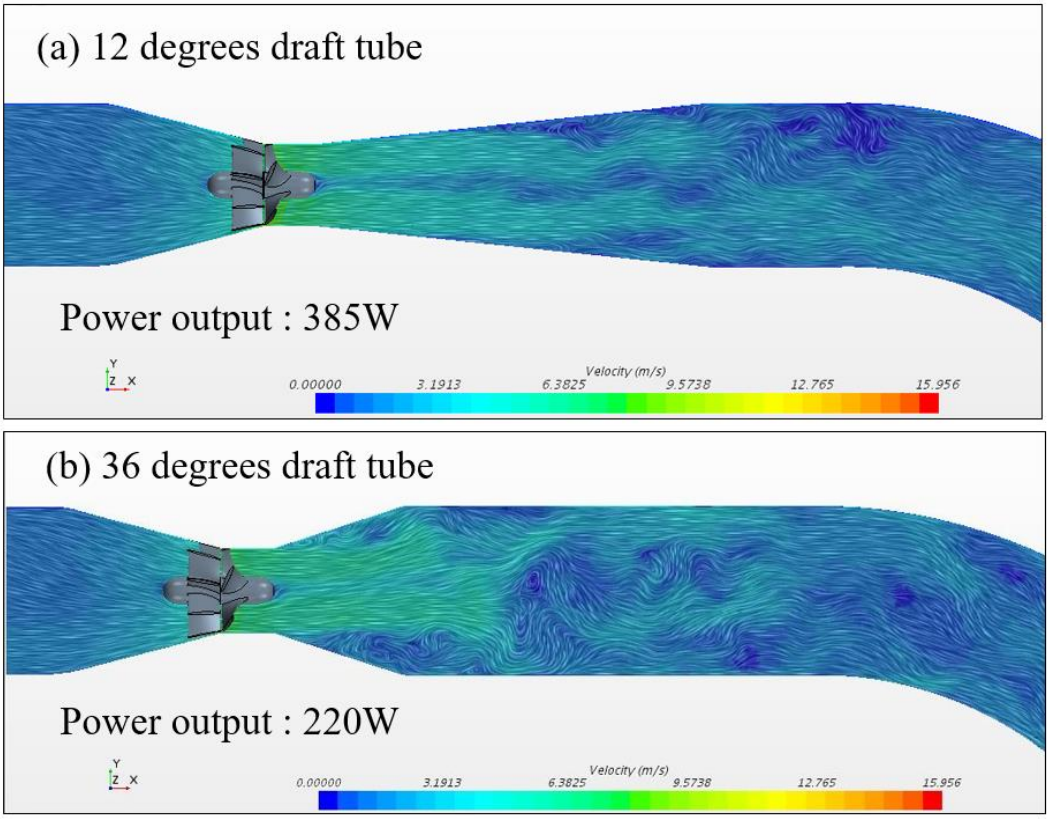

Figure 3-37: Velocity profiles with (a) 12 deg. tube and (b) 36 deg. tube (bottom); Scale 0 to 16 m/s

Furthermore, the impact on tube angles for the 90-cm vertical system is close to the impact on the 7.6 cm system. As can be seen in Figure 3-38, the maximum power and efficiency of about 92 kW and 83% respectively obtained at about 24 degrees. While for the draft tube (see Figure 3-39), the optimum performance achieved between 12 - 18 degrees, but closer to the latest angle.

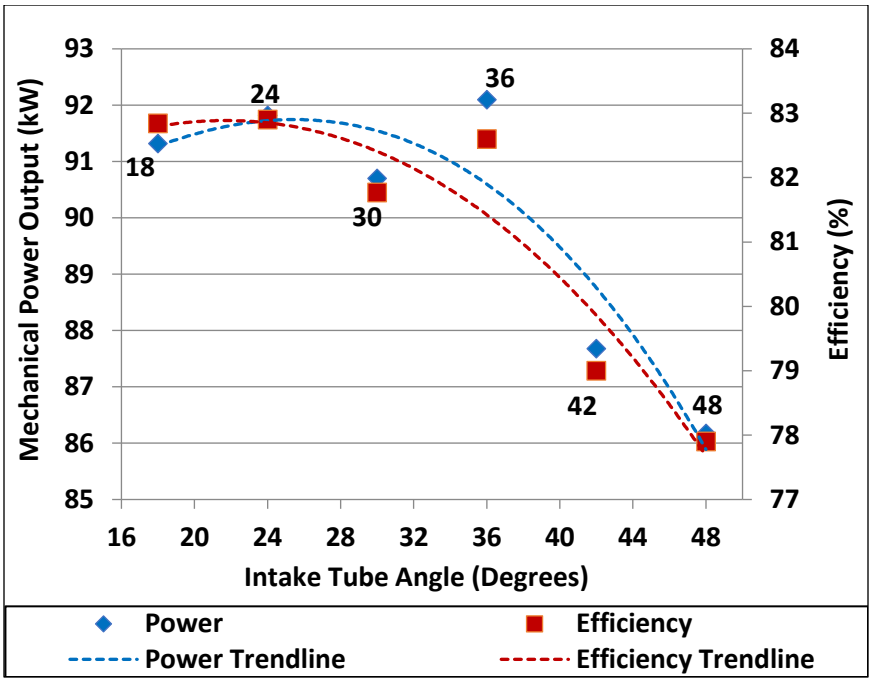

Figure 3-38: Impact of the intake tube angle on the performance of the 90 cm vertical system

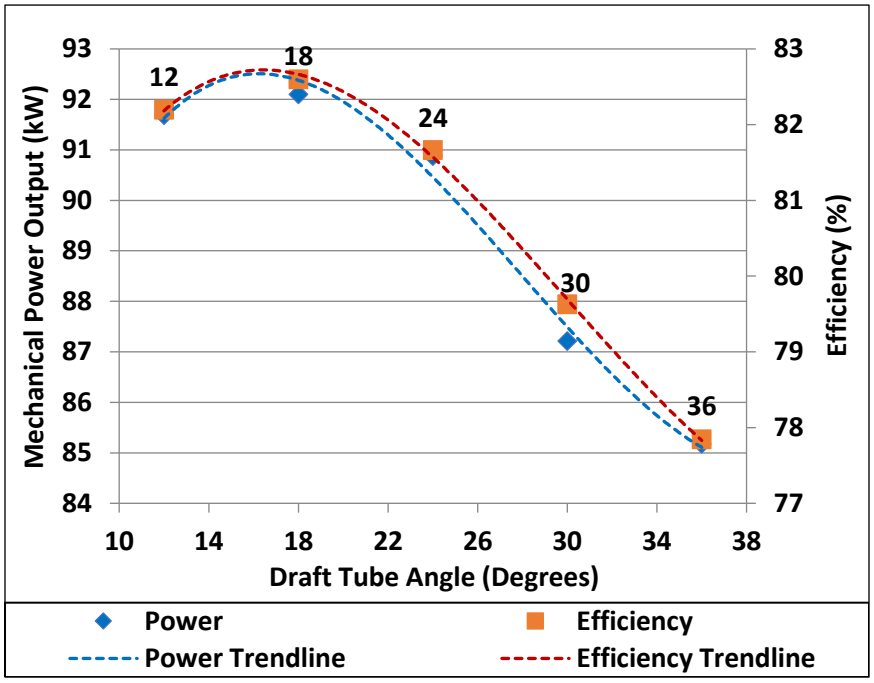

Figure 3-39: Impact of the draft tube angle on the performance of the 90 cm vertical system

3.3.3.2 *Lengths*

Four lengths picked for each tube (0.4, 0.9, 1.4 and 1.9 m) as shown in Figure 3-40 for the intake tube and Figure 3-41 for the draft tube, and based on these lengths the result of simulations was as concluded in Figure 3-42 and Figure 3-43. Again, the draft tube has a higher impact than the intake tube on both the output power and the efficiency of the system as its parameters varied, i.e. angle and length of the tube. As the exit, kinetic energy at the draft tube (diffuser) considered as one of the most efficiency losses in hydro turbines, besides the friction and the tip leakage.

It can be noticed from Figure 3-42 that the best length for the intake tube is in the range of 0.9 – 1.4 meter. In constrast, for the draft tube (see Figure 3-43), the power and the efficiency increases with longer draft tubes, but this is not a rule for industrial applications and on-site hydro turbine setups, as there might be design or space limitations.

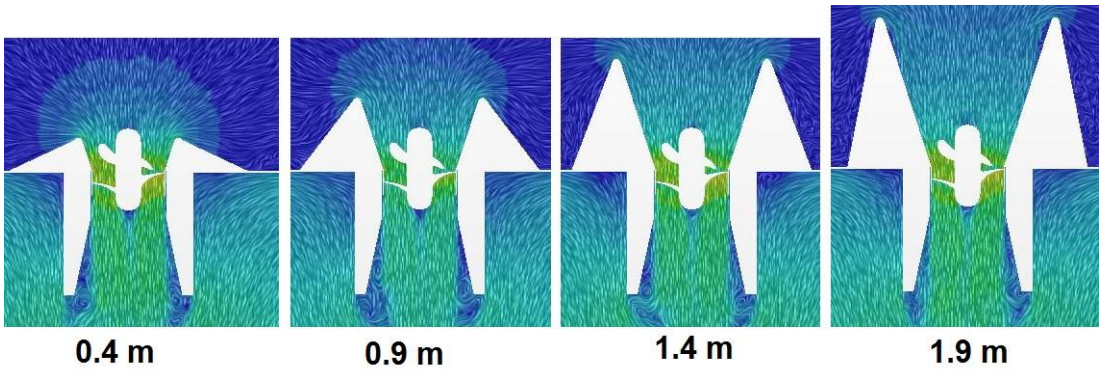

Figure 3-40: Lengths of the intake tube

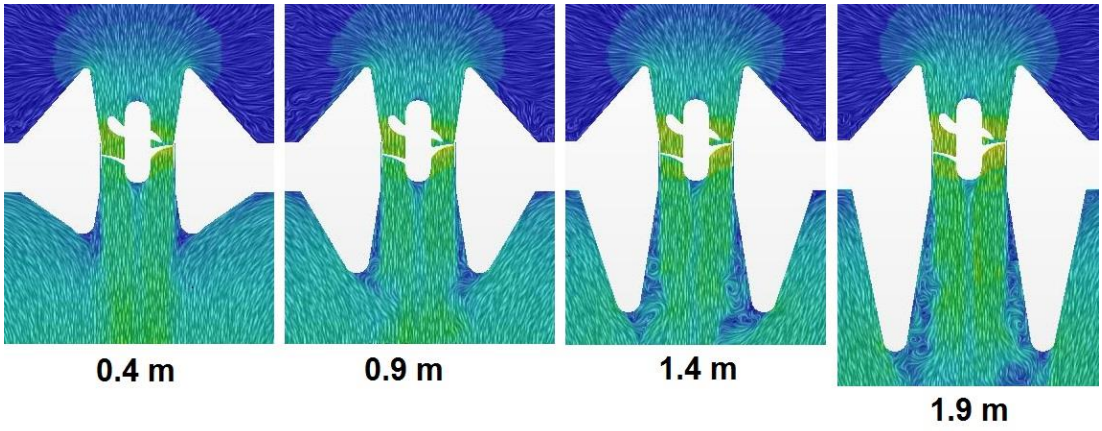

Figure 3-41: Lengths of the draft tube

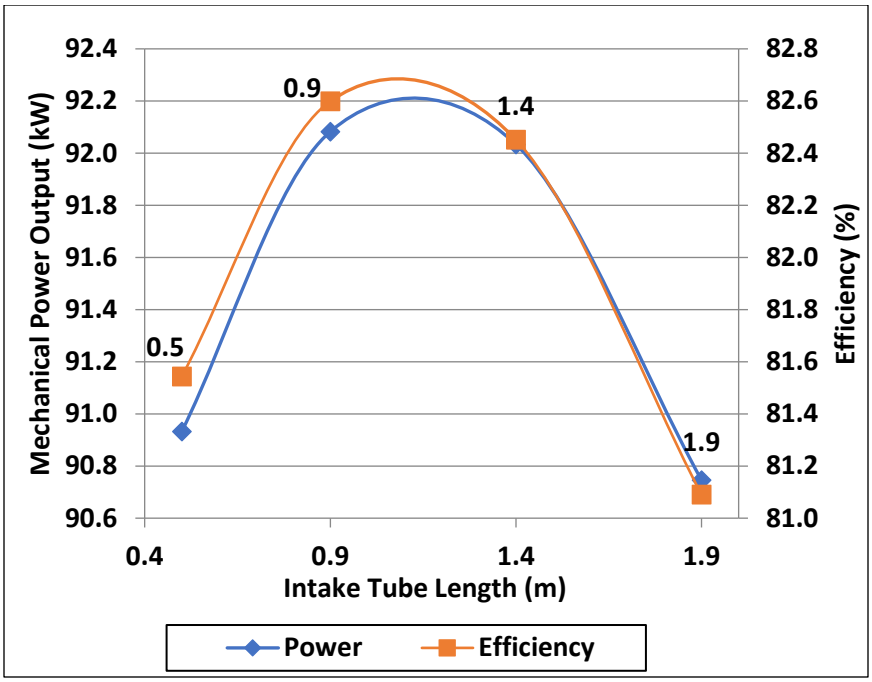

Figure 3-42: Impact of the intake tube length on the performance of the system

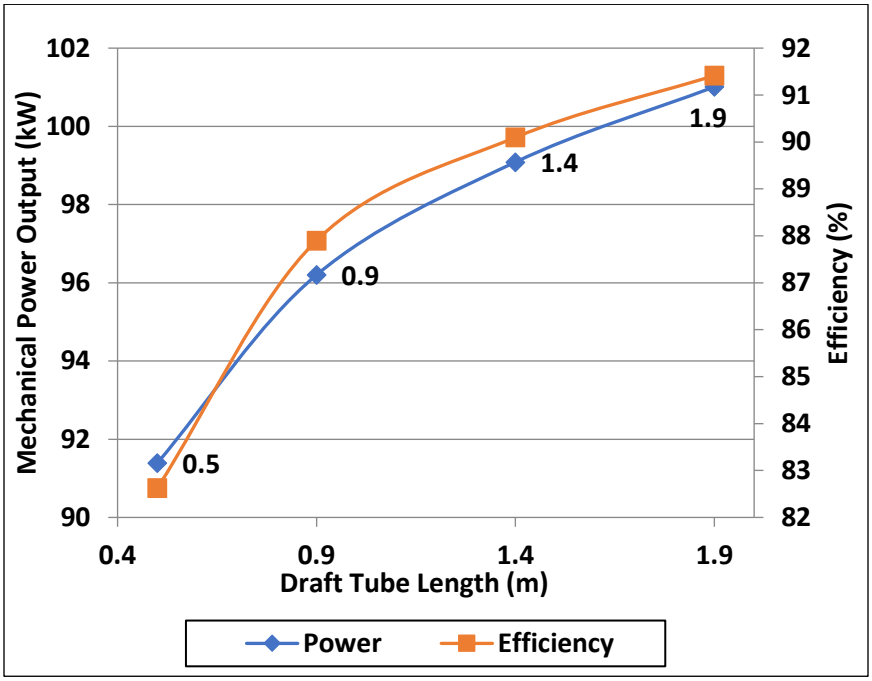

Figure 3-43: Impact of the draft tube length on the performance of the system

3.3.3.3 *Shapes*

Three basic tube shapes were analyzed (as shown in Figure 3-30): Straight tube, simple radius or bellmouth (straight side ending with a round edge), and elliptical. There is a marked improvement with having at the very least a rounded entrance to the intake tube or exit to the draft tube, see Figure 3-44 where the peak efficiency and output power are summarized. The numbers in Figure 3-44 correspond to the best in each category, with parameters such as the edge radius varied for the bellmouth shape, etc. The result is easily understood by comparing the velocity profiles for the straight and bellmouth cases, see Figure 3-45. With a straight edge, separation is visible along the sides, while the bellmouth shape helps the flow to pass smoothly without any separation. As a result, that will decrease the flow losses in the intake tube and increase the generated power and the overall efficiency. This design change leads to an improvement in peak efficiency from 76.7% to 82.6% or a gain of almost six percentage points.

Moving from bellmouth-shaped to elliptical provided further improvement, namely a gain of another 2.2 percentage points. The difference between the two shapes is that the sides are straight (bellmouth) or convex (elliptical). The elliptical shape provides for a pattern that makes for a gradual change in velocity that minimizes any loss in the intake tube.

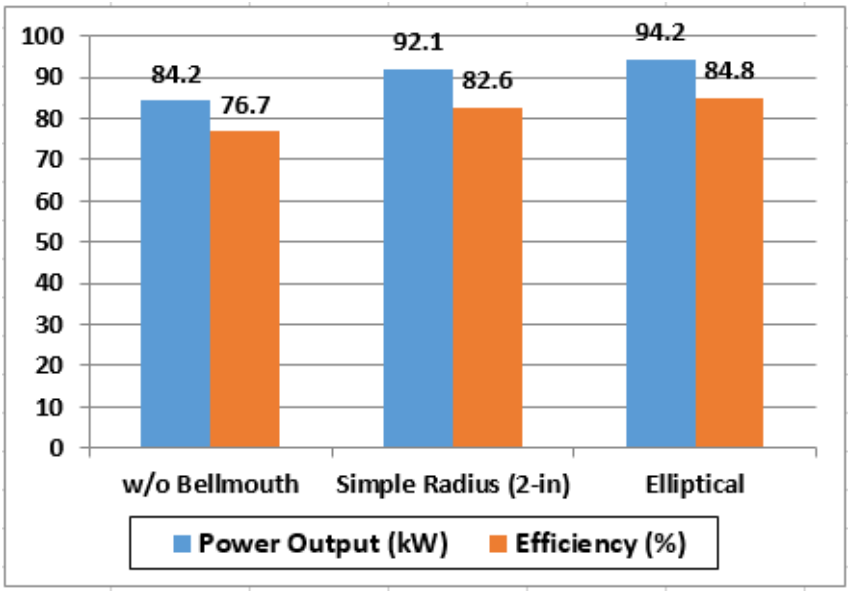

Figure 3-44: Comparison of shapes for the intake tube

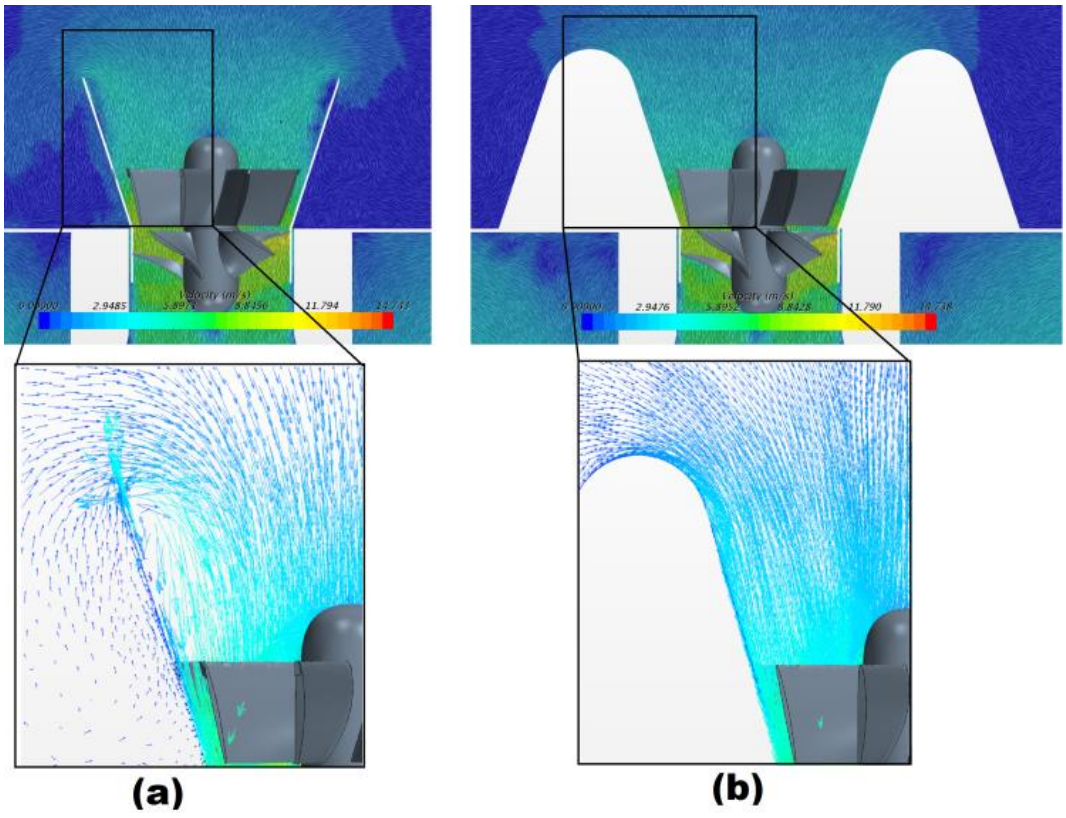

Figure 3-45: Velocity pattern of the flow at the intake tube wall (a) without bellmouth (b) with bellmouth 10-in simple radius; Color scale is 0 to 15 m/s

The important factor appears to be to avoid the sharp edge at the entrance of the intake tube. Considering the bellmouth, changing the radius of the edge had, in fact, relatively little

impact on the improvement over the straight intake tube option, such that even a relatively small radius was useful in obtaining this improvement. The outcome is evident from Figure 3-46 and Figure 3-47, where the radius of curvature for tubes (radius defined in Figure 3-29) is varied from zero to 16 inches. Any radii provide efficiencies in the 81-82% range, as opposed to 78% for the intake tube. A similar trend line can be noticed for the impact on the draft tube, in addition to that the efficiency can go up to almost 90% where the radius is between 8 - 12 inches.

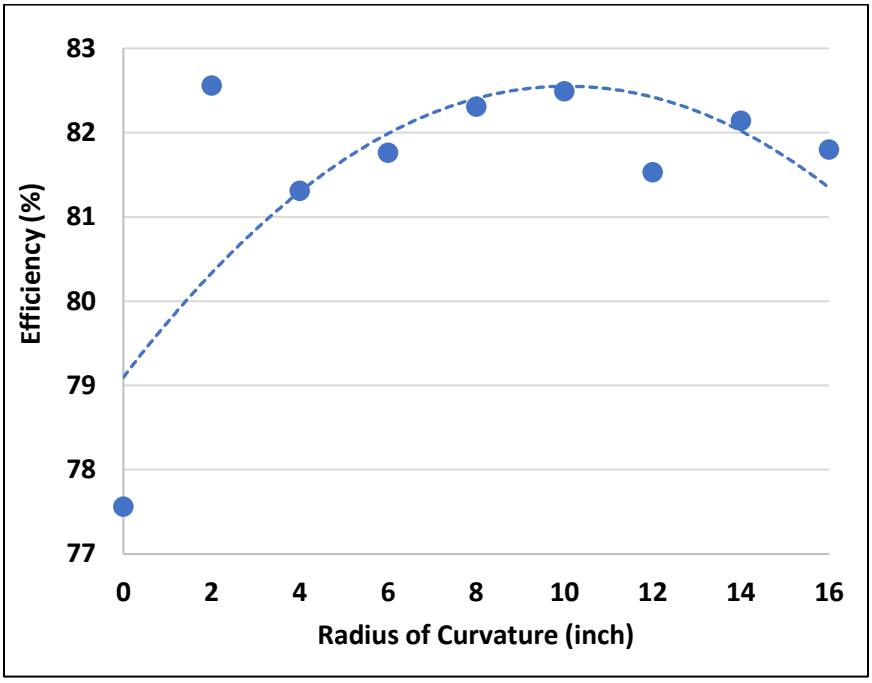

Figure 3-46: Impact of edge radius (radius of curvature) in the bellmouth simple radius intake tube on the efficiency

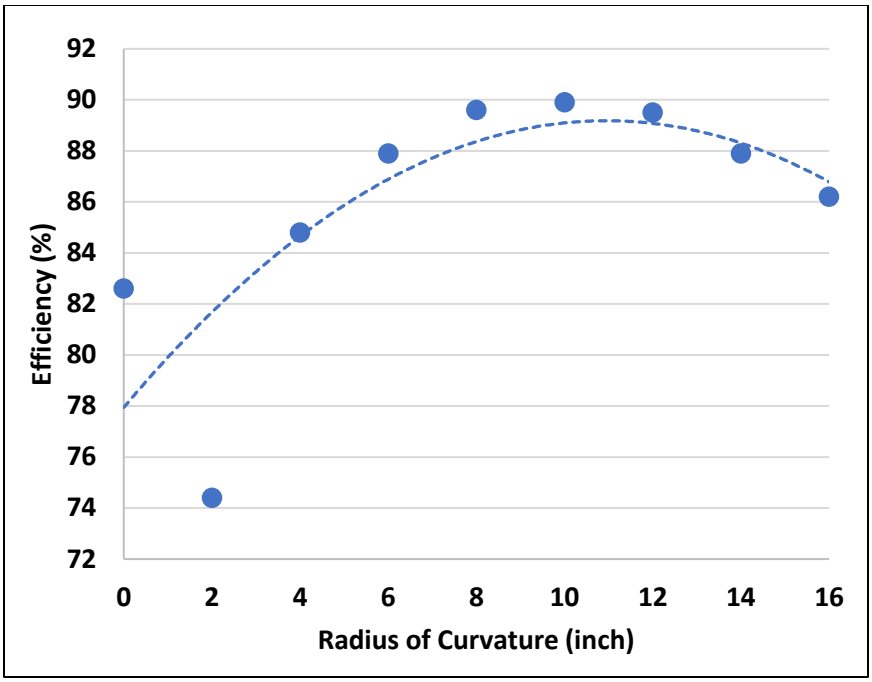

Figure 3-47: Impact of edge radius (radius of curvature) in the bellmouth simple radius draft tube on the efficiency

Correspondingly, the elliptical profile for the straight intake tube provided about 9% to the efficiency. Three trials were investigated for the design of the elliptical intake tube by changing the length and the width arbitrary. Based on the results shown in Figure 3-48, the length is an independent parameter here as for both second (50/88) and third (50/60) cases, the length of the tube was 50 inches and the two cases have 4% difference in efficiency, and that was only due to the change in the width of the tube from 88 to 60 inches. The shortest the width of the tube the higher the efficiency; and that can be referred to the increase in velocity of the flow as the short-width tubes have a steeper wall.

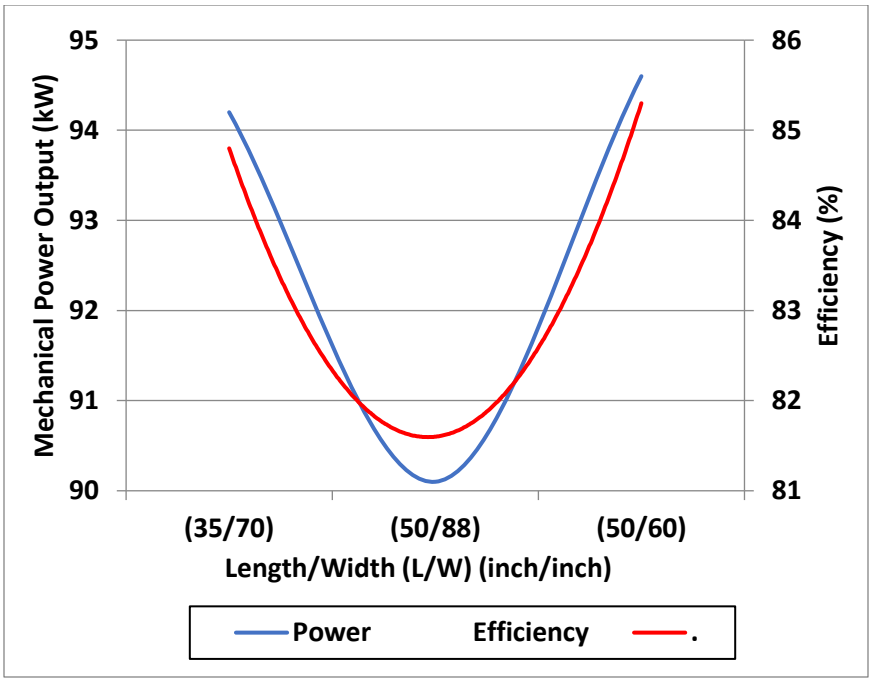

Figure 3-48: Impact of three configurations of the elliptical profile for the intake tube

3.4 Optimization of the Guide Vanes

The 7.6-cm system includes a 90-degree elbow just upstream of the turbine, see Fig. 17. Such an elbow causes pressure fluctuations and eddies due to the sudden change in flow direction when the flow enters the elbow. Of course, the best is to avoid such discontinuities, but this is not always practical. Instead, keeping in mind that one aspect of this work is aimed at investigating how 3D printing techniques can be put to beneficial use in the context of small hydropower, it was decided to see if more complex shapes could be employed to mitigate the issues brought by the presence of the elbow, for situations where such elbows cannot be avoided. 3D printing indeed makes it possible to construct parts with shapes that are impractical or too expensive by traditional manufacturing methods. Accordingly, four designs with guide vanes in the elbow were studied. The designs are shown in Figure 3-49.

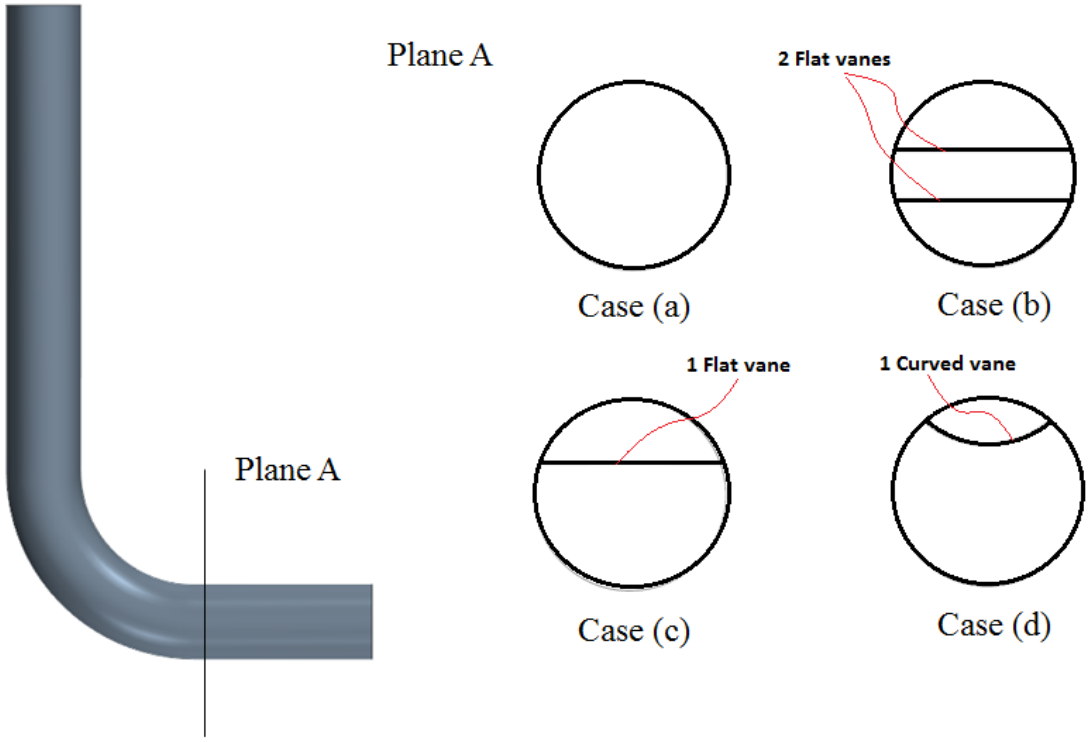

Figure 3-49: Cross-sectional view for the guide vane/vanes in the elbow. Case (a): Without guide vane. Case (b): Two flat guide vanes. Case (c): One flat guide vane. Case (d): One curved guide vane.

Figure 3-50 illustrates the ability of the guide vanes to straighten the flow in the elbow, in addition to redistributing the pressure gradient and decreasing pressure fluctuations and flow eddies. On the other hand, there is an energy loss due to the friction between the flow and the two guide vanes, with a partial flow blockage. Some optimization is thus necessary if improvements are to be obtained. Case (c) was, therefore, studied with only one flat vane as a compromise. Other elements to consider are the position and the shape of the vane in the elbow.

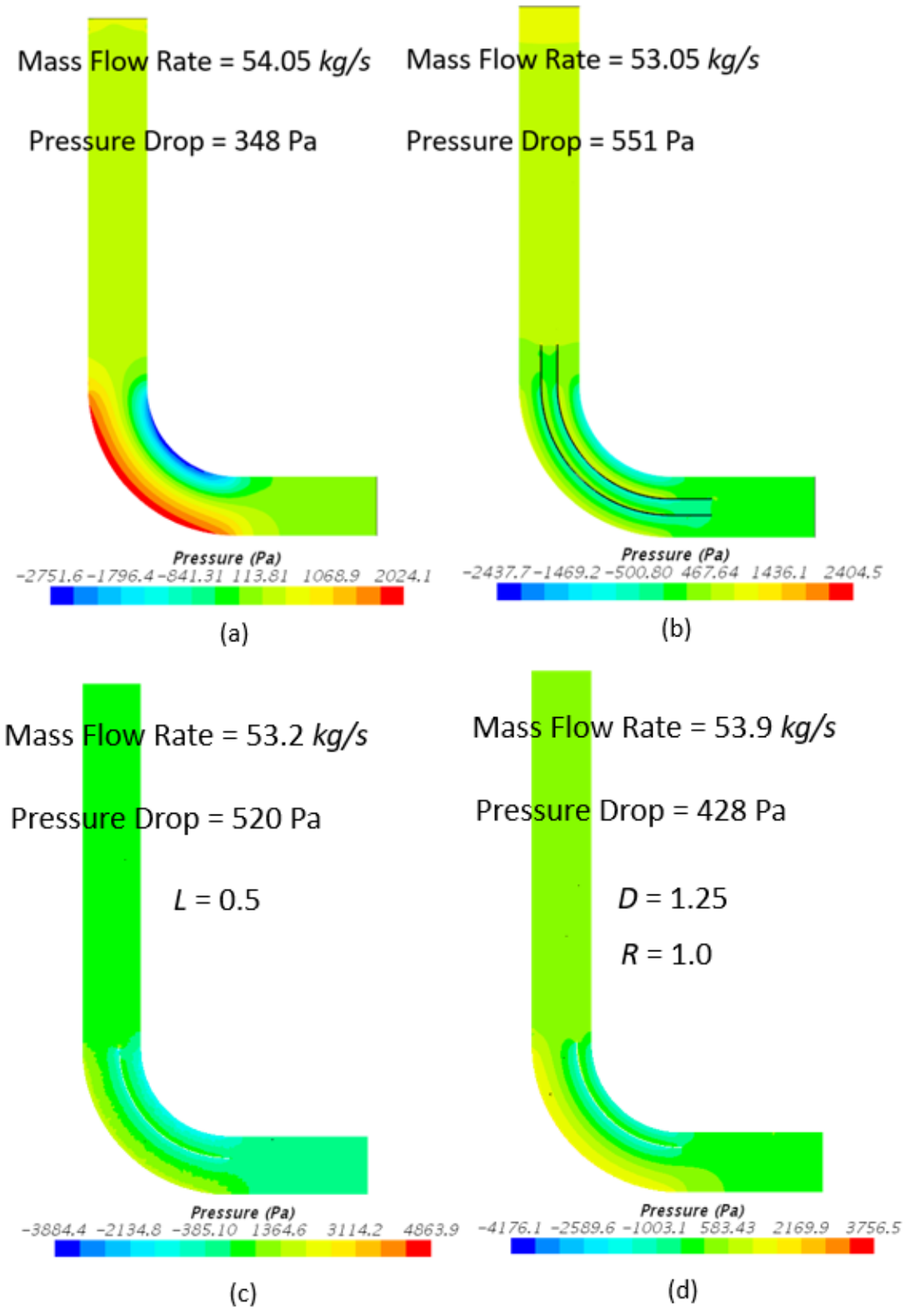

Figure 3-50: Pressure distribution (a) without guide vanes (b) with 2 flat guide vanes (c) with one flat guide vane (d) with one curved guide vane

As far as position is concerned, a new dimensionless parameter (L) was defined to express the guide vane position concerning the center of the elbow:

$$L = \frac{r}{r_o} \qquad \text{Eq. 3-5}$$

where r is the distance between the guide vane and the center of the elbow, and r_o is the radius of the elbow, which is constant at 7.6 cm (3 in.) in this case. Also, the angle Θ is defined as a design parameter. It corresponds to the ending point of the guide vane, as shown in Figure 3-51. Concerning shape, a straight vane (case c) and a curved vane (case d) were investigated. For this purpose, two new different dimensionless parameters (R and D) were defined, as detailed in Figure 3-52 and Equations 3-6 and 3-7.

$$R = \frac{r_2}{r_1} \qquad \text{Eq. 3-6}$$

$$D = \frac{l_1}{r_1} \qquad \text{Eq. 3-7}$$

where r_1 is the radius of the elbow, r_2 is the radius of curvature for the guide vane and l_1 is the distance between the center of the elbow and the center of the curved vane's circle.

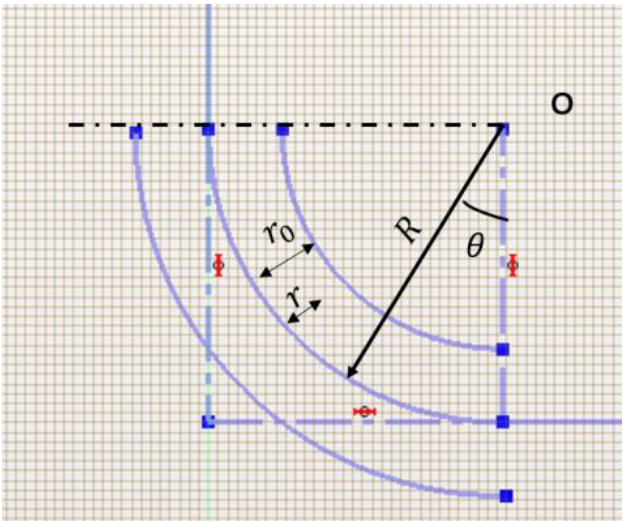

Figure 3-51: 2D sketch for the elbow with one flat guide vane

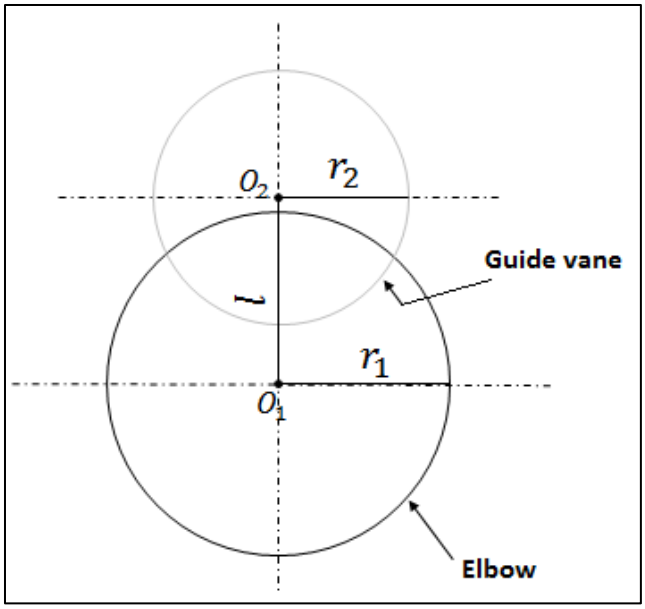

Figure 3-52: 2D sketch for the elbow and the curved guide vane

The objectives of the guide vanes design are to maximize the flow rate and minimize the pressure drop. Three values of Θ (30, 60, and 90 degrees) and three values of L (0.33, 0.50, and 0.67) were used for the flat guide vane. Also, computations were performed for two values of R (0.75 and 1.0) and three values of D (1.0, 1.25, and 1.5) for the curved guide vane. The results are shown in Figure 3-53 and Figure 3-54.

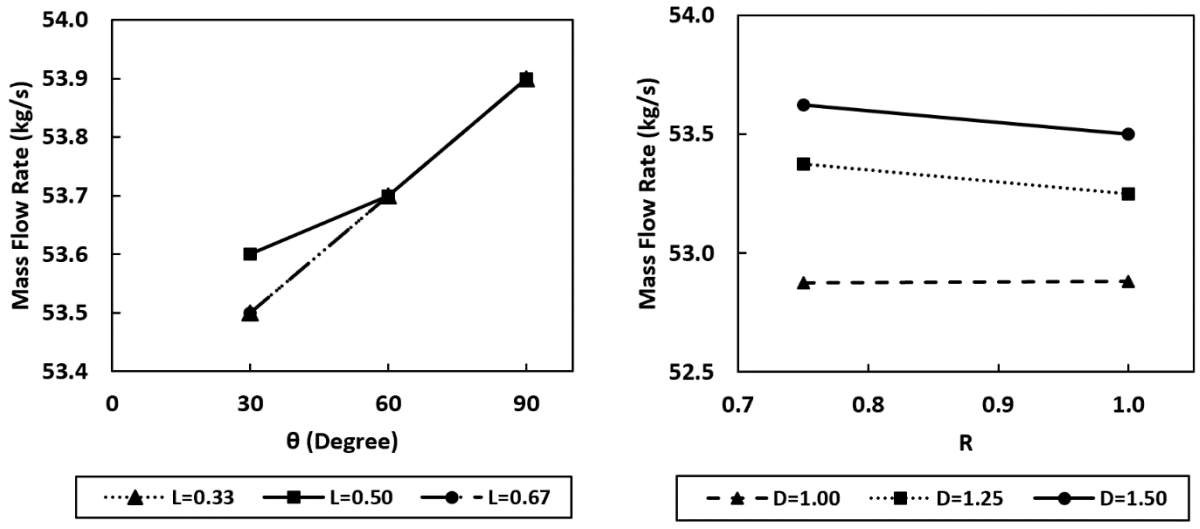

(a) **(b)**

Figure 3-53: Mass flow rate results for (a) the flat guide vane (b) the curved guide vane

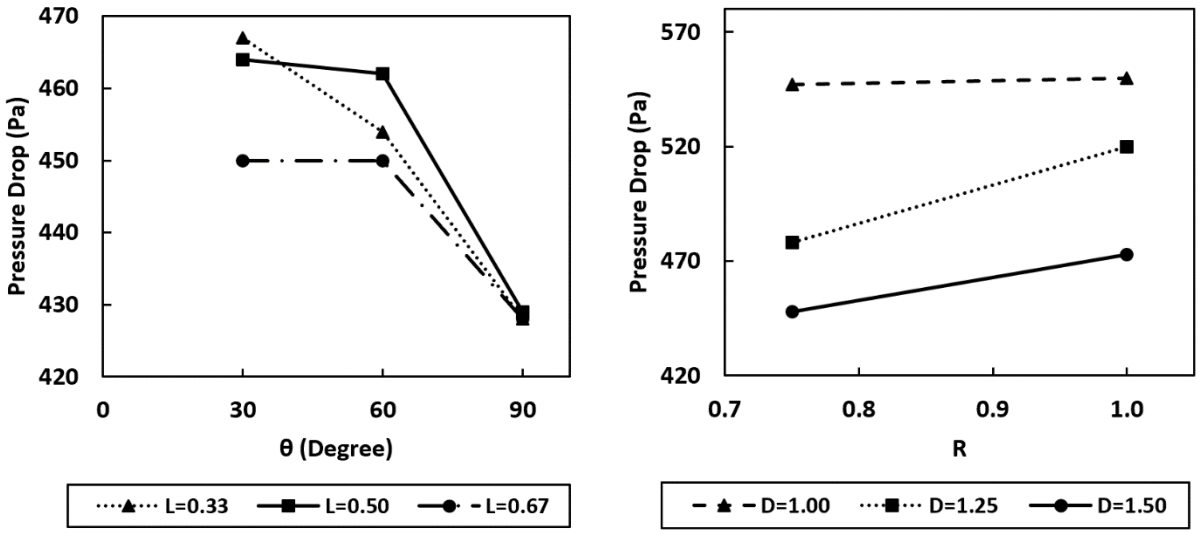

(a) **(b)**

Figure 3-54: Pressure drop results for (a) the flat guide vane (b) the curved guide vane

As shown in Figure 3-53 (a), the highest mass flow rate (53.9 kg/s) for the flat vane was obtained with Θ = 90 degrees, while changing L with this angle does not affect the flow rate. However, this is not the case when changing either D or R for the curved vane, as can be seen in Figure 3-53 (b). The maximum flow rate (about 53.6 kg/s) was obtained with the combination of R = 0.75 and D = 1.5.

Considering Figure 3-54 (a), the minimum pressure drop (427 Pa) for the flat guide vane was obtained with Θ = 90 degrees. The effect of L is almost negligible at this angle, but not so for 30 and 60 degrees. Correspondingly, as shown in Figure 3-54 (b), the pressure drop for the curved vane reaches a minimum value of about 450 Pa at the same amounts of R and D obtained for minimum flow rate, 0.75 and 1.5 respectively.

According to these different guide vane cases and regarding energy, the best choice is not to install any guide vane. However, another element needs to be considered, particularly for a hydro turbine, which is to operate continuously with minimum maintenance. The pressure fluctuations observed in the elbow could induce vibrations and cause turbine wear. If this is a concern, some

guide vanes can be implemented in the system, benefiting maintenance needs at the cost of a small energy loss due to the friction on vane surfaces.

Guide vanes were investigated to mitigate the negative impact of elbows in the water conduit ahead of the turbine, for situations where such conduit shapes are necessary. The study introduces several dimensionless parameters for the useful modeling of the guide vane design. The research indicates the advantage of guide vanes regarding durability, but at a cost regarding energy extraction and system efficiency.

3.5 Evaluating the Performance of the Turbine (Baseline Design with Shaft)

3.5.1 Introduction

The objective of the paper is to study the design and optimization of Kaplan hydro turbines for a very low head (less than 3 meters), with a particular emphasis on the use of rim-drive electrical generators. The work is based on an experimental setup and Computation Fluid Dynamics (CFD) analysis of a variety of design parameters for maximum output power and efficiency. Two designs are presented in the paper. One is a 90-cm (35-inch) diameter vertical-oriented Kaplan hydro turbine systems as an intended product capable of generating over 50 kW. The other is a smaller, 7.6-cm (3-inch) diameter horizontal-oriented system for prototyping and laboratory verification. Both are analyzed through CFD based on Large Eddy Simulation (LES) of transient turbulence. Specific design for the runner and the stator, intake tube shape, as well as guide vanes upstream of the turbine, were studied to get the most from the available head. The intent is to use 3D-printing manufacturing techniques, which may offer original design opportunities as well as the possibility of turbine and water conduit design customization as a function of the head and flow available from a specific site.

Based on the CFD analysis, the 7.6-cm diameter system achieved the highest power output and the maximum efficiency at the rotational speed range of 1500-2000 rpm, while for the experimental testing, the optimum rotational speed range was 1000-1500 rpm. Because of the mismatch between CFD and experimental results, the CFD results were correlated due to the presence of air and friction. Moreover, error and uncertainty analysis was presented for both methods. For the 90-cm case, the optimum performance was found at a rotational speed of around 350 rpm according to the CFD results.

3.5.2 Methodology

For this project, the propeller type (Kaplan) axial flow hydro turbine configuration was selected based on the maximum low-head available [103]. Such axial flow turbines are applicable with either horizontal or vertical orientation. The 7.6-cm system was designed horizontal, while the 90-cm is vertical. Kaplan runners can feature fixed or adjustable blades. With low cost being a requirement for this application, fixed-blade Kaplan turbines were exclusively investigated. Figure 3-55 shows the stator (a), the runner (b), and the runner with the rim-generator ring (c) employed in this research.

3.5.2.1 *Experimental Setup*

An experimental setup was developed in a laboratory managed by the University of Wisconsin-Milwaukee in Milwaukee's Global Water Center. It is a system with 2.7 m of the head and a maximum flow rate of 28 l/s (1.00 CFS). The turbine runner outside diameter was set at 7.6 cm, capable of a mechanical output on the order of 400 W. The setup is shown in Figure 3-6. It was used as a testbed for the computational tools for various ideas being considered and for validation.

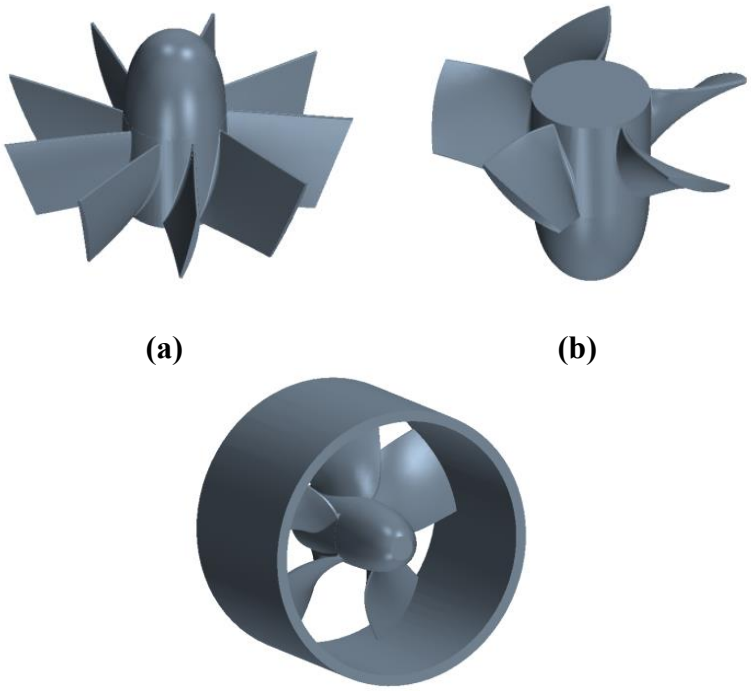

(a) **(b)**

(c)

Figure 3-55: Turbine model. (a) Stator (b) Runner (c) Runner attached to rim-generator ring

The setup included a tank to provide a head of up to 3 m (10 ft), a pump to circulate the water, two flow meters (one before the tank and one in the overflow pipe), and a turbine. The turbine had an embedded steel ring around the runner to emulate the electrical generator rotor. At this stage, the runner also had a shaft for measurement of speed and torque. As shown in Figure 3-9, this shaft was connected to a torque-meter and a DC generator. Electric power is dissipated in a resistive load bank. An electromagnetic flow-meter measured the flow rate.

The literature conjugated with the same project conditions led to the conclusion that a combination of a nine-vane stator paired with a five-blade runner provided an efficient turbine while also providing sufficient flow to power the system [154]. Also, the blade thickness fraction should be 0.07, and the tip thickness fraction should be 0.03 to provide a safety factor of 2 with the materials available for 3D printing.

The turbine includes a 9-mm thick steel ring to emulate the electrical generator rotor, which will eventually be made of permanent magnets mounted on a steel ring. The computations led to an estimation that an eventual generator rotor would be made of a 5.5-mm steel ring supporting 3.5-mm thick magnets, with a length of 10 mm. Such a generator should be able to absorb 2 N.m and generate 1 kW (electrical, assuming a generator efficiency of 88%) at 5,400 rpm. Since magnets have a specific mass close to that of steel, doing the experiments with a dummy rotor of 9-mm thickness was realistic regarding the inertia and mechanical integrity of the rotor-runner assembly.

Figure 3-56 (a) shows the tested turbine runner with a slot to slide the electrical generator rotor in place. This slot is integral to the runner, manufactured by 3D printing in a single step. Figure 3-56 (c) shows a turbine runner/rim assembly in the process of being 3D printed (the different color is immaterial - several units were built during the project from the various source material). Figure 3-56 (b) shows both turbine stator and runner before assembly.

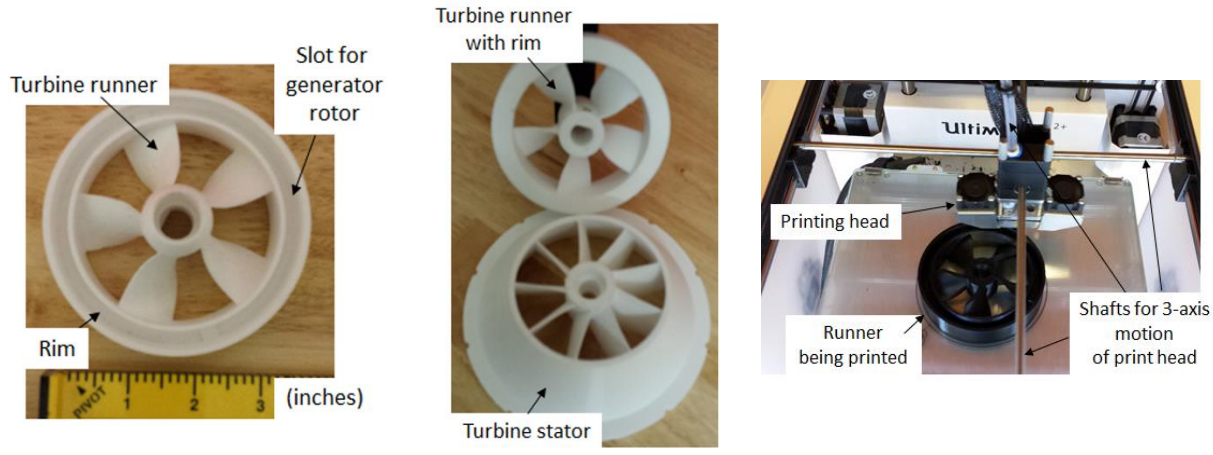

(a) (b) (c)

Figure 3-56: Turbine prototype made from 3D printing process. (a) Runner (b) Runner and stator (c) Runner being manufactured

3.5.2.2 *Computational Fluid Dynamics (CFD) Development*

With the development of numerical simulation, the accurate prediction of the flow behavior in the turbine has become easier. The simulation technique is particularly needed in this study where the object is the design of a turbomachine (hydro turbine) with rotational motion and turbulent flow. Still, experimental studies are required to corroborate the results, hence the work at a reduced size.

Figure 3-57 shows the simulation model for the horizontal 7.6-cm hydro turbine system, which includes a cylindrical tank (0.75 m^3) as a reservoir, with 15-cm (6-inch) diameter pipes. The figure also shows the location and orientation of the stator/runner set in the system. Figure 3-58 shows the simulation model for the vertical 90-cm hydro turbine system.

The first system includes a 7.6-cm diameter runner with a horizontal orientation, operating at rotational speeds of 1000-4500 rpm and with a flow rate of around 28 l/s (1.0 CFS). This system is estimated to be able to generate electrical power below 700 W. The second system features a 90-cm diameter runner with a vertical orientation, operating at rotational speeds of 200-500 rpm and flow rates in the range of 3400-4250 l/s (120-150 CFS). The objective of this study is to exceed 50 kW electrical output power with this system.

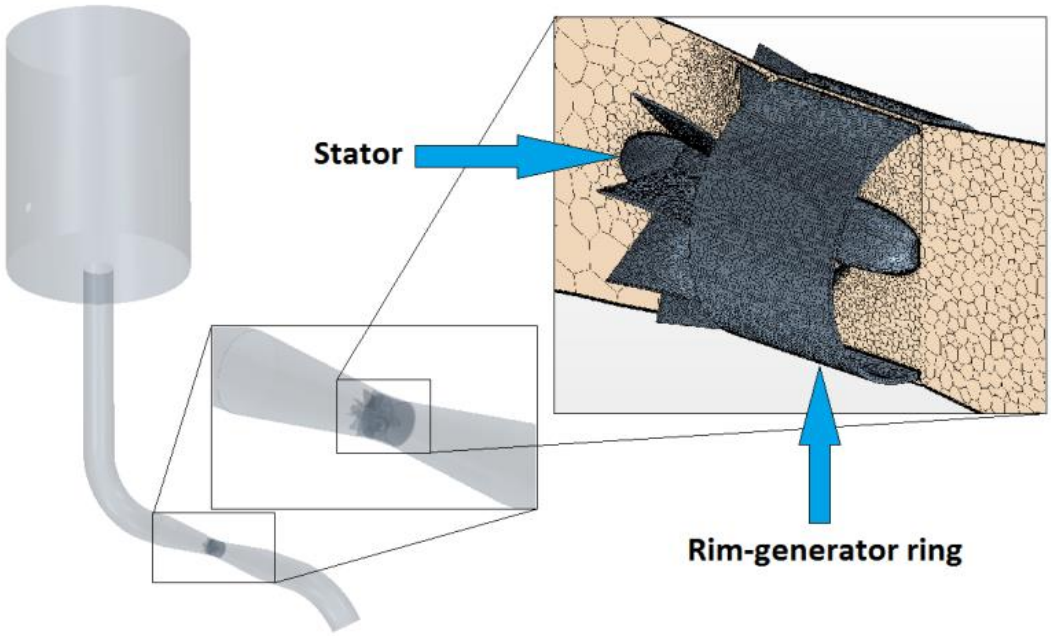

Figure 3-57: Simulation model, 7.6-cm hydro turbine system

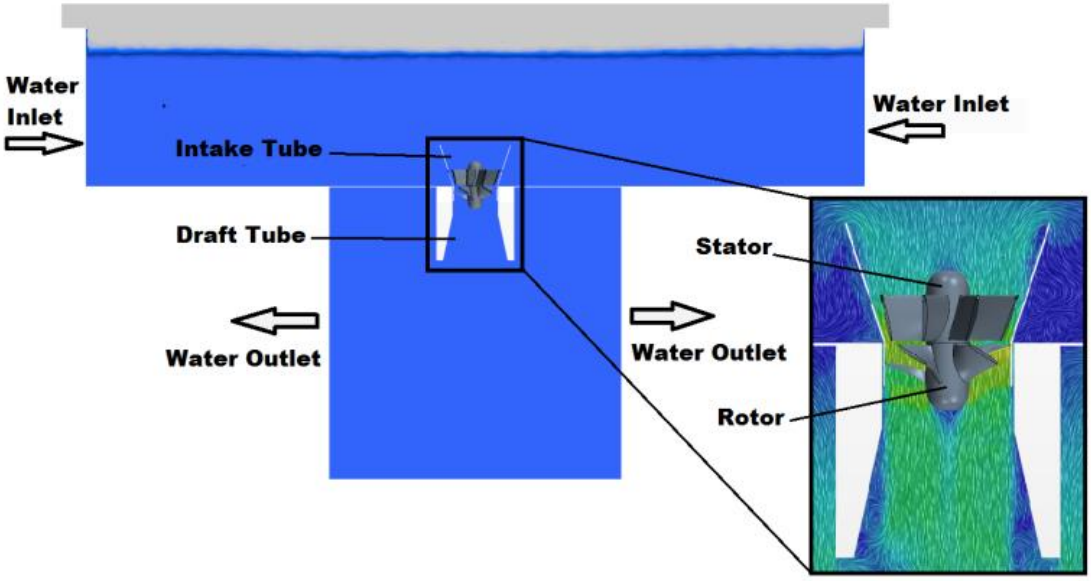

Figure 3-58: Simulation model, 35-inch hydro turbine system

For both cases, the flow rates, rotational speeds, and intake tube (nozzle) and draft tube (diffuser) geometry designs were investigated. Outputs were mechanical power and efficiency. Five different intake tube angles (20, 25, 30, 35, and 40 degrees) and two draft tube angles (12 and

18 degrees) were studied in this paper. Also, a study was conducted for the smaller system of including guide vanes upstream of the turbine.

3.5.2.3 *Simulation Approach*

In hydro turbine systems, large-scale and small-scale eddies are generated due to turbulence in the flow resulting from the high swirl in the rotating part. The simulation must capture these. Navier-Stokes (N-S) equations have to be augmented to include terms of random character, as is done, for instance, in Reynolds's Averaged Navier-Stokes (RANS) equations which are the sum of the averaged component and fluctuation components.

For this study, the CFD approach is based on Large Eddy Simulation (LES), where LES is more accurate than the Unsteady Reynolds Average Navier-Stokes (URANS) approach [135], [155]. Large Eddy Simulation (LES) is a natively transient technique that solves large-scale turbulence and at the same time models the small-scale motions. On a large scale, N-S equations are used while at a small scale, subgrid-scale models (SGS) are employed. LES usually uses either a Smagorinsky or wall-adapting local-eddy (WALE) as an SGS to compute the turbulent viscosity.

The WALE SGS employs an algebraic formulation to model the subgrid-scale stresses, while Smagorinsky SGS is based on a mixed length hypothesis [156]. The Smagorinsky model is simple and not computationally extensive, but there is a limitation due to the damping effects close to the walls; hence a damping function is needed for the accurate simulation of wall-bounded calculations [157]. Altogether, WALE is the simplest method, with better performance and more precise scaling near the wall without damping effects [136]. However, LES is the best model for predicting the turbulent flow behavior at the cost of extensive computation. LES was used in this study, an approach made possible by access to the University of Wisconsin-Milwaukee high performance computing cluster.

As an implicit unsteady simulation model, a time step of 0.001 seconds was selected along with the whole solution duration with first-order solution accuracy for temporal discretization. This approach leads the simulation to stability in reasonable computational time compared to a second-order solution.

The theoretical power equation for a water stream can be calculated as follows. The formulation sets the systems boundary conditions and makes it possible to verify the results regarding power and efficiency [152]:

$$P = \eta \times \rho \times g \times H \times Q \qquad \text{Eq. 3-8}$$

Where;

P: Power (W)

η: Efficiency of the turbine (%)

ρ: Density of the water (kg/m^3)

g: Gravitational acceleration (m/s^2)

H: Head of water (m)

Q: Flow rate through the turbine (m^3/s)

The use of two different modeling scales for the hydraulic system with variables like head, flow rate, rotational speed, diameter, and power requires a computational bridge between the two. The modeling is based on the affinity laws (similarity laws). Such laws should be considered for the estimation, and the comparison between the two systems and the most relevant law based on the given variables in this study is [158], [159]:

$$\Pi_{Prototype} = \Pi_{Model} \qquad \text{Eq. 3-9}$$

$$\frac{P_p}{\rho_p D_p^5 N_p^3} = \frac{P_m}{\rho_m D_m^5 N_m^3} \qquad \text{Eq. 3-10}$$

3.5.3 Results

3.5.3.1 *Mesh Independent Study*

The first step in the study was to develop a mesh independent model. To that effect, three different polyhedral mesh setups of 0.8, 1.5, and 4.4 million cells were exercised (for the smaller 7.6 cm system), and details of these systems are shown in Table 3-9. Figure 3-59 shows the cell sizes for each setup. The performance comparison was judged based on the mass flow rate and power output from the turbine.

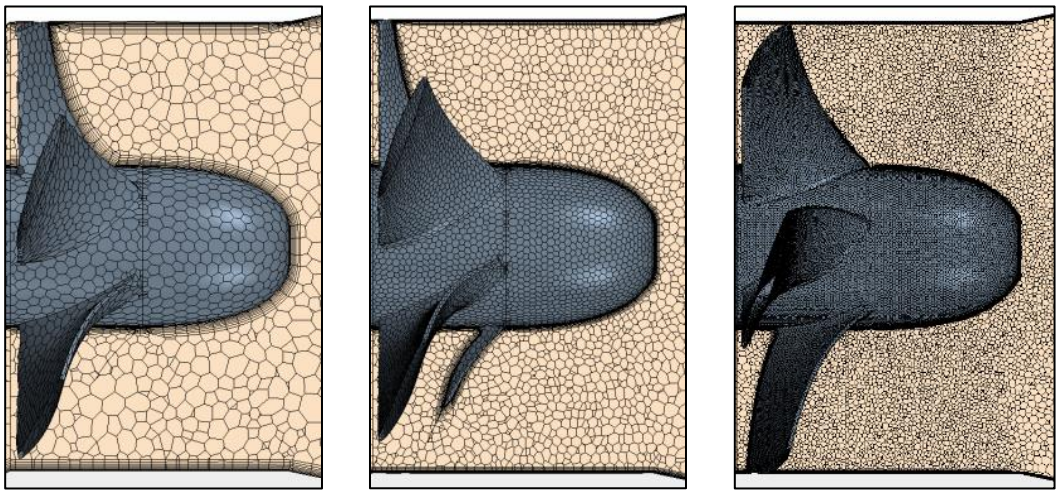

(a) (b) (c)

Figure 3-59: Mesh representation for the runner as (a) coarse mesh 0.8 M, (b) fine mesh 1.5 M and (c) very fine mesh 4.4 M

Table 3-9: Three mesh setups for the 7.6-cm system

Number of Cells	**0.8 Million**	**1.5 Million**	**4.4 Million**
Computational Time	1.0x	1.9x	5.5x
Simulation Detail	Coarse	Fine	Very Fine

Based on the results for both the power output and the flow rate, shown in Figure 3-60 and Figure 3-61, the difference between 0.8 million and 1.5 million setups is about 6.4% and 6.0% in power output and flow rate respectively. While the difference between 1.5 million and 4.4 million settings for the same perspective is 10.8% and 2.3%, respectively, it could be noticed here that

both 0.8 million and 4.4 million setups have higher values for both the power output and the flow rate. In the end, the 1.5 million cell setup was used for both the 7.6-cm and 90-cm systems simulations to provide an adequate balance between simulation resolution and computational time. Also, eight prism layers were used to keep the range of the first layer (Wall y^+) value between 0 and 5 as shown in Figure 3-62, since this is considered as an indicator for the accuracy of the results.

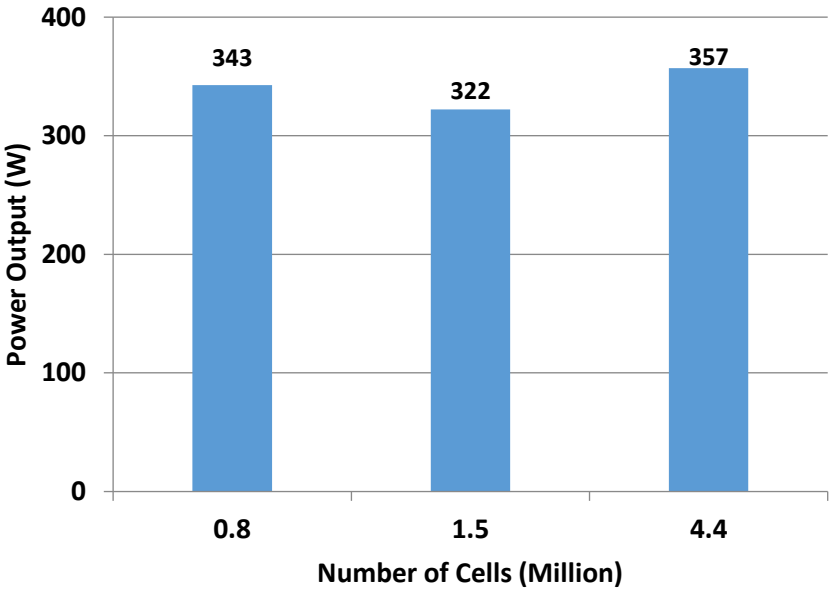

Figure 3-60: Mesh comparison in term of power output

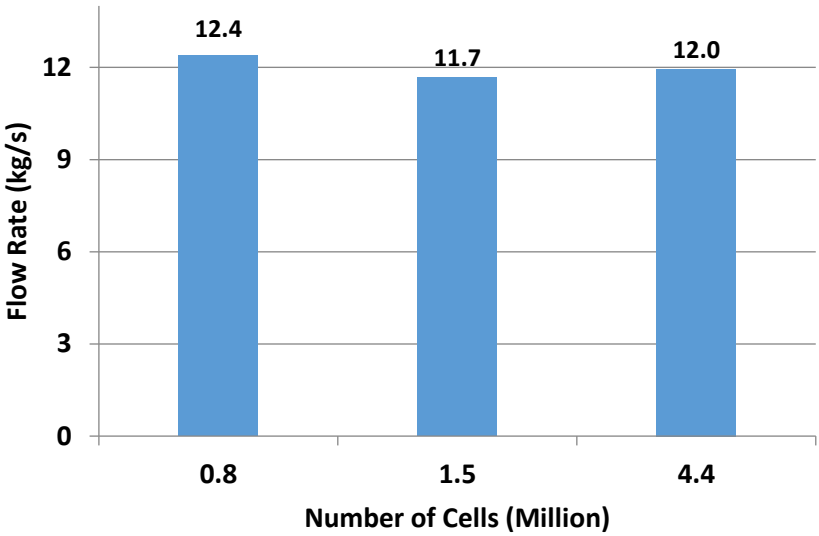

Figure 3-61: Mesh comparison in term of flow rate

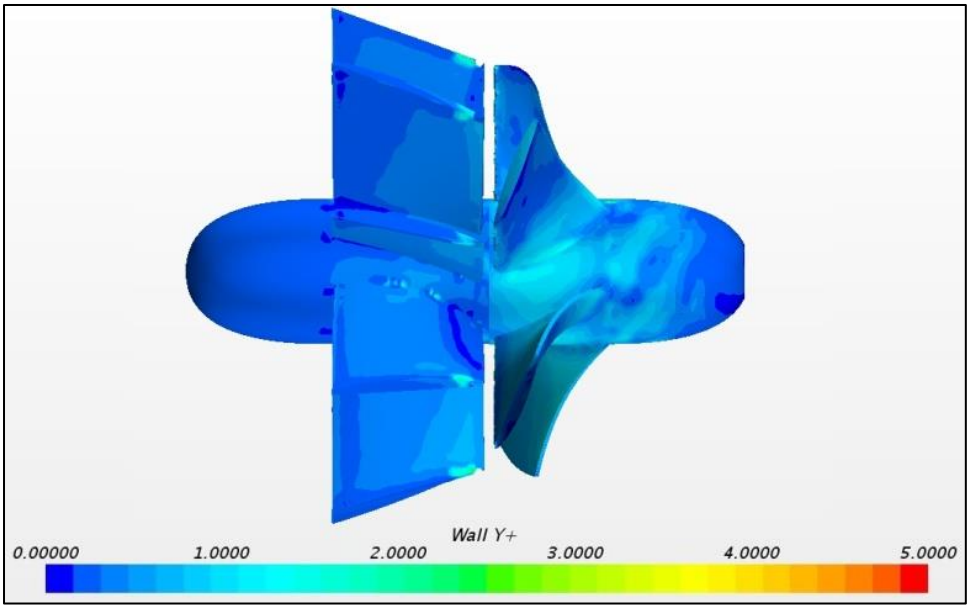

Figure 3-62: Wall y^+ values for the runner and the stator

3.5.3.2 *Test Data*

As with any other turbomachine, a hydro turbine can work at a variety of rotational speeds, depending on the design parameters of the turbine and conditions of the system. Correspondingly, the 7.6-cm turbine was tested (experiment and CFD) over a range of rotational speeds between 1000 rpm to 4000 rpm, while the 90-cm turbine was tested (CFD only) between 200 rpm to 500 rpm.

3.5.3.2.1 Initial Data

The 7.6-cm turbine was tested under two conditions, one at 2.6 m (8.5 ft) of the head and the other one at 2.0 m (6.7 ft) with the turbine located 0.2 m (0.7 ft) from tailrace in both cases as shown in Figure 3-63. The initial experimental results compared to CFD for the 7.6-cm are shown in Figure 3-64 (a) (2.6 m head) and Figure 3-64 (b) (2.0 m head). Figure 3-65 shows the turbine system efficiency comparison for both conditions. The CFD results for the 90-cm turbine are shown in Figure 3-66.

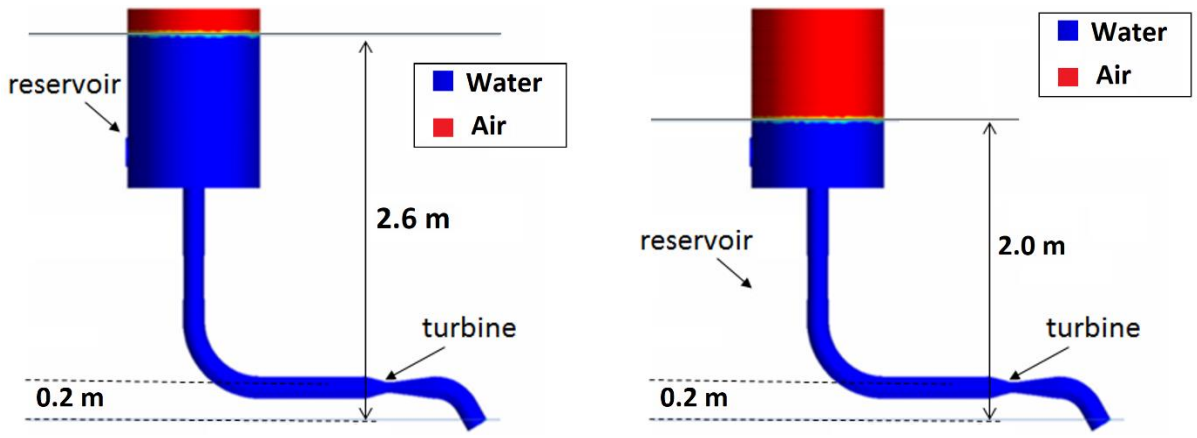

(a) **(b)**

Figure 3-63: The CFD setup (a) 2.6 m of head (b) 2.0 m of head

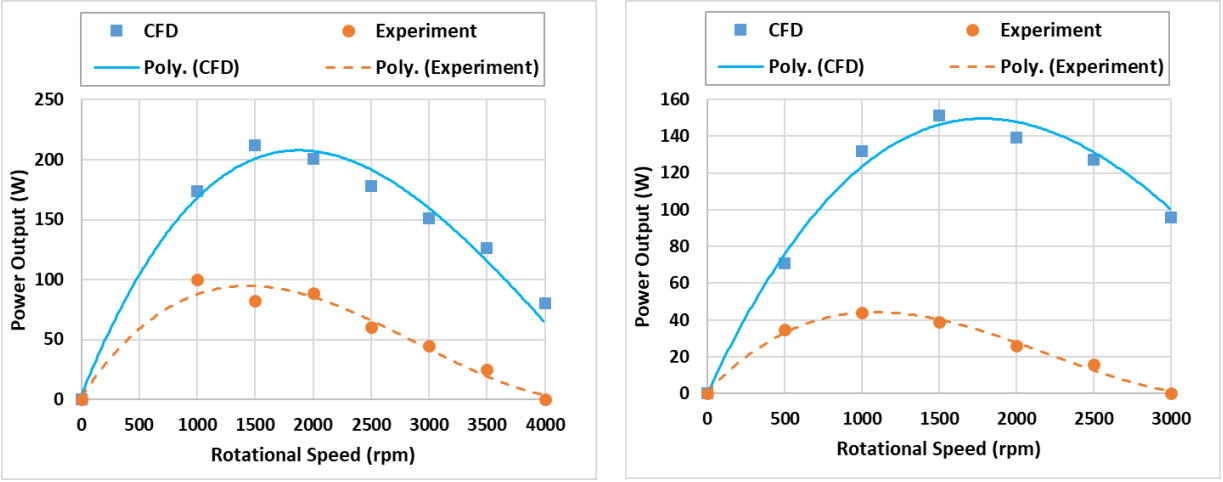

(a) **(b)**

Figure 3-64: Characteristic curve (Power output) of the 7.6-cm turbine (a) 2.6 m of head (b) 2.0 m of head

It can be noticed from Figure 3-64 (a) that the maximum power output of the CFD results (around 200 W) occurs at the rotational speed range of 1500-2000 rpm for the 7.6-cm hydro turbine system at 2.6 m of the head, while the maximum power output (approximately 150 W) at 2.0 m of the head occurs at the same range of 1500-2000 rpm as shown in Figure 3-64 (b), making the aforementioned range the optimum operating range for the 7.6-cm turbine, computationally. Herein, speeds over 3000 rpm (even 2500 rpm) should be avoided as power output approaches zero. The initial experimental maximum power output of 100 W recorded at 1000 rpm (2.6 m

head) and about 45 W in the range of 1000-1500 rpm at 2.0 m of the head. The aforementioned experimental results contradicted the CFD results regarding the maximum power output extracted from the turbine and the operational rotational speeds. A justification of this disagreement is discussed in this study in the following sections regarding the presence of air and friction estimation.

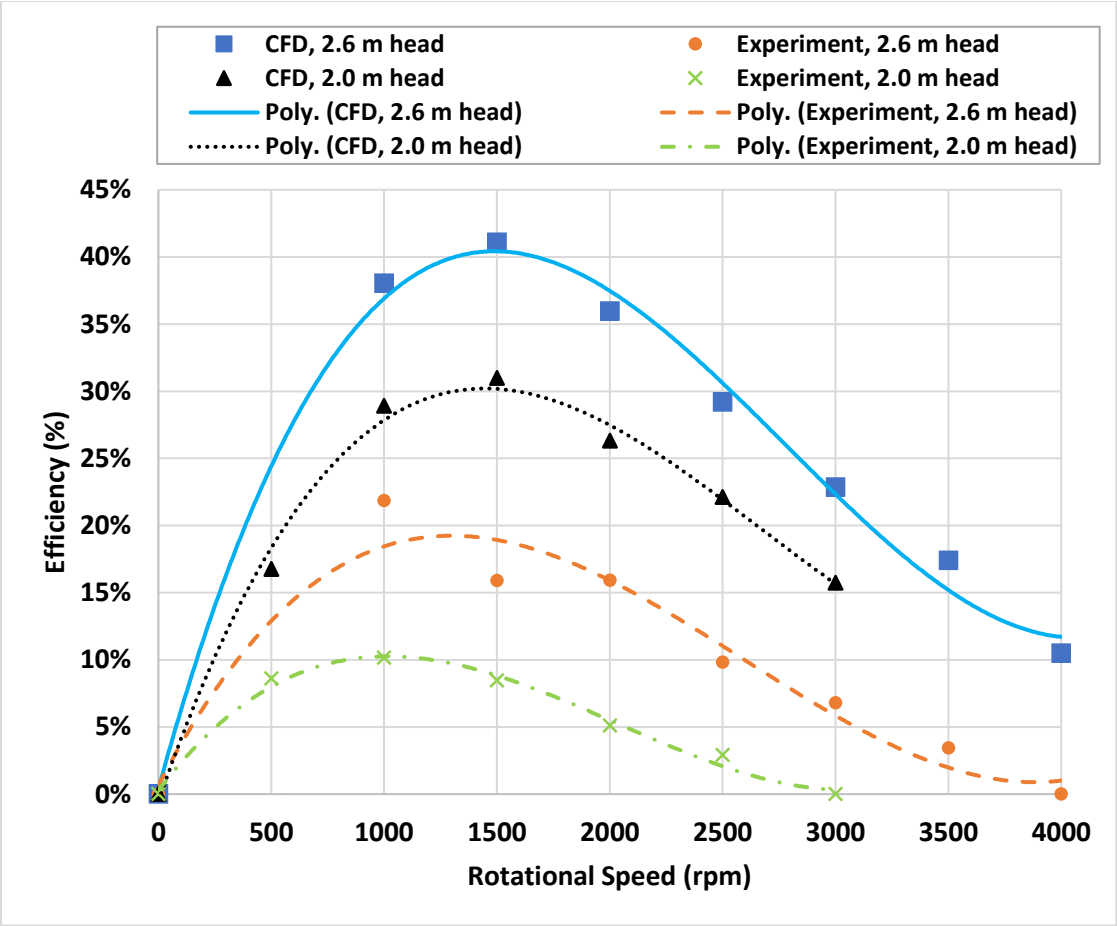

Figure 3-65: Efficiency versus speed for the 7.6-cm system at 2.6 m and 2.0 m of head

A similar pattern emerges for the 90-cm hydro turbine system (Figure 3-66), with the maximum power (about 84 kW) achieved around 300 rpm rotational speed, and very low output obtained beyond 450 rpm.

Efficiency curves tend to follow power curves, generally, with a peak over some speed range, followed by a steep decline at higher speeds. However, peak efficiency does not coincide

precisely with maximum power output. For instance, for the 90-cm system, peak power is reached at 300 rpm and peak efficiency at a slightly lower speed; 250 rpm (see Figure 3-66). All this will be a matter to consider when designing the electrical generator control system, such that either maximum power is extracted from the water, or at the best efficiency level, depending on circumstances.

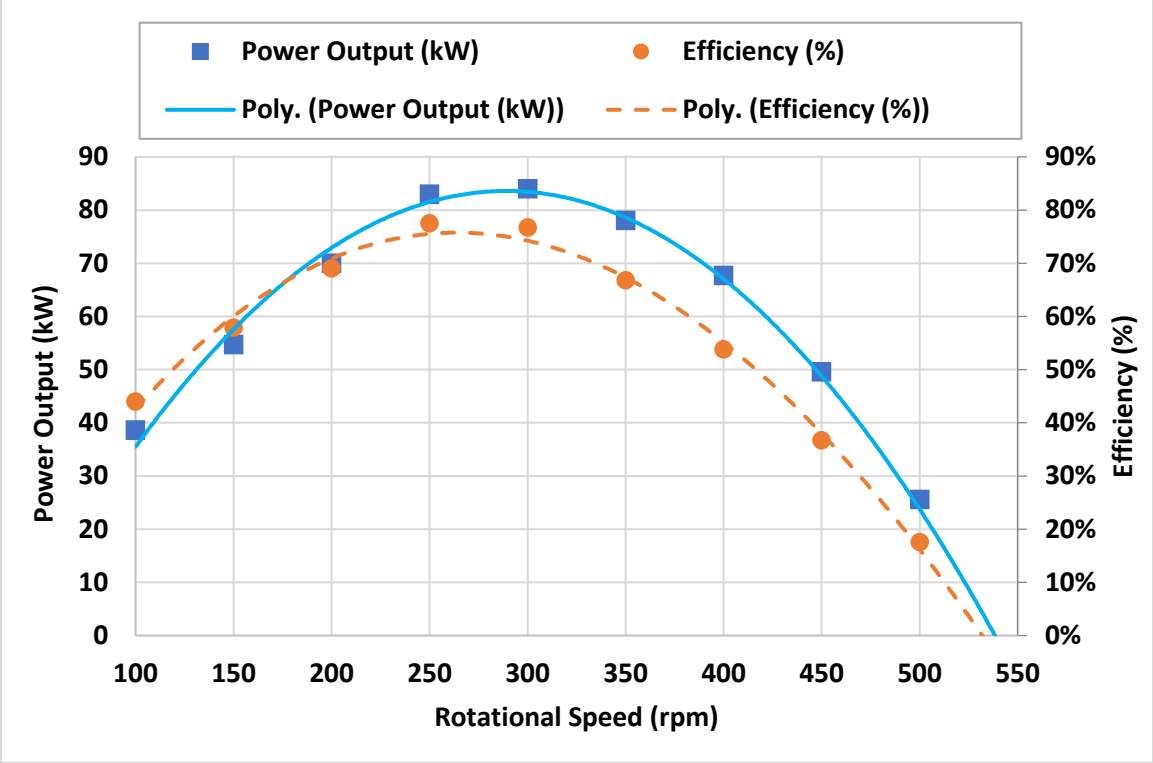

Figure 3-66: Power output and efficiency versus speed for the 90-cm system

3.5.3.2.2 Presence of Air

Figure 3-67 shows the characteristic curve of the mass flow rate of the 7.6-cm Kaplan turbine. The flow rate observed during the tests, lower than CFD where no air is present, is consistent with the presence of a significant proportion of air in the system. Both the experimental and calculated flow rates are linear with speed and can be approximated from the curves by:

$$f_c = 0.003\ N + 14.93 \qquad \text{Eq. 3-11}$$

$$f_e = 0.0027\ N + 14.20 \qquad \text{Eq. 3-12}$$

where N is the rotational speed, and fc and fe are the calculated and experimental flow rates, respectively. Defining the coefficient C_r as the ratio of mass flow rate with the ideal condition (CFD) and mass flow rate from the experiment:

$$C_r = \frac{f_e}{f_c} \qquad \text{Eq. 3-13}$$

and assuming the power output is proportional to the mass flow rate, we can obtain a corrected CFD power output, W_b, as taking into account the effect of air in the system. The correction is expressed in the equation below, and the result is plotted in Figure 3-68:

$$W_b = C_r \times W_c \qquad \text{Eq. 3-14}$$

where W_c is the ideal CFD power output.

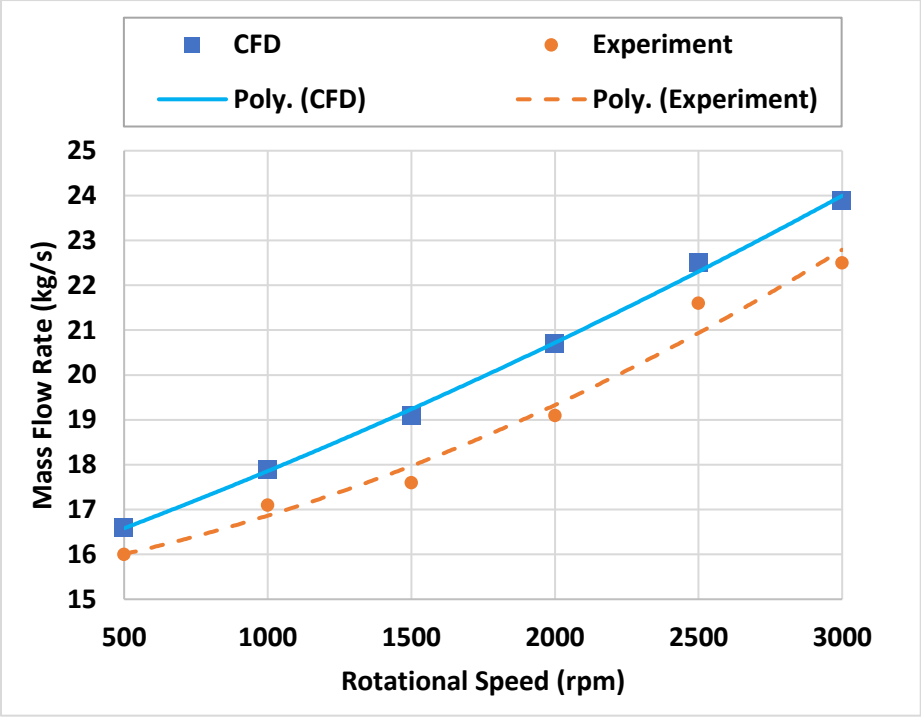

Figure 3-67: Mass flow rate versus speed for the 7.6-cm system at 2.0 m of head

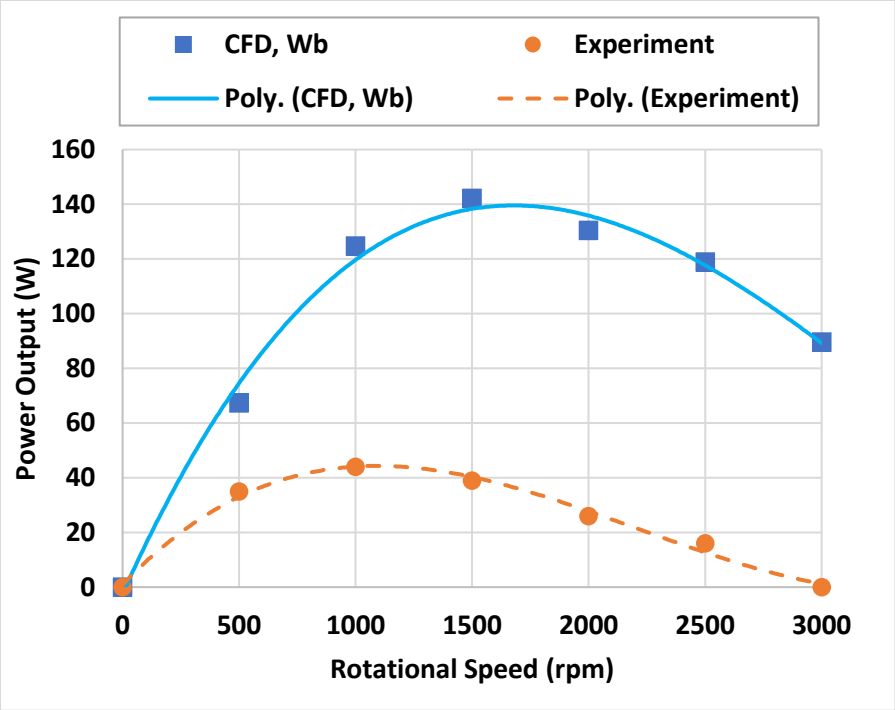

Figure 3-68: Comparison CFD-tests, with CFD corrected for the presence of air (W_b)

3.5.3.2.3 Friction Estimation

The data also show evidence of friction, perhaps exacerbated by the vibrations induced by the air in the system. Assuming the friction force F(N) is constant, the energy loss is defined as:

$$E_{loss} = F \times \left(\frac{N}{60} 2\pi \times l\right) \quad \text{Eq. 3-15}$$

where l(m) is the radius of the shaft (0.0079m), and N is the rotational speed per minute (rpm). The constant force F can be determined from the experimental point where there is no output, 3,000 rpm when friction dissipates all the energy. This is done by reading the CFD output (corrected for air), or $(Wb)_{3000rpm}$. From this, we can estimate the friction force F:

$$(w_b)_{3000rpm} = F \times (\frac{3000}{60} 2\pi \times 0.0079) \quad \text{Eq. 3-16}$$

$$F = 80.6\ N \quad \text{Eq. 3-17}$$

Figure 3-69 shows a much better correlation between calculations and tests. The remaining difference could be attributed to the water flow meter, which is less reliable in the presence of air.

Test results were initially far below CFD calculations. However, the difference can be explained by the presence of air in the system and friction. The presence of air could be reduced or eliminated with a redesign and would be expected to be less in a more extensive system. Friction is due mostly to the shaft, which is necessarily long to minimize the impact of the output elbow on flow, and relatively large in diameter compared to the small turbine. Although this could be improved, this nevertheless underscores the advantage of using a rim drive, since the shaft is eventually eliminated with no concern for an elbow after the turbine. Finally, with proper flow input and under the conditions set in the lab, a rim drive turbine should, therefore, be able to produce 250 W with a very low water head (2.0 m).

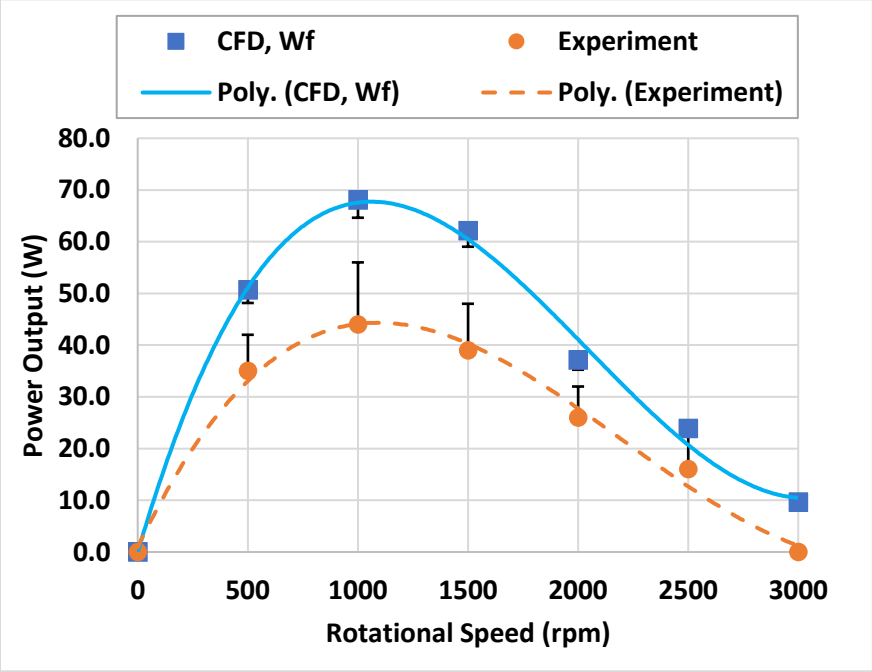

Figure 3-69: Comparison CFD-tests, with CFD corrected for presence of air and friction (W_f)

Another reason for the difference between CFD and experimental data is the uncertainty of measuring devices in the setup. Thus the uncertainty of the experimental data was estimated with a 95% confidence level, and it was represented in error bars, as shown in Figure 3-69. Both systematic and random errors were included in the uncertainty analysis. On the other hand, a fixed

error percentage of 5% was assumed for the CFD results due to some limitations in the CFD simulations, i.e. the mass of the shaft was not taken into account. Positive error bars were added to the experimental results, while negative bars considered for the CFD results to minimize the average difference percentage to 8% only.

Regarding the orientation of the turbine, the vertical 90-cm turbine exceeds the maximum efficiency of the horizontal 7.6-cm turbine by about 5%. However, this result cannot be generalized. It is expected that the use of an elbow upstream of the turbine in the 7.6-cm system may be the reason for the lower efficiency because of flow separation in the elbow which negatively impacts the kinetic energy of the water and reduces the pressure difference across the runner. The next section presents an investigation of this issue.

Chapter 4: Rim-drive Turbine Design and Performance

4.1 Introduction

The proposed research expands on these earlier results in various ways, particularly with the use of a rim-driven electrical generator similar in concept to recently introduced ship propellers [160]. It consists of a rotating ring around the outside of the runner blades. The generator stator is mounted outside the water conduit. This approach has some advantages: No shaft or other part is going from inside the water to the outside. The system has a benefit as a compact unit for easy installation, including retrofits in existing plants, maintenance, and eventual replacement. With fewer requirements for the center of the runner, one can minimize the overall system diameter, making for a more compact design. The smaller size can make better use of the low head and will facilitate manufacturing, especially with 3D printing where the cost goes up non-linearly with size. Further, it is possible to use a hubless runner and since no installation is required at the center of the rotor more water will flow through the cross-section of the turbine, thus resulting in higher power output and efficiency as well. Furthermore, the shaft-less (hubless) turbine is environment-friendly, as this design allows fish or debris to pass through it. The hubless design requires less material, which will facilitate manufacturing, considering the non-linear relation between the cost and the size in case of 3D printing.

For the current study and based on the available literature pertaining to the shaftless rim-driven ship propellers (RDPs), further in the rim-driven electric generator with a hubless turbine design is investigated.

4.2 Design and Testing

A preliminary CAD design was created to prove the concept of the Rim-Drive Hydro Turbines (RDT) as shown in Figure 4-1. Detailed sheet drawings are shown in the Appendices.

The CAD was used to 3D print the components of the setup as most of the parts are 3D printed except the electric stator, which is originally a 1 HP, 3-Phase AC induction motor designed with 4 poles (see Figure 4-2).

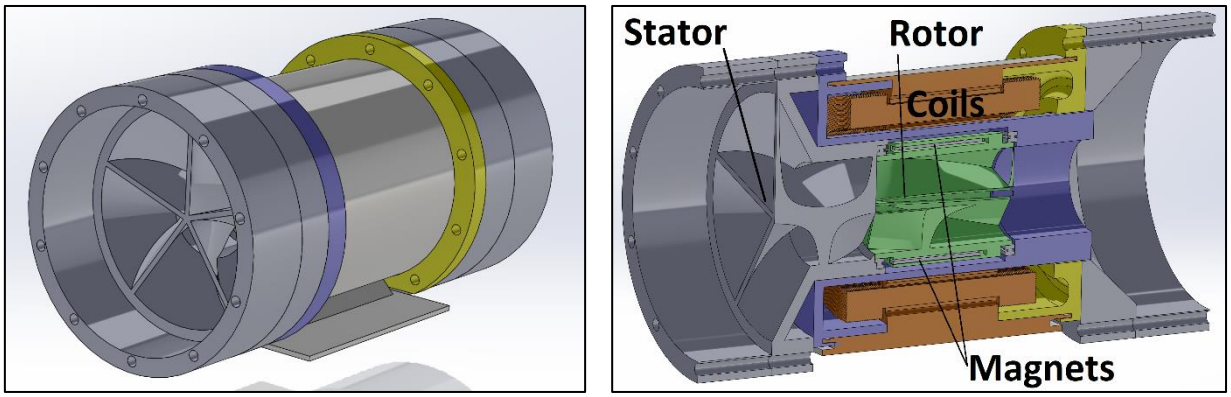

(a) **(b)**

Figure 4-1: The proposed RDT design. (a) Perspective view (b) Cross-sectional view

Figure 4-2: The electric stator of the RDT

The rotor was designed with 16 slots for magnets installation, see Figure 4-3 (a), these magnets (Figure 4-3 b) can determine the operating rotational speed of the generator as they role the number of the poles, however, for the selected electric motor it is limited with the designed

number of 4 poles. Also, the rotor will move freely by setting on two thin ball bearings (see Figure 4-3 c) on each of the rotor ends. Along with the progress in the experimental setup, two types of simulations will be conducted for the RDT. A simulation to estimate the rotating magnetic field (RMF) and the magnetic flux using software by EMWorks [161] and another CFD simulation to evaluate the fluid flow point of view and the mechanical power output using StarCCM+.

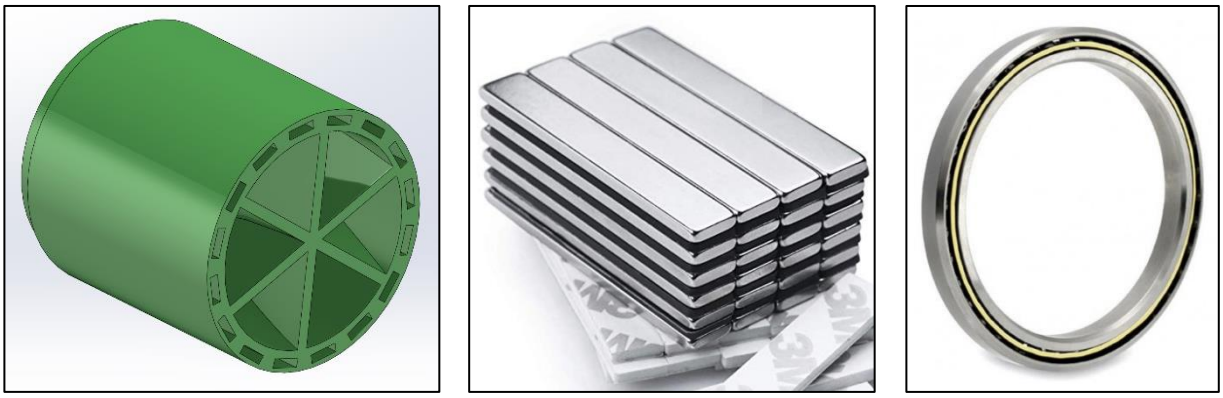

(a) (b) (c)

Figure 4-3: (a) Rotor (b) Magnets (c) Thin ball bearing

4.2.1 Experimental Setup

To evaluate the performance of the proposed design of RDT, experimental testing needs to be conducted. Also, experimentation helps in verifying the numerical computations and can be used as a tool to validate the results obtained from the EMF and the CFD simulations. It demonstrates the accuracy of the simulation results. The experimental setup of the Hydro Turbine Lab at the University of Wisconsin-Milwaukee (was explained previously in Chapter 3) is used for the RDT experimental testing. Minor changes were done on the setup to accommodate the RDT assembly includes; installing a 2-feet clear PVC pipe before the turbine, connecting the RDT assembly, building an electric circuit for monitoring the generated power, and removal of the shaft and the torque meter, as shown in Figure 4-4. The maximum head that can be achieved through the setup is still 2.6 m (8.5 ft) with the same maximum flow rate of 28 L/s (1.00 CFS).

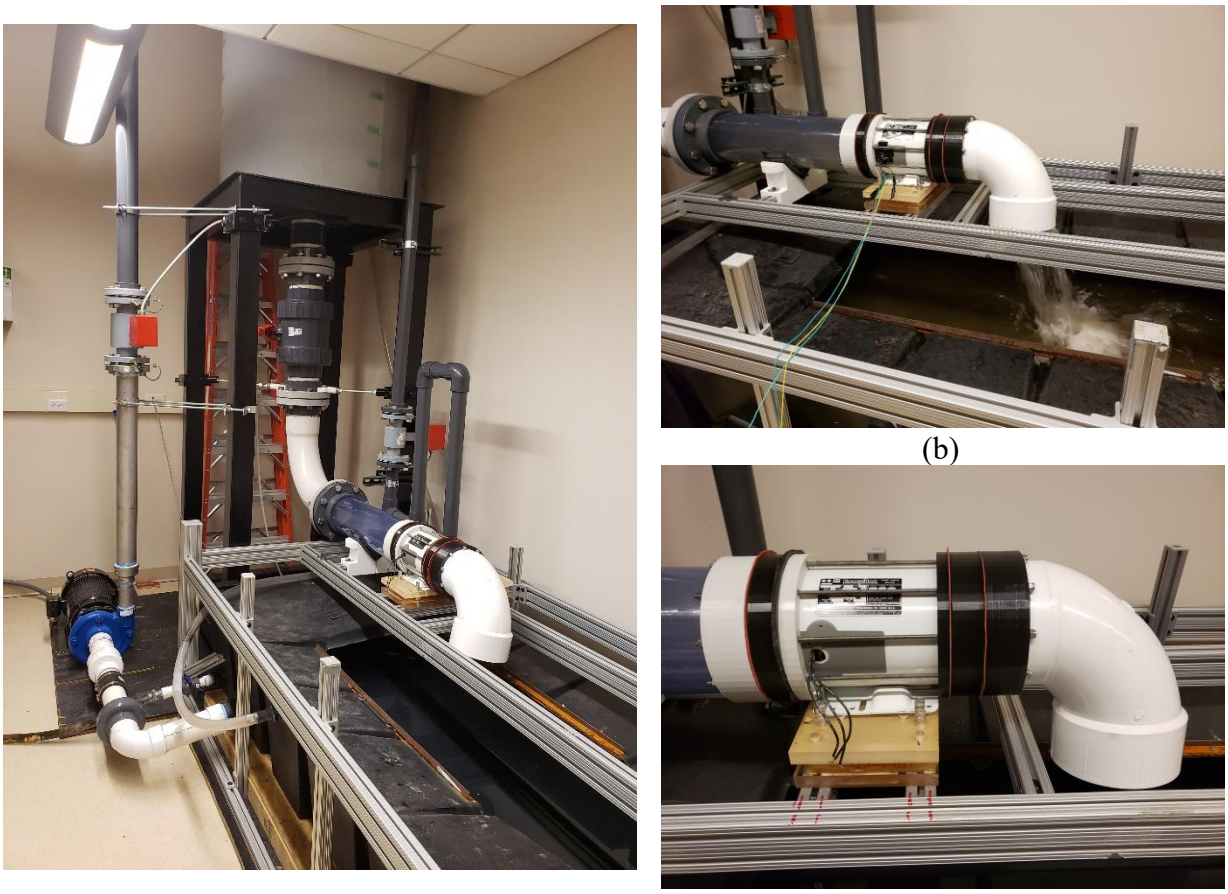

(a) (b) (c)

Figure 4-4: Experimental setup of the rim-drive turbine (RDT). (a) The whole setup including the two tanks, the turbine and the pump. (b) The setup under testing (c) the RDT assembly

For the RDT assembly and besides the stator of the electric motor (windings/coil), all other parts were 3D printed using the Ultimaker 2+ printer in the Hydro Turbine Lab. Figure 4-7 shows 3D printing under progress for the rotor of the RDT as captured by the live monitoring cam of the printer. ColorFabb nGen (multicolor) filaments were used as the printing material. All parts were printed once except the rotor, where six different rotors were printed includes two rotors for dry testing, a rotor with hub and another hubless, also a rotor with a single row of magnets and another with double rows for the wet testing. Two factors play a significant role in RDT performance. These are the design of the rotor and the type of magnets. Permanent magnets are used in this study and further details on the selection of permanents magnets are explained in the following section.

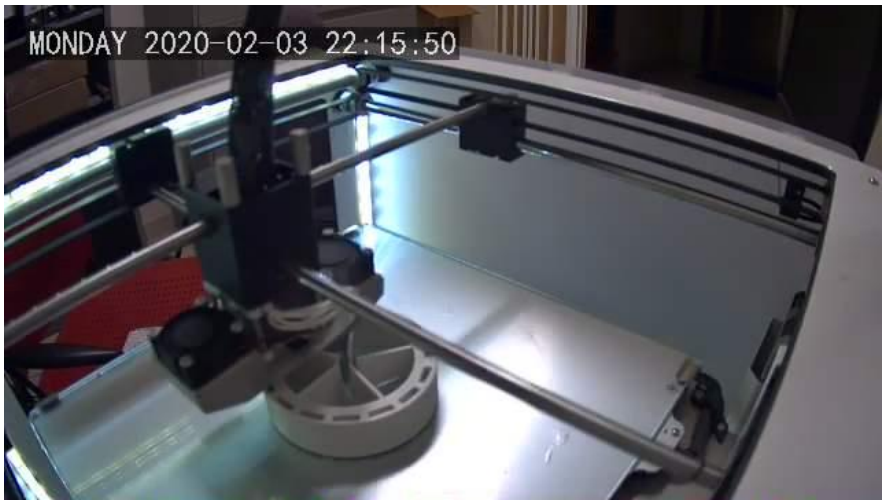

Figure 4-5: RDT's rotor during 3D printing

4.2.1.1 Permanent Magnets

A permanent magnet is a material that when inserted into a strong magnetic field will begin to exhibit a magnetic field of its own. Furthermore, it also continues to display a magnetic field once removed from the original field due to its atomic micro-structure. Indeed, the exhibited field would allow the magnet to exert force, i.e. ability to attract or repel, on other magnetic materials. Such exhibited field would then be continuous without weakening provided the material is not subjected to a change in environment such as temperature, demagnetizing field, etc. The ability to continue exhibiting a field while withstanding different environments helps to define the capabilities and types of applications in which a magnet can be successfully used [162].

Permanent magnets are usually called hard magnetic materials. This type of material is characterized by a B-H Curve (see Figure 4-6) that starts in the second quadrant if it exhibits a nonlinearity behavior. They are other magnets, but they are not permanent magnets which are called soft magnetic materials whose B-H Curve is limited to the first quadrant [163]. They are similar to permanent magnets in that they exhibit a magnetic field of their own in the presence of an external magnetic field. However, they do not continue to exhibit a magnetic field once the

applied field is reduced to zero. These materials are useful for carrying, concentrating and shaping magnetic fields. They are used throughout the magnetic industry and are often as vital in the design of a magnetic assembly as the permanent magnet.

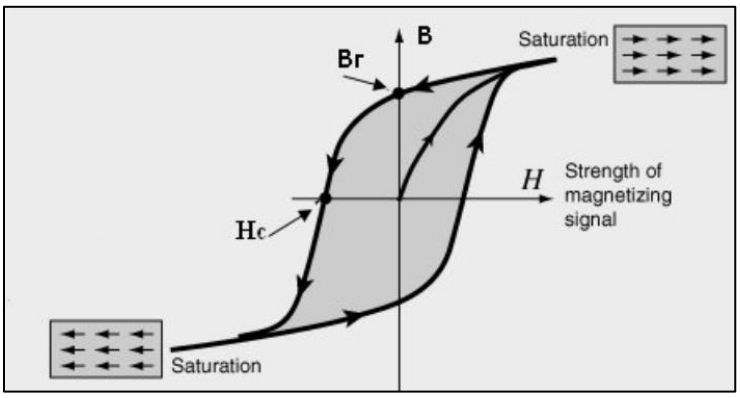

Figure 4-6: B-H curve for permanent magnets

Two important permanent magnets quantities must be considered for the design selection:

- **Coercivity** or the coercive force: Commonly denoted by the letter Hc, it is the intensity of the magnetic field needed to reduce the magnetization of a ferromagnetic material to zero after it has reached saturation. On a Hysteresis loop, as shown in Figure 4-6, it is the point where the loop intersects the H axis. The coercivity is measured in Amperes per meter (A/m) in MKS units and Oersted in Gaussian units.
- **Residual induction** or remanence: Commonly denoted by the letter Br, it is the amount of magnetic flux density remaining in a ferromagnetic material after an external magnetic field is removed after saturation in a closed circuit. On a Hysteresis loop, it is the point where the loop intersects the B axis. The Br represents the maximum magnetic flux density output of this material without an external magnetic field. The Residual induction is measured in Tesla for MKS units and in Gauss for Gaussian units.

Four main types of permanent magnets are commonly used nowadays in various magnetic applications [164], [165]:

1) **NdFeB (Neodymium-Iron-Boron)** or the so-called 'rare-earth' permanent magnets. They are very powerful magnets as they have the highest (B[3], Br, BHmax[4]) and high Hc. They are however very brittle, hard to machine, and sensitive to corrosion and high temperatures. They are generally the most expensive magnets. The NdFeB magnets have multiple grades; examples of these grades are presented in Table 4-1. In general, grade's name contains four parts; letter-xx-letter or two, where the "xx" is a two-digit number and indicates the value of the maximum energy product (BHmax) in the CGS unit and it varies from 28 to 55, the first letter is usually N as the initial letter of Neodymium, while the last part could be one letter or two to describe the level of intrinsic coercivity (Hci). The levels include "M" (Hci ≥ 14 kOe), "H" (Hci ≥ 17 kOe), "SH" (Hci ≥ 20 kOe), "UH" (Hci ≥ 25 kOe), "EH" (Hci ≥ 30 kOe) and "AH" (Hci ≥ 35 kOe), they are abbreviations for "Medium", "High", "Super High", "Ultra High", "Extreme High" and "Abnormal High", respectively. It should also be mentioned that there is a level where the letter is not available or default. In that situation, the Hcj is not less than 12 kOe [166].

   Taking grade N45SH as an example, it has a BHmax of 45 MGOe and its Hci is above the level of 20 kOe in the CGS unit system (1592 kA/m in SI unit system). In this work, two grades of NdFeB were selected; N52 and N35. The key difference is that their BHmax is 35 MGOe and 52 MGOe, respectively. As a permanent magnet's remanence Br is closely linked to its BHmax, it also means that the N35 magnet's Br is lower than that of the N52 magnet, i.e. the latter has higher magnetic flux density. As a result, a

[3] B is the magnetic flux density (tesla, T or gauss, G)
[4] BHmax is the maximum energy product (kJ/m^3 or MGOe)

motor or device using the N52 magnet can have higher power and/or can become smaller/lighter than that using the N35 magnet.

Table 4-1: Typical magnetic properties of some NdFeB grades

Grade	Residual Induction (Gauss) Br	Coercivity (Oersteds) Hc	Max. Energy Prod (MGOe) BHmax
N55	15,000	12,000	55
N52	14,700	10,300	52
N48	14,100	12,700	48
N42	13,200	12,000	42
N36	12,400	11,100	36
N35	11,900	10,700	34

2) **Ferrite (Ceramic)** or the so-called 'hard ceramic' permanent magnets. They are generally made from Strontium or Barium Ferrite. Lower in power (B, Br, BHmax) compared to other magnets, and are very brittle. However, they have very high Hc and good Tc[5] and are quite corrosion-resistant. A very cost-effective choice. Less expensive than NdFeB magnets, but still very powerful and resistant to demagnetization.
3) **AlNiCo (Aluminum-Nickel-Cobalt)** for medium strength and excellent machinability. They perform much better than plain steel but are much weaker in strength (lower B, Br, and BHmax). They must be carefully stored because they are prone to demagnetization.
4) **SmCo (Samarium Cobalt)** or the so-called 'first rare earth' magnets. They have high power and resistance to high temperatures and corrosion. They are almost as powerful as NdFeB magnets, and far more powerful than all the others (high B and Br). Usually only used where resistance to high temperatures and corrosion is needed. Also, very brittle and hard to machine. They are the most expensive magnets.

[5] Curie temperature (T_C) is the temperature at which the material loses its magnetism.

For the RDT setup, the performance was tested with several numbers of poles (2, 4, 8, and 16). However, the maximum power output was maintained at the four poles setup. And since the rotor has 16 slots (where each slot can fit one 60 mm × 10 mm × 3 mm N52 or N35 magnet), the recommended distribution then is four groups, each with four magnets with alternating the group's pole with the neighbor groups as detailed in Figure 4-7. Further, adding an extra row/rows of magnets were investigated, i.e. instead of having just one magnet in each slot, two, three, and four magnets were tested. The single and double-row setups were calculated using the RMF simulation and tested experimentally; nonetheless, the triple and quadruple-row setups were only calculated using the RMF simulation due to the machinability limitations.

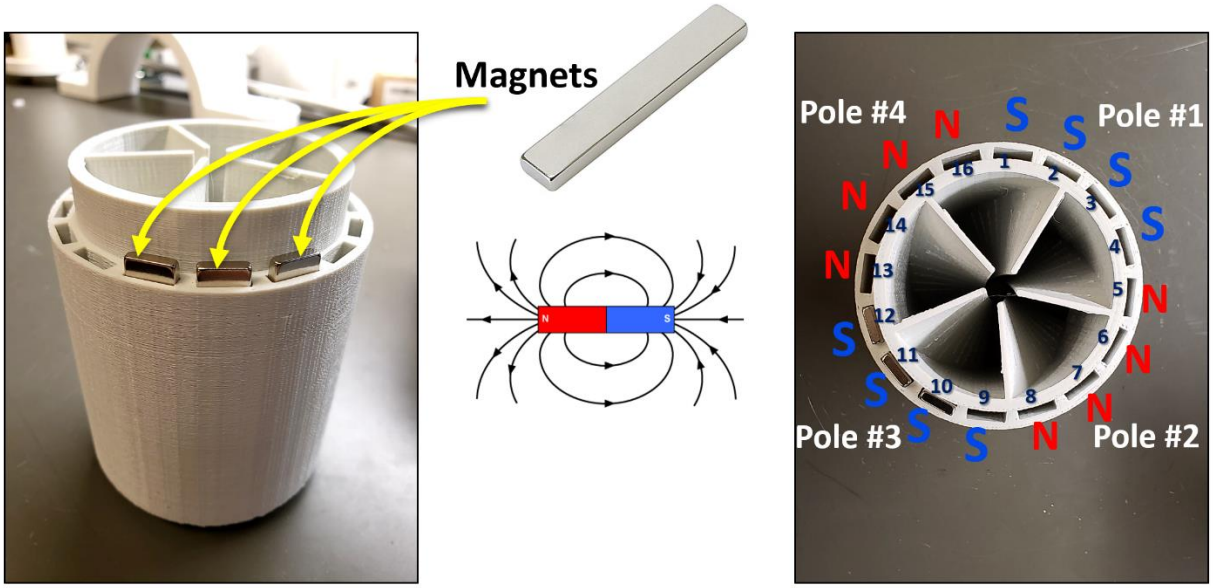

Figure 4-7: Magnets distribution (single row) on the 3D printed rotor perimeter

4.2.1.2 RDT Power Monitoring Setup

Since the raw electrical (ampere and voltage) output of the generator due to the rotation is 3-Phase AC, an electric circuit is needed (as shown in Figure 4-8) to convert the 3-phase (3-ph) to a single-phase (1-ph) and to convert the current from AC to DC, also, to regulate the voltage output. A motor starter capacitor with a capacity of 189-227 μf is used to convert the 3-ph to 1-ph, where

two out of the three wires (of the generator) are connected to the capacitor and the third one is directly connected to the AC (~) pole of a bridge rectifier diode (50A, 1000V) where the purpose of the diode is to convert the current from AC to DC. An additional DC-DC regulator is installed for constant output, then the ampere, the voltage, and the power can be obtained by connecting the plus/negatives poles of the diode with a load (bulb) and a power monitor in parallel. Since the bulb is a constant load with a fixed resistor, a resistance substitution box (see Figure 4-9) is used as a variable resistor starting with 1 Ohm (Ω) and up to 110 Megaohms (MΩ) with 1Ω increment to test the RDT performance at different loads, however, the maximum resistance used in this study is 900Ω only. The setup of the electric circuit is shown in Figure 4-10.

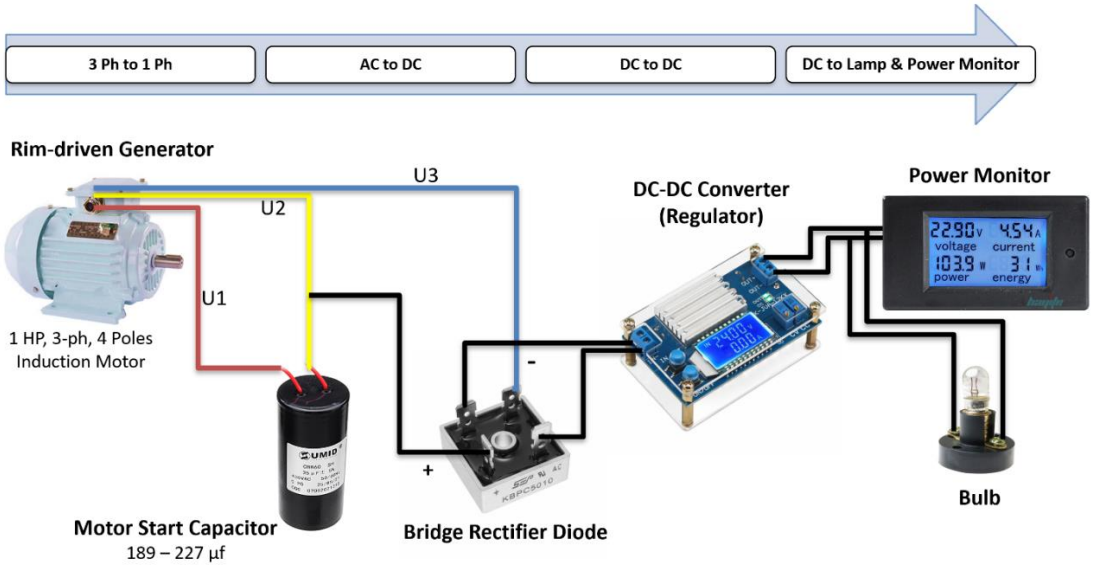

Figure 4-8: Basic schematic of the RDT generated power monitoring electric circuit

Figure 4-9: Resistance substitution box

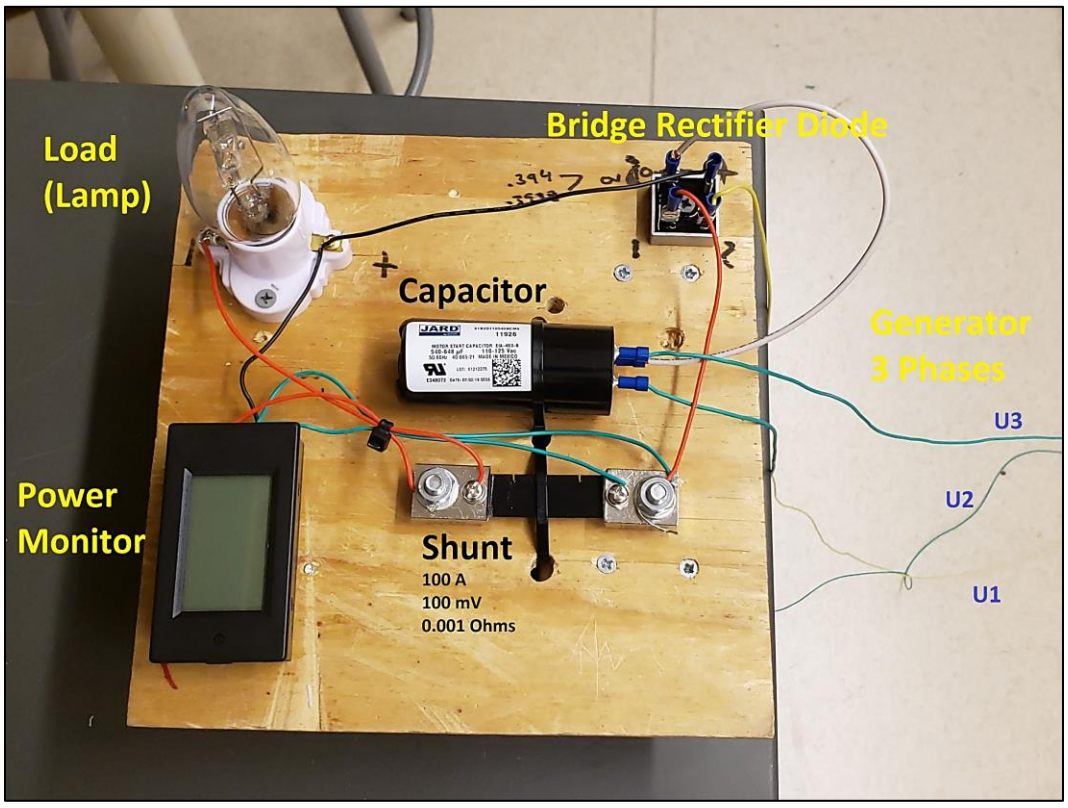

Figure 4-10: Electric circuit of the RDT generator

In addition to the aforementioned components of the electric circuit, a shunt is used (aka a current shunt resistor or an ammeter shunt), which is a high precision resistor that can be used to measure the current flowing through a circuit. Considering Ohm's Law, the voltage dropped across a resistor divided by the resistance of that resistor is equal to the current, therefore if the voltage is measured across a shunt resistor in a circuit, then the current can be easily calculated. Considering the used shunt in Figure 4-10 as an example, which is a typical 100 Amp Shunt Resistor. This shunt can be used to measure currents of up to 100 Amps. It is calibrated such that the voltage drop across it is 100mV when the current flowing through it is 100 Amps. Therefore, the resistance of this shunt is calculated to be voltage divided by current = 0.1 / 100 = 0.001 Ohms. Therefore, if a voltage drop of 28mV is measured using a standard multimeter, then the current flowing is 0.028/0.001 = 28 Amps.

4.2.2 Rotating Magnetic Field (RMF) Simulations

One important component of the RDT is the electrical generator, and since the generator was customized for this specific RDT setup, a design procedure including studying the rotating magnetic field (RMF) by using a simulation tool was completed. Electromagnetic Simulation (EMS), a software product of EMWorks company, was utilized. EMS is an electromagnetic field simulation software which calculates fields (electric / magnetic / flux / potential / eddy currents), circuit parameters (inductance / capacitance / resistance / impedance / flux linkage), mechanical parameters (force / torque), and losses (eddy/core/hysteresis/ohmic) and able to simulate the electrical machines, motors, generators, sensors, transformers, high voltage apparatus, high power machines, electrical switches, valves, actuators, PCB's, levitation machines, loudspeakers, permanent magnet machines, NDT equipment, inverters, converters, bus bars, inductors, bushings, or biomedical equipment [167].

In EMS, six types of analysis can be performed relevant to the electromagnetic and electromechanical engineering design process and these include; Electrostatic, Electric Conduction, AC Electric, Magnetostatic, AC Magnetic, and Transient Magnetic. For the RDT and in light of applying the permanent magnets machine concept, the best-fit analysis model is the Magnetostatic. All analysis models in EMS are using Maxwell's equations to calculate the needed outputs.

4.2.2.1 Maxwell's Equations

Maxwell's equations are a set of partial differential equations that govern the behavior of electromagnetic devices. They are linear in space and time. When electromagnetic fields interact with materials, the equations can become nonlinear. The main quantities involved in Maxwell's equations are:

- The electric field intensity, E
- The electric flux density or electric displacement, D
- The magnetic field intensity, H
- The magnetic flux density or magnetic induction, B
- The surface current density, J
- The volume charge density, r

In addition to below quantities defined by EMS:

- The magnetic permeability, m
- The electric permittivity, e
- The electric conductivity, s

The four Maxwell's equations (Eq. 4-1 to Eq. 4-4) are:

$$\nabla \times H = J + \frac{\partial D}{\partial t} \quad \text{Eq. 4-1}$$

$$\nabla . B = 0 \quad \text{Eq. 4-2}$$

$$\nabla \times E = -\frac{\partial B}{\partial t} \quad \text{Eq. 4-3}$$

$$\nabla . D = \rho \quad \text{Eq. 4-4}$$

The above field equations are supplemented with the constitutive relations (Eq. 4-5 to Eq. 4-7) that describe the behavior of general electromagnetic material or media:

$$D = \varepsilon E \quad \text{Eq. 4-5}$$

$$B = \mu H \quad \text{Eq. 4-6}$$

$$J = \sigma E \quad \text{Eq. 4-7}$$

Maxwell's equations relevant to Magnetostatic Analysis fields are:

$$\nabla . H = J_s \quad \text{Eq. 4-8}$$

$$\nabla . B = 0 \quad \text{Eq. 4-9}$$

where H is the magnetic field, J_s is the source current density, and B is the magnetic flux density. The constitutive relation connects B and H:

$$B = \mu(H + H_c) \quad \text{Eq. 4-10}$$

where μ is the magnetic permeability, in general, a function of H. H_c is the coercive force or coercivity. Thus, the Magnetostatic Analysis solves the above two of Maxwell's equations.

After selecting the analysis model, the CAD models of the RDT parts are imported. Not all the parts are important, only the electrical stator (which has the coils), the rotor, and the 16 magnets are involved in the simulation, as shown in Figure 4-11. The CAD model was simplified as the current stator geometry is very detailed and will result in an expensive and time-consuming simulation. The geometry was revised to be a hollow cylinder, while the rotor was revised with no blades included. These changes do not affect the output of the RMF simulation, meanwhile, less complex simulation and shorter computational time.

Each part is assigned a material; copper for the coils, plastic for the rotor, and N52 and N35 NdFeB for the magnets (one grade only at once). Then the coercivity direction of the magnets (poles) is set as two groups as north poles (red arrows) and two groups as south poles (blue arrows), see Figure 4-12. Other simulation parameters and the mesh count are listed in Table 4-2. While the 3D generated mesh for cases of single and quadruple-row are presented in Figure 4-13.

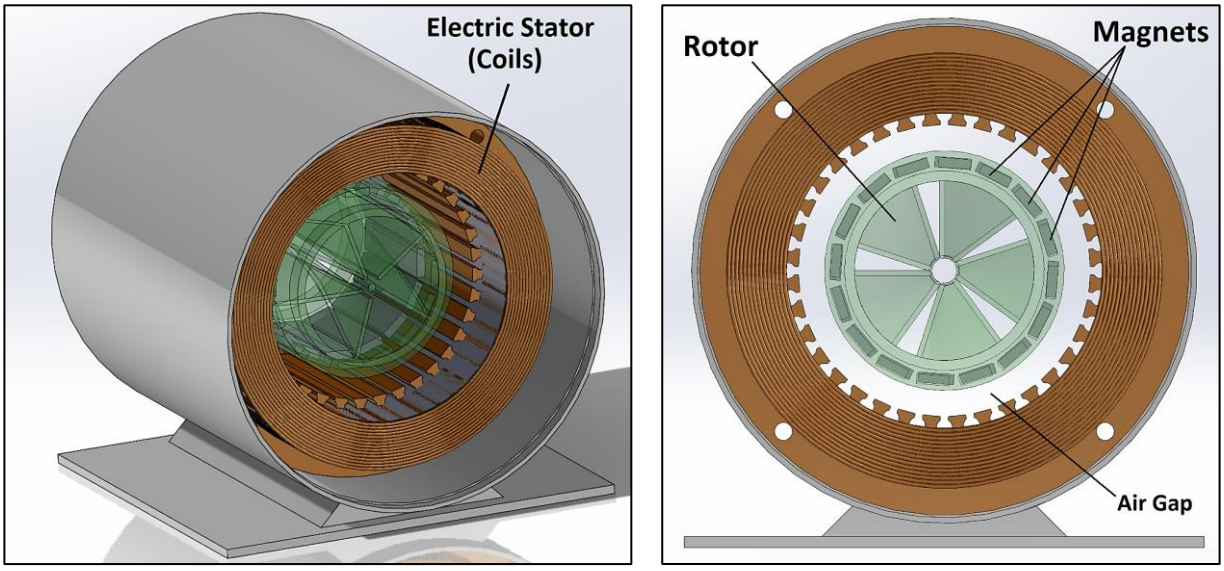

(a) (b)

Figure 4-11: CAD model for the RMF simulation. Parts included; electric stator (coils), rotor, and magnets. (a) Isometric view (b) Front view

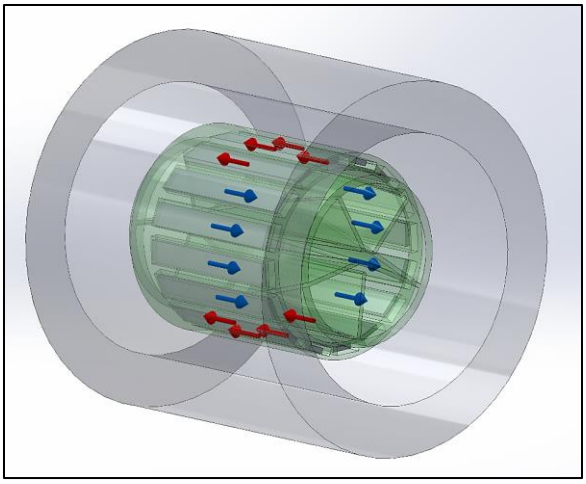

Figure 4-12: Coercivity direction (poles) of the magnets inside the rotor's slots. Red arrows = north poles, blue arrows = south poles

Table 4-2: RMF simulation parameters and mesh count

Parameter	**Value**
Rotor rotational speed (RPM)	415 – 2,130
Timestep (s)	0.04
Total solution time (s)	5
Relative residual error for iterative solver	1×10^{-6}
Mesh Details	
Number of nodes	~20,000
Number of elements	~105,000
Global element size (in)	0.523
Tolerance (in)	5.23×10^{-4}
Enabled Models	
Magnetostatic study	
Motion study coupled	
Mutli-core iterative solver	

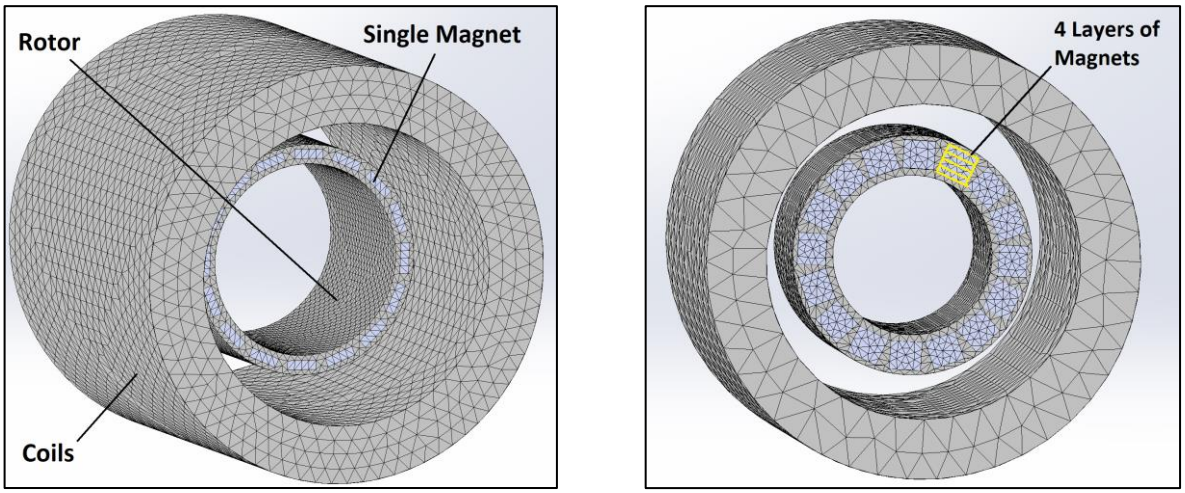

(a) (b)

Figure 4-13: Mesh plotting for (a) single-row (b) quadruple-row of magnets

4.2.3 CFD Setup of the RDT

The performance of the RDT is calculated by the RMF simulation from the electrical point-of-view, yet, evaluating the performance from the mechanical aspect and predicting the potential of the proposed turbine is needed by utilizing CFD. The theoretical (maximum) power output of the RDT is calculated by conducting CFD simulations using Star-CCM+ software. Similar conditions and parameters of the previously conducted simulations (in Chapter 3) are considered here, despite the changes in the geometry near the turbine assembly, as shown in Figure 4-14.

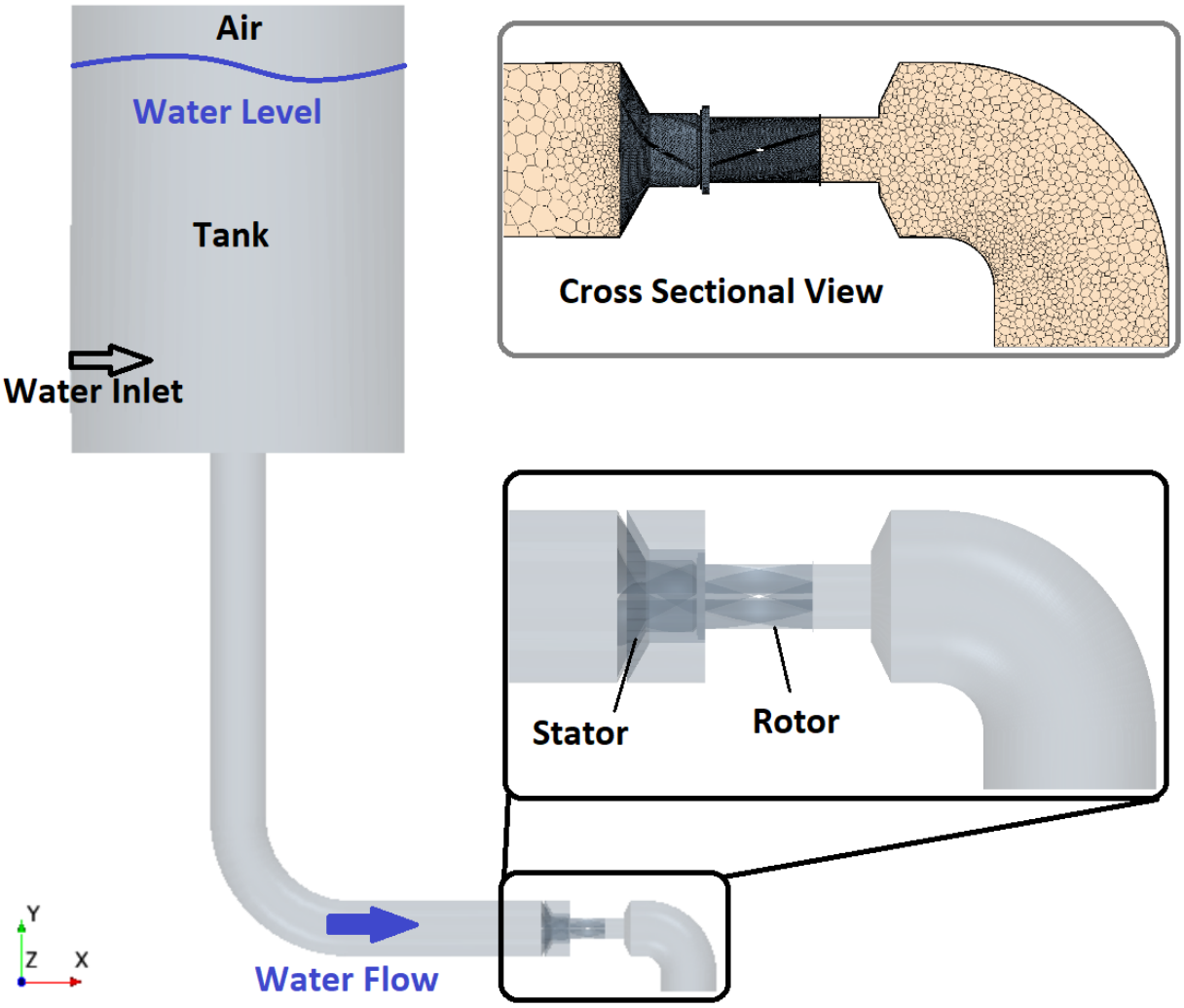

Figure 4-14: CFD setup of the RDT

4.3 Results

After considering the three RDT evaluation procedures i.e. experimentally, RMF simulations, and CFD simulations, one common parameter was taken into account to compare and validate the results which is the generated electric power (power output) out of the electric generator because of the developed rotating magnetic field as a result of the rotor's rotational motion along with the attached magnets on the perimeter by the potential and kinetic energy of the water flow through the turbine. In this section, the RDT is evaluated as follows:

1) Two rotors designs; a rotor with hub and another hubless (Experiment and CFD)
2) N52 vs. N35 magnets (Experiment and RMF)
3) Number of magnets' rows (Experiment and RMF)
4) Overall performance of the RDT (Experiment, RMF, and CFD)

4.3.1 Hub versus Hubless Rotor

What distinguishes the RDT is that there is no need for the shaft to transmit the rotational motion to a generator as the rotor is supported with two bearings, one on each side, and the generation occurs directly in-place at the outer diameter of the rotor. Accordingly, there is no need to have a hub for the rotor, which may allow for more flow to pass through the turbine, but necessary to increase the power output. Another advantage of considering the environmental aspects into account by allowing debris or fish to pass through, especially in the case of run-a-river. The hubless rotor might have one disadvantage as its structure is weaker than the rotor with a hub. Figure 4-15 shows the front view of the two rotors; (a) the rotor with hub and (b) the hubless rotor.

The rotors were compared by conducting CFD simulations, and then the results are validated with experimental testing (see Figure 4-18). The flow behavior is also compared by

looking into the velocity profile and pressure drop in both cases, as presented in Figure 4-16 and Figure 4-17.

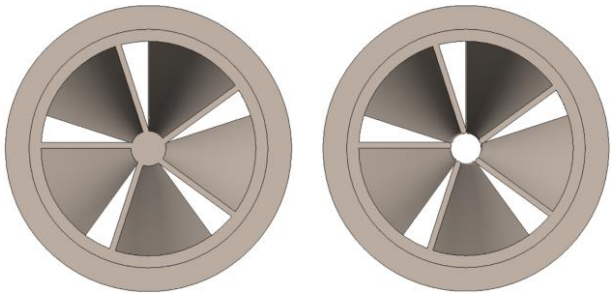

(a) (b)

Figure 4-15: (a) Rotor with Hub (b) Hubless rotor

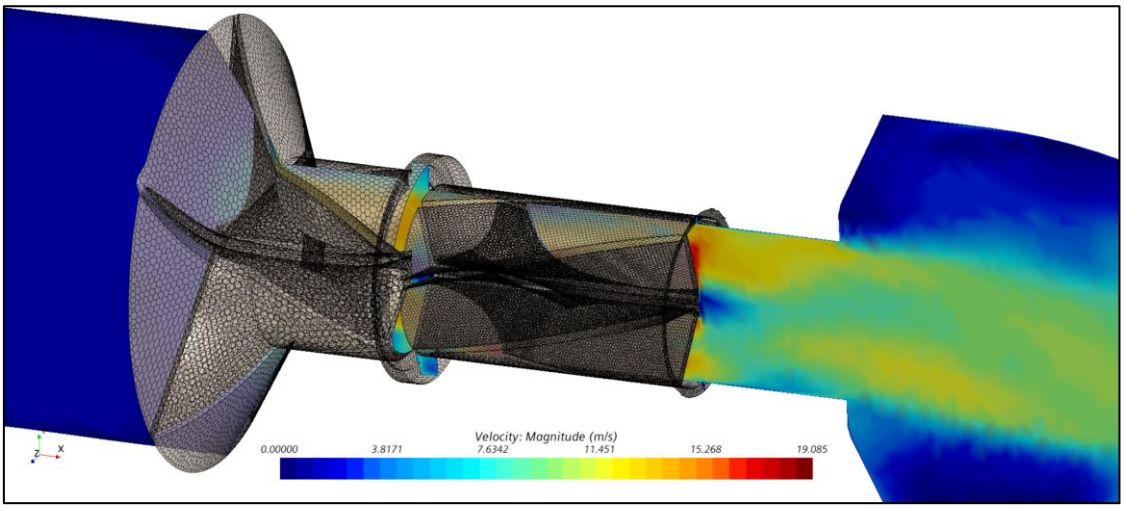

(a)

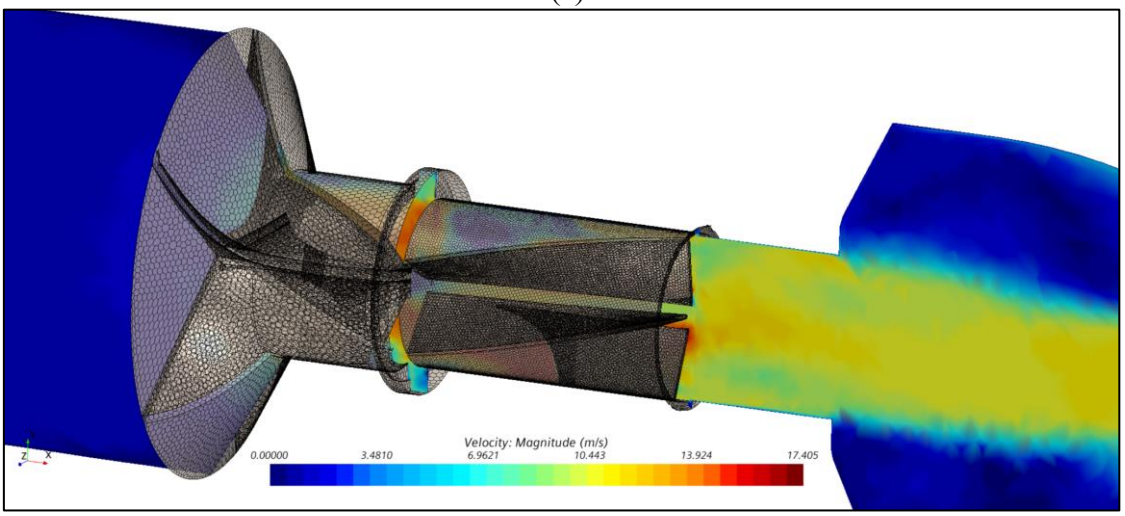

(b)

Figure 4-16: Scalar scene of the velocity magnitude for (a) the RDT with hub design and (b) the hubless RDT

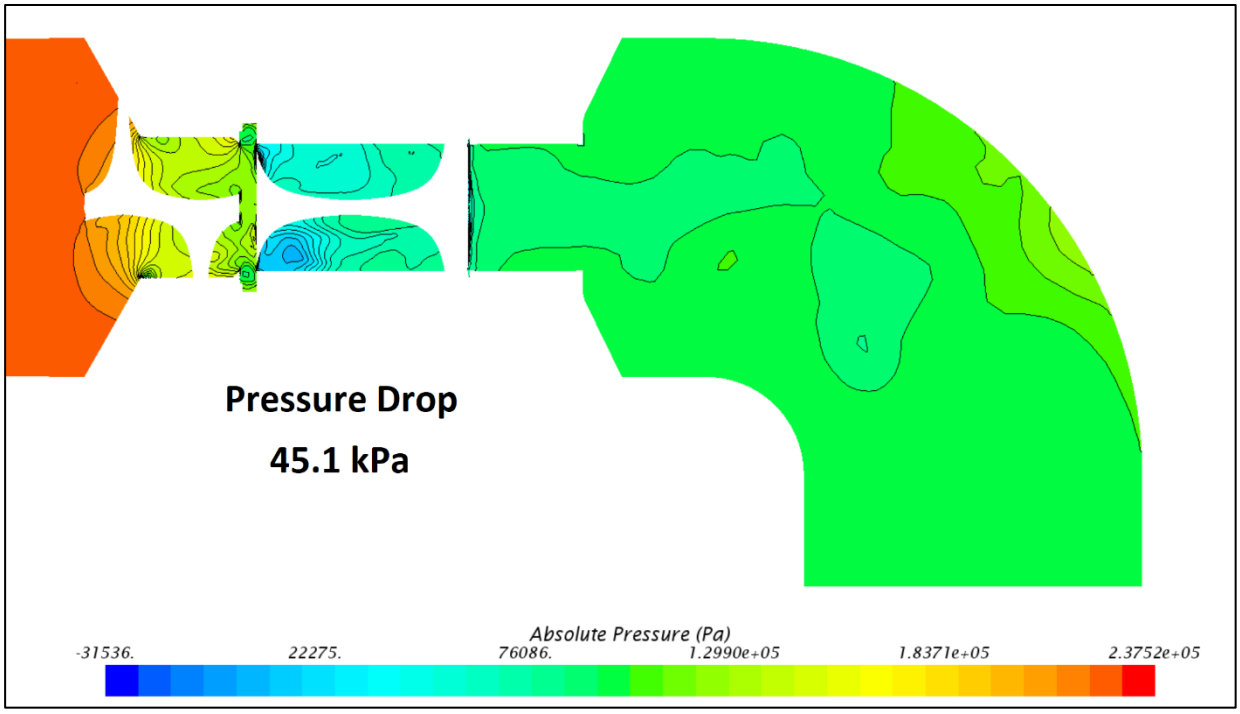

(a)

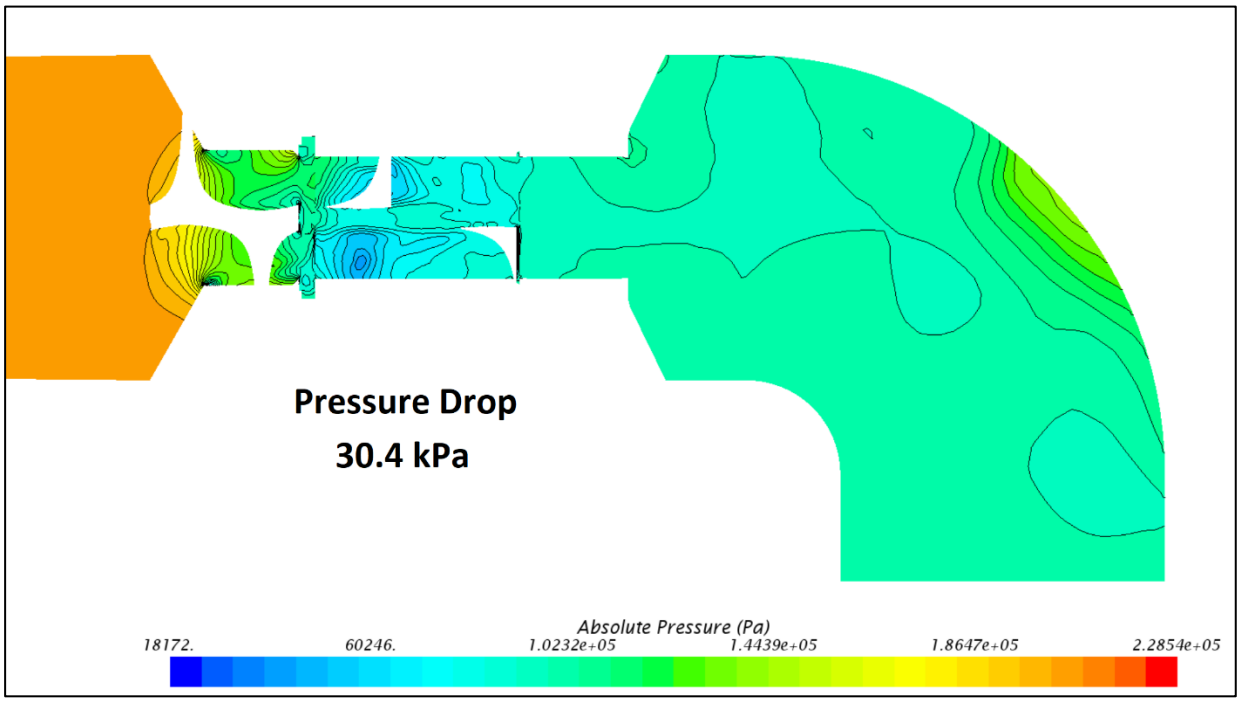

(b)

Figure 4-17: Scalar scene of the absolute pressure for (a) the RDT with hub design and (b) the hubless RDT

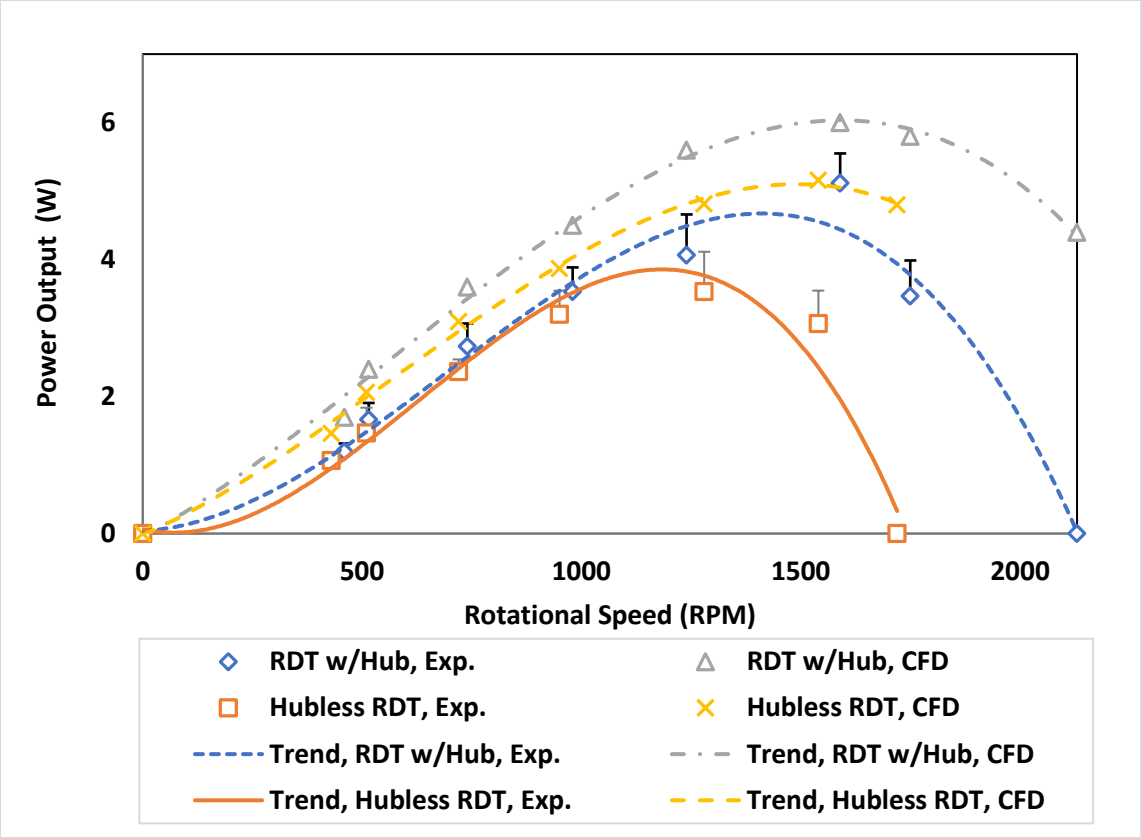

Figure 4-18: Performance comparison of the RDT with hub versus the hubless RDT

It can be noticed from Figure 4-16 (a) that the rotor with hub has a stagnation at the exit of the rotor and near the hub which led to an increase in the exit losses, but the same scene showed higher velocity values inside the rotor and near blades, as the water flow is forced to pass in the blade passage only as the hub is existed, while for the hubless rotor as shown in Figure 4-16 (b) the flow pass more freely inside the rotor and right after the exit, however, slower velocity values are indicated in the scene inside the rotor. Also, when the pressure drop was calculated for the two cases (see Figure 4-17), it was noticed that the hubless has lower pressure drop (30.3 kPa) than the rotor with the hub (45.1 kPa) which means less energy extracted in the turbine and thus, less power output.

As a result, the power output of both cases over a range of rotational speeds is presented in Figure 4-18. The rotor with hub showed higher power output over the hubless rotor, with an

average difference of 13% for the experimental data and 16% for CFD data. The error was calculated for the experimental data by using the 95% confidence level and represented as error bars with an average error of 15%. It can also be concluded that the hubless design tends toward the lower range of the rotational speeds as the maximum power output was recorded around 1200 rpm but around 1400-1500 rpm for the rotor with the hub.

4.3.2 N52 versus N35 Magnets

For this work, two grades were used for the experimental testing, N52 and N35, where generally the N52 magnet is considered a stronger magnet than the N35. It is evident from Figure 4-19 that the RDT has higher power output with N52 magnets over the N35 magnets by 67.2% for the single-row arrangement and 63.4% for the double-row. The highest power value recorded was 8.6 W at 1480 rpm for the N52 magnets, while the highest for the N35 magnets was 5.3 W at 1430 rpm.

4.3.3 Number of magnets' rows

As was mentioned earlier, multiple rows of magnets i.e. single, double, triple, and quadruple were tested to see how the power output of the RDT can be affected. Figure 4-19 shows the results of the experimental testing of the single-row versus double-row magnets, and it can be seen that the double-row RDT achieved an average of 83% more power than the single-row turbine for the N52 magnet grade, while it has an average of 89% more power output for the N35 magnets. It can also be noticed that the highest power output of the double-row RDT is obtained at rotational speeds around 1250 rpm, while the highest power output for the single-row occurred around 1400 rpm. Further, the triple and the quadruple setups are calculated by the RMF simulations. Figure 4-20 shows the highest magnetic field intensity captured for the quadruple-row RDT over the single-row. The RDT performance at different rows' arrangement is shown in Figure 4-21.

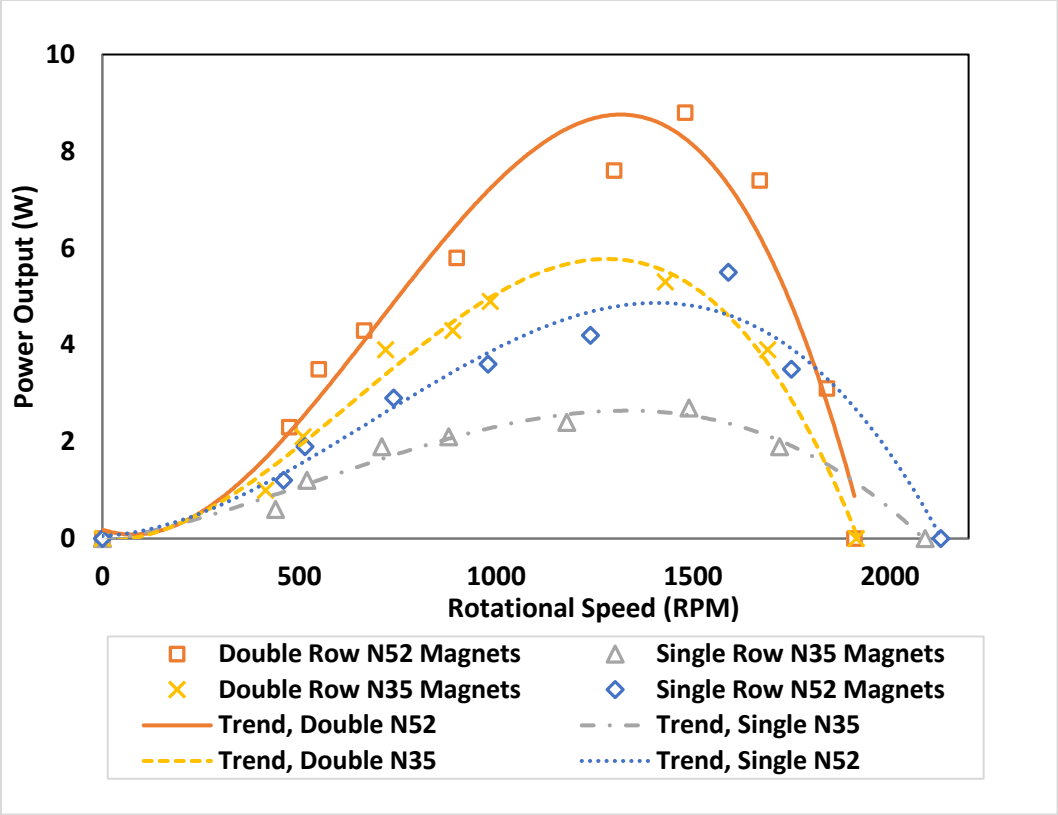

Figure 4-19: Experimentally measured power output of the RDT with N52 and N35 magnets for two arrangements; single row and double row

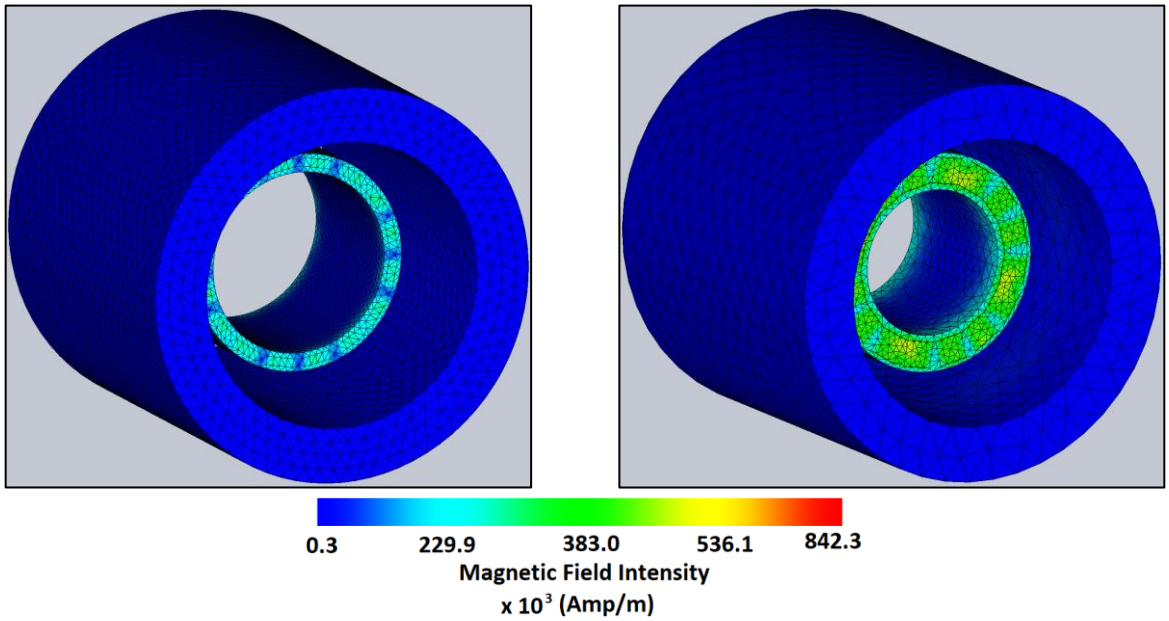

(a) (b)

Figure 4-20: Magnetic field intensity for (a) single-row of magnets (b) quadruple-row of magnets

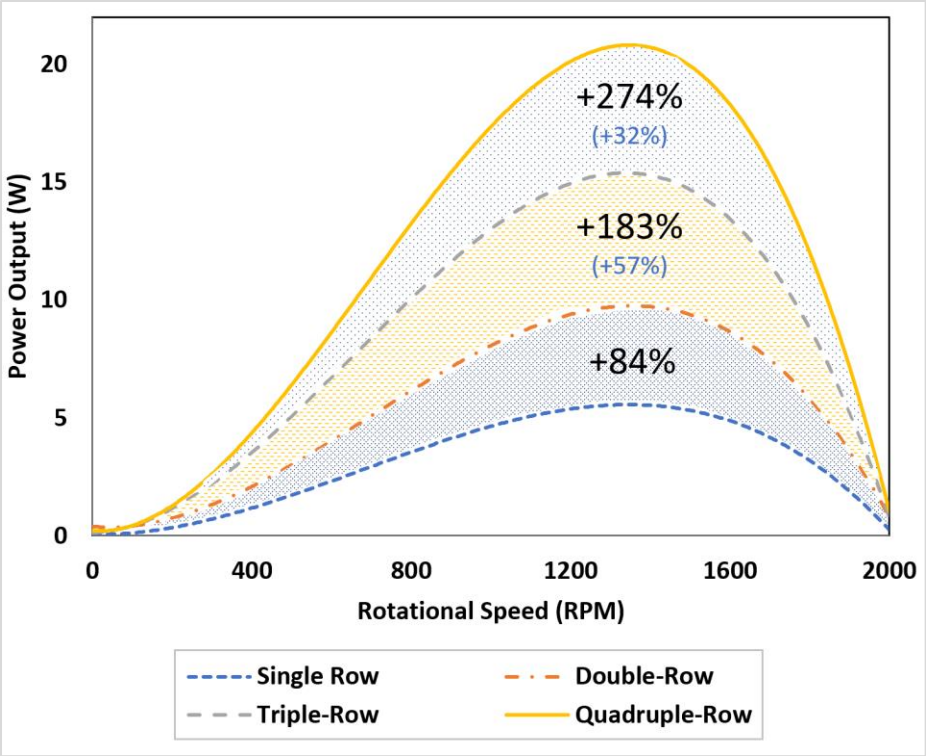

Figure 4-21: The RMF simulated power output of the RDT with four arrangements for N52 magnets; single-row, double-row, triple-row, and quadruple-row

The increase in the RDT power output for the double-row as calculated by the RMF simulation is 84%, as shown in Figure 4-21, which is almost the same gain was recorded in the experimental data. Similarly, adding another row (triple-row) can contribute to increasing the power output in an average of 57% compared to the double-row RDT and an average of %183 when compared to the single-row turbine. The power can jump up to 274% when quadruple-row RDT is utilized when it is compared with the single-row and 32% when compared with the triple-row RDT.

4.3.4 Overall performance of the RDT

In this section, the power extracted from the proposed RDT is evaluated within its limit of rotational speeds (0 to ~2000 rpm) experimentally, and by RMF and CFD simulations. The next four figures are presenting the performance of RDT with single and double rows, and the performance for N52 and N35 grades of magnets. In general, the experimental data and the RMF

simulation results are following the same trend for all the cases, where the peak power is located between 1000 rpm – 1500 rpm. While for the CFD results, the curve is shifted to the right with the peak located at a higher range of rotational speeds, i.e. 1500 rpm – 1700 rpm. Also, the first two cases have a common error value of around 7% between the experiment and the RMF results and an average of 14% error between the experiment and the CFD results. In the case of the single-row N35, the error between the experiment and RMF is 12%, and between experiment and CFD is 18%. For the last case of double-row N35, the error between experiment, RMF, and CFD is 9% and 21%, respectively. For these four cases, the case of double-row N52 has the highest power output (a maximum of 8.6 W), while the single-row N35 has the lowest power output (a maximum of 2.6 W). Then the case of the double-row N35 ranked second after the double-row N52 (maximum power of 5.3 W) followed by the single-row N52 case with a maximum power of 5.1 W. The error in all cases was presented by error bars and it was calculated by using the 95% confidence level.

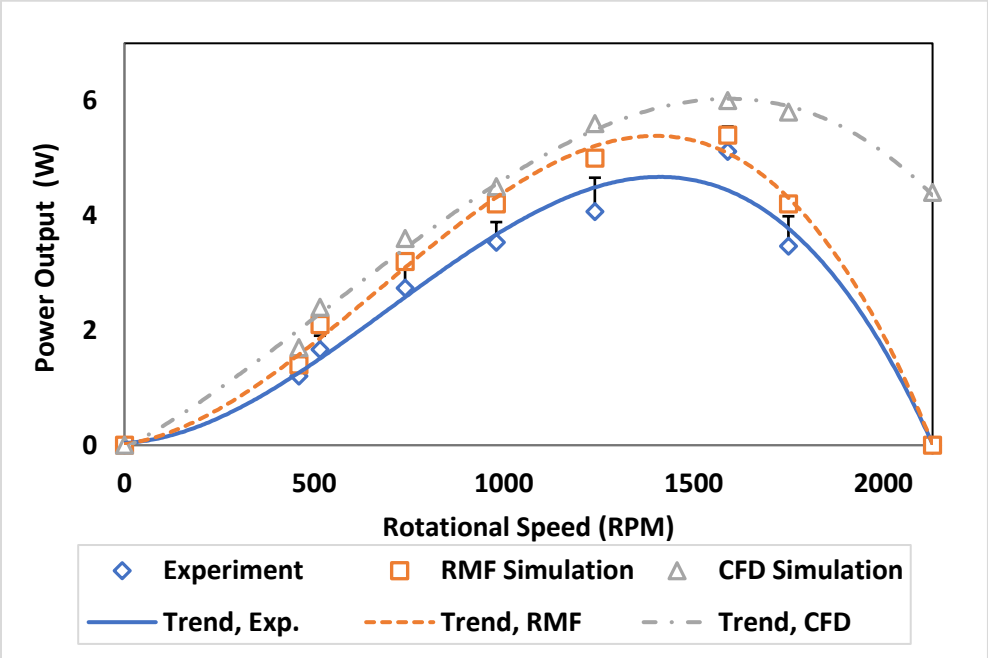

Figure 4-22: RDT performance with a single row of N52 magnets

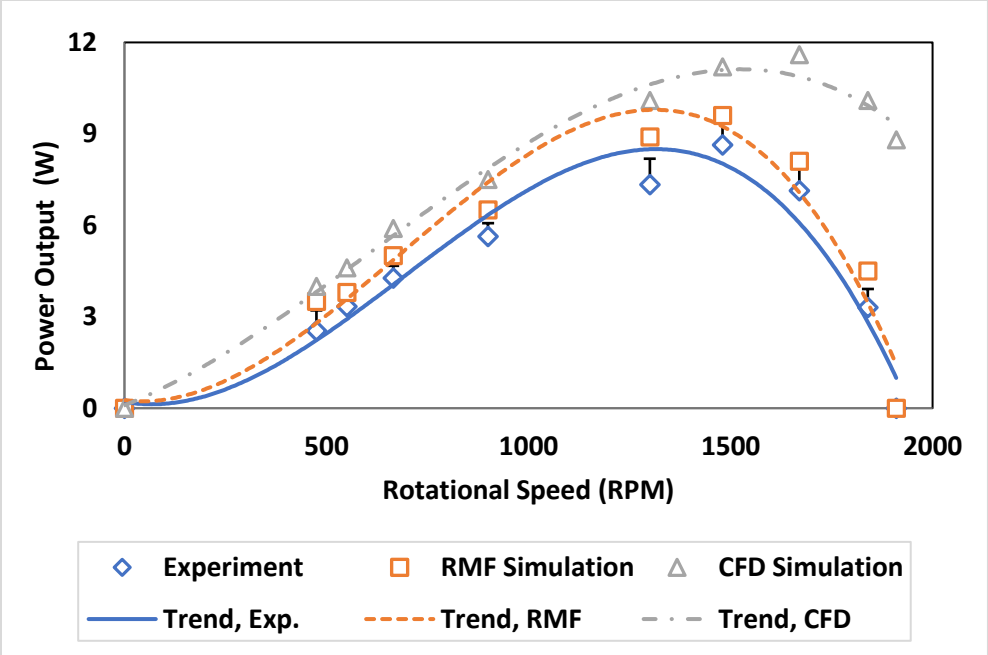

Figure 4-23: RDT performance with a double row of N52 magnets

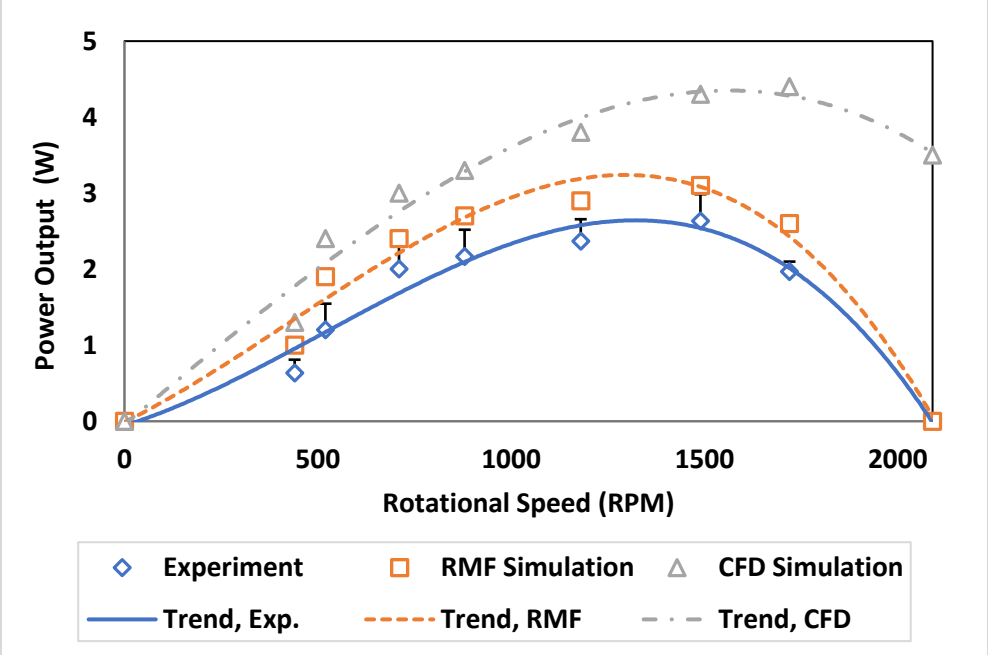

Figure 4-24: RDT performance with a single row of N35 magnets

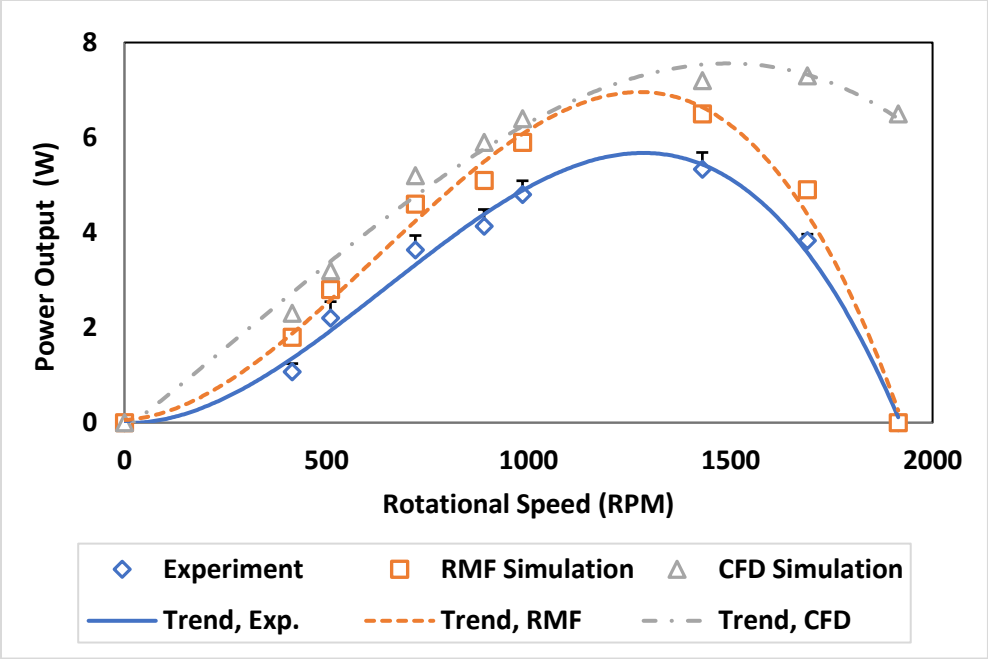

Figure 4-25: RDT performance with a double row of N35 magnets

Chapter 5: Rim-drive Turbines (RDT) Applications – WWTPs

5.1 Introduction

Wastewater treatment plants (WWTPs) are a major energy consumer, yet there are several opportunities for implementing on-site power generation systems. Within the treatment process, a high flow rate of effluent is produced and discharged to a nearby water body by gravity. Thus, hydro turbines can be utilized to generate power in such an application due to a difference in elevation and high flow rate. This paper presents a case study of introducing a hydro turbine in a wastewater treatment plant in Wisconsin and evaluating the power output in addition to determining the energy savings. The wastewater treatment plant considered in this study has an effluent flow rate of 190 MGD (million gallons per day) and an elevation difference of 3 meters (10 feet) between the final stage of treatment and the discharge point. Based on the aforementioned parameters, hubless rim-drive Kaplan type hydro turbine (RDT) is the optimal choice to be used in such an application. The RDT is designed and optimized by using an in-house code. A computational fluid dynamics (CFD) software is applied to evaluate the performance of the proposed model and the system is simulated through HOMER software to validate the results generated by the CFD. The expected savings are estimated to be 1,564 MWh/year.

5.2 Methodology

Hydroelectric power is referred to as the electric power generation converted from the potential and kinetic energy stored in a water source (like dams, rivers) by using hydro turbines. Hydro turbines are selected based on different parameters such as flow rate, head, and application in addition to other parameters. Since WWTPs have a high effluent flow rate with an acceptable elevation difference between the effluent and the final discharge point, hydropower can be a

significant renewable energy generation source [168]–[170], yet, hydropower can decrease greenhouse gases generation [2], [3].

A recent design of shaft-less rim-driven thruster for ships showed some advantages over the traditional designs with the shaft by reducing the vibration and noise, providing more compact design with less weight, and more flexibility in installations [42]. Also, rim-driven propellers (RDP) configuration can be more cost-effective than traditional design since fewer components are required. Such technology has reduced the spatial requirements for installation as well as the maintenance needed to operate the system. Moreover, the hubless RDP and thrusters demonstrated higher efficiencies than the hub ones [43], [44].

Since the WWTP in this study has a high water flow rate (around 190 MGD) and a low head difference (around 3 m), a Kaplan hydro turbine was selected [14]. For modeling the system and sizing the turbine capacity, HOMER software was used. HOMER is a modeling software developed by the U.S. National Renewable Energy Laboratory (NREL) to further the design of the power system and provide a comparison of different power generation technologies in a wide range of applications. The design of the rim-driven Kaplan hydro turbine was optimized using an in-house code in which the efficiency of Kaplan turbine can reach up to 92% compared to normal efficiency (80-88%) for traditional design one [140]. Finally, CFD software (STAR-CCM+) was used to investigate the performance of the newly designed Kaplan turbine.

For the current study and based on the available literature pertaining to the shaft-less rim-driven ship propellers (RDP) or thrusters, furthering in the rim-driven electric generator with a hubless turbine design is investigated. The rim-drive turbine (RDT) comprises of a ring that rotates around the rotor blades and an electric generator stator that is mounted on the water pipe. This approach has several advantages, including no shaft or other components are installed on the inside

which will not hinder the water flow neither create losses due to such installations. Also, a compact hydro-turbine unit can be easy to implement as new construction or for retrofitting an existing installation, including maintenance and operation of hydro turbine setups. Additionally, since no installation is required at the center of the rotor, more water will flow through the cross-section of the turbine, thus resulting in higher power output and efficiency as well. The hubless design requires less material which will facilitate manufacturing, considering the non-linear relation between the cost and the size in case of the 3D printing. Furthermore, the shaft-less turbine is environment-friendly, as this design allows fish to pass through it.

The head in the investigated WWTP is 3 meters, which is considered low for hydro turbine applications. However, Kaplan (propeller) type is applicable for such scenarios of low head and high flow rate, therefore, Kaplan hydro turbine is selected in this study. Figure 1-10 [28] shows the classification of hydro-turbines based on both head (in meters) and flow rate (in L/s) and indicates the range of operation of Kaplan turbines.

5.2.1 System Sizing by HOMER

The average daily effluent flow rate for each month was obtained by the WWTP's personnel, as shown in Figure 5-1. It can be noticed that the maximum average flow rate of 9,000 L/s occurred in February, while the minimum flow rate of around 6,500 L/s recorded in June, with an average yearly flow rate of 7,750 L/s per day. As both the head and flow rate are known, HOMER software can be used with some other assumptions as a design reference point (see Table 5-1) to estimate the performance of the hydro turbine system.

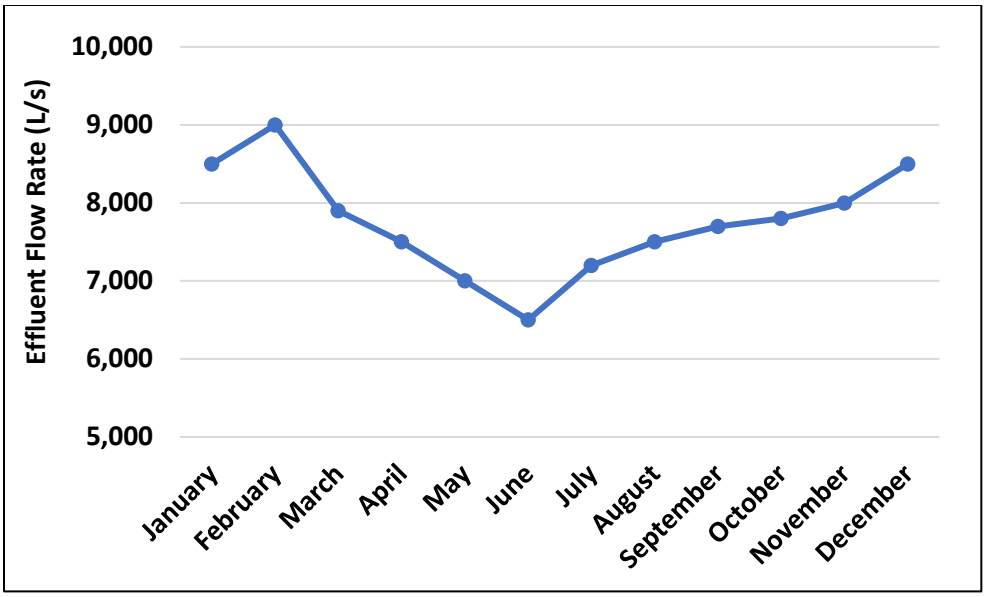

Figure 5-1: Average daily WWTP's effluent flow rate for each month (in L/s)

Table 5-1: Design reference parameters for the hydro turbine

Parameter	Value
Available head (meter)	3
Design flow rate (L/s)	10,000
Minimum flow rate ratio (%)	50
Maximum flow rate ratio (%)	150
Efficiency (%)	92
Pipe head loss (%)	15

Through the system simulation using HOMER, the nominal capacity of the system (in kW) can be determined as well as the energy generated (in kWh) around the year based on the effluent flow rate available. However, to validate the capacity of the system, the theoretical hydro turbines power equation (Eq. 3-8) [152] is used, considering the system boundary conditions.

5.2.2 Hydro Turbine Design with In-house Code

The hubless RDT is somewhat unique in its design. Therefore, a special in-house code is used to optimize blades design for both the stator and the rotor with known system conditions (i.e., head, flow rate, and rotational speed). We proposed five blades-rotor, while nine blades for the

stator are used [119]. Also, the optimization process covers that the diameter of the turbine is two meters. Table 5-2 describes other parameters of the stator and the RDT.

Table 5-2: Hydro turbine rim-rotor and stator parameters

Parameter	Value
Number of blades for the rotor	5
Number of meridional sections (rotor)	3
Number of blades for the stator	9
Number of meridional sections (stator)	5
Turbine diameter (meter)	2.0
Rotational speed (rpm)	100 - 200
Specific speed (nq)	138.7 - 277.5
Swirl angle (degrees)	90
Rim (shroud) length (m)	0.7
Rim (shroud) thickness (m)	0.02

Kaplan turbines can be of both blades type configuration: fixed or adjustable. Fixed-blade Kaplan turbine is assumed for this case, taking into consideration less initial cost and simplicity of manufacturing. Figure 5-2 shows the proposed CAD for the hubless RDT (a) front view and (b) isometric view, and Figure 5-3 shows the CAD for the hubless stator with front and isometric views.

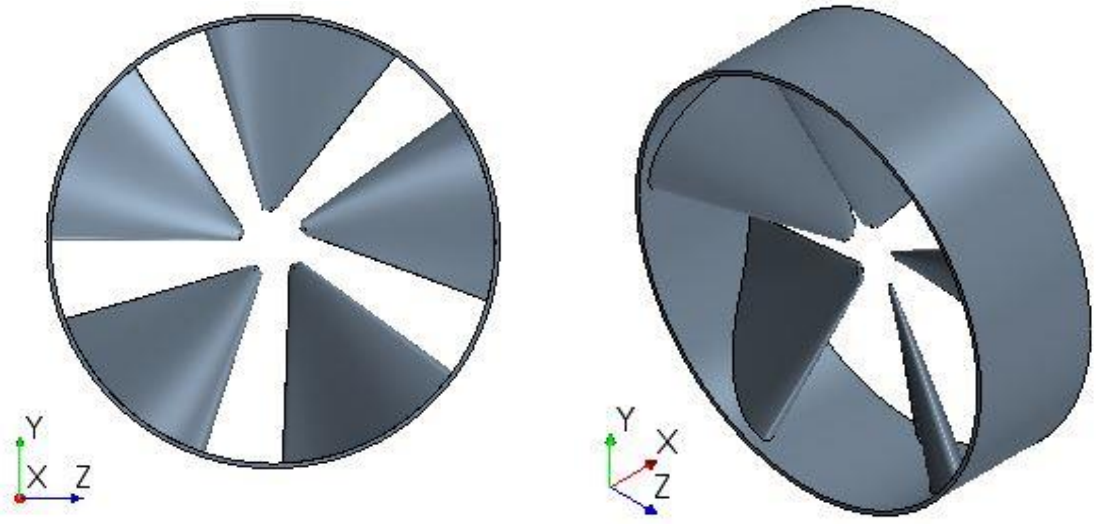

(a) (b)

Figure 5-2: CAD for the proposed hubless RDT (a) Front view (b) Isometric view

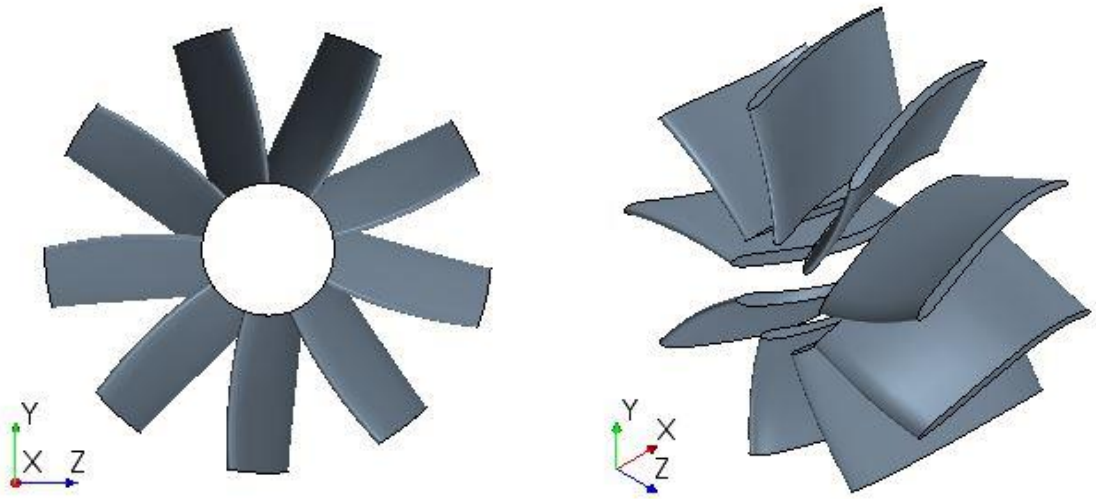

(a) (b)

Figure 5-3: CAD for the Proposed hubless turbine stator (a) Front view (b) Isometric view

5.2.3 Performance of Hydro Turbine by CFD

To predict the system performance with different boundary conditions, such as flow rate and rotational speed, a numerical solution is used in this study. The numerical solution is obtained by utilizing a 3D-CFD simulation with Large Eddy Simulation (LES) for transient turbulence modeling since such a turbomachine device generates a rotational motion with high swirl and turbulent flow as well. Design reference parameters from HOMER and in-house code CAD designs for the RDT and the stator are considered as an input for the CFD simulation.

S-type hydro turbine configuration is recommended for this WWTP. Hence, Figure 5-4 shows the simulation model for the turbine casing (includes the hubless RDT and the hubless stator), intake and draft tube parts of the system based on the proposed configuration. The figure also indicates the location and the horizontal orientation of the stator/rotor set in the system, as well as the inlet and the outlet of the flow. The selected intake and draft tubes angles are 24 degrees, and 12 degrees, respectively, based on an optimization study was done before with almost the same

system conditions [171]. Figure 5-5 indicates a 3D meshed view of the turbine configuration within the system.

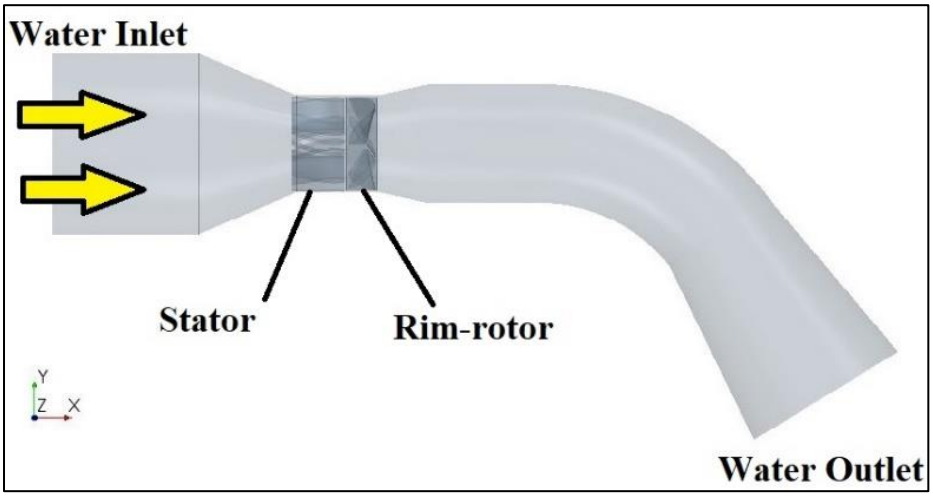

Figure 5-4: Geometry of hydro turbine simulation model

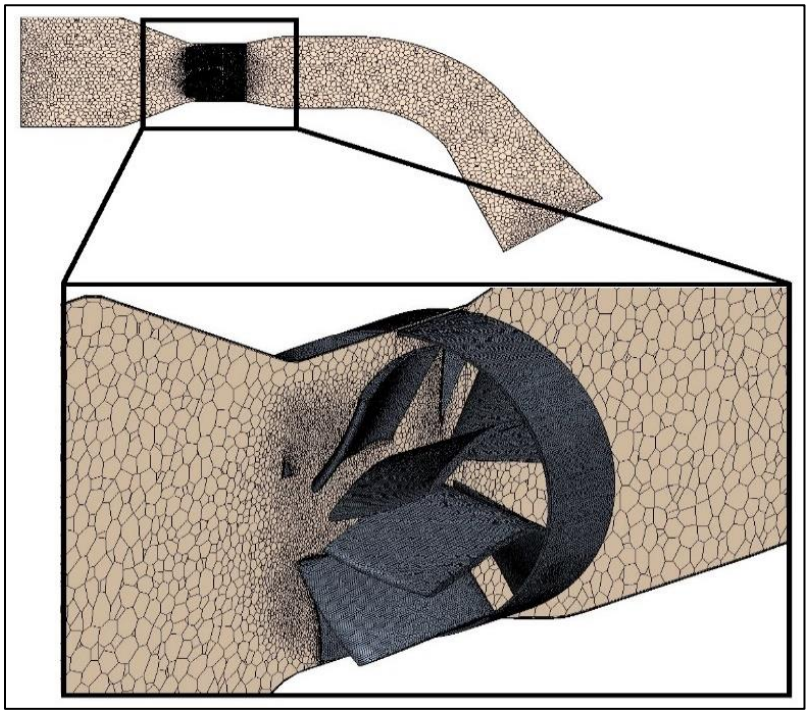

Figure 5-5: Hydro turbine configuration within the system

Turbulent transient status of the flow due to the high swirl generates large and small-scale eddies with spatial and temporal variations, and to capture and simulate these eddies; Large Eddy

Simulation (LES) is considered for the CFD approach as the transient turbulence model; since it is more accurate than the Unsteady Reynolds Average Navier-Stokes (URANS) approach [135].

Large Eddy Simulation (LES) solves large-scale eddies with Navier-Stokes (N-S) equations, while models the small-scale motions by wall-adapting local-eddy (WALE) as subgrid-scale models (SGS) rather than Smagorinsky SGS to compute the turbulent viscosity.

The WALE SGS is based on algebraic equations, while Smagorinsky SGS is based on a multi-length hypothesis. The latter is simple and not computationally extensive, but there are some limitations (i.e., damping effects near walls). Correspondingly, WALE is the most straightforward method, with superior performance and extra accurate modeling near the wall without damping effects [136]. Even though LES is an expensive and extensive computational approach, however, it is the best model to utilize where turbulent flow behavior exists.

A time-step of 10^{-3} seconds along with an implicit unsteady solution with the first-order accuracy for temporal discretization is selected for this CFD simulation. These models lead to a stable simulation solution with a reasonable computational time. Table 5-3 states the physical parameters, conditions, and enabled models for the simulation.

Table 5-3: Physical parameters, conditions, and enabled models for the simulation

Parameter	Value
Total Head (m)	3.0
Mass flow at the inlet (kg/s)	5,000 - 15,000
Outlet pressure (kPa)	101.325
Rotor rotational speed (rpm)	100 - 200
Timestep (s)	10^{-3}
Number of iterations (per time step)	5
Enabled Models	
Gravity	
Gradients, Three dimensional	
Turbulent, Segregated Flow**,** Implicit Unsteady, Transient	
Large Eddy Simulation (LES), WALE Subgrid Scale	
Multiphase Interaction, Volume of Fluid (VOF)	

5.3 Results

The approach followed in this study comprises sizing the hydro turbine system, design the hubless RDT and the hubless stator CADs and testing the performance of the proposed turbine set, by using HOMER, in-house code, and STAR-CCM+ software, respectively. The following sections present the results of this case study.

5.3.1 System Sizing by HOMER

HOMER inputs of 3 meters of water head and an average daily flow rate of 7,750 L/s led to 1,564 MWh/year of electricity generation, which can be considered as annual energy savings for the WWTP. Taking into account the average electricity cost of $56.8/MWh, the annual cost savings is $88,835/year. Figure 5-6 shows the monthly average electric production by the turbine (in kW) in which February recorded the maximum generated power followed by January and December, corresponding with the effluent flow rate indicated at these months, while the minimum power -which is in concurrence with the drop in the effluent flow rate- was captured in June. The estimated nominal, maximum and minimum capacities of the hydro turbine is shown in

Table ***5-4***.

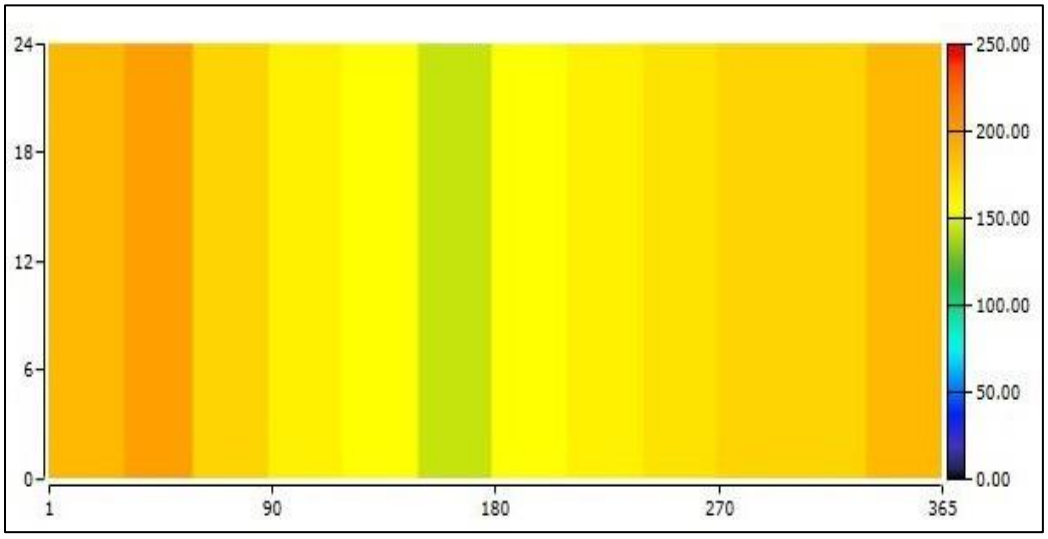

Figure 5-6: Monthly average electric production (in kW)

Table 5-4: Power output of the hydro turbine

Parameter	Value
Nominal capacity (kW)	270.8
Minimum output (kW)	149.7
Maximum output (kW)	207.3
Annual total production (MWh)	1,564
Annual hours of operation (hour)	8,760

However, to validate the nominal capacity of the system that was estimated by the software, Eq.3-8 is used with the same available conditions resulting in 270 kW of capacity. The nominal calculated capacity meets with the estimated one generated via HOMER with only 0.3% of error.

5.3.2 Mesh Independent Study

A significant factor to consider for the validity of the CFD simulation results is the mesh independent analysis. For that effect, six different polyhedral mesh setups of 0.5, 1.0, 1.5, 2.0, 2.5, and 3.0 million cells were assumed for the proposed hydro turbine system. The power output and efficiency of the turbine were the basis of the performance comparison.

Based on the results of both the power output and the efficiency, as shown in Figure 5-7, the maximum difference between these setups is only about 2.5% and 2.7% in power output and efficiency, respectively. It can also be noticed that for the 2.5 and 3.0 million cells setups the power and efficiency values are less than the values of the 2.0 million cells case. Therefore, simulation results are independent of some cells. Thus, the 2.0 million cell setup was used for the simulation model of this study, as this selection provides a reasonable balance between the simulation's resolution and the computational time.

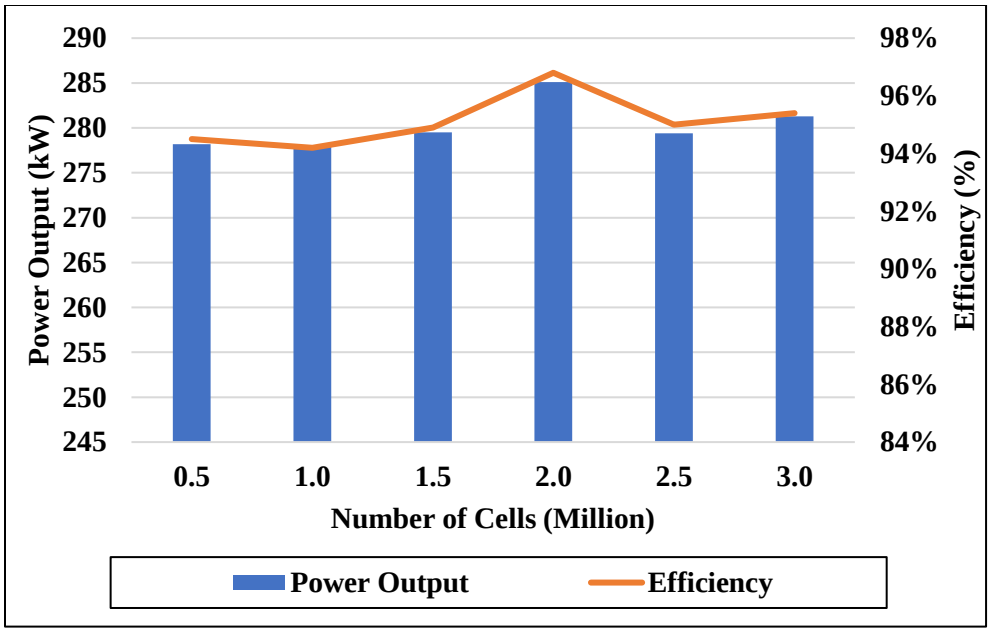

Figure 5-7: Mesh independent study results

5.3.3 CFD Simulation Results

The performance of the hubless RDT is simulated in STAR-CCM+ with pre-defined boundary conditions after importing the optimized CAD design to the simulation geometry. As a result, simulations matrix of 15 different cases for the proposed turbine were performed by varying the flow rate between 5,000 L/s and 10,000 L/s as well as the rotational speed in the range of 100 – 200 RPM. Figure 5-8 illustrates the results of these 15 simulations in a performance curve scheme. Both the power output and efficiency of the system are low as the flow rate, and the rotational speed is low, and vice versa. It can be noticed that the system performs better for the 200 RPM curve, with a maximum efficiency of 94.9% at the design reference flow rate of 10,000 L/s.

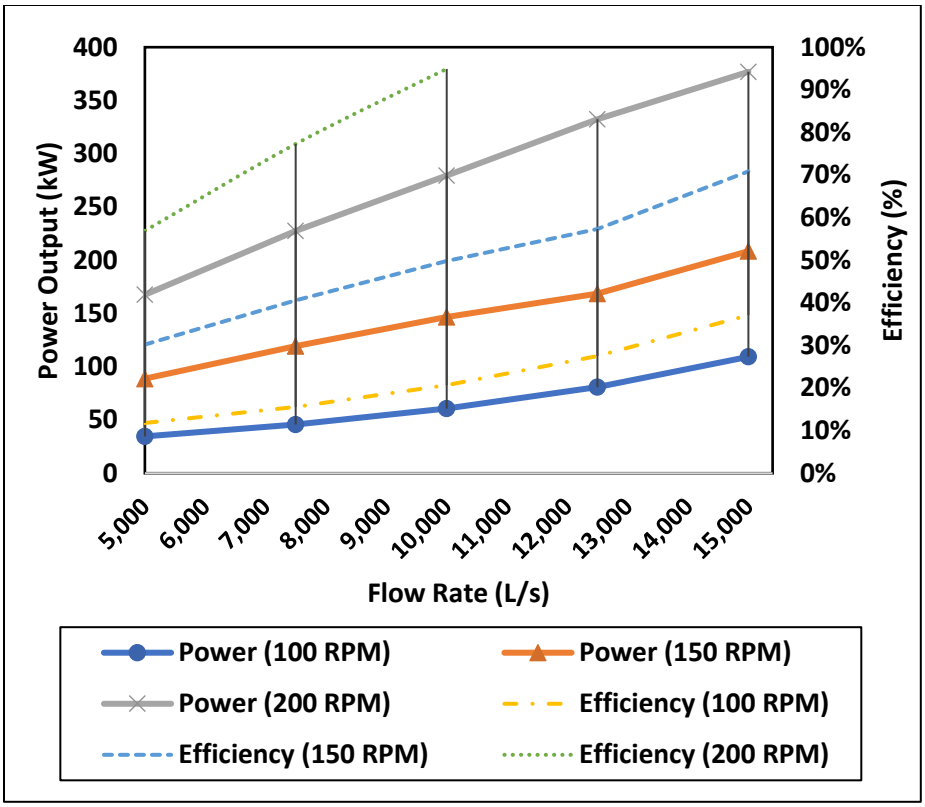

Figure 5-8: Performance curve of the proposed hydro turbine

Chapter 6: Conclusions and Future Work Recommendations

6.1 Research Conclusions

In this research, investigation of power-efficient micro and pico Kaplan hydro turbines at very-low-head with rim-driven generators to be studied and evaluated, specifically, at heads of less than 3 meters (10 ft). Optimization of performance and design for a 3D printed conventional -with shaft- 7.6 cm (3-inch) Kaplan turbine was carried out based on an experimental setup in the Hydro Turbines Laboratory of the University of Wisconsin-Milwaukee in addition to the utilization of Computational Fluid Dynamics (CFD). Then a shaftless rim-driven generator-based turbine (RDT) was introduced and optimized. Such a new hydro turbine perception can increase the efficiency (of power generation) of hydro turbines in general, and the efficiency of low-head turbines in specific.

The study covered these main points:

- Design optimization for 7.6 cm (3-inch) and 90 cm (35-inch) conventional Kaplan hydro turbines at specific boundary conditions of 2.6 m (8.5 ft) maximum water head.
- The design optimization includes; the number of the blades for the turbine's rotor (runner) and stator, the blade wrap-angle of the rotor, intake and draft tubes angles, lengths and shapes, and the guide vanes.
- Evaluating the performance (power output and efficiency) of the conventional turbine by utilizing CFD and by testing a 3D printed model of the turbine in a custom-built experimental setup.
- Evaluating the turbine at different water heads (from 2.0 m to 2.6 m) and different rotational speeds (0 – 4000 rpm).

- The CFD setup is based on 3D transient turbulent featuring the Large Eddy Simulation (LES) model, and STAR-CCM+ is the CFD software. Besides, the high-performance computing (HPC) cluster of the University of Wisconsin-Milwaukee is used for solving the complex CFD simulations.
- Introduce the rim-driven shaftless turbine (RDT) at the same boundary conditions to evaluate the advantage of the RDT over the conventional turbines.
- Evaluating the performance of the RDT by utilizing RMF and CFD simulations and by testing a 3D printed model of the turbine in a custom-built experimental setup.
- Evaluating the RDT at different a water head of 2.6 m and different rotational speeds (0 – 2000 rpm).
- Introduce some applications of the rim-driven turbines (RDT), i.e. wastewater treatment plants (WWTPs) where very-low head and high flow of water are available.

6.1.1 Conclusions of the Turbine's Blades Optimization

A multidisciplinary design optimization (MDO) method is adopted to develop and improve the performance of a horizontal micro-Kaplan hydro turbine at a very-low head (less than 3 meters), an in-house code was developed and utilized for the turbine CADs optimization and generation. Also, STAR-CCM+ software as a CFD tool for evaluation the turbine performance, followed by experimental testing for CFD results validation. Hence, the main findings are:

- A preliminary CAD for the rotor was generated based on the given boundary and operation conditions. An optimization algorithm inspired by MDO was presented.
- Two design variables were considered for the optimization process in this study; the number of the blades (3, 4, 5, 6, and 7 blades) at a range of rotational speeds (500 – 3,000

RPM) and the blade wrap angle. The investigation in these two variables resulted in over 150 3D flow simulations.

- The 6-blade rotor recorded the highest power output (121 W) at the 1,500 RPM rotational speed over the 5-blade and the 7-blade rotors, the 7-blade rotor has more losses is the reason behind being in the second place.
- The blade wrap angle has a significant effect on the power output of the turbine, where it was able to increase the power output by 23%. The optimized wrap angle is located at the range of 100^{o}-105^{o} at the hub and the shroud.
- The 6-blade rotor was 3D printed and tested in an experimental setup to validate the CFD results. The characteristics curve of the experimental results have the same trend as the CFD curve, were both showed the optimum rotational speed range of 1,400 – 1,600 RPM. There was an average percentage of 47% difference between the experimental and the CFD data; however, by considering the uncertainty and error analysis, this percentage was minimized to 35% only.

6.1.2 Conclusions of the Intake and Draft Tubes Optimization

In this study, 3D-CFD simulations with LES of transient turbulence modeling were conducted to optimize the design of both the intake and the draft tubes for two different diameter sizes Kaplan micro-hydro turbine systems to minimize the losses, increase the output power and improve the system efficiency as well. And then, the findings are:

- Six intake tube angles and five draft tube angles were studied for both the 7.6-cm horizontal and the 90-cm vertical systems; a 24-degree angle is the best for the intake tube, where the draft tube angle is best at 12 - 18-degree angle.

- Changing the angle of the draft tube has a larger effect over the intake tube regarding the output power and the efficiency; As the exit kinetic energy at the draft tube (diffuser) considered as one of the most efficiency losses in hydro turbines
- Four lengths were considered for the intake and the draft tubes (0.4, 0.9, 1.4, and 1.9 m) for the 90-cm vertical system only, as the 7.6 cm horizontal system has some length limitations. 0.9-1.4 m is the best for the intake tube, while for the draft tube, the power and the efficiency increase with longer draft tubes
- Two bellmouth designs (simple radius and elliptical) were introduced for the intake and the draft tube; such improvement added up to 9% on the efficiency of the system.
- The range of (2 - 16) inch as the radius of curvature for the simple radius bellmouth tube was investigated, in addition to three arbitrary elliptical tube designs.

6.1.3 Conclusions of the Conventional Kaplan Turbine Performance

In this study, several different parameters were investigated based on 3D-CFD simulations with LES of transient turbulence modeling to optimize the performance of two different Kaplan hydro turbine systems for very low head applications. The two systems are a 7.6-cm diameter horizontally oriented and a 90-cm diameter vertically oriented turbines. The findings are:

- The range of rotational speeds was investigated for both systems; the recommended calculated rotational speed range for the 7.6-cm system was between 2500 - 3000 rpm, and around 1000 rpm, experimentally. Also, a justification for the disagreement between the calculated and experimental results was presented in this study.
- The 90-cm system was only investigated numerically. Hence, the CFD results demonstrated a recommended rotational speed of around 350 rpm. The optimum speed is

slightly different for power output and efficiency, something to keep in mind for generation control development.

6.1.4 Conclusions of the Rim Drive Turbine (RDT) Performance

A custom-built hydro turbine assembly (RDT) inspired by the ships' Rim-driven Propellers (RDP) was developed in this study. The assembly consists mainly of a stator (coils) of a 3-ph, 1 HP induction motor, NdFeB magnets, and 3D printed parts (custom flanges, stator, rim-rotor, diffuser, and custom sleeves to separate the water flow from the electric stator). The concept of permanent magnet generators was used for the RDT. Simply, it consists of a rotating ring around the outside of the rotor blades, and the electric generator stator is mounted outside the water conduit. This design has several advantages over the conventional Kaplan turbine beside the higher power generation efficiency. The RDT was tested experimentally in the Hydro Turbine Lab of the University of Wisconsin-Milwaukee with a maximum water head of 2.6 m, and the results were validated with RMF and CFD simulations. Hence, the main findings are:

- A preliminary CAD assembly of the RDT was designed, and then 3D printed into seven parts. With an electric stator, 16 magnets, and two thin bearings, the RDT is assembled and was tested experimentally.
- Several cases were tested experimentally over a range of rotational speeds (0 rpm to ~2000 rpm); two for comparing the grade of the magnets (N52 and N35), one for evaluating the effect of increase another row of magnets, and then another two for comparing the RDT rotor with hub versus the hubless design.
- Two simulation models were developed for evaluating the performance theoretically; a rotating magnetic field (RMF) simulation by using a software called EMS by EMWorks to calculate the generated magnetic field flux/intensity and thus the generated power, and

a CFD simulation by using Star-CCM+ software to study the behavior of the water and to predict the maximum theoretical power available from the RDT.

- The optimum range of rotational speeds is between 1000 rpm to 1500 rpm, while the peak power output recorded was 8.6 W at 1480 rpm with a double-row of N52 magnets' arrangement.
- The N52 magnets were found to generate an average of 65% more power over the N35 magnets, as the N52 magnets are stronger than the N35 magnets. Likewise, the double-row of magnets achieved an average of 85% more power than the single-row arrangement. In general, a higher number of magnets' rows can achieve higher power output as the magnetic field become stronger. Upgrading to quadruple-row arrangement recorded a 274% increase in power output over the single-row RDT.
- The hubless design was presented and compared with a rotor with the hub, in this case, and without any optimization for the design, the hubless design show no improvement on the power output. However, this design has an advantage of allowing debris or fish to pass through especially in the case of run-a-river
- The RDT shows a higher capability of theoretical power generation with up to 460 W. On the other hand, the conventional turbine has a theoretical power output of up to 390 W only. Hence, the RDT has 18% more power output than the conventional turbine.
- Besides the higher efficiency of the generation of the RDT, this approach has some other advantages such as reducing the vibration and noise, considered a compact design with less weight, more flexible in installations, cost-effective, and less maintenance.

6.1.5 Conclusions of the RDT Applications – WWTP Case Study

In this study, utilization of a hubless RDT combined with a hubless stator for a very-low head (3 meters) and high effluent flow rate WWTP is presented, with the aid of HOMER for sizing the turbine, in-house code for turbine CADs and STAR-CCM+ for testing the turbine performance. Hence, the main findings are:

- The average daily effluent flow rate for the selected WWTP ranges between 6,500 L/s to 9,000 L/s with an average flow rate of 7,750 L/s. Such flow rate accommodates a hydro turbine of 270 kW nominal capacity. This capacity was validated with the theoretical hydro turbine power equation.
- The simulation performed through HOMER indicated that the 270-kW hydro turbine could produce total electric energy of 1,564 MWh/year. This amount can be considered as an annual energy saving for the plant with a yearly cost savings of $88,835/year leading to 16% of energy savings the designated WWTP.
- The significance of employing the in-house code concluded in optimizing the CAD design for the hubless RDT and the hubless stator. Two meters diameter turbine with five blades for the rotor and nine blades for the stator was selected.
- A performance curve for the proposed hubless RDT design was generated by 15 different CFD simulations. Such a proposed design contributes to increasing the efficiency of Kaplan hydro turbines up to 94.9%.

6.2 Future Work Recommendations

Based on the findings of the study in hand, future work is recommended as below:

- Further investigation for optimizing the turbine blades is recommended, some of the parameters were not evaluated in this study and some of these are the blade' angle over

the span (from the leading edge to the trailing edge), the blade deflection angle, the camber angle, and the stagger angle.

- The concept of generating electricity from the RDT was proven in this research. However, the electrical design of the RDT assembly need to be improved for higher power generation, and that includes but not limited to selecting different electrical stator (in size and coils' material) and sizes and arrangement of magnets.
- Optimizing the design of the RDT geometry by studying various design parameters of the rotor, the stator, and intake and draft tubes.
- Optimizing the hubless RDT design to improve the power output over the rotor with the hub as the hubless design already have other significant advantages.
- A vibration and noise study need to be conducted with the use of industrial class thin bearings to maintain a dynamically balanced system. In addition to conducting a finite element analysis (FEA) when the RDT rotor's material is selected.
- Investigating the selection of thin bearings by taking into consideration a bearing that can withstand high rotational speeds with a waterproof sealed design and non-magnetic or non-metal material.
- One last recommended work on how optimizing the turbine's design (the conventional or the RDT) can reduce and treat the developed cavitation near the rotor's blades at high flow rates and rotational speeds, as the existence of such a phenomena decreases the power output and wear the blade surface over time.

References

[1] G. Stein-Brzozowska, C. Bergins, A. Kukoski, S. Wu, M. Agraniotis, and E. Kakaras, "The Current Trends in Conventional Power Plant Technology on Two Continents From the Perspective of Engineering, Procurement, and Construction Contractor and Original Equipment Manufacturer," *J. Energy Resour. Technol.*, vol. 138, no. 4, p. 044501, Mar. 2016, doi: 10.1115/1.4032731.

[2] K. Vincent Wong, "Engineering Solutions to the Greenhouse Gases Generated by Hydroelectric Plants," *J. Energy Resour. Technol.*, vol. 136, no. 2, p. 024701, Apr. 2014, doi: 10.1115/1.4027260.

[3] B. G. S. Prasad, "Energy efficiency, sources and sustainability," *J. Energy Resour. Technol. Trans. ASME*, vol. 132, no. 2, pp. 1–2, 2010, doi: 10.1115/1.4001684.

[4] REN21 Secretariat, "Renewable Energy Policy Network for the 21st Century, 2019, Renewables 2019 Global Status Report," Paris, France, 2019.

[5] REN21 Secretariat, "Renewable Energy Policy Network for the 21st Century, 2018, Renewables 2018 Global Status Report," Paris, France, 2018.

[6] REN21 Secretariat, "Renewable Energy Policy Network for the 21st Century, 2017, Renewables 2017 Global Status Report," Paris, France, 2017.

[7] REN21 Secretariat, "Renewable Energy Policy Network for the 21st Century, 2016, Renewables 2016 Global Status Report," Paris, France, 2016.

[8] REN21 Secretariat, "Renewable Energy Policy Network for the 21st Century, 2015, Renewables 2015 Global Status Report," Paris, France, 2015.

[9] B. Hamududu and A. Killingtveit, "Assessing climate change impacts on global hydropower," *Energies*, vol. 5, no. 2, pp. 305–322, 2012, doi: 10.3390/en5020305.

[10] "Total Energy Annual Data - U.S. Energy Information Administration (EIA)." [Online]. Available: https://www.eia.gov/totalenergy/data/annual/. [Accessed: 27-Aug-2019].

[11] "Electric Power Monthly - U.S. Energy Information Administration." [Online]. Available: https://www.eia.gov/electricity/monthly/. [Accessed: 27-Aug-2019].

[12] World Energy Council, "World Energy Resources: 2016 Survey," London, 2016.

[13] International Energy Agency, "Key World Energy Statistics 2017 Report," Paris, France, 2017.

[14] S. Derakhshan and N. Kasaeian, "Optimization, Numerical, and Experimental Study of a Propeller Pump as Turbine," *J. Energy Resour. Technol.*, vol. 136, no. 1, p. 012005, Feb. 2014, doi: 10.1115/1.4026312.

[15] Oak Ridge National Laboratory, “2017 Hydropower Market Report,” Oak Ridge, 2018.

[16] V. Nelson and K. Starcher, *Introduction to Renewable Energy*, Second Edi. CRC Press, 2015.

[17] B. of Reclamation, “Hoover Dam | Bureau of Reclamation.” [Online]. Available: https://www.usbr.gov/lc/hooverdam/index.html. [Accessed: 16-Nov-2019].

[18] Bureau of Reclamation, “Grand Coulee Dam | Bureau of Reclamation.” [Online]. Available: https://www.usbr.gov/pn/grandcoulee/index.html. [Accessed: 16-Nov-2019].

[19] H.-J. Wagner and J. Mathur, *Introduction to Hydro Energy Systems*. 2011.

[20] S. van Vuuren, C. Blersch, and M. van Dijk, “Modelling the feasibility of retrofitting hydropower to existing South African dams,” *Water SA*, vol. 37, no. 5, 2011, doi: 10.4314/wsa.v37i5.5.

[21] E. Oud, “The evolving context for hydropower development,” *Energy Policy*, vol. 30, no. 14, pp. 1215–1223, Nov. 2002, doi: 10.1016/S0301-4215(02)00082-4.

[22] G. W. Frey and D. M. Linke, “Hydropower as a renewable and sustainable energy resource meeting global energy challenges in a reasonable way,” *Energy Policy*, vol. 30, no. 14, pp. 1261–1265, Nov. 2002, doi: 10.1016/S0301-4215(02)00086-1.

[23] U.S. Department of Energy, “Five Promising Types of Water Power,” 2017. [Online]. Available: https://www.energy.gov/sites/prod/files/2017/06/f35/Five Types of Hydropower Infographic.pdf. [Accessed: 13-Nov-2019].

[24] Japan International Cooperation Agency, “Guideline and Manual for Hydropower Development Vol. 1 Conventional Hydropower and Pumped Storage Hydropower,” 2011.

[25] A. Singh, “Principles of renewable energy technologies—biomass and hydropower,” in *Talking Renewables: A renewable energy primer for everyone*, First Edit., IOP Publishing, 2018.

[26] A. Carravetta, S. D. Houreh, and H. M. Ramos, *Pumps as Turbines: Fundamentals and Applications*, First Edit. Springer, 2018.

[27] U.S. Department of Energy, “Types of Hydropower Turbines | Department of Energy.” [Online]. Available: https://www.energy.gov/eere/water/types-hydropower-turbines. [Accessed: 14-Nov-2019].

[28] J. Chen, W. Lu, Z. Hu, Y. Lei, and M. Yang, “Numerical studies on the performance of a drag-type vertical axis water turbine for water pipeline,” *J. Renew. Sustain. Energy*, 2018, doi: 10.1063/1.5027551.

[29] P. Breeze, “Power Generation Technologies,” in *Power Generation Technologies, Second Edition*, Second Edi., Elsevier Science, 2014, pp. 1–396.

[30] E. L. Wolf, *Physics and technology of sustainable energy*. Oxford University Press, 2018.

[31] Renewables First, “Hydropower Head and Flow - Renewables First.” [Online]. Available: https://www.renewablesfirst.co.uk/hydropower/hydropower-learning-centre/head-and-flow-detailed-review/. [Accessed: 15-Nov-2019].

[32] S. Davis, *Microhydro : Clean Power from Water*. New Society Publishers, 2003.

[33] “Classification of Hydroelectric Power Plants.” [Online]. Available: https://www.engineeringenotes.com/power-plants-2/hydroelectric-power-plant/classification-of-hydroelectric-power-plants/29422. [Accessed: 16-Nov-2019].

[34] D. G. Hall and K. S. Reeves, “A Study of United States Hydroelectric Plant Ownership,” 2006.

[35] I. Renewable Energy Agency, “RENEWABLE ENERGY TECHNOLOGIES: COST ANALYSIS SERIES,” 2012.

[36] UK’s Department for International Development (DFID), “Hands On: Pico-Hydro - Vietnam,” 2004. [Online]. Available: https://web.archive.org/web/20070807184919/http://www.tve.org/ho/doc.cfm?aid=1636&lang=English. [Accessed: 16-Nov-2019].

[37] Aurora Power & Design, “1000W Low-Head Kaplan Hydro Turbine.” [Online]. Available: http://www.aurorapower.net/products/categoryid/4/list/1/level/a/productid/234.aspx. [Accessed: 16-Nov-2019].

[38] S. (Scott L. . Davis, *Serious Microhydro: Water Power Solutions from the Experts*. New Society, 2010.

[39] P. A. Breeze, *Hydropower*, First Edit. Academic Press, 2018.

[40] US Army Corps of Engineers, “How Hydropower Works.” [Online]. Available: https://www.sas.usace.army.mil/About/Divisions-and-Offices/Operations-Division/J-Strom-Thurmond-Dam-and-Lake/Hydropower/How-Hydropower-Works/. [Accessed: 17-Nov-2019].

[41] N. Smith, *Motors as Generators For Micro Hydro Power*. Practical Action Pub, 2008.

[42] X. Yan, X. Liang, W. Ouyang, Z. Liu, B. Liu, and J. Lan, “A review of progress and applications of ship shaft-less rim-driven thrusters,” *Ocean Engineering*, vol. 144. Elsevier Ltd, pp. 142–156, 01-Nov-2017, doi: 10.1016/j.oceaneng.2017.08.045.

[43] B. W. Song, Y. J. Wang, and W. L. Tian, “Open water performance comparison between hub-type and hubless rim driven thrusters based on CFD method,” *Ocean Eng.*, vol. 103, pp. 55–63, May 2015, doi: 10.1016/j.oceaneng.2015.04.074.

[44] P. M. Tuohy, “Development of Canned Line-start Rim-driven Electric Machines,” 2011.

[45] U.S. Department of Energy, “Hydropower Technology Development.” [Online]. Available: https://www.energy.gov/eere/water/hydropower-technology-development. [Accessed: 18-Nov-2019].

[46] U.S. Department of Energy, “Hydropower Resource Assessment and Characterization.” [Online]. Available: https://www.energy.gov/eere/water/hydropower-resource-assessment-and-characterization. [Accessed: 18-Nov-2019].

[47] B. Hadjerioua, Y. Wei, and S.-C. Kao, “An Assessment of Energy Potential at Non-Powered Dams in the United States Report,” 2012.

[48] M. T. L. Barros, F. T. C. Tsai, S. li Yang, J. E. G. Lopes, and W. W. G. Yeh, “Optimization of large-scale hydropower system operations,” *J. Water Resour. Plan. Manag.*, 2003, doi: 10.1061/(ASCE)0733-9496(2003)129:3(178).

[49] E. Cristian Finardi and M. Reolon Scuzziato, “Hydro unit commitment and loading problem for day-ahead operation planning problem,” *Int. J. Electr. Power Energy Syst.*, 2013, doi: 10.1016/j.ijepes.2012.07.023.

[50] M. S. Babel, C. Nguyen Dinh, M. R. A. Mullick, and U. V. Nanduri, “Operation of a hydropower system considering environmental flow requirements: A case study in La Nga river basin, Vietnam,” *J. Hydro-Environment Res.*, 2012, doi: 10.1016/j.jher.2011.05.006.

[51] J. W. Labadie, “Optimal operation of multireservoir systems: State-of-the-art review,” *J. Water Resour. Plan. Manag.*, 2004, doi: 10.1061/(ASCE)0733-9496(2004)130:2(93).

[52] N. Kishor, R. P. Saini, and S. P. Singh, “A review on hydropower plant models and control,” *Renewable and Sustainable Energy Reviews*. 2007, doi: 10.1016/j.rser.2005.06.003.

[53] Q. Goor, R. Kelman, and A. Tilmant, “Optimal multipurpose-multireservoir operation model with variable productivity of hydropower plants,” *J. Water Resour. Plan. Manag.*, 2011, doi: 10.1061/(ASCE)WR.1943-5452.0000117.

[54] L. Le Ngo, H. Madsen, and D. Rosbjerg, “Simulation and optimisation modelling approach for operation of the Hoa Binh reservoir, Vietnam,” *J. Hydrol.*, 2007, doi: 10.1016/j.jhydrol.2007.01.003.

[55] J. I. Pérez-Díaz, J. R. Wilhelmi, and L. A. Arévalo, “Optimal short-term operation schedule of a hydropower plant in a competitive electricity market,” *Energy Convers. Manag.*, 2010, doi: 10.1016/j.enconman.2010.06.038.

[56] D. Connolly, H. Lund, P. Finn, B. V. Mathiesen, and M. Leahy, “Practical operation strategies for pumped hydroelectric energy storage (PHES) utilising electricity price arbitrage,” *Energy Policy*, 2011, doi: 10.1016/j.enpol.2011.04.032.

[57] M. Mahmoud, K. Dutton, and M. Denman, “Dynamical modelling and simulation of a cascaded reserevoirs hydropower plant,” *Electr. Power Syst. Res.*, 2004, doi: 10.1016/j.epsr.2003.12.001.

[58] S. C. Chang, C. H. Chen, I. Kong Fong, and P. B. Luh, “Hydroelectric generation scheduling with an effective differential dynamic programming algorithm,” *IEEE Trans. Power Syst.*, 1990, doi: 10.1109/59.65900.

[59] S. Soares and A. A. F. M. Carneiro, “Optimal operation of reservoirs for electric generation,” *IEEE Trans. Power Deliv.*, 1991, doi: 10.1109/61.85854.

[60] R. Naresh, “Hydro system scheduling using ANN approach,” *IEEE Trans. Power Syst.*, 2000, doi: 10.1109/59.852149.

[61] Z. K. Shawwash, T. K. Siu, and S. O. Denis Russell, “The B.C. hydro short term hydro scheduling optimization model,” *IEEE Trans. Power Syst.*, 2000, doi: 10.1109/59.871743.

[62] B. Mo, A. Gjelsvik, A. Grundt, and K. Kåresen, “Optimisation of hydropower operation in a liberalised market with focus on price modelling,” in *2001 IEEE Porto Power Tech Proceedings*, 2001, doi: 10.1109/PTC.2001.964603.

[63] C. T. Cheng, W. C. Wang, D. M. Xu, and K. W. Chau, “Optimizing hydropower reservoir operation using hybrid genetic algorithm and chaos,” *Water Resour. Manag.*, 2008, doi: 10.1007/s11269-007-9200-1.

[64] B. Xu, P. A. Zhong, X. Wan, W. Zhang, and X. Chen, “Dynamic feasible region genetic algorithm for optimal operation of a multi-reservoir system,” *Energies*, 2012, doi: 10.3390/en5082894.

[65] G. S. Bastos, E. C. Bortoni, B. M. M. L. Augusto N. C. Viana, and F. Micerino, “Hydro Power Plants Operation Optimization Using An On Offline Approach - Powid 2011,” in *54th POWID Annual ISA Symposium 2011*, 2011.

[66] J. C. Grygier and J. R. Stedinger, “Algorithms for Optimizing Hydropower System Operation,” *Water Resour. Res.*, 1985, doi: 10.1029/WR021i001p00001.

[67] M. A. Mariño and B. Mohammadi, “Reservoir Operation by Linear and Dynamic Programming,” *J. Water Resour. Plan. Manag.*, vol. 109, no. 4, pp. 303–319, Oct. 1983, doi: 10.1061/(ASCE)0733-9496(1983)109:4(303).

[68] M. Sharif and R. Wardlaw, “Multireservoir systems optimization using genetic algorithms: Case study,” *J. Comput. Civ. Eng.*, 2000, doi: 10.1061/(ASCE)0887-3801(2000)14:4(255).

[69] M. R. Jalali, A. Afshar, and M. A. Mariño, “Reservoir operation by ant colony optimization algorithms,” *Iran. J. Sci. Technol. Trans. B Eng.*, 2006.

[70] J. A. Ahmed and A. K. Sarma, “Genetic algorithm for optimal operating policy of a multipurpose reservoir,” *Water Resour. Manag.*, 2005, doi: 10.1007/s11269-005-2704-7.

[71] M. R. Jalali, A. Afshar, and M. A. Mariño, “Multi-colony ant algorithm for continuous multi-reservoir operation optimization problem,” *Water Resour. Manag.*, 2007, doi: 10.1007/s11269-006-9092-5.

[72] Howard CDD, “Hydroelectric system operations optimization,” in *In Great Wall World Renewable Energy Forum and Exhibition. Beijing, China: Chinese Wind Energy Association*, 2006.

[73] L. Duckstein and S. Opricovic, “Multiobjective optimization in river basin development,” *Water Resour. Res.*, 1980, doi: 10.1029/WR016i001p00014.

[74] J. R. Stedinger, B. F. Sule, and D. P. Loucks, “Stochastic dynamic programming models for reservoir operation optimization,” *Water Resour. Res.*, 1984, doi: 10.1029/WR020i011p01499.

[75] T. W. Archibald, K. I. M. McKinnon, and L. C. Thomas, “An aggregate stochastic dynamic programming model of multireservoir systems,” *Water Resour. Res.*, 1997, doi: 10.1029/96WR02859.

[76] R. Oliveira and D. P. Loucks, “Operating rules for multireservoir systems,” *Water Resour. Res.*, 1997, doi: 10.1029/96WR03745.

[77] S. R. Mishra, S. K. Singal, and D. kumar Khatod, “Effect of Variation of Penstock Parameter on Mechanical Power,” *Int. J. Energy Sci.*, 2012.

[78] H. D. Jacoby and D. P. Loucks, “Combined use of optimization and simulation models in river basin planning,” *Water Resour. Res.*, 1972, doi: 10.1029/WR008i006p01401.

[79] A. Ahmadi, J. Aghaei, H. A. Shayanfar, and A. Rabiee, “Mixed integer programming of multiobjective hydro-thermal self scheduling,” *Appl. Soft Comput. J.*, 2012, doi: 10.1016/j.asoc.2012.03.020.

[80] L. Duckstein, A. Tecle, H. P. Nachnebel, and B. F. Hobbs, “Multicriterion Analysis of Hydropower Operation,” *J. Energy Eng.*, vol. 115, no. 3, pp. 132–153, Dec. 1989, doi: 10.1061/(ASCE)0733-9402(1989)115:3(132).

[81] J. Garrido, Á. Zafra, and F. Vázquez, “Object oriented modelling and simulation of hydropower plants with run-of-river scheme: A new simulation tool,” *Simul. Model. Pract. Theory*, 2009, doi: 10.1016/j.simpat.2009.08.007.

[82] J. S. Anagnostopoulos and D. E. Papantonis, “Optimal sizing of a run-of-river small hydropower plant,” *Energy Convers. Manag.*, 2007, doi: 10.1016/j.enconman.2007.04.016.

[83] Y. Aslan, O. Arslan, and C. Yasar, “A sensitivity analysis for the design of small-scale hydropower plant: Kayabogazi case study,” *Renew. Energy*, 2008, doi: 10.1016/j.renene.2007.04.011.

[84] S. J. Williamson, B. H. Stark, and J. D. Booker, “Low head pico hydro turbine selection using a multi-criteria analysis,” *Renew. Energy*, 2014, doi: 10.1016/j.renene.2012.06.020.

[85] S. K. Singal, R. P. Saini, and C. S. Raghuvanshi, “Analysis for cost estimation of low head run-of-river small hydropower schemes,” *Energy Sustain. Dev.*, 2010, doi:

10.1016/j.esd.2010.04.001.

[86] O. B. Haddad, M. Moradi-Jalal, and M. A. Mariño, “Design-operation optimisation of run-of-river power plants,” *Proc. Inst. Civ. Eng. Water Manag.*, 2011, doi: 10.1680/wama.2011.164.9.463.

[87] M. Najmaii and A. Movaghar, “Optimal design of run-of-river power plants,” *Water Resour. Res.*, vol. 28, no. 4, pp. 991–997, Apr. 1992, doi: 10.1029/91WR02528.

[88] S. Basso and G. Botter, “Streamflow variability and optimal capacity of run-of-river hydropower plants,” *Water Resour. Res.*, 2012, doi: 10.1029/2012WR012017.

[89] C. L. T. Borges and R. J. Pinto, “Small hydro power plants energy availability modeling for generation reliability evaluation,” *IEEE Trans. Power Syst.*, 2008, doi: 10.1109/TPWRS.2008.926713.

[90] M. Karami, H. A. Shayanfar, J. Aghaei, and A. Ahmadi, “Mixed integer programming of security-constrained daily hydrothermal generation scheduling (SCDHGS),” *Sci. Iran.*, 2013.

[91] H. Moghimi Ghadikolaei, A. Ahmadi, J. Aghaei, and M. Najafi, “Risk constrained self-scheduling of hydro/wind units for short term electricity markets considering intermittency and uncertainty,” *Renewable and Sustainable Energy Reviews*. 2012, doi: 10.1016/j.rser.2012.04.019.

[92] A. Ahmadi, J. Aghaei, and H. A. Shayanfar, “Stochastic self-scheduling of hydro units in joint energy and reserves markets,” in *2011 19th Iranian Conference on Electrical Engineering, ICEE 2011*, 2011.

[93] S. Yadav, “Some Aspects of Performance Improvement of Pelton Wheel Turbine with Reengineered Blade and Auxiliary Attachments,” *Int. J. Sci. Eng. …*, 2011.

[94] A. A. Williams, “Pumps as turbines for low cost micro hydro power,” *Renew. Energy*, 1996, doi: 10.1016/0960-1481(96)88498-9.

[95] S. R. Huang, Y. H. Ma, C. F. Chen, K. Seki, and T. Aso, “Theoretical and conditional monitoring of a small three-bladed vertical-axis micro-hydro turbine,” *Energy Convers. Manag.*, 2014, doi: 10.1016/j.enconman.2014.05.098.

[96] A. H. Elbatran, O. B. Yaakob, Y. M. Ahmed, and H. M. Shabara, “Operation, performance and economic analysis of low head micro-hydropower turbines for rural and remote areas: A review,” *Renewable and Sustainable Energy Reviews*. 2015, doi: 10.1016/j.rser.2014.11.045.

[97] A. Židonis, D. S. Benzon, and G. A. Aggidis, “Development of hydro impulse turbines and new opportunities,” *Renewable and Sustainable Energy Reviews*. 2015, doi: 10.1016/j.rser.2015.07.007.

[98] K. Gaiser, P. Erickson, P. Stroeve, and J. P. Delplanque, “An experimental investigation of design parameters for pico-hydro Turgo turbines using a response surface methodology,” *Renew. Energy*, 2016, doi: 10.1016/j.renene.2015.06.049.

[99] A. A. Khan, A. Shahzad, I. Hayat, and M. S. Miah, “Recovery of flow conditions for optimum electricity generation through micro hydro turbines,” *Renew. Energy*, 2016, doi: 10.1016/j.renene.2016.05.052.

[100] A. Bozorgi, E. Javidpour, A. Riasi, and A. Nourbakhsh, “Numerical and experimental study of using axial pump as turbine in Pico hydropower plants,” *Renew. Energy*, 2013, doi: 10.1016/j.renene.2012.11.016.

[101] A. Date, A. Date, A. Akbarzadeh, and F. Alam, “Examining the potential of split reaction water turbine for ultra-low head hydro resources,” in *Procedia Engineering*, 2012, doi: 10.1016/j.proeng.2012.10.128.

[102] K. H. Motwani, S. V. Jain, and R. N. Patel, “Cost analysis of pump as turbine for pico hydropower plants - A case Study,” in *Procedia Engineering*, 2013, doi: 10.1016/j.proeng.2013.01.103.

[103] A. N. Gorban’, A. M. Gorlov, and V. M. Silantyev, “Limits of the turbine efficiency for free fluid flow,” *J. Energy Resour. Technol. Trans. ASME*, 2001, doi: 10.1115/1.1414137.

[104] S. Derakhshan and A. Nourbakhsh, “Experimental study of characteristic curves of centrifugal pumps working as turbines in different specific speeds,” *Exp. Therm. Fluid Sci.*, 2008, doi: 10.1016/j.expthermflusci.2007.10.004.

[105] M. Sinagra, V. Sammartano, C. Aricò, A. Collura, and T. Tucciarelli, “Cross-Flow turbine design for variable operating conditions,” in *Procedia Engineering*, 2014, doi: 10.1016/j.proeng.2014.02.170.

[106] T. Ikeda, S. Iio, and K. Tatsuno, “Performance of nano-hydraulic turbine utilizing waterfalls,” *Renew. Energy*, 2010, doi: 10.1016/j.renene.2009.07.004.

[107] Y. Yassi and S. Hashemloo, “Improvement of the efficiency of the Agnew micro hydro turbine at part loads due to installing guide vanes mechanism,” *Energy Convers. Manag.*, 2010, doi: 10.1016/j.enconman.2010.02.029.

[108] K. A. S. M. Mishra A *et al.*, “Development and Testing of a Cross Flow Turbine,” *IGHEM-2010*, 2010.

[109] J. De Andrade, C. Curiel, F. Kenyery, O. Aguilln, A. Vásquez, and M. Asuaje, “Numerical investigation of the internal flow in a Banki turbine,” *Int. J. Rotating Mach.*, 2011, doi: 10.1155/2011/841214.

[110] Pereira and Borges, “A Study on the Efficiency of a Cross-Flow Turbine Based on Experimental Measurements,” *Proc. 5th Int. Conf. Fluid Mech. Heat Mass Transf.*, 2014.

[111] M. A. Khan and S. Badshah, “Design and analysis of cross flow turbine for micro hydro power application using sewerage water,” *Res. J. Appl. Sci. Eng. Technol.*, 2014, doi: 10.19026/rjaset.8.1040.

[112] Girma Misrak and Dribssa Edessa, “Flow Simulation and Performance Prediction of Cross Flow Turbine Using CFD Tool,” *Int. J. Eng. Res. Gen. Sci.*, 2014.

[113] N. Acharya, C. G. Kim, B. Thapa, and Y. H. Lee, “Numerical analysis and performance enhancement of a cross-flow hydro turbine,” *Renew. Energy*, 2015, doi: 10.1016/j.renene.2015.01.064.

[114] B. R. Cobb and K. V. Sharp, “Impulse (Turgo and Pelton) turbine performance characteristics and their impact on pico-hydro installations,” *Renew. Energy*, 2013, doi: 10.1016/j.renene.2012.08.010.

[115] A. Date, A. Date, and A. Akbarzadeh, “Investigating the potential for using a simple water reaction turbine for power production from low head hydro resources,” *Energy Convers. Manag.*, 2013, doi: 10.1016/j.enconman.2012.09.032.

[116] S. J. Williamson, B. H. Stark, and J. D. Booker, “Performance of a low-head pico-hydro Turgo turbine,” *Appl. Energy*, 2013, doi: 10.1016/j.apenergy.2012.06.029.

[117] D. R. Giosio, A. D. Henderson, J. M. Walker, P. A. Brandner, J. E. Sargison, and P. Gautam, “Design and performance evaluation of a pump-as-turbine micro-hydro test facility with incorporated inlet flow control,” *Renew. Energy*, 2015, doi: 10.1016/j.renene.2014.12.027.

[118] V. Bijukchhe, “Comparison of experimental results of horizontal kaplan turbine with computational fluid dynamics,” University of Iowa, Iowa City, Iowa, USA, 2012.

[119] Y. H. Yen, T. El Gammal, R. S. Amano, J. Millevolte, B. Lequesne, and R. J. Mueller, “Numerical optimization of Micro Kaplan hydro turbine system,” in *American Society of Mechanical Engineers, Fluids Engineering Division (Publication) FEDSM*, 2016, vol. 1A-2016, doi: 10.1115/FEDSM2016-7575.

[120] T. El Gammal, Y. H. Yen, R. S. Amano, J. Millevolte, R. J. Mueller, and B. Lequesne, “Numerical investigations on intake tube design of Micro Kaplan hydro-turbine system,” in *American Society of Mechanical Engineers, Fluids Engineering Division (Publication) FEDSM*, 2016, vol. 1B-2016, doi: 10.1115/FEDSM2016-7569.

[121] C. Abeykoon and T. Hantsch, “Design and analysis of a Kaplan turbine runner wheel,” in *Proceedings of the World Congress on Mechanical, Chemical, and Material Engineering*, 2017, doi: 10.11159/htff17.151.

[122] M. M. Ujwala, P. C. K. Chowdary, and L. S. Naik, “Design and Analysis of Low Head , Light weight Kaplan Turbine Blade,” *Int. Ref. J. Eng. Sci.*, 2017.

[123] A. B. Janjua, M. S. Khalil, and M. Saeed, “Blade Profile Optimization of Kaplan Turbine Using CFD Analysis,” *Mehran Univ. Res. J. Eng. Technol.*, 2013.

[124] E. Permana and Y. Rudianto, “Design and velocity distribution of runner blade of kaplan turbine using CFD (computer fluid dynamic) for small hydroelectric power plant,” in *IOP Conference Series: Materials Science and Engineering*, 2017, doi: 10.1088/1757-899X/180/1/012269.

[125] D. Jošt, A. Škerlavaj, and A. Lipej, “Improvement of efficiency prediction for a Kaplan turbine with advanced turbulence models,” *Stroj. Vestnik/Journal Mech. Eng.*, 2014, doi: 10.5545/sv-jme.2013.1222.

[126] D. Nan, T. Shigemitsu, S. Zhao, T. Ikebuchi, and Y. Takeshima, “Study on performance of contra-rotating small hydro-turbine with thinner blade and longer front hub,” *Renew. Energy*, 2018, doi: 10.1016/j.renene.2017.10.046.

[127] R. K. Ranjan, N. Alom, J. Singh, and B. K. Sarkar, “Performance investigations of cross flow hydro turbine with the variation of blade and nozzle entry arc angle,” *Energy Convers. Manag.*, 2019, doi: 10.1016/j.enconman.2018.12.075.

[128] H. Hoghooghi, M. Durali, and A. Kashef, “A new low-cost swirler for axial micro hydro turbines of low head potential,” *Renew. Energy*, 2018, doi: 10.1016/j.renene.2018.05.086.

[129] V. Yildiz and J. A. Vrugt, “A toolbox for the optimal design of run-of-river hydropower plants,” *Environ. Model. Softw.*, 2019, doi: 10.1016/j.envsoft.2018.08.018.

[130] J. R. R. A. Martins and A. B. Lambe, “Multidisciplinary design optimization: A survey of architectures,” *AIAA J.*, 2013, doi: 10.2514/1.J051895.

[131] S. K. Singh, “A novel concept for non-linear multidisciplinary aerodynamic design optimization,” *Aerosp. Sci. Technol.*, 2017, doi: 10.1016/j.ast.2017.08.043.

[132] L. Wang, C. Xiong, J. Hu, X. Wang, and Z. Qiu, “Sequential multidisciplinary design optimization and reliability analysis under interval uncertainty,” *Aerosp. Sci. Technol.*, 2018, doi: 10.1016/j.ast.2018.07.029.

[133] W. Yao, X. Chen, W. Luo, M. Van Tooren, and J. Guo, “Review of uncertainty-based multidisciplinary design optimization methods for aerospace vehicles,” *Progress in Aerospace Sciences*. 2011, doi: 10.1016/j.paerosci.2011.05.001.

[134] M. Zhang, W. Gou, L. Li, X. Wang, and Z. Yue, “Multidisciplinary design and optimization of the twin-web turbine disk,” *Struct. Multidiscip. Optim.*, 2016, doi: 10.1007/s00158-015-1373-2.

[135] R. S. Amano and B. Sunden, *Computational Fluid Dynamics and Heat Transfer*, First Edit. Southampton, Boston: WIT Press, 2010.

[136] F. Nicoud and F. Ducros, “Subgrid-scale stress modelling based on the square of the velocity gradient tensor,” *Flow, Turbul. Combust.*, 1999, doi: 10.1023/A:1009995426001.

[137] A. I. Abbas, M. D. Qandil, M. R. Al-Haddad, and R. S. Amano, “Performance investigation

of very-low-head kaplan hydro-turbines," in *AIAA Scitech 2019 Forum*, 2019, doi: 10.2514/6.2019-0241.

[138] A. I. Abbas, M. D. Qandil, M. R. Al-Haddad, M. S. Saravani, and R. S. Amano, "Utilization of Hydroturbines in Wastewater Treatment Plants," *J. Energy Resour. Technol. Trans. ASME*, vol. 141, no. 6, 2019, doi: 10.1115/1.4042969.

[139] A. I. Abbas, R. S. Amano, M. S. Saravani, M. D. Qandil, and T. Sakamoto, "Optimization of Kaplan Hydroturbine at Very Low Head with Rim-Driven Generator," *J. Energy Resour. Technol. Trans. ASME*, vol. 141, no. 11, 2019, doi: 10.1115/1.4043710.

[140] A. I. Abbas, R. S. Amano, M. S. Saravani, M. D. Qandil, and T. Sakamoto, "Optimization of Kaplan Hydroturbine at Very Low Head with Rim-Driven Generator," *J. Energy Resour. Technol. Trans. ASME*, 2019, doi: 10.1115/1.4043710.

[141] "Eastman Amphora™ 3D Polymer AM3300 Application/Uses Production of 3D Printing filaments."

[142] "Ultimaker 2+: Robust single extrusion." [Online]. Available: https://ultimaker.com/3d-printers/ultimaker-2-plus. [Accessed: 03-Dec-2019].

[143] "M2000 Electromagnetic Flow Meter User Manual M2000 Electromagnetic Flow Meter," 2019.

[144] Magtrol, "TM 300 Series In-Line Torque Transducers User's Manual."

[145] "2.25 HP Icon Health And Fitness Treadmill Motor F-237595 | Special Purpose DC Motors | DC Motors | Electrical | www.surpluscenter.com." [Online]. Available: https://www.surpluscenter.com/Electrical/DC-Motors/Special-Purpose-DC-Motors/2-25-HP-Icon-Health-And-Fitness-Treadmill-Motor-F-237595-10-3034.axd. [Accessed: 03-Dec-2019].

[146] "ATM 10 HP pump." [Online]. Available: http://amtpumps.com/site/wp-content/uploads/2017/01/STE-15-16.pdf. [Accessed: 03-Dec-2019].

[147] "ABB ACS310 VSD." [Online]. Available: https://library.e.abb.com/public/f54878880ad34bbd855ee0008d6d13a6/3AUA0000159910_REVG.pdf. [Accessed: 03-Dec-2019].

[148] Stephen B. Pope, *Turbulent Flows by Stephen B. Pope*, First Edit. Cambridge University Press, 2000.

[149] B. E. Launder and D. B. Spalding, *Lectures in Mathematical Models of Turbulence*. 1972.

[150] D. Anderson, J. C. Tannehill, and R. H. Pletcher, *Computational fluid mechanics and heat transfer, Third edition*. 2016.

[151] A. J. Wheeler and A. R. Ganji, *Wheeler & Ganji, Introduction to Engineering*

Experimentation, 3rd Edition | Pearson. Pearson, 2010.

[152] S. L. Dixon and C. Hall, *Fluid Mechanics and Thermodynamics of Turbomachinery: Seventh Edition*. 2013.

[153] F. M. White, *Fluid Mechanics 8th Ed.*, 8th Editio. McGraw Hill, 2016.

[154] Y. H. Yen, T. El Gammal, R. S. Amano, J. Millevolte, B. Lequesne, and R. J. Mueller, "Numerical optimization of Micro Kaplan hydro turbine system," in *American Society of Mechanical Engineers, Fluids Engineering Division (Publication) FEDSM*, 2016, doi: 10.1115/FEDSM2016-7575.

[155] L. Bravo, S. Wijeyakulasuriya, E. Pomraning, P. K. Senecal, and C.-B. Kweon, "Large Eddy Simulation of High Reynolds Number Nonreacting and Reacting JP-8 Sprays in a Constant Pressure Flow Vessel With a Detailed Chemistry Approach," *J. Energy Resour. Technol.*, 2016, doi: 10.1115/1.4032901.

[156] J. SMAGORINSKY, "GENERAL CIRCULATION EXPERIMENTS WITH THE PRIMITIVE EQUATIONS," *Mon. Weather Rev.*, 1963, doi: 10.1175/1520-0493(1963)091<0099:gcewtp>2.3.co;2.

[157] H. Hattori, T. Houra, A. Kono, and S. Yoshikawa, "Computational Fluid Dynamics Study for Improvement of Prediction of Various Thermally Stratified Turbulent Boundary Layers," *J. Energy Resour. Technol.*, 2017, doi: 10.1115/1.4036177.

[158] W. W. Peng, *Fundamentals of turbomachinery*, First Edit. J. Wiley, 2008.

[159] G. Morrison, W. Yin, R. Agarwal, and A. Patil, "Development of Modified Affinity Law for Centrifugal Pump to Predict the Effect of Viscosity," *J. Sol. Energy Eng. Trans. ASME*, 2018, doi: 10.1115/1.4039874.

[160] Ø. Krøvel, R. Nilssen, S. E. Skaar, E. Løvli, and N. Sandøy, "Design of an Integrated 100kW Permanent Magnet Synchronous Machine in a Prototype Thruster for Ship Propulsion," in *ICEM 2004*, 2004.

[161] "Electromagnetic and Magnetic Software | EMWorks." [Online]. Available: https://www.emworks.com/. [Accessed: 03-Dec-2019].

[162] J. Lucas, P. Lucas, T. Le Mercier, A. Rollat, and W. Davenport, *Rare Earths: Science, Technology, Production and Use*. Elsevier Inc., 2014.

[163] "Permanent Magnets." [Online]. Available: http://hyperphysics.phy-astr.gsu.edu/hbase/Solids/magperm.html. [Accessed: 11-Apr-2020].

[164] J. J. Croat, J. F. Herbst, R. W. Lee, and F. E. Pinkerton, "Pr-Fe and Nd-Fe-based materials: A new class of high-performance permanent magnets (invited)," *J. Appl. Phys.*, vol. 55, no. 6, pp. 2078–2082, Mar. 1984, doi: 10.1063/1.333571.

[165] M. Sagawa, S. Fujimura, N. Togawa, H. Yamamoto, and Y. Matsuura, “New material for permanent magnets on a base of Nd and Fe (invited),” *J. Appl. Phys.*, vol. 55, no. 6, pp. 2083–2087, Mar. 1984, doi: 10.1063/1.333572.

[166] “How to Understand the Grade of Sintered NdFeB Magnet? – China NdFeB Magnet, SmCo Magnet Supplier | HGT Co.,Ltd.” [Online]. Available: http://www.advancedmagnets.com/how-to-understand-the-rare-earth-permanent-magnets-grades-part-1-sintered-neodymium-iron-boron-magnets/. [Accessed: 11-Apr-2020].

[167] “Electric and Magnetic Field Simulation for SOLIDWORKS and Autodesk.” [Online]. Available: https://www.emworks.com/product/ems. [Accessed: 11-Apr-2020].

[168] K. J. Chae, I. S. Kim, X. Ren, and K. H. Cheon, “Reliable energy recovery in an existing municipal wastewater treatment plant with a flow-variable micro-hydropower system,” *Energy Convers. Manag.*, vol. 101, pp. 681–688, Jun. 2015, doi: 10.1016/j.enconman.2015.06.016.

[169] C. Power, A. McNabola, and P. Coughlan, “Development of an evaluation method for hydropower energy recovery in wastewater treatment plants: Case studies in Ireland and the UK,” *Sustain. Energy Technol. Assessments*, vol. 7, pp. 166–177, 2014, doi: 10.1016/j.seta.2014.06.001.

[170] M. Capua, J. Dzwonkoski, C. Harris Advisor, and J. D. Plummer, “Reclamation of Power in Wastewater Treatment Facilities,” 2014.

[171] A. I. Abbas and R. S. Amano, “Optimization of intake and draft tubes of a kaplan micro hydro-turbine,” in *15th International Energy Conversion Engineering Conference, 2017*, 2017.

Appendices

Appendix A: Exploded view of the RDT parts (CAD)

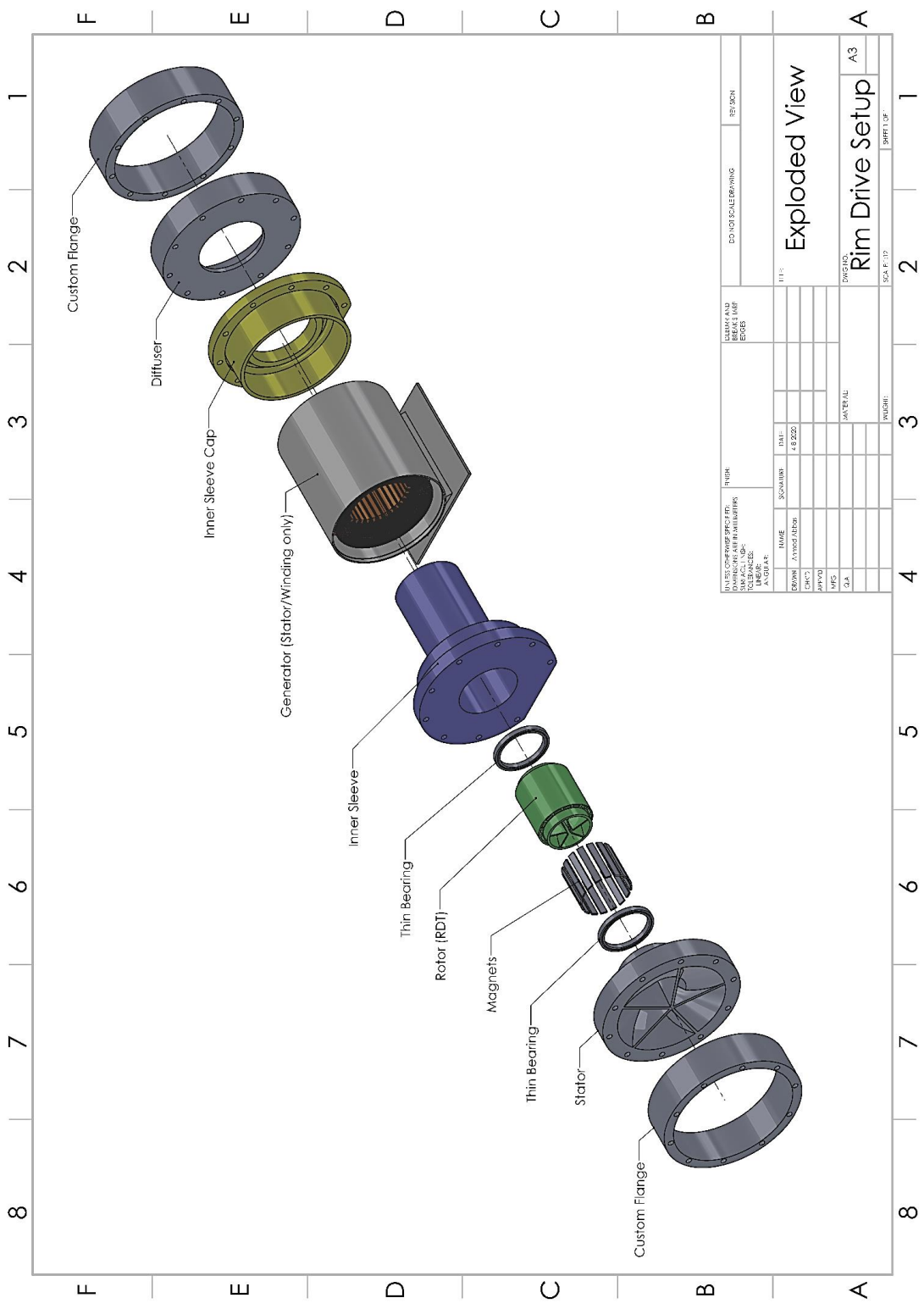

Appendix B: Exploded view of the RDT parts (Detailed)

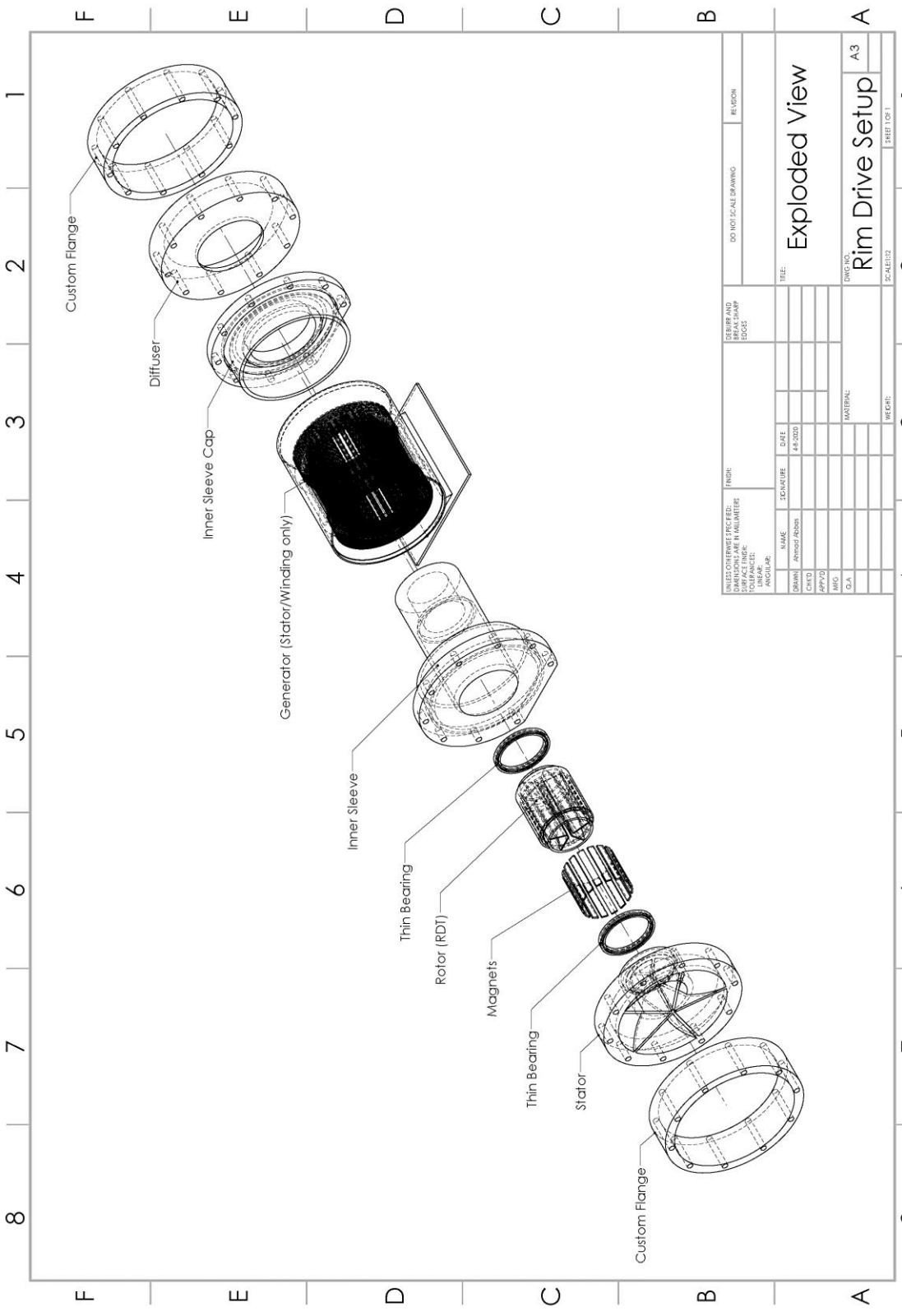

Appendix C: Multiple views of the RDT setup

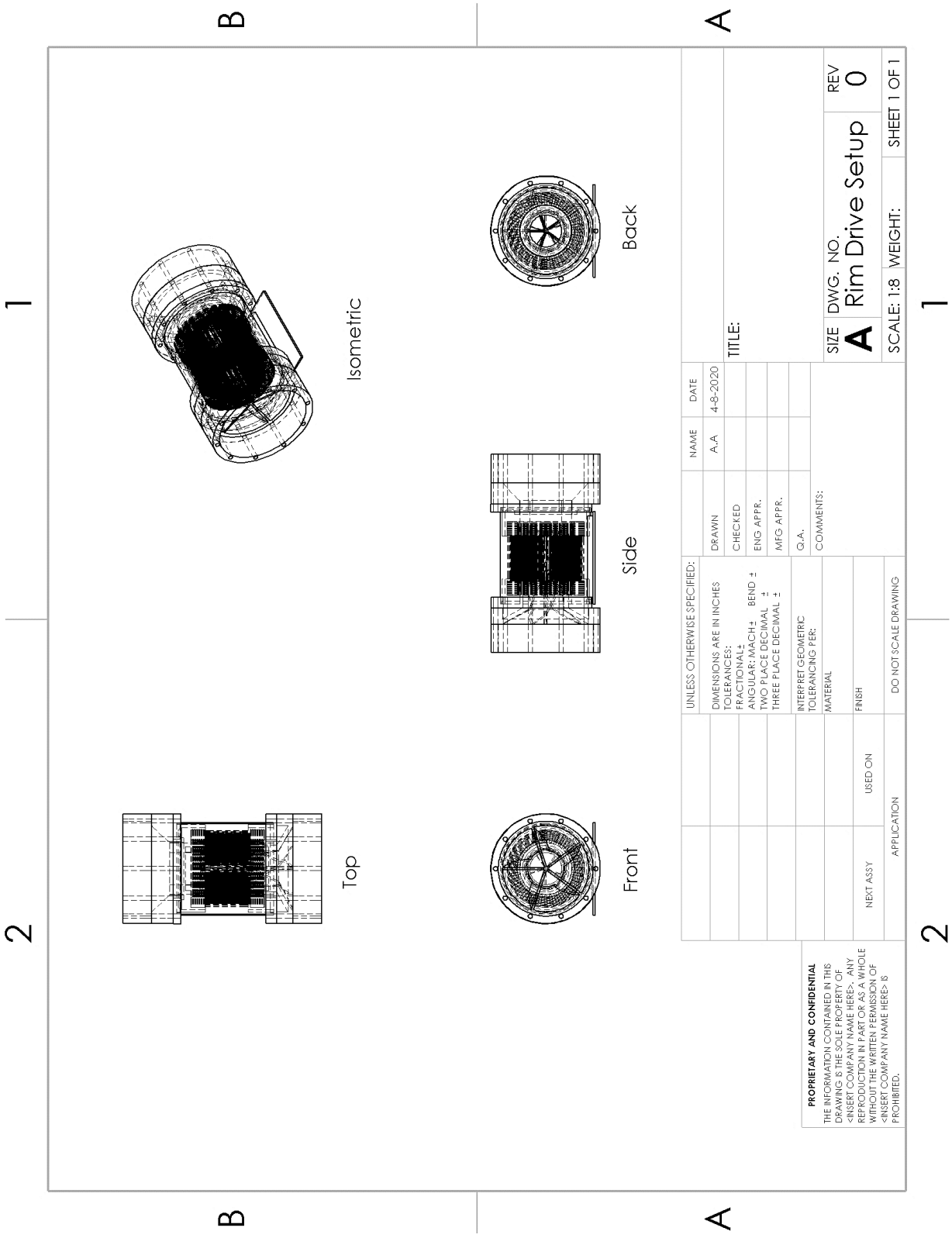

Appendix D: Front view of the RDT setup

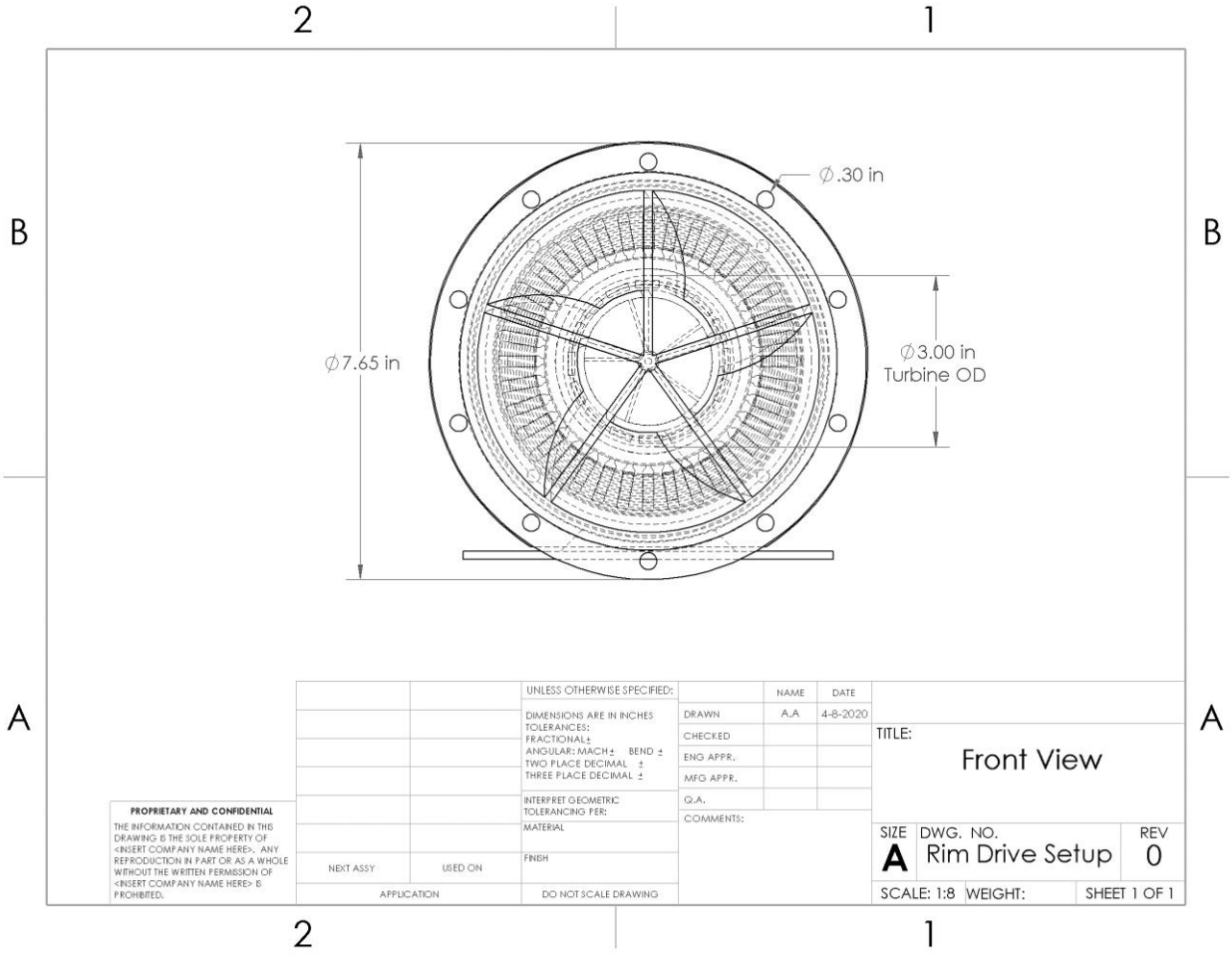

Appendix E: Side view of the RDT setup

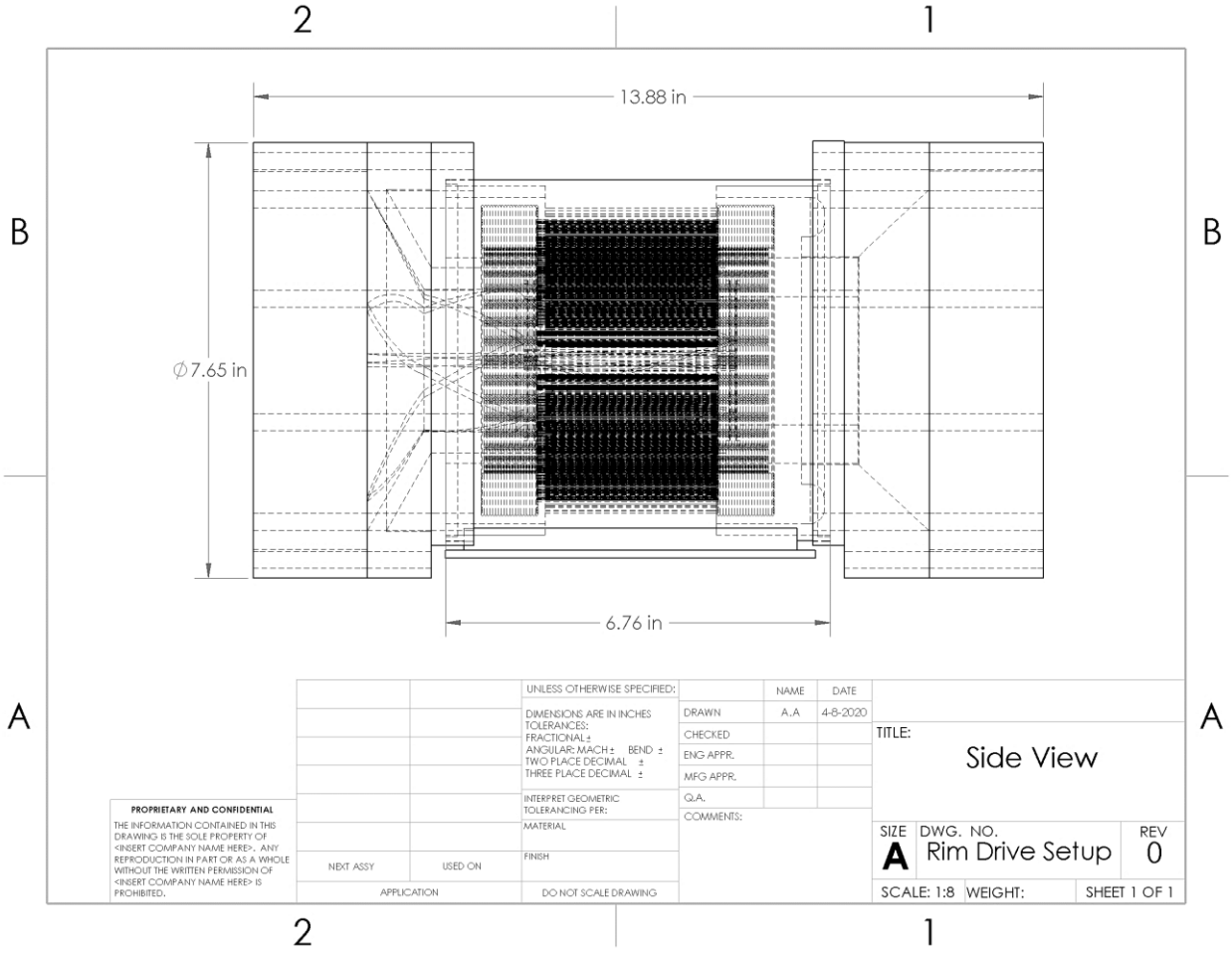

Appendix F: Back view of the RDT setup

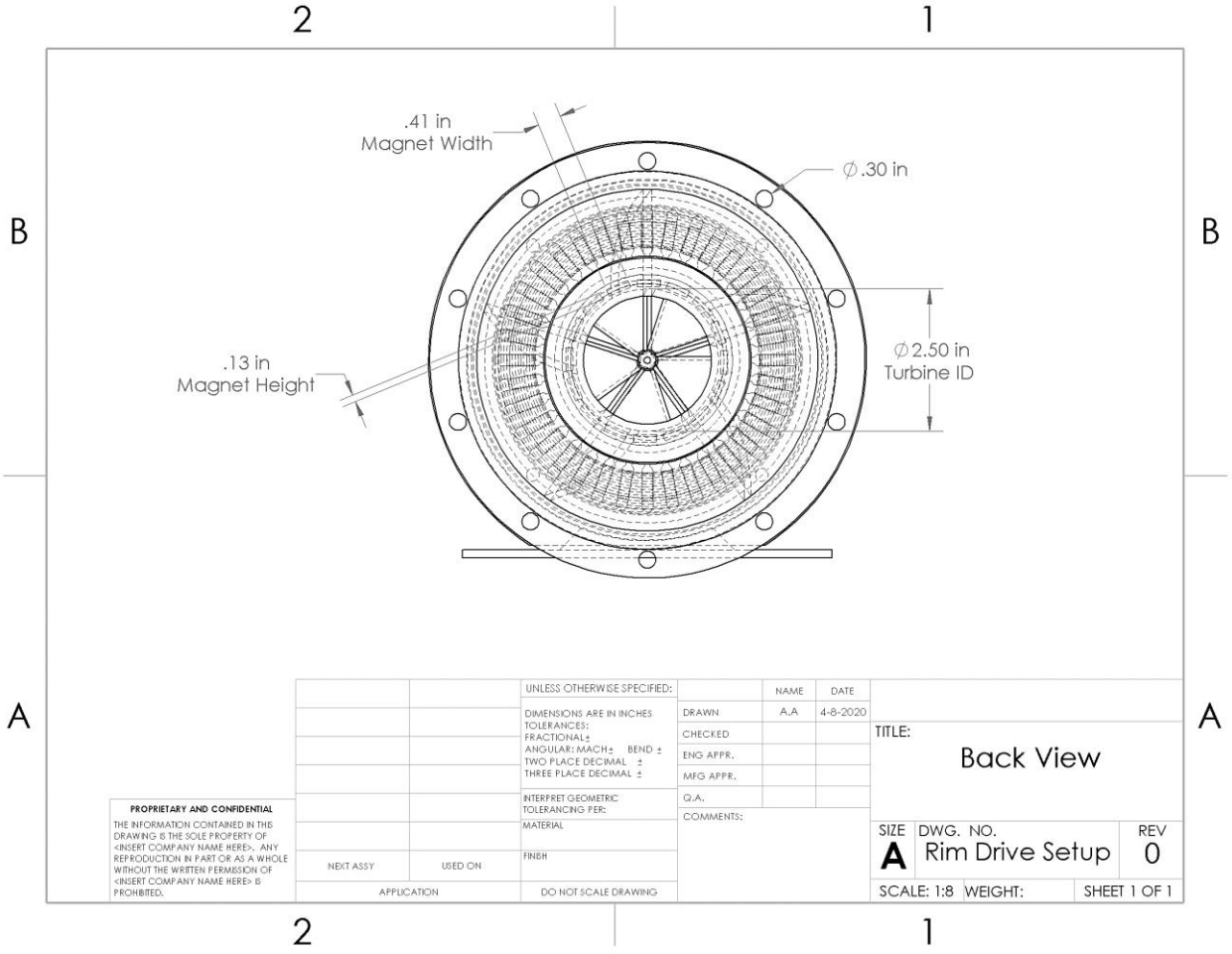

Appendix G: Top view of the RDT setup

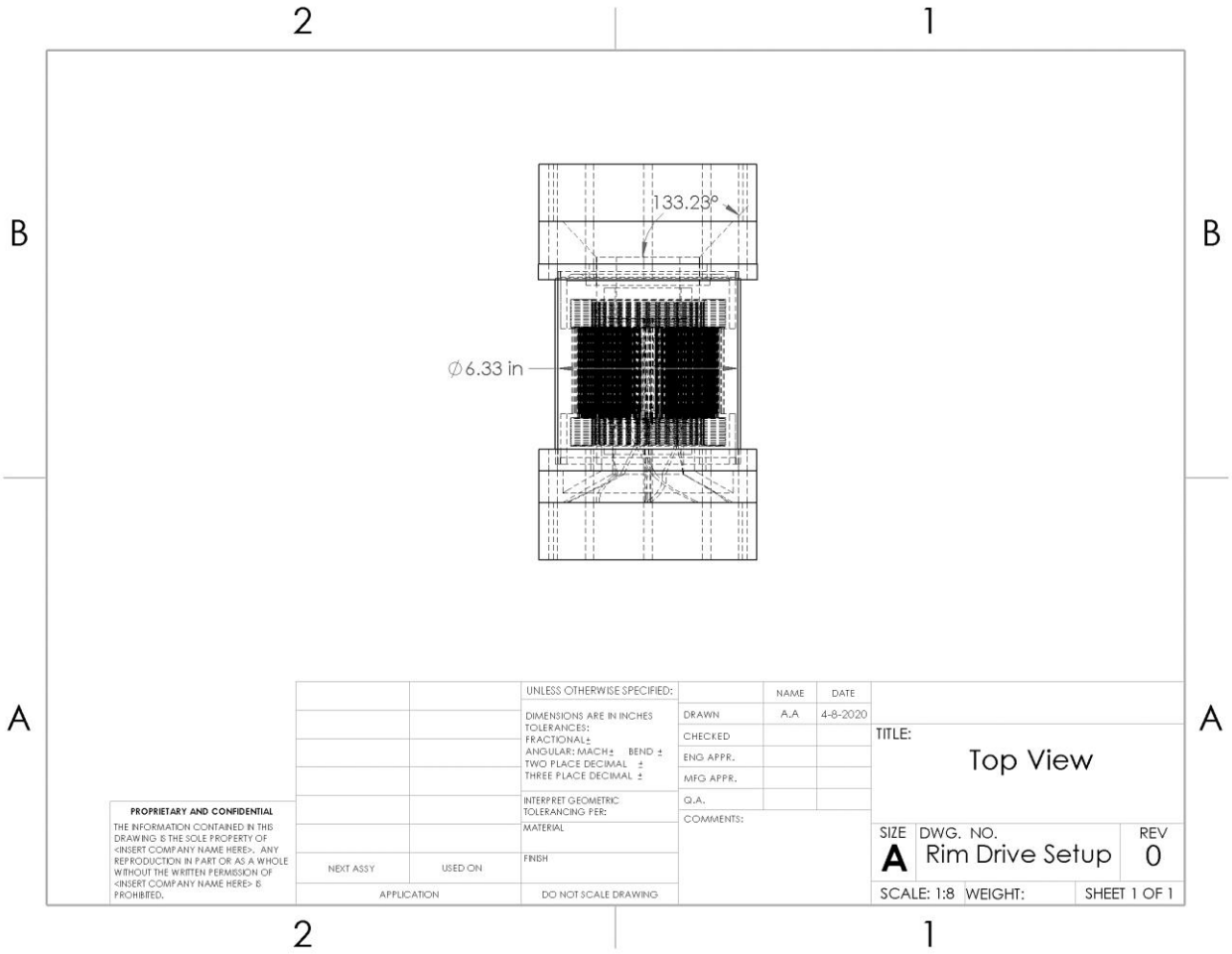

Curriculum Vitae

Objective

Enthusiastic energy engineer and research assistant with 3+ years' experience in the DOE-Industrial Assessment Center and Hydro-turbine Lab of UW-Milwaukee, seeking to pursue research in the field of energy efficiency for buildings in general and the industrial sector in specific.

Highlights

- 3+ years' experience as a Lead Energy Engineer in the DOE-Industrial Assessment Center of UW-Milwaukee (Participated in 45+ assessments).
- 3+ years' experience as a Research Assistant in the Hydro-turbine Lab at UW-Milwaukee with utilizing Star-CCM+ for CFD tests.
- 4+ years of work experience; 3 years as a Technical Support/Application Engineer in HVAC Industry and 1 year as a Maintenance Engineer in Dairy Industry.

Experience

November 2016 – Present | Lead Energy Engineer

DOE-Industrial Assessment Center of UW-Milwaukee| Milwaukee, WI

- Perform ASHRAE level I and II energy audits on industrial facilities as part of the U.S. Department of Energy-Advanced Manufacturing Office program.
- Prepare audit reports delineating the outcomes of the assessment in terms of energy savings, cost reduction in utility bills, and return of investment.
- Analyze and assess equipment, systems and processes to provide energy savings and improve productivity.
- Evaluate utility bills and carry out a comprehensive analysis to trace the energy usage trend.
- Contact clients arrange assessments and manage audit teams.
- Conducted 45+ assessments and led 8 energy audits on various industrial facilities.
- Evaluated energy usage and identified over $5 million worth of energy savings.
- Certified by U.S. DOE's IAC program since October 2017.
- The Lead Student for the Center starting November 2018.

January 2016 – Present | Research Assistant/CFD Engineer

University of Wisconsin-Milwaukee/Global Water Center | Milwaukee, WI

- Working on micro & pico-scale Kaplan hydro-turbines:
  - To investigate and improve the performance of turbines (Project with US DOE)
  - To investigate cavitation in hydro-turbines (Project with Rexnord)
- Utilize STAR-CCM+ as a CFD tool for testing hydro-turbines performance and various design parameters along with CFturbo software for CAD optimization,
- Utilize each of 3D printing, High-Speed Camera, and High-Performance Computing (HPC) clusters.
- Highlighted Project: DOE DE-FOA-0001417 - SBIR/STTR FY2016 Phase I Release 2: Topic 15.a WATER - Innovative Very Low-head and Instream Current Waterpower Turbine-Generator Technologies (under grant no. DE-SC0015757/$150,000)

August 2016 – August 2017 | Teaching Assistant

University of Wisconsin-Milwaukee/Main Campus | Milwaukee, WI

- Teaching Assistant with the Mechanical Engineering Department
- Instructor for Fluid Mechanics Laboratory (Fall 2016 & Summer 2017)

March 2013 – December 2015 | Application Engineer / Technical Support

PETRA Engineering for HVAC Industries | Amman, Jordan

- Study client's inquiries for central air conditioning systems
- Prepare technical and financial quotations for the client
- Send job orders for production department

May 2012 – March 2013 | Maintenance Engineer

Hammoudeh Food Industries Co. (Cheese Plant) | Al-Mafraq, Jordan

- Plan the routine maintenance of equipment and machines
- Design maintenance strategies, procedures and methods
- Diagnose breakdown problems
- Make scheduled checks on machinery and parts

Education

January 2016 – Present | Ph.D. in Engineering

- University of Wisconsin-Milwaukee - Mechanical Engineering Department
- Thesis topic: Numerical and Experimental Investigation of Performance for Very-Low-Head Micro and Pico Kaplan Hydro-Turbines with Rim-Driven Generators
- GPA of (3.7/4.0)
- Expected Graduation Date: May 2020

Jan, 2013 - June, 2015 | M.Sc. of Mechanical Engineering/Energy Systems

- The Hashemite University - Mechanical Engineering Department
- Zarqa, Jordan
- GPA of (3.54/4.00), Grade: Excellent
- Thesis Title: Repowering Conventional Power Plants by Introducing Concentrated Solar Power (CSP) Systems
- Fields of Study: Solar Energy, Renewable Energy Systems, Energy Management and Energy & Environment

September 2008 - May 2012 | B.Sc. of Mechanical Engineering

- Al-Balqa' Applied University – Faculty of Engineering Technology
- Amman, Jordan
- GPA of (3.16/4.00), Grade: Very good
- Graduation Project/Senior Design: Energy Audit for Administration Building in Faculty of Engineering Technology (Award in Graduation Projects/Senior Design Competition-2013 at Jordan Engineers Association)

Computer Software's

- STAR-CCM+ (3+ years' experience): Simulate flow motion (3D simulation, unsteady, turbulent flow, VOF, and rotational motion models) for micro hydro-turbines projects.
- CFturbo: Generate CAD and design optimization for rotor/stator sets of hydro-turbines.
- SolidWorks: Draw/edit CAD models related to micro hydro-turbines.
- System Advisor Model (SAM) by NREL: Used for my master's research to simulate and to study the performance of a concentrated solar power (CSP) field in Jordan.

Skills

- Analytical: research, problem-solving, data and metrics interpreting, reporting, organization, communication, troubleshooting, diagnostics, creativity, and brainstorming.
- Critical and Creative Thinking
- Management: leadership, people management, collaboration & teamwork, time management, negotiating, planning, and training.
- Decision Making: team and shared decision-making skills.
- Technical: writing, spreadsheets, computer, video creation, presenting.

Publications

Journal Papers:

1. Ahmad I. Abbas, Mohammad D. Qandil, Muhannad R. Al-Haddad, and Ryoichi S. Amano, "Investigation of Horizontal Micro Kaplan Hydro Turbine Performance Using Multi-Disciplinary Design Optimization", Transactions of the ASME, Journal of Energy Resources Technology (Impact Factor: 2.759), May 2020, Vol. 142, No. 5, pp. 052101 (8 pages) https://doi.org/10.1115/1.4045821
2. Wei-Lin Chen, Ahmad I. Abbas, Ryan Ott, and Ryoichi S. Amano, "Investigation of Liquid Breakup Process Solid Rocket Motor Part A: Horizontal C-D Nozzle", Transactions of the ASME, Journal of Energy Resources Technology (IF: 2.759), May 2020, Vol. 142, No. 5, pp. 052102 (7 pages) https://doi.org/10.1115/1.4046081
3. Mandana S. Saravani, Nicholas J. DiPasquale, Ahmad I. Abbas, and Ryoichi S. Amano, "Heat Transfer Evaluation for a Two-Pass Smooth Wall Channel: Stationary and Rotating Cases", Transactions of the ASME, Journal of Energy Resources Technology (IF: 2.759), June, 2020, Vol. 142, No. 6, pp. 061305 (13 pages) https://doi.org/10.1115/1.4045535
4. Mohammad D. Qandil, Ahmad I. Abbas, Hasan D. Qandil, Muhannad R. Al-Haddad, and Ryoichi S. Amano, "A Stand-Alone Hybrid Photovoltaic, Fuel Cell, and Battery System: Case Studies in Jordan", Transactions of the ASME, Journal of Energy Resources Technology (IF=2.759), May 2019, Vol. 141, No.11, pp. 111201 (10 pages). https://doi.org/10.1115/1.4043656
5. Ahmad I. Abbas, Ryoichi S. Amano, Mandana S. Saravani, Mohammad D. Qandil, and Tomoki Sakamoto, "Optimization of Kaplan Hydroturbine at Very Low Head With Rim-Driven Generator", Transactions of the ASME, Journal of Energy Resources Technology (Impact Factor: 2.759), May 2019, Vol.141, No.11, pp. 111204 (12 pages). https://doi.org/10.1115/1.4043710
6. Ahmad I. Abbas, Mohammad D. Qandil, Muhannad R. Al-Haddad, Mandana S. Saravani, and Ryoichi S. Amano, "Utilization of Hydroturbines in Wastewater Treatment Plants", Transactions of the ASME, Journal of Energy Resources Technology (IF=2.759), April 2019, Vol.141, No.6, pp. 062011 (5 pages). https://doi.org/10.1115/1.4042969
7. Taieseer Abu Rahmeh, Ahmad Abbas, Jamal Jaber and Aiman Alawin, "Repowering Old Thermal Power Station by Integrating Concentrated Solar Power Technology", Jordan Journal of Mechanical and Industrial Engineering, June 2016, Vol.10, No.2, pp. 85-98
8. http://jjmie.hu.edu.jo/vol%2010-2/JJMIE-19-16-01.pdf
9. Wei-Lin Chen, Ahmad I. Abbas, Ryan Ott, and Ryoichi S. Amano, "Investigation of Liquid Breakup Process Solid Rocket Motor Part B: Vertical C-D Nozzle", Transactions of the ASME, Journal of Energy Resources Technology, February 2020. (Manuscript Accepted)
10. Mohammad D. Qandil, Ahmad I. Abbas, Ahmad I. Abdelhadi, Abdel-Rahman S. Salem, and Ryo S. Amano, "Energy Analysis: Ways to Save Energy and Reduce the Emissions in Wastewater Treatment Plants (WWTPs) In Wisconsin," Energy (IF: 5.537), in review.
11. Ahmad I. Abbas, Mohammad D. Qandil, Ryo S. Amano, "Comprehensive Comparative Study of Turbulence Models and Efficient CFD Simulations of Hydro Turbines in The World of High-performance Computing (HPC)", Applied Energy (IF: 8.426), in review.
12. Ahmad I. Abbas, Muhannad R. Al-Haddad, Mandana S. Saravani, and Ryoichi S. Amano, "How much Wastewater Treatment Plants (WWTPs) are far from Net-zero Energy? An approach of Energy-Efficiency, Combined Heat and Power (CHP), and Solar PV-Wind Hybrid Renewable Energy System", Sustainable Cities and Society (IF: 4.624), in review.

Conference Papers (peer-reviewed):

1. Ryoichi S. Amano, Ahmad I. Abbas, Mohammad D. Qandil, and Muhannad Al-Haddad, "Multi-Disciplinary Design Optimization of a Horizontal Micro Kaplan Hydro Turbine", ASME Turbo Expo 2019, Phoenix, AZ, USA. https://doi.org/10.1115/GT2019-90509
2. Ryoichi S. Amano, Ahmad I. Abbas, Muhannad Al-Haddad and Mohammad D. Qandil, "Energy Consumption, Energy-saving and Emissions Reduction of Wastewater Treatment Plants (WWTPs) in Wisconsin", AIAA Propulsion and Energy 2019 Forum, Indianapolis, IN, USA. https://doi.org/10.2514/6.2019-4239

3. Ryoichi S. Amano, Mandana S. Saravani, Ahmad I. Abbas, "The Opportunity for Energy Saving in Foundry-Case Study", AIAA Propulsion and Energy 2019 Forum, Indianapolis, IN, USA. https://doi.org/10.2514/6.2019-4072
4. Ryoichi S. Amano, Ahmad I. Abbas, Abdel Rahman S. Salem, Ahmad I. AbdelHadi, and Mohammad D. Qandil, "Study of industrial energy assessments for different sectors", AIAA Propulsion and Energy 2019 Forum, Indianapolis, IN, USA. https://doi.org/10.2514/6.2019-4238
5. Mohammad Qandil, Tarek Elgammal, Ahmad I. Abbas, Ahmad Abdelhadi, and Ryoichi S. Amano, "Predicting the Cavitation Phenomena Over the Hydrofoil: CFD Validation", AIAA Scitech 2019 Forum, San Deigo, CA, USA. https://doi.org/10.2514/6.2019-0783
6. Ahmad I. Abbas, Mohammad Qandil, Muhannad Al-Haddad, and Ryoichi S. Amano, "Performance Investigation of Very-Low-Head Kaplan Hydro-Turbines", AIAA Scitech 2019 Forum, San Deigo, CA, USA. https://doi.org/10.2514/6.2019-0241
7. Muhannad Al-Haddad, Ahmad I. Abbas, Mohammad Qandil, Mandana Saravani, and Ryoichi S. Amano, "Energy Value Analysis (EVA) of an Office Building: Case Study", AIAA Scitech 2019 Forum, San Deigo, CA, USA. https://doi.org/10.2514/6.2019-1276
8. Ahmad I. Abbas, Mohammad D. Qandil, Muhannad R. Al-Haddad, Mandana S. Saravani, and Ryoichi S. Amano, 2018, "Utilization of Hydro-Turbines in Wastewater Treatment Plants (WWTPS)", Proceedings of the ASME 2018 Power Conference, Orlando, FL, USA, Paper No. PowerEnergy2018-7349. https://doi.org/10.1115/ES2018-7349
9. Ahmad I. Abbas, Muhannad R. Al-Haddad, Mandana S. Saravani, Mohammad D. Qandil, and Ryoichi S. Amano, 2018, "A Comparative Study of Industrial Energy Assessments For Small and Medium-Sized Industrial Facilities", Proceedings of the ASME 2018 Power Conference, Orlando, FL, USA, Paper No. PowerEnergy2018-7550. https://doi.org/10.1115/ES2018-7550
10. Mohammad D. Qandil, Ryoichi S. Amano, and Ahmad I. Abbas, 2018, "A Stand-Alone Hybrid Photovoltaic, Fuel Cell and Battery System: Case Studies In Jordan", Proceedings of the ASME 2018 Power Conference, Orlando, FL, USA, Paper No. PowerEnergy2018-7121. https://doi.org/10.1115/ES2018-7121
11. Ahmad Abbas, Mandana S. Saravani, Muhannad Al-Haddad, and Ryoichi S. Amano. "Net-Zero-Energy (NZE) Wastewater Treatment Plants (WWTPs)." In 2018 AIAA Aerospace Sciences Meeting. American Institute of Aeronautics and Astronautics. https://doi.org/10.2514/6.2018-1712.
12. Ahmad Abbas, Muhannad Al-Haddad, Mandana S. Saravani, , and Ryoichi S. Amano. "An Analytical Study of Energy Efficiency Opportunities in Some Industrial Facilities." In 2018 AIAA Aerospace Sciences Meeting. American Institute of Aeronautics and Astronautics. https://doi.org/10.2514/6.2018-1710.
13. Ahmad Abbas, and Ryoichi S. Amano. "Optimization of Intake and Draft Tubes of a Kaplan Micro Hydro-Turbine." In 15th International Energy Conversion Engineering Conference (2017). American Institute of Aeronautics and Astronautics. https://doi.org/10.2514/6.2017-4807.
14. Ahmad Abbas, and Ryoichi S. Amano. "Integration of Linear Fresnel Reflectors (LFR) with Conventional Power Plants." In 15th International Energy Conversion Engineering Conference (2017). American Institute of Aeronautics and Astronautics. https://doi.org/10.2514/6.2017-4624.
15. Ahmad I. Abbas, Tomoki Sakamoto, Mandana S. Saravani, Ryoichi S. Amano, Joseph Millevolte, and Bruno Lequesne, 2017, "Optimization of Kaplan Hydro-Turbine at Very Low Head with Rim-Driven Generator", Proceedings of the ASME 2017 Power Conference Joint with ICOPE-17, Charlotte, NC, USA, Paper No. POWER-ICOPE2017-3564. https://doi.org/10.1115/POWER-ICOPE2017-3564
16. Ahmad I. Abbas, Mohammad D. Qandil, and Ryoichi S. Amano, "Optimization of Computational Fluid Dynamics (CFD) Simulations for Hydro Turbines Applications," ASME FEDSM 2020, Orlando, FL, USA. (in-review).
17. Mohammad D. Qandil, Ahmad I. Abbas, Ahmad I. Abdelhadi, and Ryoichi S. Amano, "The Cavitation Characteristics That Occurs Over a Hydrofoil in a Water Tunnel," ASME FEDSM 2020, Orlando, FL, USA. (in-review).

18. Farah N. Nazifa, Ahmad I. Abbas, and Ryoichi S. Amano, "An Analytical Study to Use the Excess Digester Gas of Wastewater Treatment Plant in Wisconsin," ASME FEDSM 2020, Orlando, FL, USA (in review).

Technical Reports:

Bruno Lequesne, Ryoichi S. Amano, Joseph Millevolte, Ahmad Abbas, Tomoki Sakamoto, Mandana Saravani, Muhannad Al-Haddad, Tarek El-Gammal, and Hisham Alyahya,"DOE-EMotors-15757-1 3D-printed, integrated plug-and-play turbine-generator set for very-low-head hydro", No. DOE-EMotors-15757-1, March 2017, DOI: 10.2172/1348117

Presentations at Conferences

1. ASME Turbo Expo Turbomachinery Technical Conference & Exposition 2019, June 17-21, 2019, Phoenix, AZ, USA.
2. AEE 37th West Coast Energy Management Congress 2019, June 4-6, 2019, Santa Clara, CA, USA.
3. AEE 41st World Energy Engineering Congress (WEEC) 2018, October 17-19, 2018, Charlotte, NC, USA.
4. AIAA Propulsion and Energy Forum and Exposition 2018, July 9-11, 2018, Cincinnati, OH, USA.
5. AIAA SciTech Forum and Exposition 2018, January 8-12, 2018, Kissimmee, FL, USA.
6. AEE 40th World Energy Engineering Congress (WEEC) 2017, September 27-29, 2017, Atlanta, GA, USA.
7. AIAA Propulsion and Energy Forum and Exposition 2017, July 10-12, 2017, Atlanta, GA, USA.
8. ASME 2017 Power Conference joint with ICOPE-17 collocated with the ASME 2017 11th International Conference on Energy Sustainability, the ASME 2017 15th International Conference on Fuel Cell Science, Engineering and Technology, and the ASME 2017 Nuclear Forum, June 26-30, 2017, Charlotte, NC, USA.
9. AEE 35th West Coast Energy Management Congress (EMC) 2017, June 7-8, 2017, Long Beach, CA, USA.
10. ASME 2016 Fluids Engineering Division Summer Meeting, FEDSM 2016, collocated with the ASME 2016 Heat Transfer Summer Conference and the ASME 2016 14th International Conference on Nanochannels, Microchannels, and Minichannels, July 10-14, 2016, Washington, DC, USA.

Awards and Certificates

- Distinguished Graduate Student Fellowship (DGSF) 2019-2020 Award at University of Wisconsin-Milwaukee
- Chancellor's Award, Spring 2020 at UW-Milwaukee
- Chancellor's Award, Fall 2018 at UW-Milwaukee
- Chancellor's Award, Spring 2016 at UW-Milwaukee
- U.S. DOE's Industrial Assessment Center Program, Certificate of Achievement, October 2017 by the US Department of Energy (DOE).

Editorial/Peer-Review Work

- Reviewer in ASME Journal of Energy Resources Technology (7 reviews)
- Reviewer in International Journal of Rotating Machinery (1 review)

Administrative Services

- Member of the Graduate Student Fellowships Committee (GSFC) (2019-2020)

Courses/Training

- July 2012 – August 2012 | Technical Writing (18 Hours)
  Jordan Engineers Association | Amman, Jordan
- April 2011 – May 2011 | SolidWorks (30 Hours)
  JEA, (Engineers Training Center) | Zarqa, Jordan

Languages

- Arabic: Native language
- English: Overall score of 7.0 in IELTS

Associations

- Association of Energy Engineers (AEE) – Student Member
- American Institute of Aeronautics and Astronautics (AIAA)–Student Member
- American Society of Mechanical Engineers (ASME)-Student Member
- American Institute of Aeronautics and Astronautics (AIAA) (Vice-President for UW-Milwaukee chapter)
- Association of Energy Engineers (AEE) (President for UW-Milwaukee chapter)
- Arab American Association of Architects and Engineers (AAAEA) (Founder & Vice-President for UW-Milwaukee chapter)
- The Jordan Engineers Association (JEA) as a Mechanical Engineer.

Other

- Google Scholar: https://scholar.google.com/citations?user=nAFHT7MAAAAJ&hl=en#
- LinkedIn: https://www.linkedin.com/in/ahabbas/